

Design and Synthesis of Supramolecular Assemblies and their Photophysical studies

**Thesis Submitted to AcSIR for the Award of the Degree
of**

**DOCTOR OF PHILOSOPHY
In Chemical Science**



(Academy of Scientific and Innovative Research)

By

Monalisa Gangopadhyay

(Reg.No. 10CC12A26086)

Under the guidance of

Dr. Amitava Das

CSIR-National Chemical Laboratory
Pune, Maharashtra, India– 411008

June 2017

CANDIDATE'S STATEMENT

I hereby declare that the work incorporated in the present thesis is original and has not been submitted to any University/Institution for the award of a Diploma or a Degree. Research material obtained from other sources has been duly acknowledged in the thesis. Any text, illustration, table etc., used in the thesis from other sources, have been duly cited and acknowledged." further declare that the results presented in the thesis and the considerations made therein, contribute in general to the advancement of knowledge in chemistry and in particular to "**Design and Synthesis of Supramolecular Assemblies and their Photophysical studies**".

Monalisa Gangopadhyay

Monalisa Gangopadhyay

Certificate

This is to certify that the work incorporated in this Ph.D. entitled "**Design and Synthesis of Supramolecular Assemblies and their Photophysical studies**" submitted by **Ms. Monalisa Gangopadhyay**, to Academy of Scientific and Innovative Research (AcSIR) in fulfillment of the requirements for the award of the Degree of Doctor of Philosophy, embodies original research work under my supervision. I further certify that this work has not been submitted to any other University or Institution in part or full for the award of any degree or diploma. Research material obtained from other sources has been duly acknowledged in the thesis. Any text, illustration, table etc., used in the thesis from other sources, have been duly cited and acknowledged.

Monalisa Gangopadhyay

(Student)

Amitava Das

(Supervisor)

Acknowledgment

ACKNOWLEDGEMENTS

I whole heartedly express my deep sense of gratitude to **Dr. Amitava Das** – My Guide. I am extremely grateful to him for his continuous encouragement, timely advise, scholarly monitoring and invaluable suggestions. I am really thankful for the freedom that he gave to my research life. I grew as a research student watching him working till late night every day, which has been the source of inspiration to me.

I wish to convey my gratefulness to **Dr. Rajamohanam, Dr. Sapna Ravindranathan** for fruitful discussions on research problems, appreciative comments, and continuous guidance whenever I approached which helped me to explore various aspects of the chemistry.

I wish to express my sincere thanks to my Doctoral advisor committee **Dr. J Nithyanandan, Dr. D S Reddy** and **Dr. A Sudalai** for their continued encouragement and valuable suggestions.

I wish to express my word of thanks to **Dr. P. K. Ghosh** (Former Director, CSMCRI, Bhavnagar), **Dr. Sourav Pal** (Former Director, NCL-Pune), **Dr. Ashwini K. Nangia** (Director, NCL), **Dr. Parimal Paul** (Discipline Coordinator, CSMCRI) **Dr. Pradeep Kumar**, Head, Division of Organic Chemistry for providing me opportunity and all necessary facilities to carry out my research work.

My sincere thanks to **Dr. Sakya Sen, Dr. S. B. Sukumaran, Dr. R. A. Joshi, Dr. Rahul Banerjee, Dr. Sayam Sengupta, Dr. B. L. V. Prasad, Dr. P. S. Subramaniyan, Dr. Ramrup sarkar, Dr. S. P. Mukherjee, Dr. A. K. Siddhanta, Dr. R. I. Kureshi and Dr. Adimurthy** and all other scientists of NCL and CSMCRI for their motivation, constant encouragement and support.

I would like to express my special thanks to my seniors **Dr. Moorthy Suresh, Dr. Prasenjit Mahato, Dr. Amal Kumar Mandal, Dr. Priyadip Das, Dr. Sukdeb Saha, Dr. Tanmay Banerjee, Dr. Upendar Reddy, Dr. Vadde Ramu, Dr. Hridesh Agarwalla**. They all taught me in my initial days of my research carrier and took me along with them.

I feel fortunate enough to have wonderful group of colleagues **Arunava, Firoj, Dr. Praveen L., Dr. Sovan Roy, Dr. Shilpi Kushwaha, Dr. Ketan Patel, Dr. Suman Pal, Dr. Ajoy Pal, Sunil, Anil, Koushik, Sanjukta and Ananta** with whom I worked all these five year. Each one of them equally contributed in different way to take up my course so fruitfully throughout these five years. I thank all of them individually from the bottom of my heart.

Acknowledgment

My Sincere thanks to my friends and collaborators **Tuhin Khan, K. Prajitha, Santanu Basu, Dinesh More** who are an important part of my journey.

My sincere thanks to all my friends for their support and to my make my journey joyful and a memorable one. I thank all of you **Dibyendu, Milan, Jaswanta, Pritam, Arnab, Debashis, Debdeep da, Anup, Santi, Pravat da, Partha da, Kanak da, Achintya da, Susanta da, Arpan da, Arya da, Saikat da, Shyam da, Chandan da, Himadri da, Krishanu da, Arijit da, Tamas da, Prathit da, Tanaya di, Munmun di, Jhumur di, Subhadi, Soumen da, Siba, Subhrasis, Tapas, Tamal, Pronob, Manzoor, Saibal, Subrata, Avijit, Pranoy, Sandipan, Mohitosh, Somsuvra, Indrwadeep, Sutanu, Anirban, Piyali, Rupa, Ruchi, Bhawana, Veenita, Soumya di.**

My sincere thanks to new hostel saturday night group. My pune stay would have been boring without you people **Chayanika, Manik, Santanu, Sudip, Suman, Bittu, Atanu, Atryee, Manoj da, Gabluda, Munna.**

I would like to extend my sincere thanks to my teachers Rana Sir, Chandan Saha, Chandan Kumar Pal Sir for their sincere efforts and patience in guiding me from my college days.

I wish to thank **CSIR** for financial assistance and **AcSIR** for allowing me to submit my work in the form of thesis.

At this moment, I invariably feel short of words to express my sincere thanks to My Grand Parent Late **Kalyani Gangopadhyay** and, Late **Anondomoyi Banerjee** my grand father **Sri. Satyna Narayan Banerjee** and father **Manas Mohan Gangopadhyay** mother **Smt. Kakali Gangopadhyay** and beloved sister **Mohini** and uncle **Gopi Mohan Gangopadhyay**, for their love, prayers and support which inspired me and strengthen throughout my life. I thank all my well-wishers whose continuous encouragement and support in completion of this tough task.

I am also thankful to **Almighty God** for all your blessings to me and for the strength you give me each day.

List of Abbreviation

CD ₂ Cl ₂	Deuterated dichloromethane
CDCl ₃	Deuterated chloroform
CD ₃ OD	Deuterated Methanol
DMSO-d ₆	Deuterated Dimethyl sulfoxide
CD ₃ CN	Deuterated acetonitrile
DMF	N,N'-dimethylformamide
DMSO	Dimethyl sulfoxide
THF	Tetrahydrofuran
ACN	Acetonitrile
ESI	Electrospray Ionization
ET	Energy Transfer
HOMO	Highest Occupied Molecular Orbital
LUMO	Lowest Unoccupied Molecular Orbital
ICT	Intramolecular Charge Transfer
TOF	Time of Flight
MALDI	Matrix-assisted laser desorption/ionization
PET	Photo-induced Electron Transfer
COSY	Correlation Spectroscopy
NOESY	Nuclear Overhauser effect spectroscopy
ROESY	Rotating-frame Overhauser Spectroscopy
HSQC	Heteronuclear single quantum coherence spectroscopy
TCOSY	Total Correlation Spectroscopy

List of Abbreviation

NMR	Nuclear Magnetic Resonance
FTIR	Fourier Transform Infrared
FRET	Förster Resonance Energy Transfer
CB	Cucurbituril
CD	Cyclodextrin
TPA	Triphenylamine
B-H plot	Benesi–Hildebrand plot
Fc/Fc ⁺	Ferrocene/Ferrocenium cation
CV	Cyclic Voltametry
TCSPC	Time Correlated Single Photon Counting

Contents

Chapter	Section	Title	Page No
1		Introduction	1
	1.1	A Brief Introduction of Supramolecular Chemistry	2
	1.2	Molecular Interactions, Molecular complementarity, Cooperativity, Multivalency	2
	1.2.1.	Electrostatic interactions	3
	1.2.2.	Hydrogen Bonding	3
	1.2.3.	π -interactions	4
	1.2.4.	Hydrophobic interactions	4
	1.2.5.	Cooperativity	5
	1.2.6.	Molecular complementarity	5
	1.2.7.	Multivalency	6
	1.3	Photophysical Mechanisms involved in self assembled systems	7
	1.3.1.	Photoinduced Electron Transfer (PET)	7
	1.3.2.	Energy Transfer Mechanisms	9
	1.3.2.1.	Radiative Energy Transfer	9
	1.3.2.2.	Non-radiative Energy transfer	9
	1.3.3.	Intamolecular Charge Transfer	10
	1.4	Different kinds of Self-assembled structure	10
	1.5	Recognition of Organic Cations such as Imidazoilium and Ammonium Cations: Pseudorotaxane Based Interlocked Molecules	10

Contents

	1.5.1. Ammonium ion binding	11
	1.5.2. Imidazolium/pyridinium cation binding	15
	1.5.3. Multivalency based pseudorotaxane	19
	1.5.4. Self-sorting based pseudorotaxane	23
1.6	Chiral recognition on self-assembled systems	27
1.7	1.7. Logic gates on self-assembled systems	30
1.8	References	33
2	Tuning Emission Responses of a TPA Derivative in Photoresponsive Pseudorotaxane and an Unusual Dynamic Inclusion Phenomenon	37
2.1	Introduction	38
2.2	Experimental section	39
	2.2.1. Materials	39
	2.2.2. Analytical Methods	39
	2.2.3. Generalised methodology for spectroscopic studies	40
	2.2.4. Synthesis	41
2.3	Results and Discussions	41
	2.3.1. NMR studies of $[1 \cdot \{3CB[7]\}]Cl_3$	42
	2.3.2. NMR studies of $[1 \cdot \{\beta\text{-CD}\}]Cl_3$	47

Contents

	2.3.3. Association Constant and Thermodynamic Parameters	59
	2.3.4. Photophysical studies	60
2.4	Conclusion	65
2.5	References	67
3	[2]pseudorotaxane Formation With FRET-Based Luminescence Response: Demonstration of Boolean Operations Through Self-Sorting on Solid Surface	70
3.1	Introduction	71
3.2	Experimental section	73
	3.2.1. Materials	73
	3.2.2. Analytical Methods	73
	3.2.3. Synthesis	74
3.3.	Results and Discussions	77
	3.3.1. Photophysical studies	77
	3.3.2. Time resolved emission studies	82
	3.3.3. NMR studies	85
	3.3.4. Electrochemical studies	90
	3.3.5. Isothermal Titration Calorimetry studies	91
	3.3.6. Self-sorting	92
	3.3.7. Photophysical properties in film and construction of Logic gates	95

Contents

	3.4	Conclusion	99
	3.5	References	100
4		Chiral Discrimination Through FRET Based Process in Supramolecular Assemblies	102
	4.1	Introduction	103
	4.2	Experimental section	105
		4.2.1 Materials	105
		4.2.2 Analytical Methods	105
		4.2.3. Synthesis	106
	4.3	Results and Discussions	108
		4.3.1. Photophysical studies	108
		4.3.2. Time resolved emission studies	113
		4.3.3. Electrochemical studies	116
		4.3.4. Isothermal Titration Calorimetry studies	117
		4.3.5. Circular Dichroism	118
		4.3.6. NMR studies	119
	4.4.	Conclusion	131
	4.5	References	132
5		Tuning of Monomer/Excimer Emission of a bis-crown ether By Dicationic Ammonium Guests	135
	5.1	Introduction	136

Contents

5.2.	Experimental section	138
	5.2.1. Materials	138
	5.2.2. Analytical Methods	138
	5.2.3. Synthesis	138
5.3.	Results and Discussions	142
	5.3.1. Spectroscopic studies	142
	5.3.2. Temperature dependent fluorescence studies	148
		149
	5.3.3. Time resolved emission studies	
5.4.	Conclusion	151
5.5	References	152
	Conclusion of Thesis	154
	Appendix	156
	List of Publication	182
	List of Conferences attended	183

CHAPTER 1

INTRODUCTION

Chapter 1

1.1. A Brief Introduction of Supramolecular Chemistry

Supramolecular chemistry primarily deals with molecular assemblies involving a discrete number of molecular components that are held through weak and reversible non-covalent interactions. Understanding the nature of such weak and reversible non-covalent interactions that govern the assembly formation in a host-guest assembly is crucial in achieving the desired specificity in the recognition process. Reversible non-covalent interactions allow the disassembly process too in presence of certain external stimuli. Any such assembly and disassembly process for a supramolecular host-guest system generally leads to a conformational change(s) of the host and (or) guest molecules. Such change(s) in molecular conformation has/have immense significance for constructing the artificial molecular-level machines following bottom-up strategies that enables manipulation of molecules, the smallest entities that have distinct properties. With appropriate design in a bottom-up approach, one can actually control the three-dimensional superstructure of individual (macro) molecules and the architecture of their assemblies.¹⁻³ Mechanically interlocked structures⁴ are attractive to chemists not only because they are aesthetically appealing but also due to their potential applications in molecular machines and smart materials.⁵ Consequently, complex architecture and functionality in an assembly can be achieved with comparatively simple and well defined molecular building blocks. Supramolecular structures are the result of not only additive but also cooperative interactions, including hydrogen bonding, hydrophobic interactions as well as coordinative interaction(s). Such supramolecular assemblies generally possess property(ies) that is/are different than the sum of the properties of each individual component.

Complementarity plays an important role in biological and supramolecular systems in terms of size, shape and active synthon for the specific host-guest interactions. This is also important for molecular recognition and inclusion complex formation as well as imparting stability to it. A brief summary of various factors that influence the inclusion complex formation and molecular recognition process is provided in the next section.⁶

1.2. Molecular Interactions, Molecular complementarity, Cooperativity, Multivalency

Several types of molecular interactions such as electrostatic, hydrogen bonding, ion-dipole, dipole-dipole, hydrophobic and Vander Walls interactions act individually or simultaneously for the formation of stable supramolecular architectures. These interactions are considerably weaker than covalent interactions.

Chapter 1

1.2.1. Electrostatic interactions

Electrostatic interactions are important for ionic species like cations and anions as well as for species with formal charge. In supramolecular self assembled systems, electrostatic interactions generally occur in the form of ion–ion, ion–dipole, ion–quadrupole, and quadrupole–quadrupole interactions (Figure 1.1). Molecules with permanent dipole interact with cations as well as anions and accounts for the ion–dipole interaction. Difference in electronegativity and the spatial orientation of the associated atoms in the molecule plays a crucial role for the effective charge polarization and the dipole moment of the overall molecule. Among various electrostatic interactions, dipole–dipole interaction is the weakest one (5–50 KJ mol⁻¹) but such an interaction is highly directional in nature.⁷

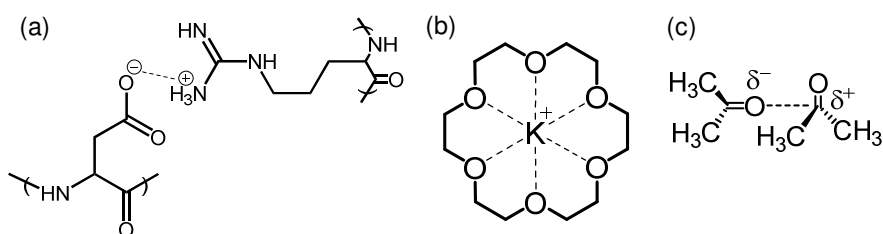


Figure 1.1: Schematic presentation of various molecular interactions: (a) ion-ion interaction in cationic amino acid (arginine) and anionic amino acid (aspartic acid), (b) ion-dipole interaction in the K⁺ complex of [18]crown-6, (c) dipole-dipole interaction in acetone.

1.2.2. Hydrogen Bonding

Hydrogen bonding (H-bonding) plays a very crucial role in supramolecular self-assembly formation or generation of self-assembled architecture (Figure 1.2).⁸ This interaction ranges from 1 to 5 kcal mol⁻¹.⁸ The strength of hydrogen bonds depends on the electronegativity of the atom to which the hydrogen atom is attached and the geometry that the hydrogen bond adopts in the structure. For example, in HF₂⁻ ion, linear H-bond formation between two fluoride ions [F...H...F]⁻ attributes to a much stronger interaction. Moderate H-bonding interaction does not have linear geometry but bent in nature. Here interaction takes place between neutral donor and neutral acceptor via its electron lone pairs. Slightly bent hydrogen bonding is observed in self-association of carboxylic acids due to moderate interaction between donor and acceptor atoms.

1.2.3. π -interactions

Various types of π -interactions are observed in self-assembled supramolecular structures, namely cation- π , π - π , anion- π , polar- π interactions (Figure 1.2). π - π interactions are associated with the interaction between the π -orbitals of a molecular system.⁹ All these interactions are self-explanatory. Polar- π interaction involves interaction of molecules with permanent dipole(s) with the quadrupole moment of a π -system. Strength of such interactions generally ranges between ~ 1 to 2 kcal/mol.

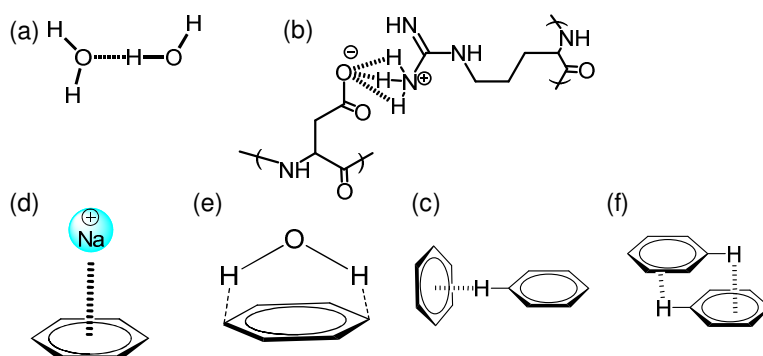


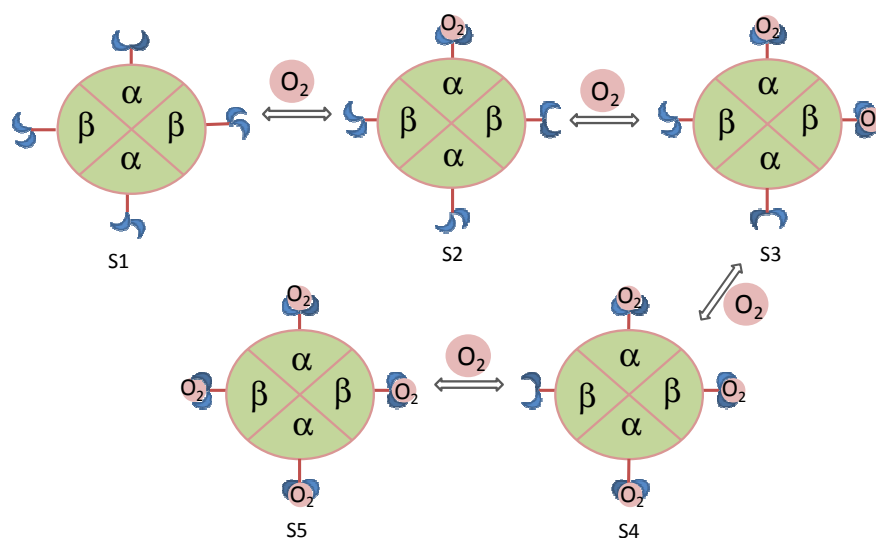
Figure 1.2: Schematic representation of hydrogen bond interactions between (a) two water molecules, (b) amino acid pairs (arginine and aspartic acid), (c) cation- π interaction, (d) polar- π interactions, (e) π - π interactions (edge to face), (f) displaced interactions.

1.2.4. Hydrophobic interactions

Hydrophobic effect relies on the minimization of the energetically unfavourable surface between polar/protic and unpolar/aprotic molecules. This demonstrates the influence of the environment on molecular property. It is namely of two types, enthalpic component and entropic component of hydrophobic effect. Enthalpic component favours the water-water hydrogen bonds in the solvation shell due to the reduced mobility of water molecules and this situation arises when a guest displaces the water within a cavity. Once the water has been replaced by a guest, the energy is lowered by the interaction of the former water guest with the bulk solvent outside the cavity. The hydrophobic effect is mostly entropy-driven at room temperature due to the reduced mobility of water molecules in the solvation shell of the non-polar solute.

1.2.5. Cooperativity

Cooperativity is a concept for understanding molecular recognition and supramolecular self-assembly.¹⁰ It is one of the most important phenomena that is associated with the binding processes in biology.^{11a} Cooperativity generally arises from the role of two or more interactions, so that the system as a whole behaves differently from expectations based on the properties of the individual interactions that exists in isolation. Coupling of interactions can lead to positive or negative cooperativity, depending on whether one interaction favours or disfavours another. Cooperativity is the key feature of systems chemistry that leads to collective properties not present in the individual molecular components. One of the common example of positive cooperativity in molecular recognition is the O₂-binding process of the mammalian haemoglobin (Hb) tetramer. In Hb, both concerted and sequential models of cooperativity are operational.^{11b} Other factors like media polarity, solvation and conformational change(s) associated with individual active site of the receptor influences the binding thermodynamics.



Binding of O₂ induced structural changes in the protein structure and that inturn helps in favouring the binding of the next. Oxygen affinity of S4 > S3 > S2 > S1

Figure 1.3: Representation of processes that display positive cooperativity, haemoglobin binding oxygen.

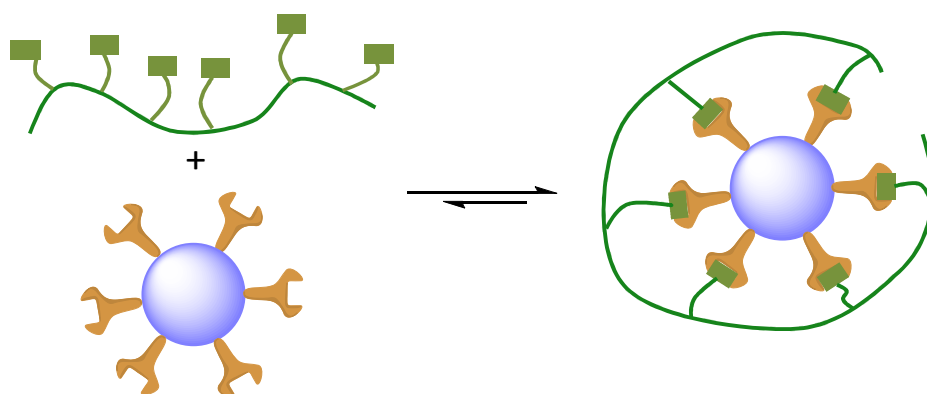
1.2.6. Molecular complementarities

Complementarity is one of the key issues for molecular recognition in supramolecular assembly, which primarily depends how well the host and guest molecules/ ions

Chapter 1

complement each other in terms of size, shape and electronically. More recently it has been argued that recognition is a phenomenon of organisation. Prediction of the molecular recognition events is not the static snapshot of a single frame between the guest and the host. One needs to have a better insight in free energy landscape to understand the change(s) in entropies, as that plays a crucial role in binding thermodynamics and entropies. For understanding a real binding model, dynamic molecular recognition involving positive or negative cooperativity are important. Other factors like media polarity, solvation, conformational changes etc. also play key a role.

1.2.7. Multivalency



Cartoon representation multiple host-guest interactions through simultaneous binding events may significantly enhance the stability of the host-guest complex formation through various non-covalent and complementary interactions.

Cartoon representation multiple copies of guest fragment on a specified surface



Cartoon representation multiple copies of host fragment on a specified surface



Cartoon representation multiple host-guest interactions through simultaneous binding events

Figure 1.4: Cartoon representation for describing how multivalency may help in stabilizing the host-guest adduct formation.

Multivalency describes the unique thermodynamic features arising from binding a host and a guest each equipped with more than one binding site. One should use the term “multivalency” only for those host-guest complexes, in which the dissociation into free host and guest requires at least the cleavage of two recognition sites. The concept of multivalency has been introduced to adequately describe the properties of biomolecules.¹²

Chapter 1

Multivalent binding is associated with simultaneous interaction of multiple complementary functionalities, which significantly increases the significance of 'weak' intermolecular forces, such as hydrogen bonding, π - π interactions and electrostatic interactions, in a manner analogous to how Velcro work (Figure 1.4).

1.3. Photophysical Mechanisms involved in self assembled systems

In molecular recognition, binding process involves a spontaneous analyte-receptor binding and such binding process often induces significant changes in the energies of the frontier orbitals of the individual host and (or) guest molecule or the energies of the frontier orbitals of the chromophore(s) covalently bound to the receptor or/and analyte molecule(s). Binding process in molecular recognition also induces change(s) in the electronic environment of the binding sites of the host and guest components. Such changes in electronic environment and the energies of the frontier orbitals help us to probe the binding phenomena by monitoring changes in magnetic resonance spectroscopy and optical spectroscopy, respectively. Among these options, ease of using optical spectroscopy has provided this an obvious edge over other process for probing the binding processes in molecular recognition. For this one needs to have a guest and/or host molecule(s) that is covalently linked to a chromophore through a conduit that allows transmission of the binding induced changes with necessary changes in the optical properties. Such measurable change(s) in optical or photophysical properties help us in probing the recognition phenomena. As the focus of this dissertation lies in utilizing the changes in luminescence properties for probing the recognition of cationic ammonium or imidazolium ions by synthetic crown ether based host molecules or naturally occurring carbohydrate residues like cyclodextrin or cucurbituril, discussions are restricted in various photophysical processes that are associated with luminescence changes that are associated with such binding phenomena. In the following section, brief discussions on few photophysical processes that are pertinent for the present dissertation are provided.

1.3.1. Photoinduced Electron Transfer (PET)

The working principle of a PET-based Photophysical process is shown in Figure 1.5. The essential criterion for a PET based process involves covalent linking of a fluorophore to a receptor unit having an unshared pair of electrons with distinctly lower redox potential value for the HOMO of the receptor when that unshared pair of electrons is bound or coordinated to a proton or a metal ion.¹³ As shown in Figure 1.5, the energetically feasible

Chapter 1

electron transfer quenches the fluorescence of the luminophore and this is attributed to a relatively higher HOMO energy level for the receptor with lone pair of electrons. On association of the receptor lone pair of electrons either through H-bonding or through coordination to a H^+ or a cation, energy for the HOMO is effectively lower to a level that prohibits any electronic transition to the HOMO levels of the photo-excited fluorophore and subsequently interrupt the PET process. This accounts for a significant enhancement or fluorescence ON responses.

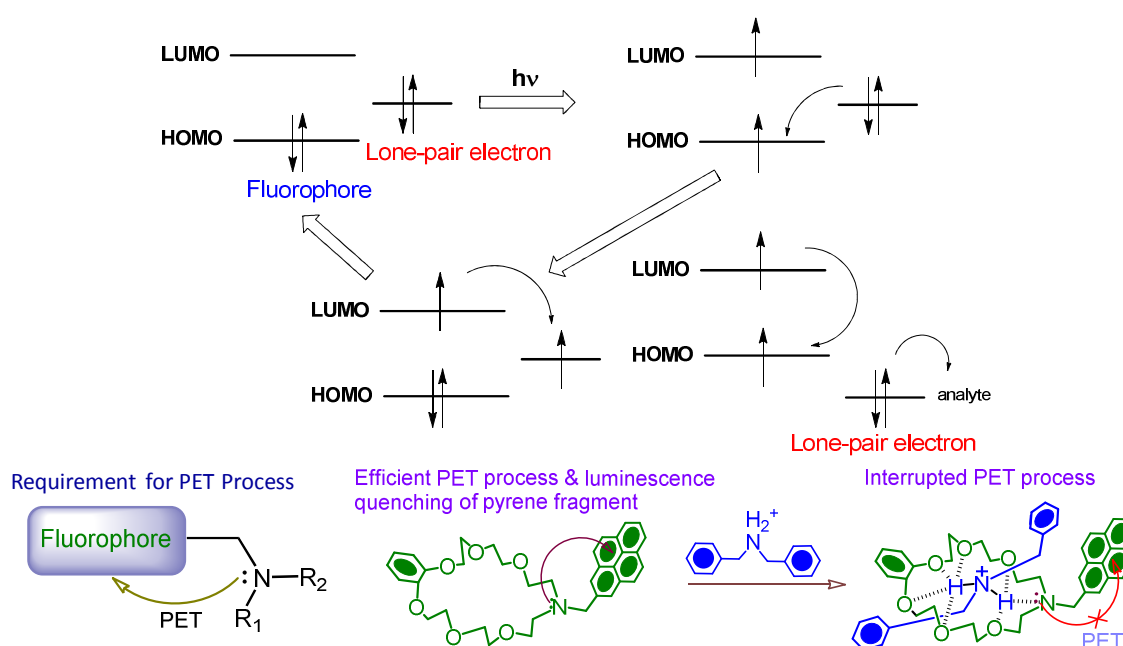


Figure 1.5: Photophysical mechanism of PET and fluorescence enhancement (top), cartoon representation as well as the molecular structures of a receptor and the host-guest assembly with interrupted PET process (bottom).

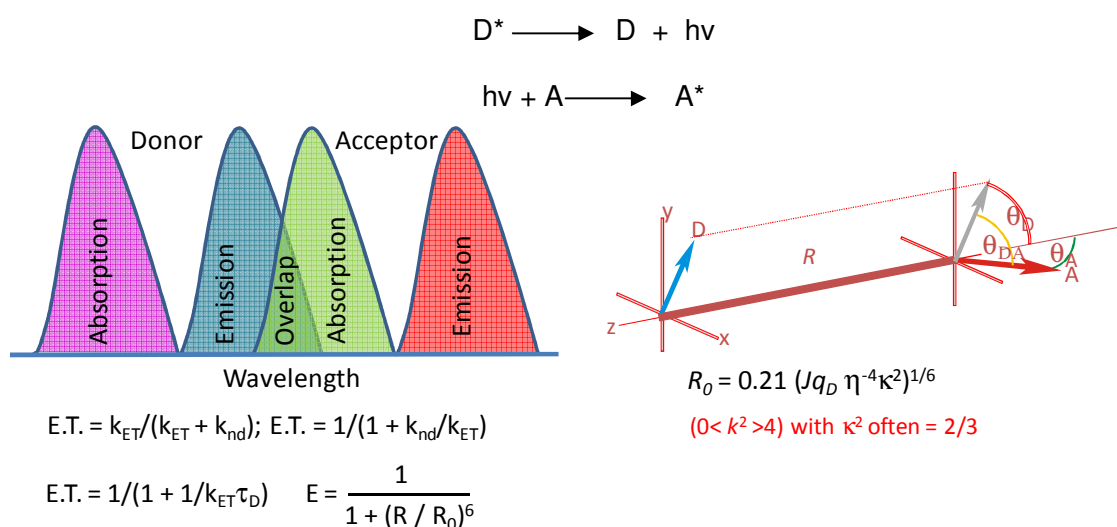
As shown in Figure 1.5 a lone pair of electrons is located in a receptor's HOMO that lies between the HOMO and LUMO of the fluorophore. On photoexcitation, electronic transition from HOMO generates a hole in the HOMO of the fluorophore, which triggers a thermodynamically feasible electronic transition from the lone pairs of electron of the receptor moiety. On effective lowering of the energy of the lone pairs of electron such process is inhibited and favours the radiative deactivation of excited state with fluorescence ON response. Figure 1.5 shows the design aspect for achieving the interrupted PET process in understanding the host-guest complexation by monitoring the luminescence change.

1.3.2. Energy Transfer Mechanisms

Interaction between two chromophores in the excited state mainly manifested in photophysical process called electronic energy transfer, which play a key role in supramolecular chemistry. Electronic energy transfer process involves either radiative or non-radiative energy transfer from an excited donor molecule to an acceptor molecule.

1.3.2.1. Radiative Energy Transfer

Radiative energy transfer is two-step processes which involve the absorption of a photon by acceptor molecule (A), emitted from a Donor molecule (D) and this transfer happens when the average distance between D and A is larger than the wavelength (Figure 1.6).



- J is the normalized spectral overlap of the donor emission and acceptor absorption
- q_D is the quantum efficiency (or quantum yield) for donor emission in the absence of acceptor and is evaluated as the number of photons emitted divided by number of photons absorbed).
- η is the index of refraction (1.33 for water; 1.29 for many organic molecules).
- κ^2 is a geometric factor related to the relative orientation of the transition dipoles of the donor and acceptor and their relative orientation in space.

Figure 1.6: Photophysical mechanism of Förster Resonance Energy Transfer mechanism.

1.3.2.2. Non-radiative Energy transfer

Non-radiative energy transfer is an electrodynamic phenomenon and transfers the excitation energy by long range dipole-dipole interactions between the donor (D) and acceptor (A) fragments. Spectral overlap between the donor and acceptor allows the several vibronic transitions of the donor to be coupled with the corresponding transition of the acceptors that have same energy levels, a favourable relative orientation of the donor

Chapter 1

and acceptor dipoles and the distance between the donor and acceptor molecules (Figure 1.6). Such energy transfer processes called as resonance energy transfer process.¹⁴

1.3.3. Intramolecular Charge Transfer

This mechanism involves the transfer of an electron between electron donor and acceptor functionalities within the molecule, which eventually results an altered “push-pull” interaction in the excited state in a π -electron system.

1.4. Different kinds of Self-assembled structure

Various non-covalent interactions like H-bonding and π - π stack interactions are generally operational for the formation of an inclusion complex and induce a change in molecular conformation or movement in the participating molecules. These reversible molecular movements provide the basis for the construction of artificial molecular machine. Appropriate design of the individual host and/or guest fragment(s) helps in achieving an inclusion complex like pseudorotaxanes, rotaxanes, and catenanes,³ (Figure 1.7) where such host-guest assembly as a unit can perform function in predictable fashion. Pseudorotaxane is a supramolecular assembly, where plugs like component threads into a socket like cyclic component.¹⁵ Such system can be subjected to disassemble to form the individual free components under the influence of an external stimulus and eventually reassemble on appropriate counter stimulation. For rotaxanes, two bulky substituents are placed at both the ends of the thread and this prevents dethreading.¹⁶ Catenane is a mechanically-interlocked molecular architecture consisting of two or more interlocked macrocycles.¹⁷

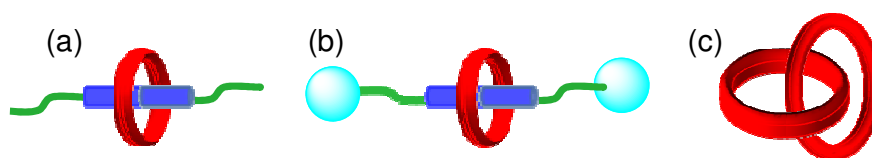


Figure 1.7: Representative structures of (a) pseudorotaxane, (b) rotaxane and (c) catenane.

1.5. Recognition of Organic Cations such as Imidazolium and Ammonium Cations: Pseudorotaxane Based Interlocked Molecules

Due to the important role of substituted ammonium and imidazolium/pyridinium ions in chemistry and in biology,^{18a,b} development of synthetic receptors for the recognition of these organic cations such as ammonium and imidazolium cations are of great interest.

Chapter 1

Studies of such recognition processes with tailored-made receptors and ammonium or imidazolium ion-based guests are expected to help in developing a better insight in unravelling the complicated multitopic recognition process in biology, which are operational through weak interaction forces like H-bonding, dipole-dipole/induced dipole interactions, and π - π stack interactions.

1.5.1. Ammonium ion binding

Pedersen was the first to report the use of different crown ether derivatives for the recognition of alkali metal cations as well as ammonium cations.^{18c} Since then, there are innumerable reports on studies with analogous host-guest assemblies. It has been argued that thermodynamic stabilities of such assemblies are favoured primarily by certain non-bonding interactions like $[C-H...O]/[C-H...N_{[NHR_1R_2]^+}]$ and $[C-H...π]/[π-π]$ interactions. Michael *et al.* reported Multiple $[-NH^+...O_{Ether}]$ H-bonding involving primary ammonium ion effects the binding and inner-sphere solvation with mono-, bi-, tri- and tetra-dentate ethers (Figure 1.8).¹⁹ Increasing stabilities of the complexes with increasing size of the cyclic crown ethers was observed in the case of cyclic polyethers due to the preorganised geometry. Molecular models show that the $-NH^+...O_{CrownEther}$ angles becomes more favourable for the larger ethers.

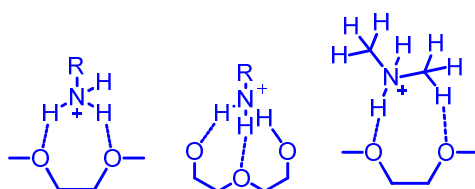


Figure 1.8: Possible modes of interaction between O_{crown} and H_{NR_2H+2} and H_{NR_3H+} .

Among three cyclic crown ether derivatives 12-crown-4, 15-crown-5 and 18-Crown-6, the highest affinity for primary ammonium ions was found for 18-Crown-6.²⁰ Ionic diameter of an ammonium ion is 286 pm which is very close to the cavity size of 18-crown-6 (260 - 320 pm). The ionic diameter of an ammonium ion is 286 pm, which is very similar to potassium ions with 266 pm. Ammonium ion prefers to bind at a tetrahedral co-ordination site while potassium ion prefers an octahedral coordination site.²⁰ Trueblood proposed that an ammonium or substituted ammonium ion is too large to fit into an 18-crown-6 ring.²¹ The relative strength of the inclusion complexes is dependent on the depth of penetration of the ammonium group into the cavity. Secondary ammonium ions prefer to bind to a larger

Chapter 1

crown ether (24-crown-8) and slips through the crown ether ring to form “pseudorotaxane” structures. Balzani *et al.* was first to use the concept of H-bonding in an inclusion phenomenon of aromatic crown ether and fluorescent ammonium ions, which gave modulation in photophysical properties after adduct formation.²² The host crown ether (DB24C8) forms pseudorotaxane with protonated 9-methylaminomethylanthracene (**1**) in CH_2Cl_2 solution. Results of the photo physical studies reveal that FRET process is operation due to an efficient energy transfer process involving the donor host (DB24C8) and the anthracene moiety as acceptor fluorophore in the guest moiety (Figure 1.9).

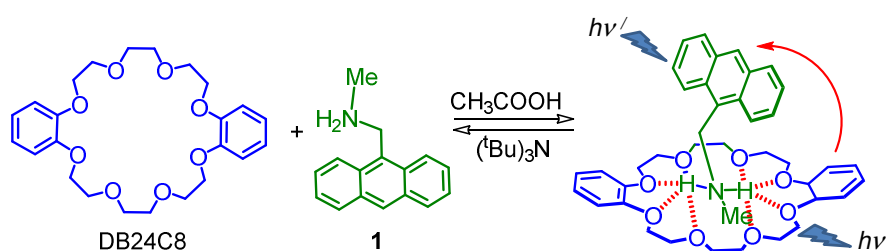


Figure 1.9: Schematic representation of the energy transfer process between DB24C8 and protonated form of 9-methylaminomethylanthracene (**1**).

A report from the same research group reveals a molecular level plug/socket system using a crown ether (**2**) derived from the binaphthyl (binap) unit and a secondary ammonium ion-based guest molecule (**3,4**) that is functionalized with an anthracenyl unit (Figure 1.10). The pseudorotaxane formation leads to an resonance energy transfer from the donor binap moiety to the acceptor anthracene moiety.²³

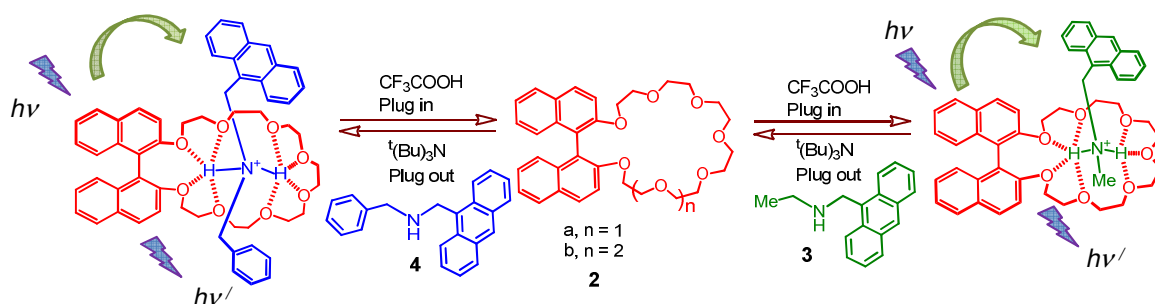


Figure 1.10: Molecular level *plug/socket* behaviour in the H-bonded pseudorotaxane between binap-crown ether (host) and anthracenyl ammonium ion (guest). (Figure is adopted from the reference Chem. Soc. Rev., 2015, 44, 663)

More recently it is demonstrated that the host-guest type complex formation between different host molecules like cucurbit[7]uril (CB[7]), β -cyclodextrin (β -CD), and dibenzo

Chapter 1

[24]crown-8 ether (DB24C8) and a triphenylamine (TPA) derivative (**5**) as the guest component (Figure 1.11).²⁴ Restriction of internal rotation of the guest molecule (**5**) on inclusion complex formation with either of these two host molecules (CB[7] or β -CD) is reflected in the enhancement of the emission quantum yield and the excited-state lifetime of the TPA moiety. The inclusion complex formation with DB24C8 as a host component offers a binding-induced FRET process with DB24C8 as the donor moiety and TPA-derivative as the acceptor fragment. MALDI-TOF Mass, ^1H NMR and 2D-NOESY experimental studies reveal a 1:3 binding stoichiometry for all binding processes. ^1H -NMR studies also reveal a cooperative binding process for CB[7], whereas statistical binding prevails for hosts like β -CD and DB24C8.

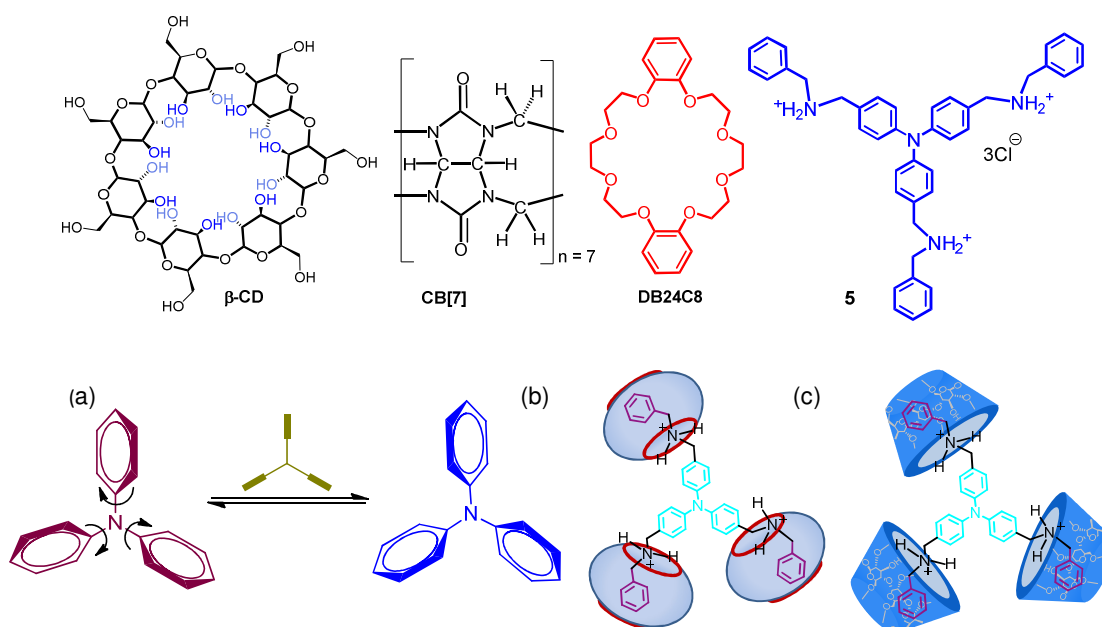


Figure 1.11: Schematic representation of different macrocyclic hosts and the guest molecules, used to study the conformational restriction through complexation, (a) Conformational change of a Triphenylamine core through internal bond rotation, Mode of complexation of **5** with (b) CB[7], (c) β -CD.

A more recent report reveals that threading phenomenon results in an interrupted PET and a fluorescence ON response, which in turn initiates a FRET-based luminescence response.²⁵ The purpose built azacrown ether moiety (**6**), used as the host, is separated from the photoactive donor unit through a $-\text{CH}_2-$ spacer, which allows the unshared pair of electrons of the tertiary N-Crown to participate effectively in PET process (Figure 1.12). On formation of an inclusion complex formation with the guest molecule (**7**), an enhancement in the pyrene based emission at 378 nm is observed due to an efficient interrupted PET

Chapter 1

process. On further addition of **7** ($[7]/[6] > 1$) to this solution, the pyrene based emission at 378 nm is found to decrease with concomitant increase in the anthracene based emission at 425 and 450 nm. This could be explicitly ascribed to an efficient FRET process (Figure 1.12). Subtle variation of the acidity in the secondary ammonium ion derivatives (**8**, **9** and **10**) and their abilities for H^+ -exchange are found to influence the efficiency of this FRET process. Reasons for such observations are also rationalized by appropriate molecular modelling studies.

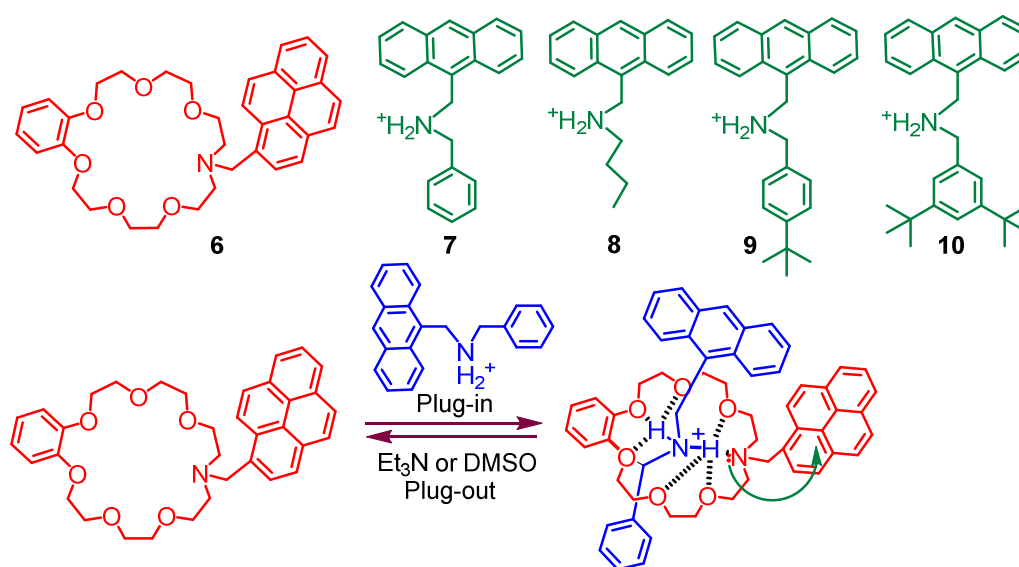


Figure 1.12: The structure of the azacrown based host and the hexafluorophosphate salt of different guest molecules with varying stopper size. Schematic illustration of the inclusion phenomena and the associated photoinduced processes.

A recent article reports formation of a trichromophoric pseudorotaxane with a two-step FRET-based of sequential energy transfer ($1 \rightarrow 2 \rightarrow 3$) along with direct energy transfer ($1 \rightarrow 3$) processes.²⁶ The crown ether-based host molecule (**11**, functionalized with naphthalene or coumarin moiety) self-assembles in a non-polar medium to form a pseudorotaxane adduct with a secondary ammonium salt (**12**, having a pyrene moiety as a fluorophore) (Figure 1.13). Results of time resolved and steady-state emission studies confirm that the sequential resonance energy transfer (FRET: naphthalene \rightarrow pyrene \rightarrow coumarin) as well as the direct resonance energy transfer (FRET: naphthalene \rightarrow coumarin) processes are operational simultaneously, where pyrene acts as a transmitter. The formation of the trichromophoric interwoven complex was confirmed by 1D and 2D 1H NMR studies. Single crystal X-ray structure for the pseudorotaxane also confirms the inclusion complex formation in solid state.

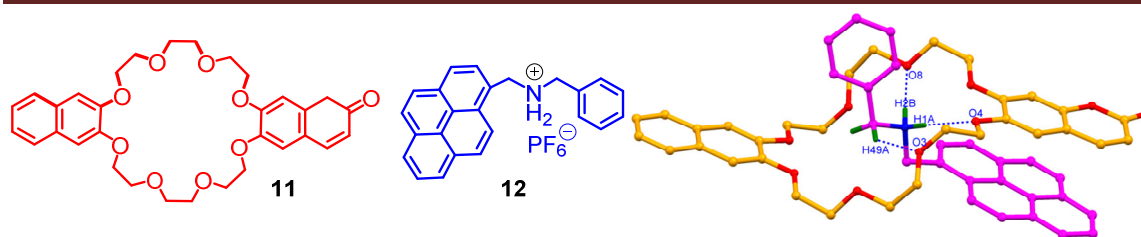


Figure 1.13: The structure of the used host and guest components. Single crystal X-ray diffraction structure of the pseudorotaxane assembly.

Macartney *et al.* first demonstrate the host-guest approach for tuning the dual emission i.e.; green to blue fluorescence of 2-aminoanthracene (**13**) on protonation with subsequent inclusion complex formation with CB[7] (Figure 1.14). The formation of a 1:1 host-guest complex between protonated 2-aminoanthracene, $\mathbf{13.H}^+$ and CB[7] is confirmed by spectroscopic techniques.²⁷ A switch in the fluorescence of $\mathbf{13.H}^+$ from green to blue is observed on formation of an inclusion complex CB[7] and this is attributed to the pronounced decrease in acidity of the excited state of $\mathbf{13.H}^+$ on formation of the inclusion complex. Interaction of the NH_3^+ protons with the portal oxygen atoms with lone pair of electrons of CB[7] accounts the observed changes its acidity in ground as well as in the excited states. Changes in the optical (UV-visible and fluorescence) spectra are primarily due to the reduction of polarity that is experienced by the guest within macrocyclic cavity, CB[7] with respect to those in the bulk.

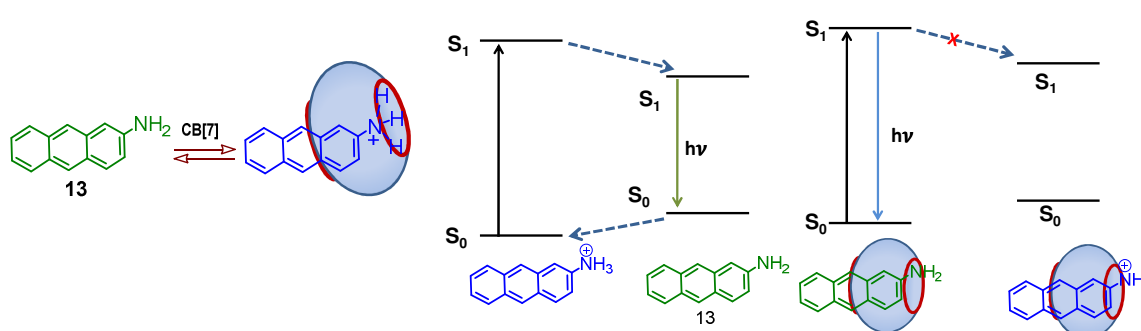


Figure 1.14: Schematic representation of the energy levels that are associated with excitation and emission spectra of $\mathbf{13.H}^+$ in absence and presence of CB[7] in acidic aqueous solution.

1.5.2. Imidazolium/pyridinium cation binding

As an effective structural unit, imidazole in its protonated and non-protonated form plays a vital role in their biological function at the active sites of various proteins. Use of imidazolium derivatives as a suitable guest for inclusion complex formation was also

Chapter 1

demonstrated with macrocyclic ligands such as crown ethers and cucurbituril as host fragments from past decades.^{28a,b} In 1979 Lehn *et al.* had shown that a chiral 1,2,10,11,19,20-hexacarboxylate-27- crown-9 derivative (**14**) formed a relatively stable (formation constant 350 M^{-1}) complex with an imidazolium ion in aqueous solutions (Figure 1.15).^{28c} Stolwijk *et al.* proposed that for the efficient binding of imidazolium ion, a ring size of at least 30 ring atoms of a crown ether (**15**) was needed (Figure 1.15).²⁹

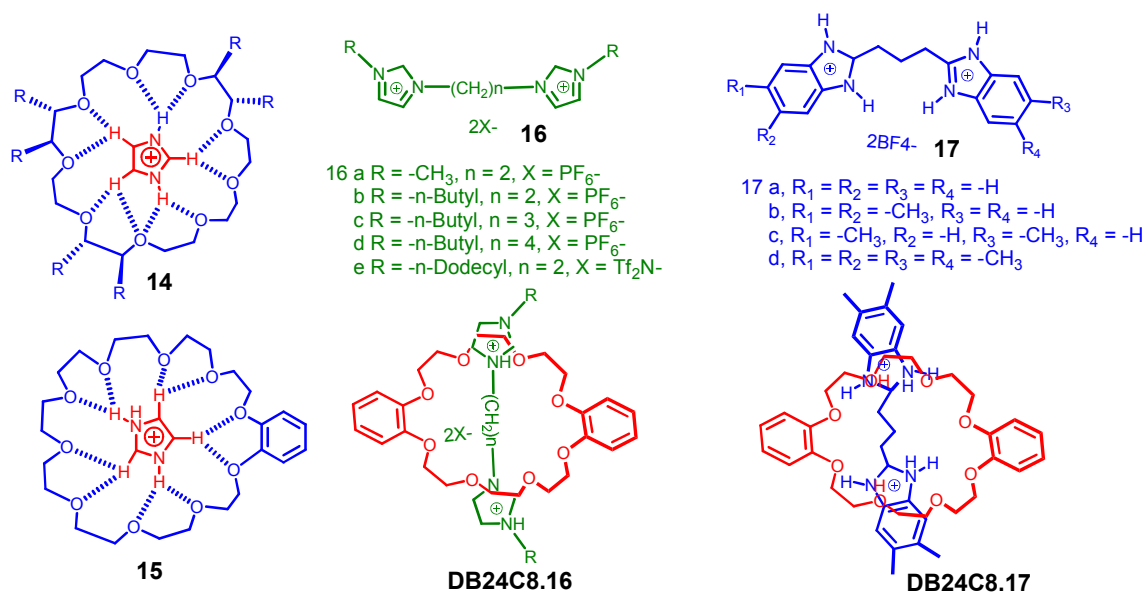


Figure 1.15: Schematic presentation of the inclusion complexes (**14**) and (**15**) crown ethers formed with imidazolium salt and the structure of the different imidazolium based guests **16,17** and their inclusion complex with DB24C8.

A report from Gibson *et al.* reveals that 1,2-Bis[N-(N'-alkylimidazolium)ethane] salts (**16**), with varying alkyl chain lengths form pseudorotaxanes with DB24C8 as a host.³⁰ The association constants for pseudorotaxane-like complex formation from 1,2-bis[N-(N'-alkylimidazolium)]ethane with DB24C8 are 24 and 30 M^{-1} in MeCN or CHCl₃, respectively (Figure 1.15). A decrease of association constant is observed with the increase in spacer length. Mukhopadhyay *et al.* have demonstrated that the threading of various bisbenzimidazolium moieties (**17**) having three methylene spacer through the macrocycle DB24C8 is influenced by the position of the aromatic methyl substituent (Figure 1.15).³¹ This report also confirms formation of pseudorotaxanes (DB24C8.16 and DB24C8.17) with similar methylene spacers and equal number of methyl substituents on the thread.

Chapter 1

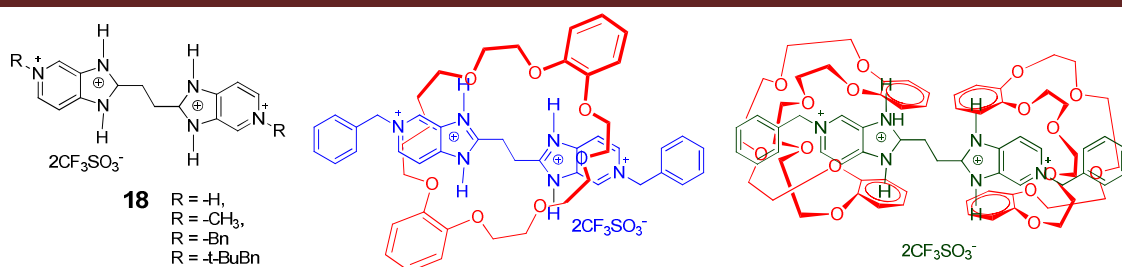


Figure 1.16: Structure of different imidazolium based guests and formation of different type of complexes between N-Functionalized 1,2-Bis(imidazopyridine-2-yl)ethane Cations and Dibenzo-24-Crown-8 Macrocycles.

Tiburcio *et al.* have reported a series of 1,2-bis(imidazopyridin-2-yl)ethane (**18**) that could fully or partially penetrate the cavity of the macrocyclic DB24C8 and result a new family of host-guest complexes.³² These new guests possess two pyridinium sites along with bis(benzimidazolium)-ethane motif. Different types of inclusion complexes are found to be formed depending upon the substituent on the pyridinium moiety (Figure 1.16). For a linear guest with a benzyl substituent, a [2]pseudorotaxane geometry involving the bis(benzimidazolium)ethane motif is formed, partially threaded complexes with two crown ethers near each of the pyridinium sites are formed with methyl group as the substituent.

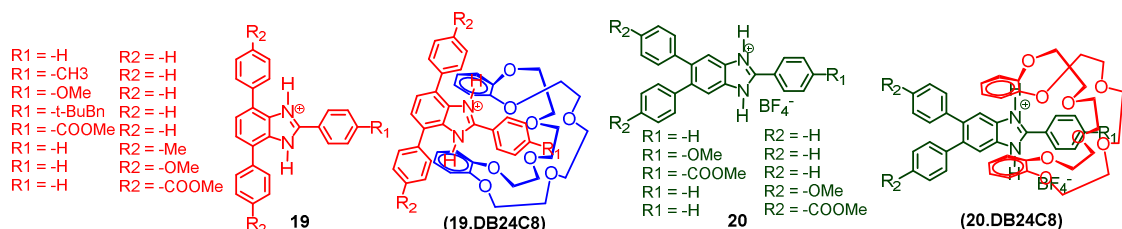


Figure 1.17: Structure of different imidazolium based T and Y shaped guests and their inclusion complexes with Dibenzo-24-Crown-8 Macrocycles.

[2]pseudorotaxanes is reported by using T-shaped axles (**19**) having a benzimidazolium core and different [24]crown-8 ether derivatives (([24]crown-8, dibenzo[24]crown-8, and dinaphtho[24]crown-8) as wheels.³³ Experimental results reveal that T-shape of the benzimidazolium cation forms stronger association between axle and crown ether wheel (Figure 1.17). It is demonstrated that despite weak interaction between dibenzo[24]crown-8 (DB24C8) and imidazolium ($K_a = 8 \text{ M}^{-1}$) or phenylbenzimidazolium ($K_a = 54 \text{ M}^{-1}$) cation, presence of an extra phenyl substituent on the T-shaped cations helps in achieving a much higher association constant ($1.78 \times 10^3 \text{ M}^{-1}$ for the parent T-shaped axle).

Chapter 1

Same research group have also shown that the Y-shape of the axle (**20**) effectively enhances the association between axle and wheel when compared to simple imidazolium cations (Figure 1.17).³⁴ Presence of the electron-donating -OMe group effectively decreases the possibility the H-bonding, ion–dipole, and π -stacking interactions by lowering the acidity of hydrogen bond donors as well as the charge on the imidazolium rings and these have a clear bearing in lowering the association constant.

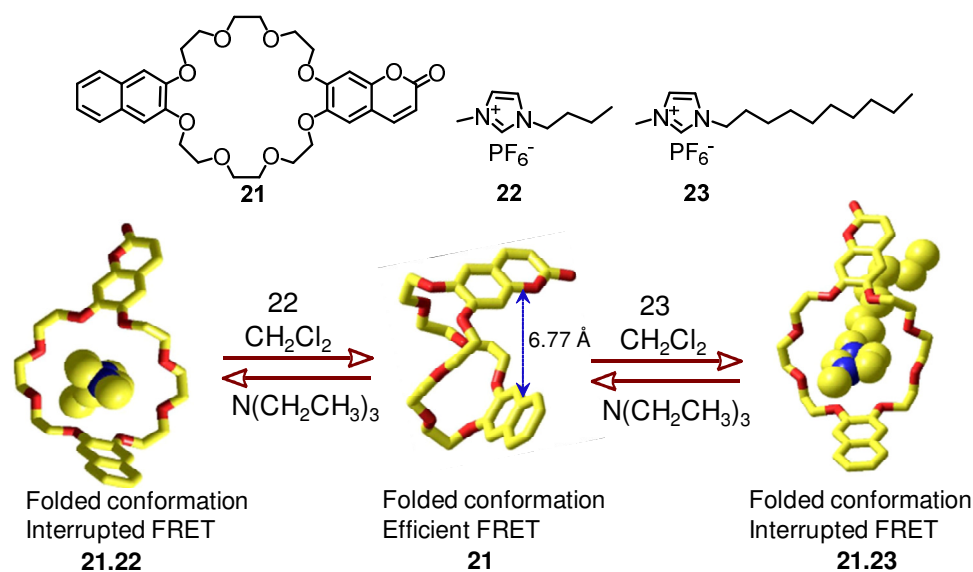


Figure 1.18: The structure of the host **21** and its reversible complexation with **22** and **23**. (Figure is adopted from the reference Chem. Soc. Rev., 2015, 44, 663)

Recently das et. al. have shown that for a donor-acceptor assembly, imidazolium ion could induce a folding-unfolding movement in an appropriately functionalized dibenzo crown ether moiety with resulting tuning of resonance energy transfer process.³⁵ A new dibenzo[24]crown-8 derivative (**21**) functionalized with naphthalene and coumarin units is found to adopt a folded conformation (Figure 1.18). Steady-state and time-resolved fluorescence studies (resonance energy transfer between the donor naphthalene moiety and acceptor coumarin fragment), NMR spectra and computational studies support a folded conformation for the crown ether moiety in solution phase. This crown ether derivative is found to form a [2]pseudorotaxane complex with imidazoliumion derivatives as the guest molecule (**22** and **23**) having varying alkyl chain lengths. Experimental results confirm that [2]pseudorotaxane adopts an open conformation and this accounts for an increase of the effective distance between the naphthalene and coumarin moieties as well as the decrease / interruption of the FRET based energy transfer, which was otherwise

Chapter 1

operational between two naphthalene and coumarin in the folded conformation. This changes in luminescence help in monitoring the relative conformational changes. This is further corroborated by computational, $^1\text{H NMR}$ and single crystal X-ray structural studies.

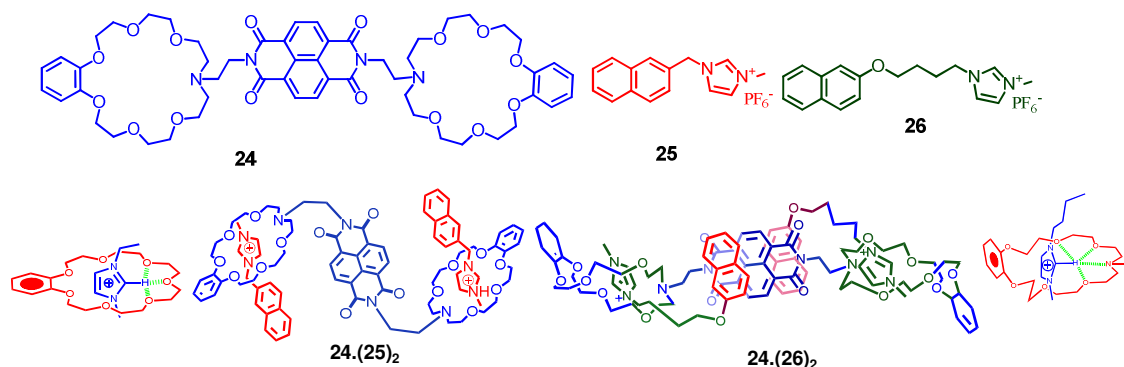


Figure 1.19: The structure of the divalent host (**24**) and the two guest molecules (**25**) and (**26**) and schematic presentation of the [3]pseudorotaxane **24.(25)₂** and **24.(26)₂** in CH_2Cl_2 .

A recent report reveals that on the basis of the length of the covalent linker in an imidazolium derivative, corresponding [3]pseudorotaxane adducts adopt different conformation or orientation.³⁶ A bis-azacrown ether moiety (**24**) functionalized with naphthalene diimide functionality is used for this study. Naphthalene diimide is well known to show a strong π - π interaction with aromatic ring like naphthalene (Figure 1.19) and such an interaction is exploited for studying the receptor-analyte interaction with two Naphthalene diimide derivatives (**25**) and (**26**) with varying spacer lengths. A perpendicular orientation for two imidazolium ion derivative with shorter spacer for the formation of a 1:2 complex (**24.(25)₂**, Figure 1.19) is observed. While a parallel orientation of the two imidazolium ion derivative having longer spacer is observed for the complexation of **24.(26)₂**. The longer spacer allows a better flexibility to adopt a favourable orientation with more efficient π - π stacking interactions. The mechanism for the naphthalene-based luminescence quenching by NDI fragment on [3]pseudorotaxane formation is attributed to a static as well as dynamic quenching—static quenching being the prominent one.

1.5.3. Multivalency based pseudorotaxane

The word Multivalency, as defined by Mulder et al. is *binding of two (or more) entities that involves the simultaneous interaction between multiple, complementary functionalities on these entities* (Figure 1.4).^{37a} The valency of any host or guest fragment is the number of

Chapter 1

separate but similar connections that each of these fragment can form through host-guest interactions with entities bearing the complementary functionality.

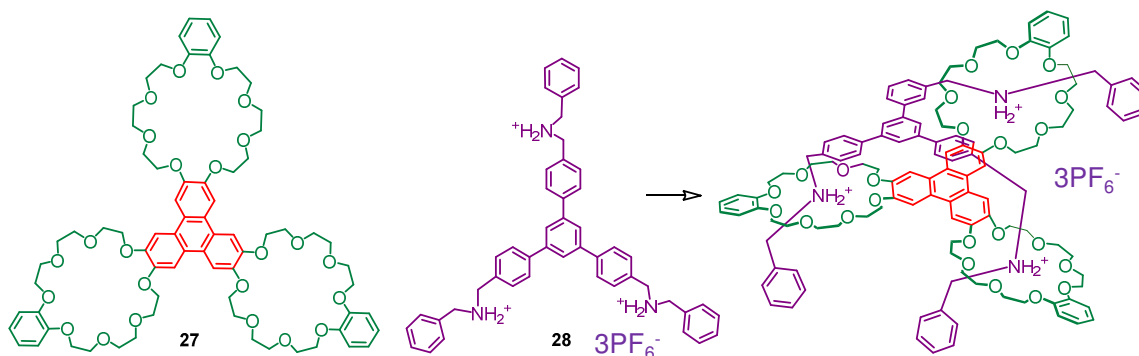


Figure 1.20: Self-assembly of a tritopic receptor **27** with a trication **28**.

To get a better fundamental understanding of the nature of multivalency, Balzani *et al.* have reported studies with a tritopic receptor (**27**)^{37b} in which three benzo[24]crown-8 macro rings are fused onto a triphenylene core and a trifurcated trication wherein three dibenzylammonium ions are linked to 1, 3 and 5 positions of a central benzenoid core (**28**). Host-guest complexation leads to a 1:1 adduct formation which constitutes a triply-threaded, two-component supramolecular bundle (Figure 1.20). In addition to [N⁺H...O] H-bonding and [C-H...O] interactions between the NH₂⁺ centres on the three dibenzylammonium ion containing arms of the trication and the three crown ether rings in the tritopic receptor, there is a stabilizing π - π stacking interaction between the two aromatic cores. Mass spectrometry and ¹H NMR spectroscopy, X-Ray crystallography has confirmed the integrity of the 1:1 adduct in acetonitrile solution. Interestingly, the supramolecular interactions and the dethreading as well as the rethreading processes associated with the 1:1 adduct could be controlled quantitatively by addition of external chemical stimuli (acid and base).

Further Schalley *et al.* reported homo- and hetero divalent crown-ammonium pseudorotaxanes with different spacers connecting the two axle ammonium (**29-32**) binding sites.³⁸ They reported that shortest spacer exhibits a chelate cooperativity much stronger with respect to that of the longer spacers for homo divalent pseudorotaxanes. With a similar series of heterodivalent pseudorotaxanes, the variation in spacer length illustrates that the shortest spacer causes a strained transition structure and consequently disfavours the second binding event. The longer spacers for hetero-divalent pseudorotaxanes reduces the enthalpic strain in the transition state than the shortest

Chapter 1

member of the series. The flexibility of the longer spacers accounts for a more unfavourable situation for the second binding event (Figure 1.21).

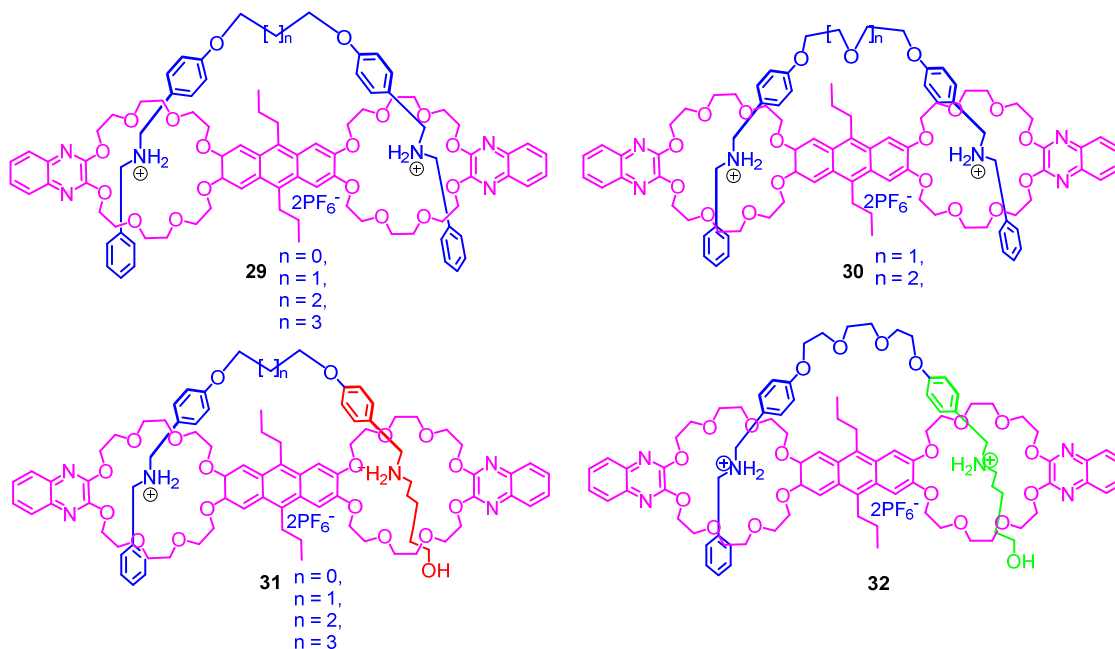


Figure 1.21: Structure of the various pseudorotaxane formed from divalent crown ether with divalent guest with varying spacer length where chelate cooperativity and spacer length of the guest drive the complexation process.

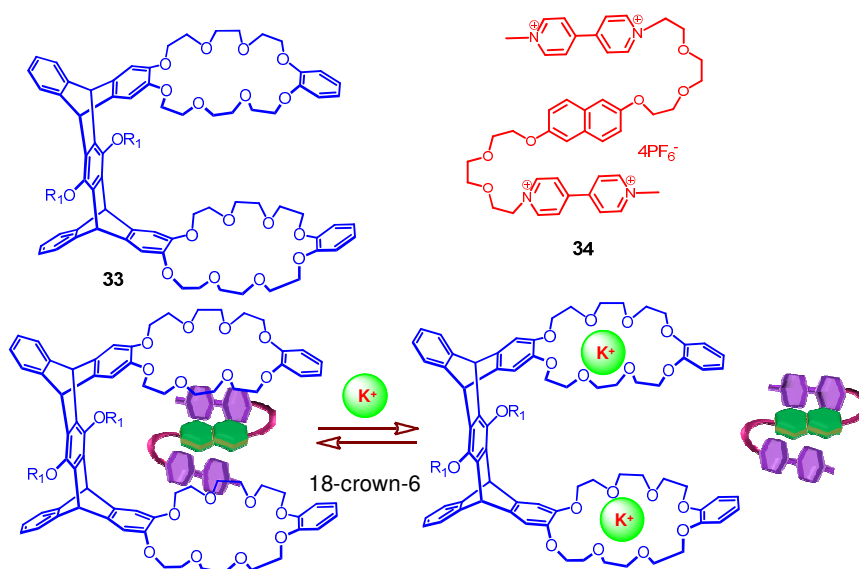


Figure 1.22: The structure of the host **33** and the guest molecule **34**. Schematic description of the K⁺ ion-controlled switchable complexation

Chapter 1

Chen *et al.* has reported a new guest **34** that participates in the self-folding process. The pentiptycene-based tweezer-like crown ether host **33** forms a 1:1 stable complexes with appropriate guests in solution (Figure 1.22).³⁹ π - π interactions between electron deficient bipyridinium ring and an electron-rich naphthalene moiety and this favours the formation of a 'S' conformation. Multiple C-H...F H-bonding interactions between the protons of the bipyridinium rings of the guests and PF_6^- has presumably played an important role in formation of the self-folding structure of the guest as well. Additionally, it was found that the binding and release of the guests in the inclusion complexes could be controlled by potassium ions (Figure 1.22).

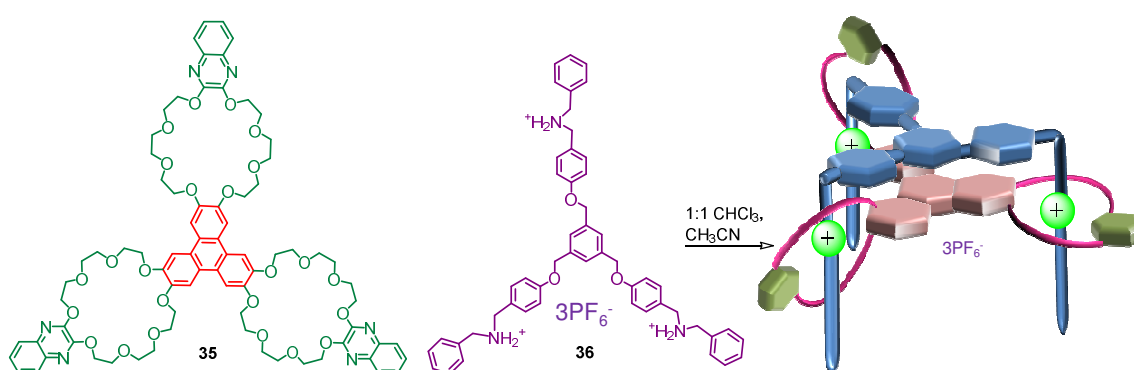


Figure 1.23: Pseudorotaxane formed from crown ether **35** with trivalent ammonium ion (**36**) containing guest.

More recently Schalley and co-workers have shown that for a multivalent system, binding strength is dependent not only on the number of binding sites but their preorganized arrangement.⁴⁰ A detailed thermodynamic analysis of the axle-wheel binding in di- and trivalent secondary ammonium as axel and [24]crown-8 derivative as wheel for formation of pseudorotaxanes (**35** and **36**) is discussed. Binding of ammonium ion-crown ether based pseudorotaxanes is enthalpy-driven and all binding entropies are negative, indicating higher order upon pseudorotaxane formation (Figure 1.23). A good geometric fit of axle and wheel and favourable spacer-spacer interactions between the two spacers are the keypoint of positive chelate cooperativity, which is important for the optimal design of multivalent pseudorotaxanes.

Hecht *et al.* has reported a pseudo[2]rotaxane assembly that is derived from a divalent crown ether as host (**37**) and a divalent photochromic azobenzene as guest (**38**).⁴¹ Photoinduced cis-trans isomerization of the azobenzene unit on irradiation with light having appropriate wavelength range of 330-380 nm is exploited for achieving the assembly and

Chapter 1

disassembly of the host-guest complex (Figure 1.24). Cis form could form inclusion complex with crown **37**. A very strong binding with an unusually high association constant ($K_a = 2.0 \times 10^5 \text{ M}^{-1}$) is observed. π - π stacking interaction of the electron deficient azobenzene and the electron-rich anthracene cores has contributed favourably for this strong binding. Interestingly, inclusion complex formation further inhibits the photoisomerization of E to Z isomer.

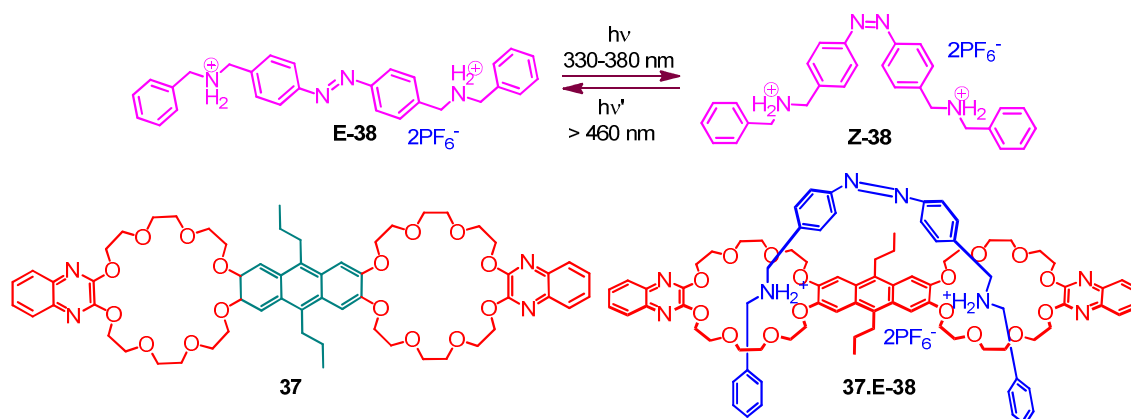


Figure 1.24: The photoinduced cis/trans isomerisation of azobenzene unit of **38**. Pseudorotaxane formed from crown ether **37** with E-**38** guest.

1.5.4. Self-sorting based pseudorotaxane

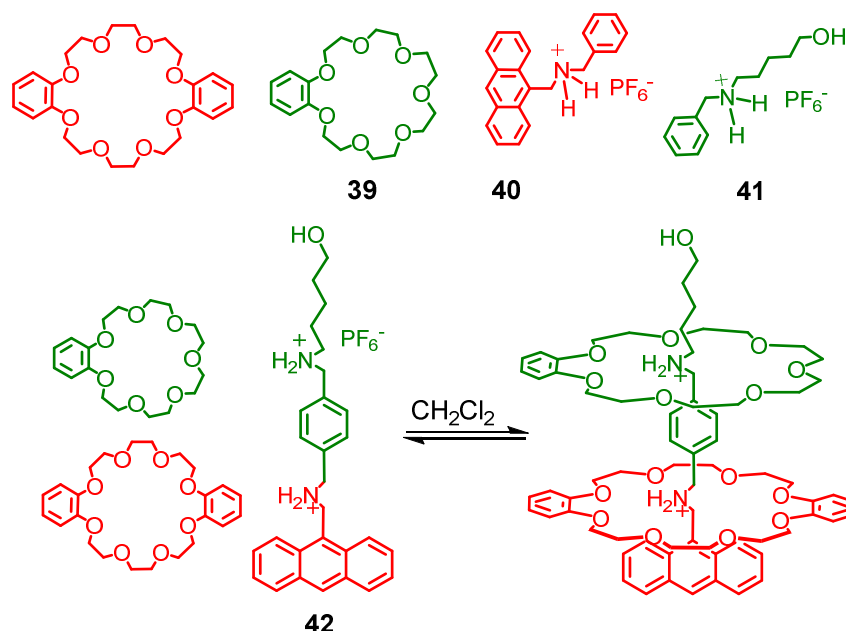


Figure 1.25: Structures of **39,40,41,42** and DB24C8. Hetero[3]pseudorotaxane formed from crown ether **39**, DB24C8 with divalent ammonium ion (**42**) containing guest.

Chapter 1

Different molecules or molecular aggregates can assemble themselves with respective recognition units following the self-sorting phenomena and offer a critical ability to distinguish between different recognition units even in a complex mixture.⁴² A variety of supramolecular systems have been explored, such as self-sorting behaviour of small molecules or self-organization of nano-structures leading to supramolecular materials.⁴³ Schalley *et al.* has demonstrated the concept of integrative self-sorting using ammonium ion based axel or thread for developing a hetero[3]pseudorotaxane system.⁴⁴

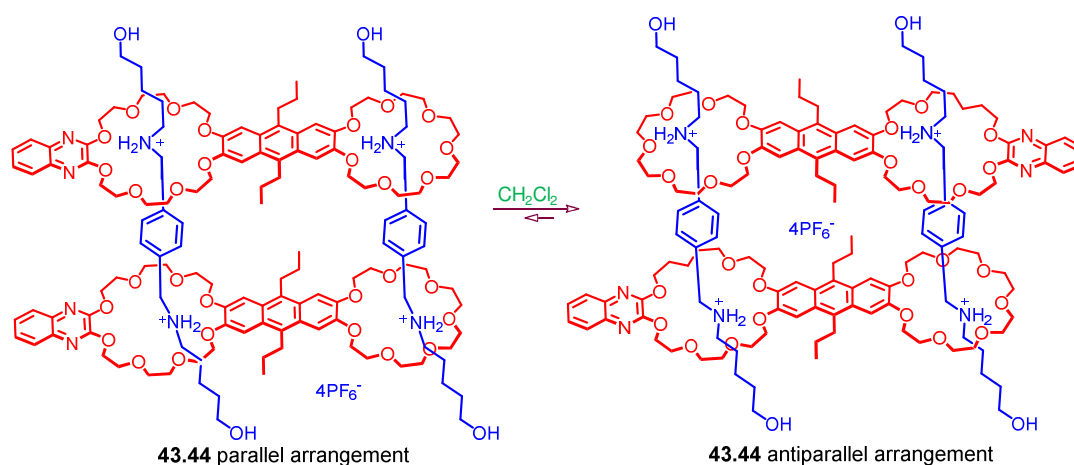


Figure 1.26: Self-assembly of [4]pseudorotaxanes including **43** and **44**. The equilibrium of [4]pseudorotaxanes is shifted far to the antiparallel crown ether arrangement.

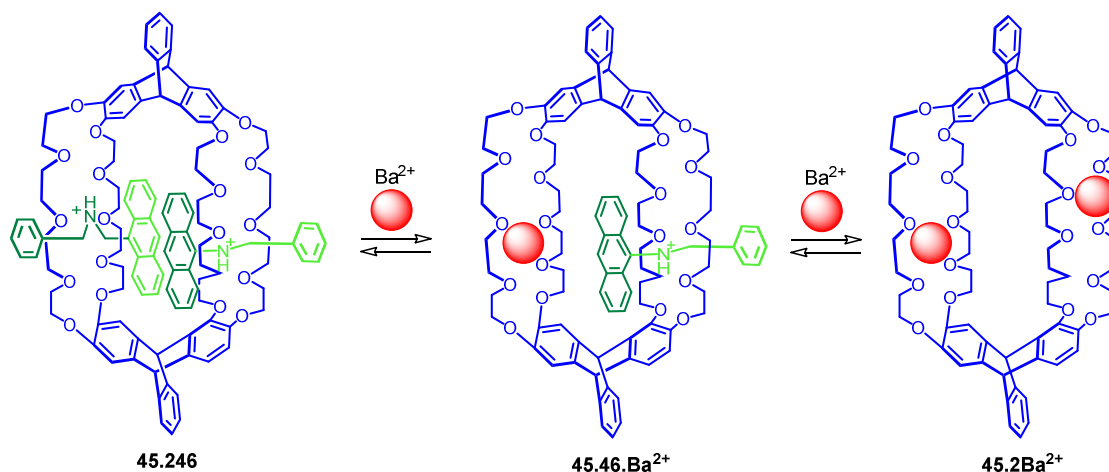


Figure 1.27: Graphic representation of the displacement of guest **46** from **45** by Ba²⁺ ion.

They designed a four component self-sorting system (DB24C8, **39**, **40**, **41**) on the basis of literature reports where the association constant for DB24C8.**40**, **39**.**41** are found to be more stable than DB24C8.**41** and **39**.**40**. A phenyl and an anthracene group are an

Chapter 1

efficient stopper for Crown-7 and Crown-8, respectively. Using this steric constrain as well as the differences in the binding affinities, the integrative self-sorting phenomenon is demonstrated by combining two axes **40** and **41** to form a divalent counterpart **42**. In non-polar solvents, for an equimolar mixture of DB24C8, **39** and **42**, phenyl part is occupied by Crown-7 and anthracene group is occupied by Crown-8 due to their complementary nature and the respective high binding constant (Figure 1.25). Thus, irrespective of the mixing order of the three components, integrative self-sorting of crown ethers by their corresponding binding sites has been achieved and established by detailed NMR as well as mass spectra studies.

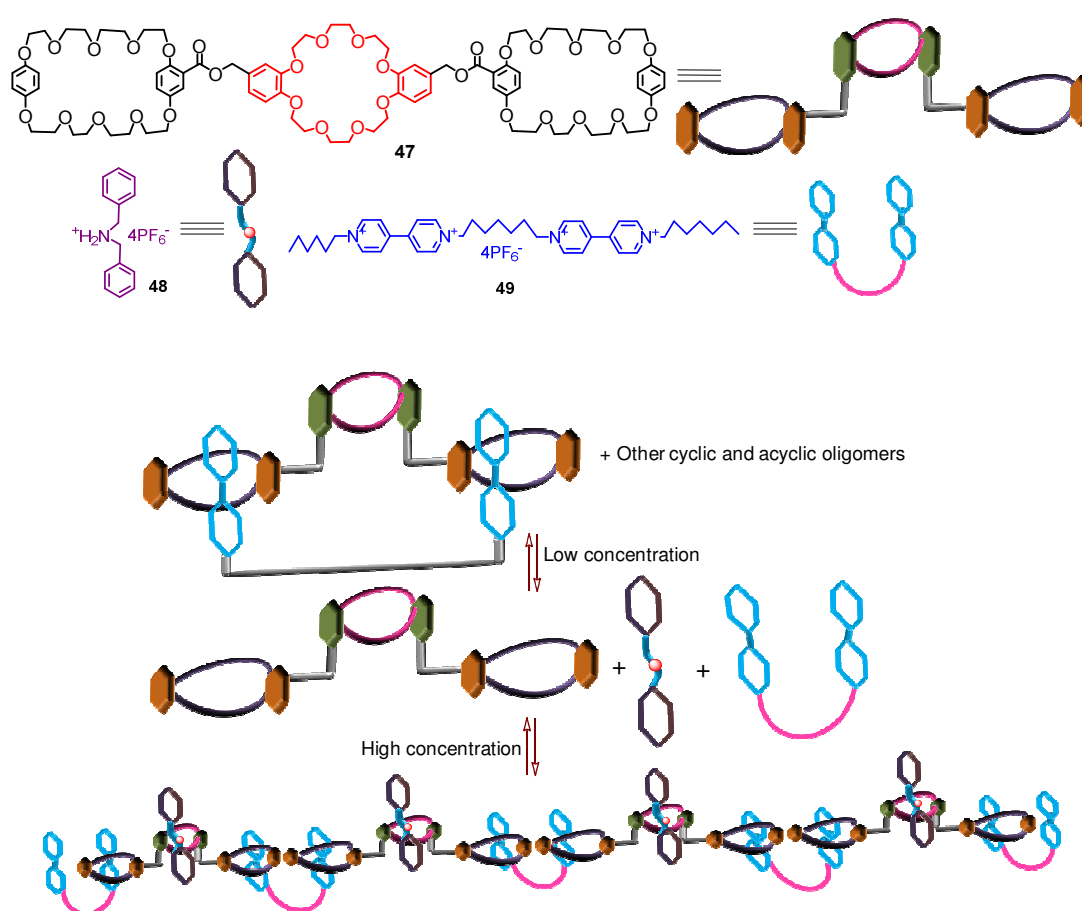


Figure 1.28: Schematic representation of the construction of supramolecular polypseudorotaxanes crown **47** with guests **48** and **49**.

Schalley and coworkers have also reported a self-assembled [4]pseudorotaxanes using orthogonal crown ether-secondary ammonium ion binding motifs (Figure 1.26).⁴⁵ They have designed a new crown ether derivative (**43**) that has two crown ether-based

Chapter 1

macrocyclic cavities with different cavity sizes. One of the reasons for the predominant formation of anti-parallel arrangement is due to favourable alignment of dipoles of the two crown ether dimers.

Triptycene-based macrotricyclic host having two dibenzo-30-crown-10 moieties (**45**) is used to form a stable 1:2 complex with (9-anthracylmethyl)benzylammonium salt (**46**) in both solution and solid state (Figure 1.27).⁴⁶ They showed that in the inclusion complexes derived from 9-anthracyl derivatives are selectively positioned inside the cavity of the host. The association and disassociation of complex could be controlled by external stimuli (acid and base). Further studies also reveal that Ba^{2+} ion could considerably replace (9-anthracylmethyl)benzylammonium salt, which might thus be utilized as a selective supramolecular fluorescence probe for Ba^{2+} ion.

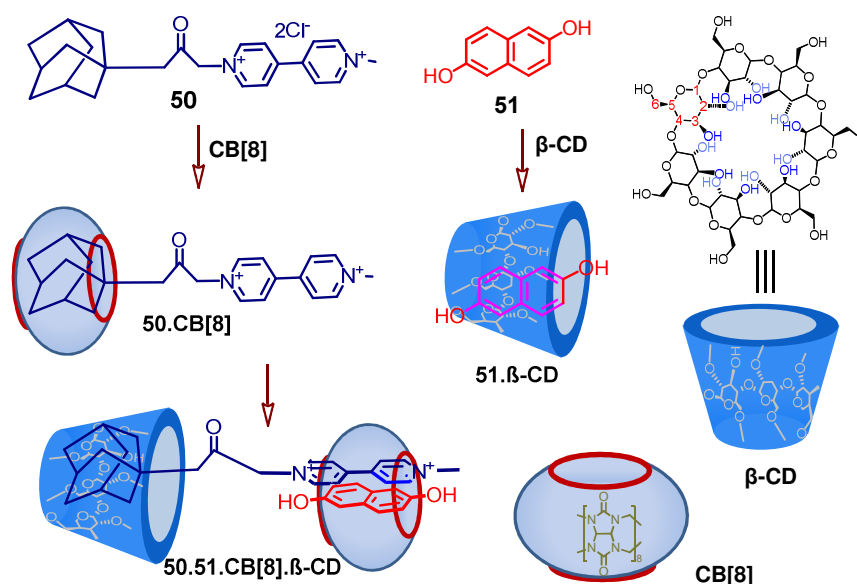


Figure 1.29: The structure of **50** and its ternary complex formed with **51** in presence of $\beta\text{-CD}$ and $\text{CB}[8]$.

Huang *et al.* has reported a linear main-chain polypseudorotaxanes with supramolecular polymer backbones using the self-sorting phenomenon (Figure 1.28).⁴⁷ Earlier report reveals that the bis(*p*-phenylene)-34-crown-10 moiety exclusively binds to the paraquat moiety while dibenzo-24-crown-8 (DB24C8) unit preferentially complexes the dibenzylammonium salt (DBA) unit in solution. They took the advantage of selective binding phenomenon of paraquat and ammonium ions towards respective crown ethers for

developing such polypseudorotaxanes. This linear supramolecular polypseudorotaxanes structures proved with the help of ^1H NMR, NOESY, UV-Vis spectroscopy, and SEM.

Liu et al. has reported a hetero-wheel [3]pseudorotaxane (**50.51**CB[8]. β -CD), which is achieved by integrating two binary inclusion complexes of β -CD with hydroxynaphthalene (**51**) and CB[8] with viologen derivative (**50**), in which the driving forces came from simultaneous molecular recognition of adamantane by β -CD and the CT interaction of **51** with the viologen nucleus of **50** in the cavity of CB[8].⁴⁸ This is a nice demonstration of the bottom-up approach for the formation of a quaternary complex as a result of guest exchange during complexation through self-sorting process (Figure 1.29).

1.6. Chiral recognition on self-assembled systems

The chirality of biological systems in the natural world has generated tremendous research interests in chiral organic molecules and studies on enantioselective recognition of chiral compounds has grown exponentially in recent past. Chiral amines and amino acids are abundant in nature and are form the basic building blocks of many biologically useful molecules. Chiral amines and amino acids also find use in many pharmaceutical preparations.

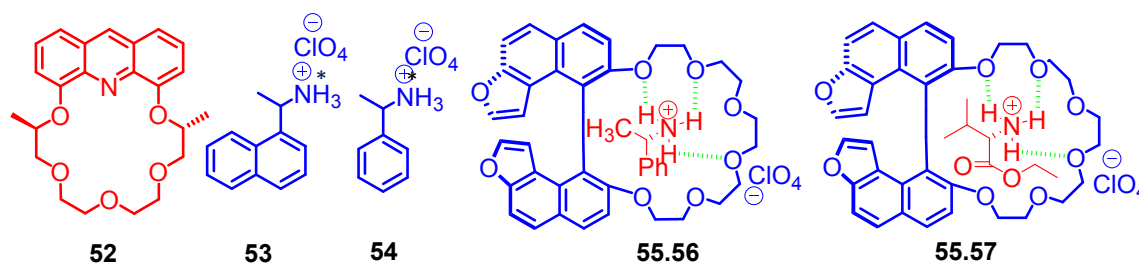


Figure 1.30: Proposed structure for complex (*R*)-(-)-**55** and (*S*)-(-)-phenylethylamine **57** and (*S*)-(+)-ethyl ester of valine **56**.

Prodi *et al.* have shown that a chiral acridino-18-crown-6 (**52**) is able to bind to organic ammonium salts (**53** and **54**) in acetonitrile with high affinity, causing pronounced changes in the luminescence properties.⁴⁹ Studies reveal that enantiomerically pure chiral macrocyclic ligand **52** shows a high enantioselectivity towards chiral organic ammonium ions with an important contribution from the π - π interaction between the chromophoric groups of the ammonium ion and the acridine unit (Figure 1.30). The possibility of monitoring the enantiomeric recognition process by means of photoluminescence

Chapter 1

spectroscopy can gain ground for the design of very efficient enantioselective chemosensors for chiral species.

Karnik *et al.* have shown that a furo-fused BINOL based chiral crown (**55**) can act as an enantioselective chiral sensor for phenylethylamine and ethyl ester of valine (**56**) (Figure 1.30).⁵⁰ Difference in fluorescence enhancements are observed when this chiral crown binds to two different enantiomers. For phenylethylamine and ethyl ester derivatives such *observed enhancements are 2.97 and 2.55 times, respectively. This enantioselectivity was attributed to the presence of a furan ring at sterically the most crucial position of BINOL.* The fluorescence studies with perchlorate salts of **56** and **57** reveal that H-bonding interactions between the lone pair of electrons on the oxygen and the quaternized nitrogen group of phenylethylamine are responsible for the fluorescence enhancement. It has been argued that the steric repulsion between the methyl group of the phenylethylamine and the ethylene oxy units of the crown is different for two diastereomeric complex.

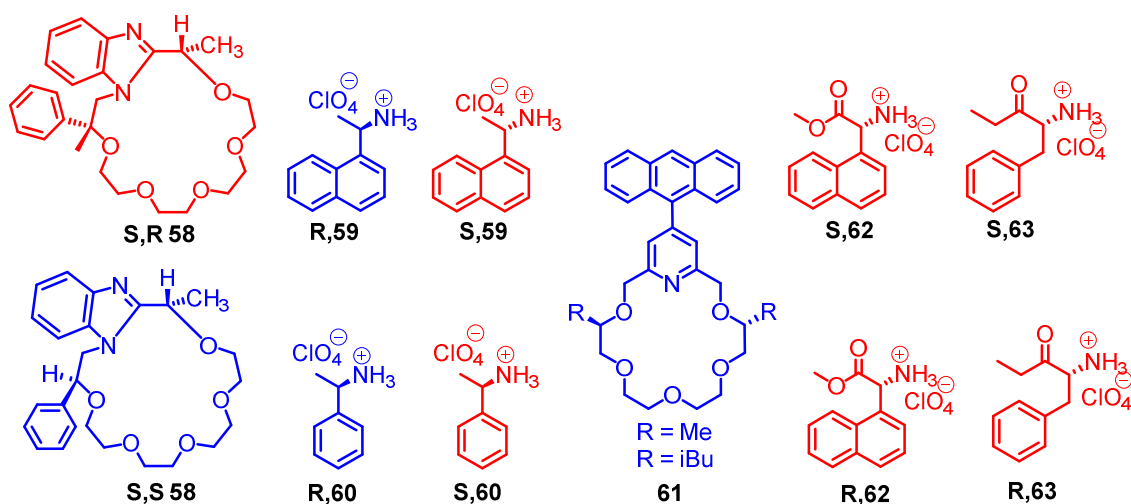


Figure 1.31: Structures of monoaza-[15]crown-5 (S,R)-**58** and (S,S)-**58** and the structures of R and S enantiomers of guests **59** and **60**, which were studied for chiral recognition. Structures of pyridino-18-crown-6 ether-based molecule **61** and optically active primary ammonium salts (**59-63**) used in the enantiomeric recognition studies.

The same research group has reported diastereomeric monoaza-[18]crown-6 compounds (S,R)-**58** and (S,S)-**58** with an additional chiral centre having a phenyl ring.⁵¹ Enantiomeric recognition of ammonium salts is attributed to an additional substituent in the form of a phenyl ring near the benzimidazole unit, as it expected to offer steric repulsion to the guests and presumably enhance the selectivity factor between the enantiomeric guests (Figure 1.31). The preferential binding to one of the two enantiomers ((S,R)-**58** and (S,S)-

Chapter 1

58) with respective organic ammonium salt (**59**, **60**) is evaluated qualitatively by ^1H NMR and circular dichroism (CD) spectroscopy and quantitatively by fluorescence spectroscopy.

Huszthy *et al.* has reported a pyridino-18-crown-6 ether-based (**61**) molecule that is functionalized with an anthracene as the fluorophore unit.⁵² The macrocyclic molecule shows appreciable preference towards an specific enantiomer of 1-phenylethylamine hydrogen perchlorate (PhEt), 1-(1-naphthyl)ethylamine hydrogen perchlorate (NapEt), phenylglycine methyl ester hydrogen (Figure 1.31).

Nau *et al.* has developed a method based on self-assembled, achiral host-dye pairs which form inclusion complex with water-soluble chiral analytes and binding process is examined through ICD effects in the preferred near-UV or visible range (Figure 1.32).⁵³ This method have an opportunity for chiral detection using an achiral host CB[8] and achiral dyes as auxiliary chromophores. Ternary complexes formation is studied using a macrocyclic host CB[8], dicationic dyes, and chiral aromatic analytes (Figure 1.32).

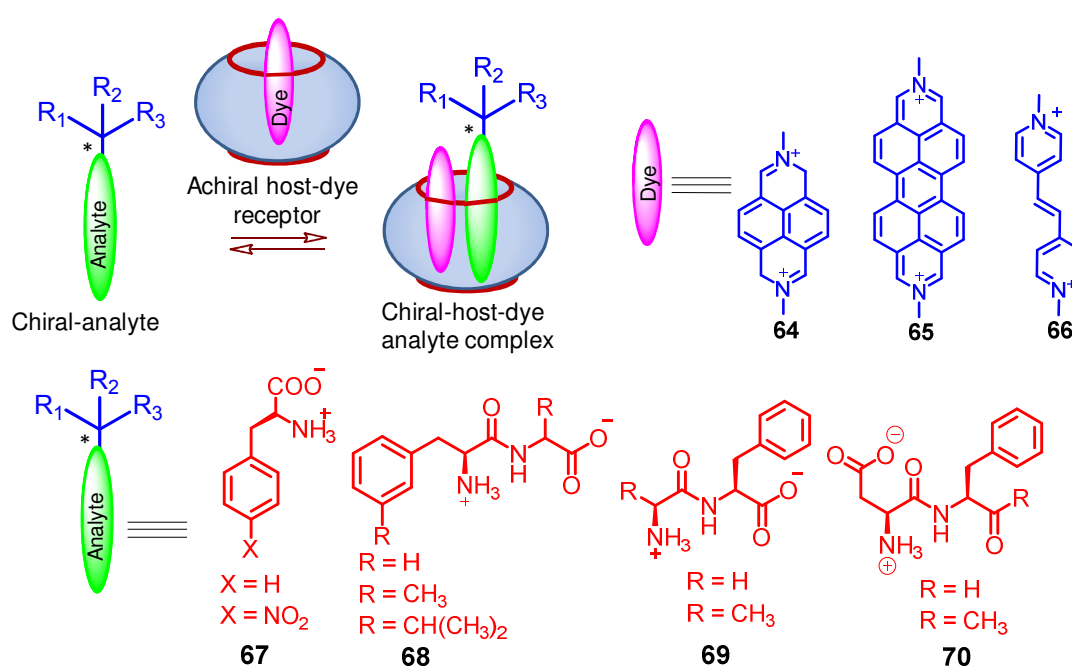


Figure 1.32: The complexation of chiral analytes by a self-assembled, achiral host-dye receptor. Chemical structures of the investigated chiral analytes and schematic representations of the macrocyclic host CB8 and the dyes.

It has been argued that such recognition process could be extended for studies for the sequence recognition of peptides and drug-related analytical applications.

1.7. Logic gates on self-assembled systems

Digital electronics is so widely used in everyday life that it is almost impossible to find an electronic device that does not make use of digital electronic components. Logic gates are basic elements processing information: they function as switches whose output (0 or 1) depends on input conditions. Now a day's all common logic operations can be mimicked with molecular devices based on chemical approaches.

The first example of a molecular logic gate is demonstrated by de Silva in 1993 for mimicking an AND function.⁵⁴ De Silva and co-workers have reported a molecule **71** that could show a combination of two YES operators (blocking of PET upon input recognition), with an associated fluorescence output. This molecule is composed of an anthracene chromophore, which is linked to two receptor units. PET process is operational for the receptor moiety **71** and this accounts for the luminescence quenching of the anthracene moiety and poor emission quantum yield. Amine (receptor1) and dialkoxybenzene (receptor2), can accommodate H^+ and Na^+ (Figure 1.33), respectively.

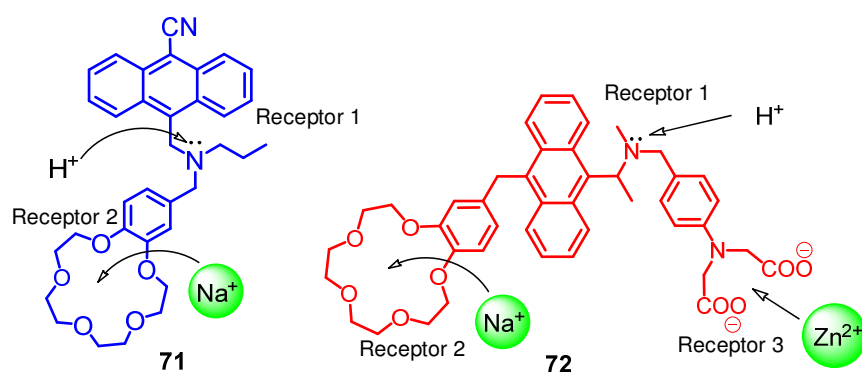


Figure 1.33: First molecular logic gate **71**, mimicking an AND operation and three-input molecular logic AND gate for molecule **72**.

This results luminescence responses that could be correlated for AND operation. Subsequently, the same group has shown that another molecule **72** serves three-input molecular logic AND gate (Figure 1.33).⁵⁵ This molecule delivers the highest fluorescence output, when all three receptors are occupied with their respective inputs, (sodium ions, protons and zinc ions).

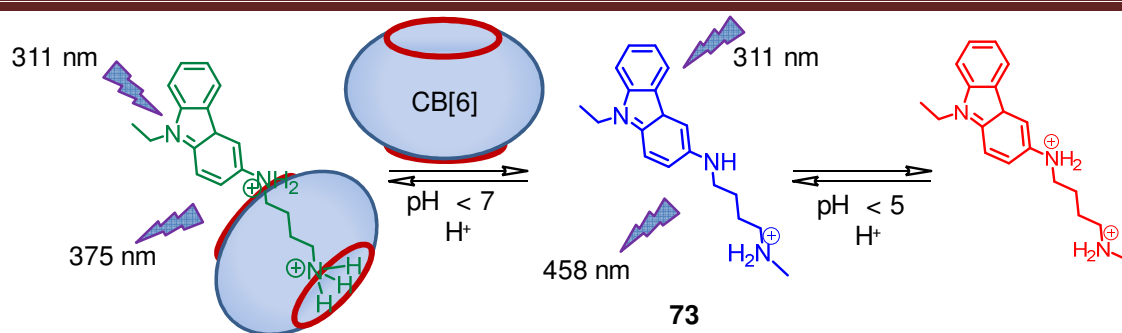


Figure 1.34: Fluorescence switching through host CB[6]-assisted guest **73** protonation giving molecular logic operation.

Nau and co-workers has reported a carbazole derivative with amino substitution in 3-position form host–guest complexes with CB[6] via complexation of derivatives of 1,4-diaminobutane.⁵⁶ Studies reveal that fluorescence of **73**, a carbazole derivative is pH sensitive. At acidic pH (pH < 5), the weaker locally excited band ($\lambda_{\text{Max}} = 375 \text{ nm}$) predominates. While at neutral pH, a band near 458 nm is observed and this is attributed to the charge transfer type electronic transition of the unprotonated anilino nitrogen. Inclusion complex formation of **73** with CB[6] promotes protonation at neutral pH values and decreases the fluorescence intensity of red-shifted ICT-related emission (458 nm). This also increases locally-excited state emission at 375 nm (Figure 1.34). Change of fluorescence behaviour upon addition of the macrocycle, CB[6] is attributed to the selective formation of an inclusion complex with the aminoalkyl anchor of the dye **73**, which has a substantially higher affinity than the carbazole chromophore. This distinct emission response system demonstrates several optical output channels.

Tian and co-workers have reported a self-assembly composed of a thread **74** with two photoisomerizable fragments (an azobenzene and a stilbene unit), fluorescent 1,8-naphthalimide stoppers, and a cyclodextrin (α -CD) macrocycle.⁵⁷ Using different irradiation wavelengths as inputs (313 nm, E to Z conversion of the stilbene unit, 380 nm, E to Z conversion of the azobenzene unit) and changes of UV absorbance and fluorescence as outputs AND and XOR logic gate is constructed (Figure 1.35).

More recently four groups have independently used a divalent luminescent crown ether based **75** as host and different paraquat derivatives (**76** and **77**) as guests for generation of reversible [3](taco complex) in nonpolar solvent (Figure 1.36).⁵⁸ Flexible host molecule forms [3](taco complex) and adopts a folded shape during binding, wherein the two

Chapter 1

paraquat units are sandwiched between the two aromatic units of the folded crown ether fragment of **75**.

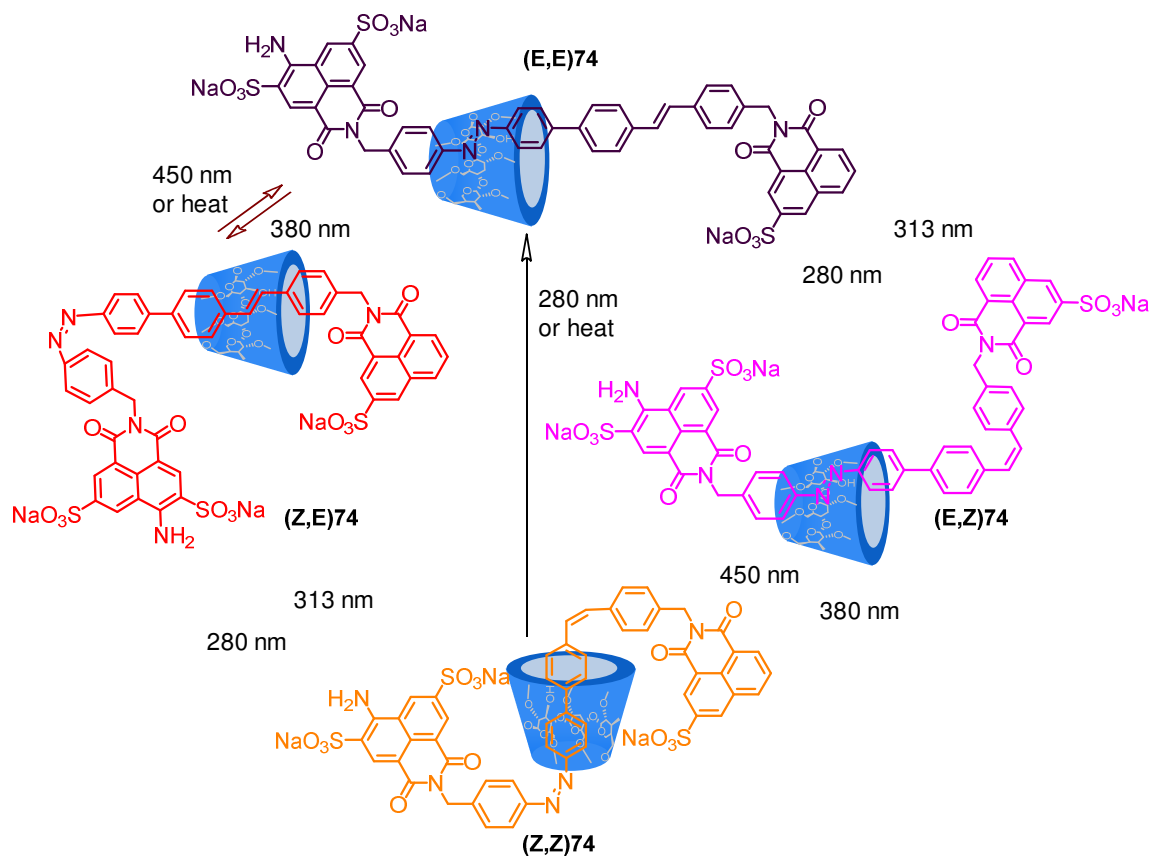


Figure 1.35: Photoisomerization processes of dyad **74** and corresponding position of the α -CD macrocycle.

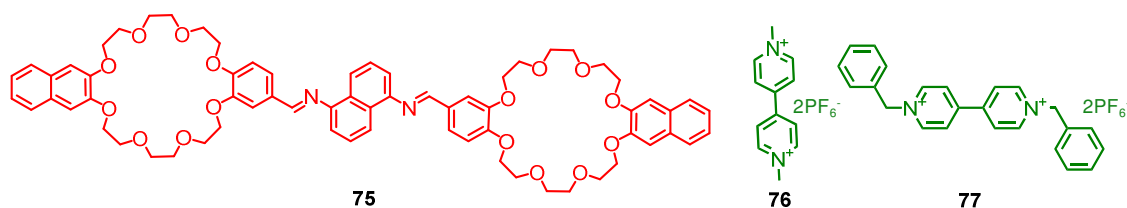


Figure 1.36: Structures of crown ether-based molecule **75** and paraquat derivatives (**76** and **77**).

Preferential binding of K^+ to crown ether moieties of **75** leads to the dissociation of the [3](taco complex) with necessary changes in luminescence responses.

Chapter 1

1.8. References

1. C. J Pedersen, *Angew. Chem., Int. Ed.* **1998**, *27*, 1021.
2. D. J. Cram, *Angew. Chem., Int. Ed.* **1998**, *27*, 1009.
3. J.-M. Lehn, *Angew. Chem., Int. Ed.* **1998**, *27*, 89.
4. (a) Stoddart, J. F.; Colquhoun, H. M. *Tetrahedron* **2008**, *64*, 8231; (b) Stoddart, J. F. *Chem. Soc. Rev.* **2009**, *38*, 1521.
5. Balzani, V.; Credi, A.; Raymo, F. M.; Stoddart, J. F. *Angew. Chem.* **2000**, *112*, 3484.
6. Lehn, J. M. *Supramolecular Chemistry: Concepts and Perspectives*; VCH: Weinheim, 1995.
7. Anslyn, E. V.; Dougherty, D. A. *Modern Physical Organic Chemistry*, University Science Books, Sausalito, CA, USA, 2006, pp.162.
8. Jeffrey, G. A. *An Introduction to Hydrogen Bonding*, Oxford University Press, Oxford 1997.
9. Hunter, C. A.; Sanders, J. K. M. *J. Am. Chem. Soc.* **1990**, *112*, 5525.
10. Shinkai, S.; Ikeda, M.; Sugasaki, A.; Takeuchi, M. *Acc. Chem. Res.* **2001**, *34*, 494.
11. (a) A. Whitty, *Nat. Chem. Biol.* **2008**, *4*, 435; (b) Nichola C. GarbettJonathan B. Chaires Binding: A Polemic and Rough Guide; *Methods in Cell Biology*, **2008**, *84*, 1.
12. M. Mammen, S.-K. Choi, G. M. Whitesides, *Angew. Chem. Int. Ed.* **1998**, *37*, 2754.
13. Fox, M. A., Chanon, M. *Photoinduced Electron Transfer*; Eds.; Elsevier: Amsterdam, **1988**. 32.
14. Barrett, E.; Dale, T. J.; Rebek, J., Jr. *J. Am. Chem. Soc.* **2008**, *130*, 2344.
15. (a) Ashton, P. R.; Chrystal, E. J. T.; Glink, P.T.; Menzer, S.; Schiavo, C.; Spencer, N.; Stoddart, J. F.; Tasker, P. A.; White, A. J. P.; Williams, D. J. *Chem. Eur. J.* **1996**, *2*, 709; (b) Mandal, A. K.; Gangopadhyay, M.; Das, A. *Chem. Soc. Rev.* **2015**, *44*, 663.
16. P. R. Ashton, I. Baxter, M. C. T. Fyfe, F. M. Raymo, N. Spencer, J. F. Stoddart, A. J. P. White, D. J. Williams, *J. Am. Chem. Soc.* **1998**, *120*, 2297.
17. Samuel P. B., A. R. Stefankiewicz, M. M. J. Smulders, D. Sattler, C. A. Schalley, J. R. Nitschke, J. K. M. Sanders *Angew. Chem. Int. Ed.* **2013**, *52*, 5749.
18. (a) Duncan, A. J.; Leo, D. J.; Long T. E., *Macromolecules*, **2008**, *41*, 7765; (b) Green, M. D.; Long, T. E. *Polym. Rev.* **2009**, *49*, 291; (c) Pedersen, C. J. *J. Am. Chem. Soc.* **1967**, *89*, 7017.

Chapter 1

19. Michael Meot-Ner, M. *J. Am. Chem. Soc.* **1983**, *105*, 4912.
20. Cantrill, S. J.; Fulton, D. A.; Heiss, A. M.; Pease, A. R.; Stoddart, J. F.; White, A. J. P.; Williams, D. J. *Chem.–Eur. J.* **2000**, *6*, 2274.
21. K. N. Trueblood, C. B. Knobler, D. S. Lawrence, R. V. Stevens, *J. Am. Chem. Soc.* **1982**, *104*, 1355.
22. M. Montalti, R. Ballardini, L. Prodi, V. Balzania, *Chem. Commun.* **1996**, 2011.
23. E. Ishow, A. Credi, V. Balzani, F. Spadola, L. Mandolini, *Chem. Eur. J.* **1999**, *5*, 984.
24. A. K. Mandal, M. Suresh, P. Das, A. Das, *Chem. Euro. J.* **2012**, *18*, 3906.
25. A. K. Mandal, M. Suresh, M. K. Kesharwani, M. Gangopadhyay, M. Agrawal, V. P. Boricha, B. Ganguly, A. Das, *J. Org. Chem.* **2013**, *78*, 9004.
26. M. Suresh, A. K. Mandal, E. Suresh, A. Das, *Chem. Sci.* **2013**, *4*, 2380.
27. R. Wang, L. Yuan and D. H. Macartney, *Chem. Commun.*, **2005**, 5867.
28. (a) Sambrook, M. R.; Beer, P. D.; Wisner, J. A.; Paul, R. L.; Cowley, A. R.; Szemes, F.; Drew, M. G. B. *J. Am. Chem. Soc.* **2005**, *127*, 2292; (b) Serpell, C. J.; Kilah, N. L.; Costa, P. J.; Felix, V.; Beer, P. D. *Angew. Chem. Int. Ed.* **2010**, *49*, 5322; (c) Lehn, J. M.; Vierling, P.; Hayward, R. C. *J. Chem. Soc. Chem. Commun.* **1979**, 296.
29. Stolwijk, T. B.; Sudhoelter, E. J. R.; Reinhoudt, D. N.; Van Eerden, J.; Harkema, S. *J. Org. Chem.* **1989**, *54*, 1001.
30. M. Lee, Z. Niu, D. V. Schoonover, C. Slebodnick, H. W. Gibson, *Tetrahedron*, **2010**, *66*, 7077.
31. C. Mukhopadhyay, S. Ghosha, A. M. Schmiedekamp, *Org. Biomol. Chem.* **2012**, *10*, 1434.
32. S. I. Moreno-Olivares, R. Cervantes, J. Tiburcio *J. Org. Chem.* **2013**, *78*, 10724.
33. N. Noujeim, K. Zhu, V. N. Vukotic, S. J. Loeb *Org. Lett.*, **2012**, *14*, 2484.
34. N. Farahani, K. Zhu, N. Noujeim S. J. Loeb *Org. Biomol. Chem.*, **2014**, *12*, 4824.
35. M. Suresh, A. K. Mandal, M. K. Kesharwani, N. N. Adarsh, B. Ganguly, R. K. Kanaparthi, A. Samanta, A. Das, *J. Org. Chem.* **2011**, *76*, 138.
36. A. K. Mandal, M. Suresh, A. Das, *Org. Biomol. Chem.* **2011**, *9*, 4811.
37. (a) Mulder, A.; Huskens, J.; Reinhoudt, D. N. *Org. Biomol. Chem.* **2004**, *2*, 3409; (b) V. Balzani, M. C. Leon, A. Credi, J. N. Lowe, J. D. Badjic, J. F. Stoddart, D. J. Williams *Chem. Eur. J.* **2003**, *9*, 5348.

Chapter 1

38. W. Jiang, K. Nowosinski, N. L. Loow, E. V. Dzyuba, F. Klautzsch, A. Schaafer, J. Huuskonen, K. Rissanen, C. A. Schalley, *J. Am. Chem.Soc.* **2012**, *134*, 1860.
39. Ying Han a,b, Jia-Bin Guo a, Jing Cao a, Chuan-Feng Chen *Tetrahedron* **2013**, *69*, 4541.
40. K.Nowosinski, L. K. S. von Krbek, N.L. Traulsen, C. A. Schalley *Org. Lett.* **2015**, *17*, 5076.
41. M. Lohse, K. Nowosinski, N. L. Traulsen, A. J. Achazi, L. K. S. von Krbek, Beate Paulus, C. A. Schalley, S. Hecht *Chem. Commun.*, **2015**, *51*, 9777.
42. (a) Mukhopadhyay, P.; Wu, A.; Isaacs, L. *J. Org. Chem.* **2004**, *69*, 6157; (b) Koevoets, R. A.; Versteegen, R. M.; Kooijman, H. A.; Spek, L.; Sijbesma, R. P.; Meijer, E.W. *J. Am. Chem. Soc.* **2005**, *127*, 2999.
43. (a) Oshovsky, G. V.; Reinhoudt, D. N.; Verboom, W. *Angew. Chem., Int. Ed.* **2007**, *46*, 2366; (b) Wang, F.; Han, C.; He, C.; Zhou, Q.; Zhang, J.; Wang, C.; Li, N.; Huang, F. *J. Am. Chem. Soc.* **2008**, *130*, 11254.
44. Jiang, W.; Winkler, H. D. F.; Schalley, C. A. *J. Am. Chem. Soc.* **2008**, *130*, 13852.
45. Wei Jiang, Dominik Sattler, Kari Rissanen, Christoph A. Schalley *Org. Lett.*, **2011**, *13*, 4502.
46. J.-M. Zhao, Q.-S. Zong, C.-F. Chen *J. Org. Chem.* **2010**, *75*, 5092.
47. F. Wang, B. Zheng, K. Zhu, Q. Zhou, C. Zhai, S. Li, N. Li, F. Huang *Chem. Commun.*, **2009**, 4375.
48. Z. J. Ding, H. Y. Zhang, L. H. Wang, F. Ding, Y. Liu, *Org. Lett.* **2011**, *13*, 856.
49. L. Prodi, F. Bolletta, M. Montalti, N. Zaccheroni, Peter Huszthy, E. Samu, B. Vermes *New J. Chem.*, **2000**, *24*, 781.
50. S. P. Upadhyay, R. R. S. Pissurlenkar, E. C. Coutinho, A. V. Karnik *J. Org. Chem.* **2007**, *72*, 5709.
51. A. D. Pandey, H. Mohammed, R. R. S. Pissurlenkar, A. V. Karnik *ChemPlusChem* **2015**, *80*, 475.
52. B. Szemenyei, I. Moczar, D. Pal, I. Kocsis, P. Baranyai, P. Huszthy *CHIRALITY*, **2016**, *28*, 562.
53. F. Biedermann, W. M. Nau *Angew. Chem. Int. Ed.* **2014**, *53*, 5694.
54. A. P. de Silva, H. Q. N. Gunaratne, C. P. McCoy, *Nature*, **1993**, *364*, 42.
55. D. C. Magri, G. J. Brown, G. D. McClean and A. P. de Silva, *J. Am. Chem. Soc.*, **2006**, *128*, 4950.

Chapter 1

56. A. Praetorius, D. M. Bailey, T. Schwarzlose and W. M. Nau, *Org. Lett.*, 2008, 10, 4089.
57. D.-H. Qu, Q.-C. Wang, H. Tian, *Angew. Chem. Int. Ed.* **2005**, 44, 5296.
58. A. K. Mandal, P. Das, P. Mahato, S. Acharya, A. Das, *J. Org. Chem.* **2012**, 77, 6789.

CHAPTER 2

TUNING EMISSION RESPONSES OF A TPA DERIVATIVE IN PHOTORESPONSIVE PSEUDOROTAXANE AND AN UNUSUAL DYNAMIC INCLUSION PHENOMENON

Publication:
J. Org. Chem. 2016, 81, 512–521

2.1. Introduction

Triphenyl amine (TPA) and its various derivatives are expected to have significance for many technological applications and in this regard understanding and control of the electroluminescence phenomenon of such derivatives is undoubtedly one of the major achievements of recent years.¹⁻³ For most of such applications, molecular rigidity plays a major role.⁴ Previous reports on structural and theoretical aspects of various TPA derivatives suggest that such molecules preferentially adopt a three-bladed propeller structure with adequate conformational flexibility, which adversely influences the photoluminescence property and thus, their application potential.^{5,6} Various research groups have put significant efforts in controlling the conformational flexibility in such derivatives. However, efforts in this regard are mostly restricted to intricate synthesis of highly rigid framework.⁷ More recently, attempt has been made to utilize host-guest inclusion complex formation with different macrocyclic hosts like cyclodextrin (CD). However, such example is scanty in the literature. Also, dual emission property remained elusive for all TPA derivatives reported till date.

Dual emission from a single molecule at room temperature, following excitation at a single wavelength, has special significance in biomedical imaging, multiplex signalling, dual labelling, opto-electronics, and display devices.⁸⁻¹² Dual emission is not an uncommon phenomenon either at low temperature or in rigid media; however, it is rather unique in the solution state at room temperature.¹³ Dual emission at room temperature has also been achieved in molecular conjugates having two or more fluorophores covalently bound to a protein backbone.¹⁴

In this chapter, a unique TPA derivative, **1Cl₃** (Figure 2.1) with two decoupled excited states which show dual emission behaviour in solution at room temperature. For example, in dimethyl formamide (DMF) solution, **1Cl₃** exhibits a high energy excitation band at ~ 370 nm for a locally excited (LE) state and a low energy band for the intramolecular charge transfer (ICT) process at ~ 440 nm. Formation of inclusion complexes with CB[7] and β -CD imparts conformational rigidity to **1Cl₃** allowing tuning of the dual emission behaviour.

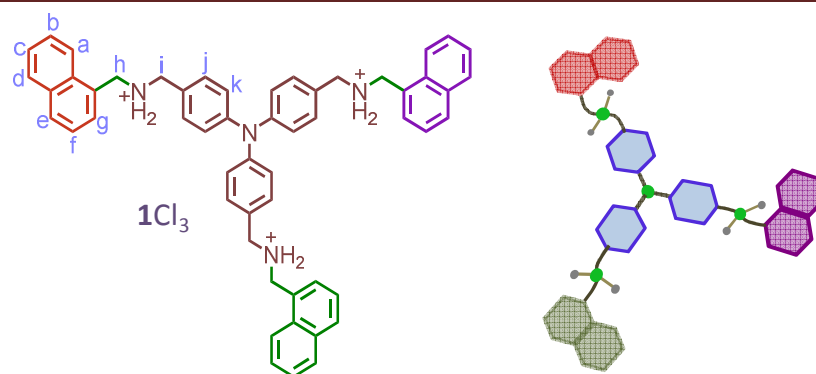


Figure 2.1: Schematic representation of the guest molecule $1Cl_3$.

2.2. Experimental section

2.2.1. Materials

1-Naphthylmethylamine, tris(para-formylphenyl) amine, CB[7], β -CD and were purchased from Sigma-Aldrich and used without further purification. All the solvents were purchased from S.D Fine Chemicals (India) and used after purification according to standard procedures.

2.2.2. Analytical Methods

NMR Spectroscopy

NMR experiments were carried out on 700 MHz and 500 MHz spectrometers. Samples were prepared in D_2O and spectra were obtained at 298 K unless stated otherwise. Homodecoupled pure shift spectra were recorded as described²⁴. Pure shift time domain data were constructed from 32 'chunks' of free induction decay measured for 20ms each. Refocusing of scalar couplings was accomplished by low flip angle CHIRP pulses in combination with a hard 180° pulse. Homonuclear 2D NMR experiments were performed with $256 \times 2K$ data points, employing a relaxation delay of 2s. Heteronuclear 2D NMR experiments were recorded with $140 \times 1K$ or $256 \times 1K$ data points. Data were acquired in Echo-Antiecho or States-TPPI mode, except for the COSY experiment which was recorded in magnitude mode. Typically, mixing times of 80ms, 250ms and 1s were employed for TOCSY, ROESY and NOESY experiments respectively. Proton NMR titration measurements were carried out by adding increasing amounts of hosts CB[7] to a 1.5 mM solution of $1Cl_3$.

Chapter 2

Isothermal titration calorimetry

Isothermal titration calorimetric (ITC) measurements were carried out by mixing solutions at 1000 rpm stirring. The complex formation between 1Cl_3 and the hosts CB[7] and β -CD was monitored in aqueous solution at 25°C. About 200 μl of the host solution was titrated against a solution of 1Cl_3 . A typical titration experiment consisted of 19 consecutive injections of 2 μl of the host at 20 s duration each with a 180 s interval between injections. Heat of dilution of the guest was determined by injecting 1Cl_3 solution into the neat solvent and the observed heats of binding were corrected for the heat of dilution. The data were analyzed to determine the binding constant (K), binding stoichiometry (N), change of enthalpy (ΔH) and the change of entropy (ΔS) associated with complex formation between 1Cl_3 and the two host molecules.

Optical Spectroscopy

The absorption and emission spectra were recorded on UV/vis-NIR spectrometer and Luminescence spectrofluorimeter at 25°C. All absorption and emission spectra measurements were performed with freshly prepared solutions and appropriate background corrections were applied. Fluorescence lifetimes were measured by Time Correlated Single Photon Counting (TCSPC) using a Luminescence spectrofluorimeter. A nano-LED was used as the excitation source ($\lambda_{\text{Ext}} = 295 \text{ nm}$). Fluorescence Quantum yield (Φ_f) was determined using quinine hemisulphate as a reference by employing the following equation,

$$\Phi_s = \Phi_R \times A_s \times (\text{Abs})_R \times \eta_s^2 / A_R \times (\text{Abs})_S \times \eta_R^2 \quad \text{Equation 1}$$

in which A_i is the integrated area under the fluorescence curve, Abs_i denotes the absorption, η_i is the refractive index of the medium and Φ_i , the fluorescence quantum yield. The subscripts $i = S, R$ refers to the parameters corresponding to the sample and reference compound, respectively.

2.2.3. Generalised methodology for spectroscopic studies

For electronic spectral studies, stock solutions of 1Cl_3 ($1.0 \times 10^{-4} \text{ M}$) were prepared in milli q water and stored in dark. Stock solutions of the CB[7] and β -CD of various anions ($1.0 \times 10^{-3} \text{ M}$) were prepared in Mili-Q water and stored in cold and dark condition. Stock

Chapter 2

solutions of $1Cl_3$ were diluted to effective final concentration of $2.08 \times 10^{-5}M$ for emission spectroscopic studies.

2.2.4. Synthesis

Synthesis of $1Cl_3$: 1-Naphthylmethylamine (0.382g, 0.607 mM) was added to tris(para-formyl phenyl) amine (0.2g, 0.243 mM) and dissolved in 30 ml of dry acetonitrile/methanol mixture with volume ratio 1:1. The reaction mixture was stirred at room temperature for 24 hrs and the solvent mixture was evaporated under reduced pressure. Methanol was added to the reaction mixture and the temperature was reduced to $0^\circ C$. $NaBH_4$ (0.6g) was then added in portions to the cooled reaction mixture. The reaction mixture was allowed to reach room temperature and stirred for 6 hrs. The solvent was removed under reduced pressure and the residue was extracted three times with DCM (30 ml) and water. The organic layers were combined and dried with anhydrous sodium sulphate. The solvent was removed under reduced pressure to collect the crude product, which was purified on a silica gel column using, chloroform/methanol (98:2, by volume) as an eluent. The desired product was obtained as a yellow sticky solid. A solution of concentrated HCl (0.2ml) in methanol was added drop wise and stirred for 24 hrs. A yellow solid was formed, (336mg, 64 %) which was isolated as a precipitate, collected by filtration and dried over P_2O_5 . 1H -NMR (500 MHz, CD_3OD , ppm): 8.00-8.04 (10H, m), 7.72 (3H, d, 7Hz), 7.57-7.68 (11H, m), 7.54 (6H, d, $J = 8.5$ Hz), 7.20 (6H, d, $J = 8.5$ Hz), 4.77 (6H, s), 4.40 (6H, s). ^{13}C -NMR (500 MHz, $DMSO-d_6$, ppm): 147.6, 133.7, 132.3, 131.5, 129.9, 129.4, 129.1, 127.1, 126.7, 125.8, 124.1, 123.9, 50.4, 46.8. Elemental Analysis : Calculated for $C_{54}H_{51}N_4Cl_3$: C, 75.21; H, 5.96; N, 6.50. Found: C, 74.93; H, 5.99; N, 6.46. ESI–Ms: Calculated: 395.16, observed: 395.21 $[M - 2Cl]^{2+}/2$, Melting point $190-195^\circ C$.

2.3. Results and Discussions

The TPA derivative, $1Cl_3$ was synthesized by reacting naphthalen-1-ylmethanamine with tris(4-formylphenyl)amine as described in the experimental section and was characterized using various analytical and spectroscopic techniques. The inclusion complex formation of $1Cl_3$ with CB[7] and β -CD were examined in detail by employing NMR spectroscopy and the thermodynamics of the binding process was studied by ITC measurements. The luminescence properties of the TPA fragment in the Free State and in the inclusion complexes were investigated by steady state and time resolved emission studies.

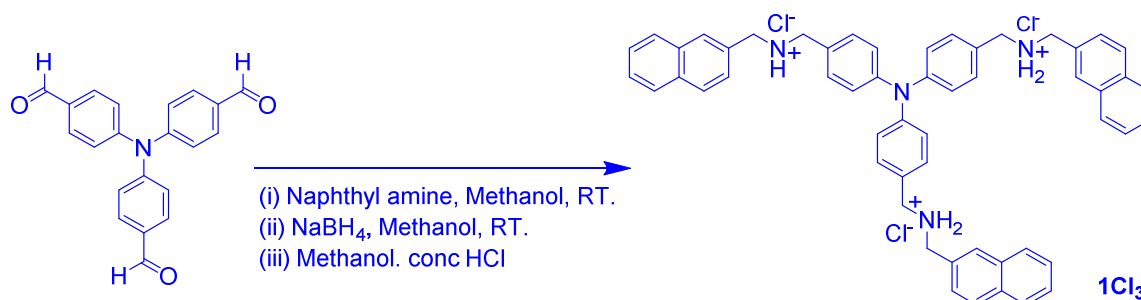


Figure 2.2: Methodology adopted for the synthesis of **1Cl₃**.

2.3.1. NMR studies of [1•{3CB[7]}]Cl₃

¹H NMR spectra of **1Cl₃**, CB[7] and the inclusion complex, [1•{3CB[7]}]Cl₃ formed by the addition of four mole equivalents of CB[7] to **1Cl₃** are shown in Figure 2.3. Titration studies showed broad NMR signals for **1Cl₃** at **1Cl₃**:CB[7] ratio of 1:1 but line narrowing was observed with further addition of CB[7] (Figure 2.4.a-e).

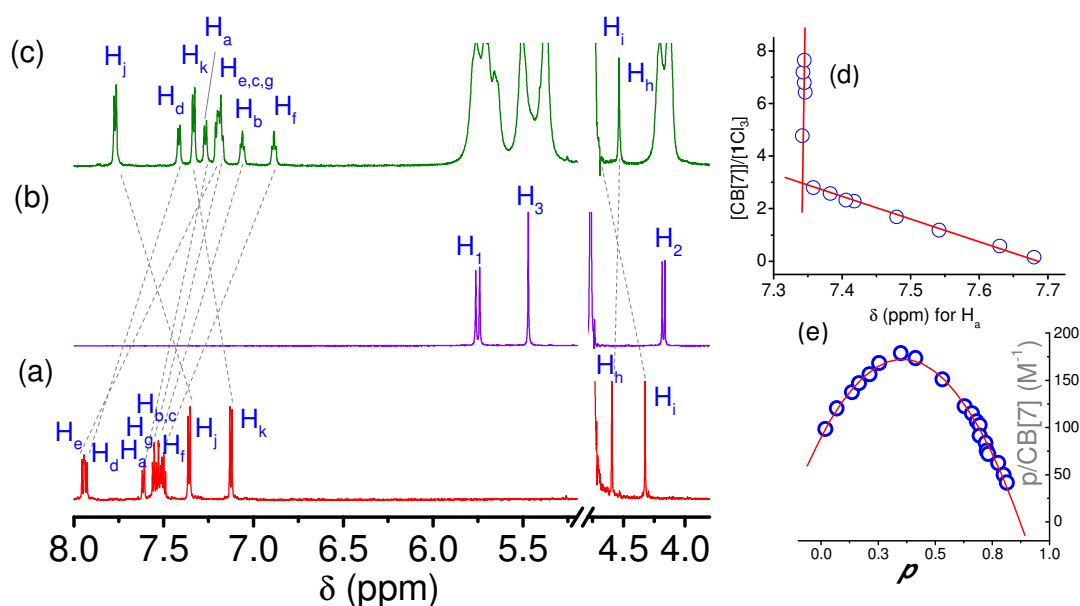


Figure 2.3: (a) Partial ¹H NMR spectra of 3.73×10^{-3} M aqueous solution of **1Cl₃**, (b) 3.73×10^{-3} M aqueous solution of CB[7] and (c) the inclusion complex with **1Cl₃**:CB[7] mole ratio 1:4, (d) mole ratio plot for the complexation of **1Cl₃** with CB[7] using $\Delta\delta$ for the H_a proton in **1Cl₃** (e) Scatchard plot for the inclusion complex formation. The data is fit by the curve $y = 89.87 + 462.84x - 648.91x^2$ ($r^2 = 0.97$).

Chapter 2

No significant changes were observed in the NMR spectrum recorded at a molar ratio of 1:3 and above. This suggests that at lower concentrations of CB[7], 1Cl_3 exchanges between the free and bound forms (inclusion complex) but at molar ratios of 1:3 and above a stable inclusion complex is formed. At a molar ratio of 1:3 for 1Cl_3 :CB[7], an inclusion complex is formed in which each of the three arms of 1Cl_3 are bound to a host molecule (CB[7]). At molar ratios exceeding 1:3, all guest molecules are bound, however the proton signals of CB[7] splits into two sets corresponding to bound and free forms of the host, with the former being more shielded and showing characteristic exchange broadened lines (Figure 2.4f-g).

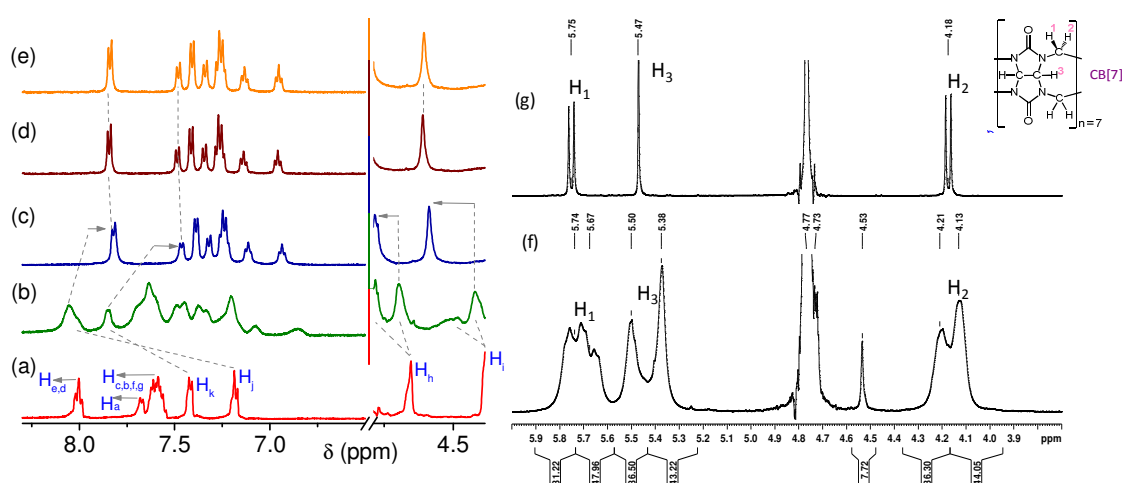


Figure 2.4: Partial ^1H NMR spectra (500 MHz, D_2O , 298K) of 1Cl_3 ($1.5 \times 10^{-3}\text{M}$) with varying concentrations of CB[7] (a) 0.0 M (b) 1.5 mM (c) 3.0 mM (d) 4.5 M and (e) 9.3 mM (left). Splitting of signals of CB[7] in the ^1H NMR spectrum. Comparison of the aliphatic region of 700 MHz ^1H NMR spectra of (f) 1Cl_3 -CB[7] complex with 1.5:5 mole ratio and, (g) CB[7].

Chemical shift assignments in $[1 \cdot \{3\text{CB}[7]\}]\text{Cl}_3$ were obtained by 1D and 2D NMR experiments (Figures 2.5a-c). Chemical shift changes in 1Cl_3 and CB[7] on complex formation are evident in Figure 2.4. In 1Cl_3 , all protons of the naphthyl moieties show upfield shifts ($\Delta\delta_{\text{H}_a} = -0.33$, $\Delta\delta_{\text{H}_c} = -0.34$, $\Delta\delta_{\text{H}_d} = -0.52$, $\Delta\delta_{\text{H}_e} = -0.76$, $\Delta\delta_{\text{H}_f} = -0.60$ and $\Delta\delta_{\text{H}_g} = -0.35$ ppm) while protons H_j and H_k of the phenyl moiety show downfield shifts ($\Delta\delta_{\text{H}_j} = 0.36$ ppm and $\Delta\delta_{\text{H}_k} = 0.21$ ppm). In addition, the aliphatic proton H_i shows a significant downfield shift ($\Delta\delta_{\text{H}_i} = 0.41$ ppm) whereas the H_h proton experiences a marginal upfield shift ($\Delta\delta_{\text{H}_h} = -0.07$ ppm). In CB[7], the diastereotopic protons (H_1 , H_2) of the methylene linkers which appear at 5.75 and 4.18 ppm as two doublets, shift to 5.67 and 4.13 ppm on complex formation. Due to symmetry, all the fourteen methylene linkers of each of the two rims of CB[7] are

Chapter 2

equivalent in free CB[7] as well as in the complex. The methine protons (H_3) of CB[7] shifts from 5.47 to 5.37 ppm on complex formation. In inclusion complexes with CB[7], protons of guest molecules experience a relatively shielded environment within the CB[7] cavity compared to the uncomplexed state.¹⁵ The observed upfield shifts of the naphthyl protons in $[1 \cdot \{3\text{CB}[7]\}] \text{Cl}_3$, implies that only the naphthyl moieties from each arm of 1Cl_3 are located within the CB[7] cavity on complex formation.

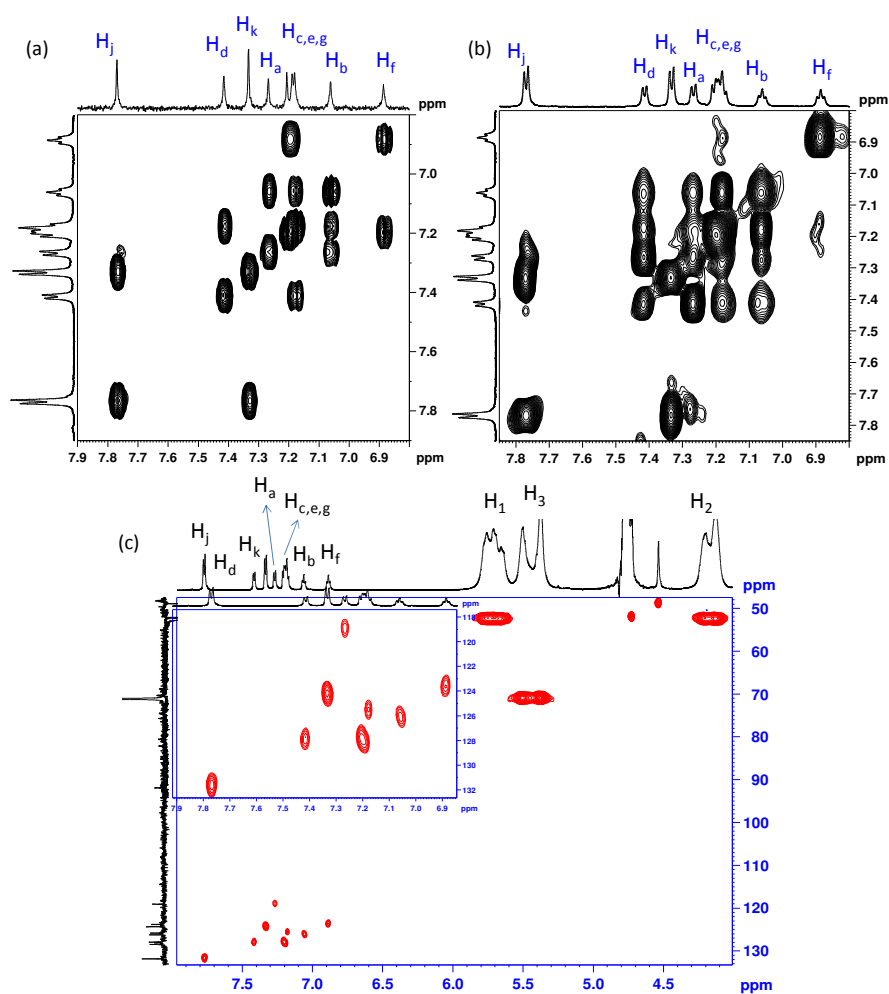


Figure 2.5: (a) Aromatic region of the 700 MHz COSY, (b) TOCSY, (c) ^1H - ^{13}C HSQC spectra of $[1 \cdot \{3\text{CB}[7]\}] \text{Cl}_3$. The conventional ^1H spectrum and homodecoupled pure shift ^1H spectrum are shown along F1 and F2 axis respectively. The spectra were acquired with $256 \times 2\text{K}$ data points, 16 scans and a relaxation delay of 2 s. The COSY spectrum was recorded in magnitude mode and the TOCSY spectrum was recorded in echo-antiecho mode with a mixing time of 80 ms. Expansion of the aromatic region of the HSQC spectrum is shown in the inset. The spectrum was acquired with $140 \times 1\text{K}$ data points, relaxation delay of 2 s and number of scans 24 for HSQC.

Chapter 2

Binding stoichiometry for the host-guest complex formation between 1Cl_3 and CB[7] was evaluated based on the data obtained from NMR titration studies. The mole ratio plot generated by monitoring the chemical shift change of the H_a proton of 1Cl_3 shows no further changes in chemical shift on addition of more than three equivalents of CB[7] (Figure 2.3d). This indicates a 1:3 binding stoichiometry and the formation of a 1:3 host-guest complex ($[1\cdot 3\{\text{CB}[7]\}]\text{Cl}_3$). This was further substantiated by MALDI-TOF mass spectral studies, which showed a molecular ion peak corresponding to $[1\cdot 3\{\text{CB}[7]\}]\text{Cl}_3$. The Scatchard plot¹⁵ was generated based on the extent of complexation p , estimated from the Benesi-Hildebrand (B-H) plot (Figure 2.6). In the case of complex formation with CB[7], the variation in the chemical shift of the H_i proton was monitored in the titration experiments. The extent of complexation, $p = \Delta/\Delta_0$ was estimated from a plot of $\Delta = \delta_c - \delta_u$ vs $1/[\text{CB}[7]]$, where δ_c and δ_u are the H_i chemical shifts in the presence and absence of CB[7], respectively and $\Delta_0 = 0.2358$. The nonlinear nature of the Scatchard plot with a maximum, confirms that positive cooperativity drives the complex formation process (Figure 2.3e).

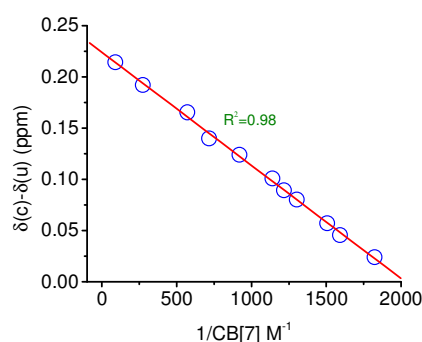


Figure 2.6: B-H Plot showing chemical shift changes of the H_i proton of 1Cl_3 with CB[7] concentration.

The initial formation of a 1:1 host-guest complex in which one arm of 1Cl_3 is bound to CB[7] favours the sequential binding of the second and third host molecules to the remaining arms of 1Cl_3 , eventually resulting in a 1:3 host-guest complex. Limited solubility of the host-guest complex ($[1\cdot 3\{\text{CB}[7]\}]\text{Cl}_3$) at the concentration level that was used for NMR studies did not allow the precise evaluation of the individual binding constant for 1:3 complex formation or the composite binding constant by NMR spectroscopy.

Further insights into the nature of the intermolecular interactions in the host-guest complex were obtained by 2D NMR experiments (NOESY and ROESY). These experiments were

Chapter 2

carried out on samples with $1\text{Cl}_3:\text{CB}[7]$ ratios of 1:3 or more to ensure conditions under which a 1:3 inclusion complex is formed. The NOESY and ROESY spectra (Figure 2.7a,b) show strong intra and inter molecular cross peaks. The positive cross peaks observed in the NOESY spectrum indicates a slowing down of the overall motion on complex formation resulting in a rotational correlation time which falls in the long correlation limit ($\omega_0 T_c \gg 1$). Intermolecular cross peaks in the NOESY spectrum can arise from the spatial proximity of the host and guest as a result of complex formation or due to exchange and spin diffusion effects. The ROESY spectrum helps to distinguish cross peaks arising due to spatial proximity (negative cross peaks) from those arising as a result of exchange (positive cross peaks). Among two inequivalent methylene protons of CB[7], those at 5.67 ppm (H_1) show intermolecular cross peaks to the naphthyl protons (H_c and H_e) located within the CB[7] cavity as well as the phenyl proton H_j located outside the cavity (Figure 2.7).

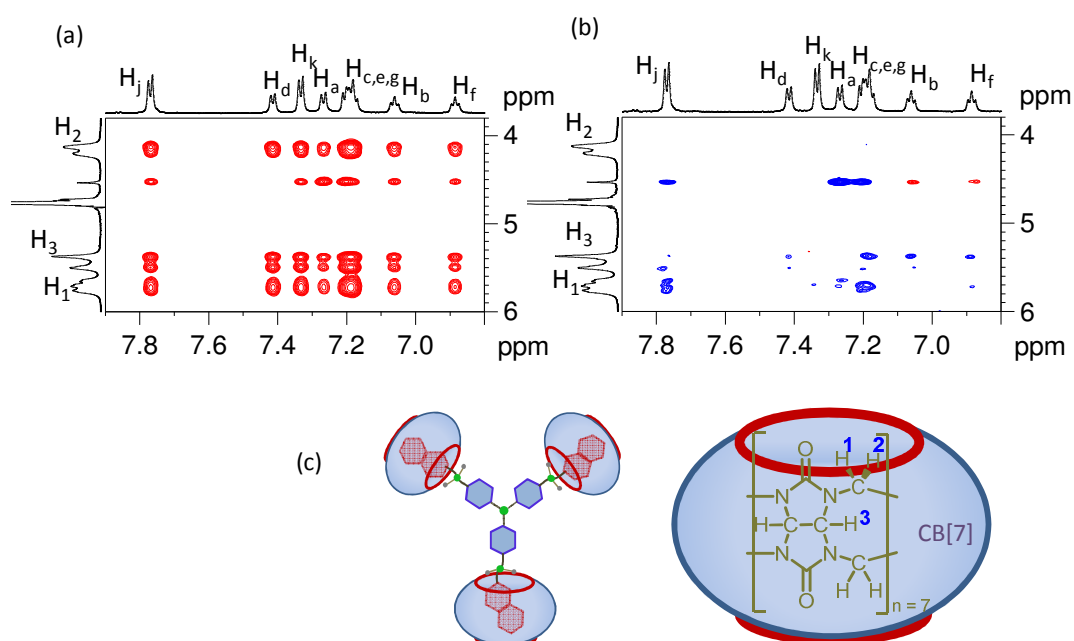


Figure 2.7: 2D NMR spectra showing intermolecular cross peaks in the $[1\bullet 3\{\text{CB}[7]\}]\text{Cl}_3$ complex (a) NOESY and (b) ROESY. (c) Schematic representation of the 1:3 host-guest complex.

On the other hand, intermolecular cross peaks to the methylene linker proton of CB[7] at 4.13 ppm is observed only in the NOESY spectrum but not in the ROESY spectrum. This implies that this cross peak in the NOESY spectrum arises from spin diffusion effects at the long mixing time (1s) employed. The structure of CB[7] shows that the inequivalent methylene linker protons at 5.67 and 4.13 ppm are present on both rims of CB[7], however

the linker protons of the two rims are indistinguishable in the spectrum due to the degeneracy of the chemical shifts imposed by symmetry. The observation of cross peaks from the methylene protons of CB[7] at 5.67 ppm to both naphthyl and phenyl units of 1Cl_3 indicates the spatial proximity of the linker protons to both these units of the guest molecule. This is because the linker protons at both rims contribute to the signal at 5.67 ppm. Thus cross peaks to the naphthyl protons arise due to spatial proximity to the linker protons at one of the rims while the phenyl protons show cross peaks to the equivalent linker protons at the opposite rim. The ROESY spectrum also shows intermolecular cross peaks between the methine protons of CB[7] at 5.37 ppm and the naphthyl protons H_c , H_e , H_b and H_f , the latter two being weaker. Based on these observations and the chemical shift changes induced in the proton spectrum on complex formation, we envisage the formation of a 1:3 inclusion complex as shown in Figure 2.7c. All the additional cross peaks seen in the NOESY spectrum which are absent in the ROESY spectrum are exchange cross peaks between free and bound forms of CB[7] since the sample had a 1Cl_3 :CB[7] mole ratio slightly in excess of 1:3.

2.3.2. NMR studies of $[1\cdot\{\beta\text{-CD}\}]\text{Cl}_3$

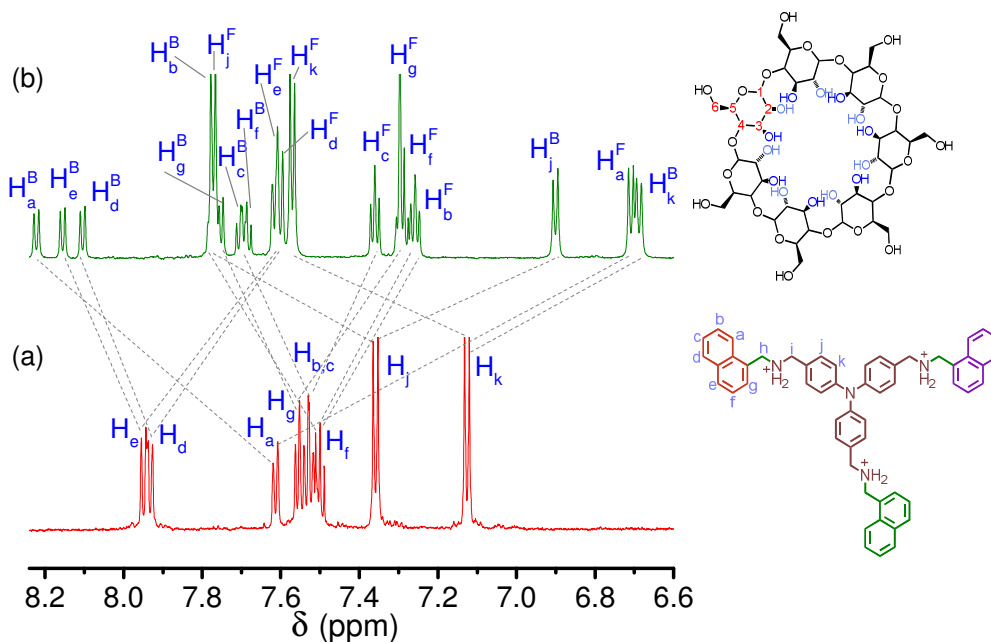


Figure 2.8. Partial ^1H NMR spectra of (a) 1.64×10^{-3} M aqueous solution of 1Cl_3 and (b) Inclusion complex, with 1Cl_3 : $\beta\text{-CD}$ mole ratio of 1:4. Signals from the 'bound' and 'free' arms of 1Cl_3 in the

Chapter 2

complex are labeled 'B' and 'F', respectively. The structures of 1Cl_3 and $\beta\text{-CD}$ with labeling of atoms are also indicated.

^1H NMR spectra of 1Cl_3 and the inclusion complex formed by the addition of four mole equivalents of $\beta\text{-CD}$ are shown in Figure 2.8. As in the case of CB[7], host-guest complex formation results in both shielding and deshielding influences on the aromatic protons of 1Cl_3 . Titration studies with $\beta\text{-CD}$ and CB[7] show striking differences in the changes occurring in the 1Cl_3 spectra as host concentration increases.

Unlike observations for the complex with CB[7], the chemical shifts of 1Cl_3 protons remain almost unchanged on addition of 1.0, 2.0, 3.0 or 6.0 mole equivalents of $\beta\text{-CD}$. Also, in contrast to complex formation with CB[7], more signals are observed in the spectrum of the complex with $\beta\text{-CD}$. This is readily visible in the homodecoupled pure shift NMR spectra shown in Figure 2.9, recorded using the PSYCHE method.¹⁶

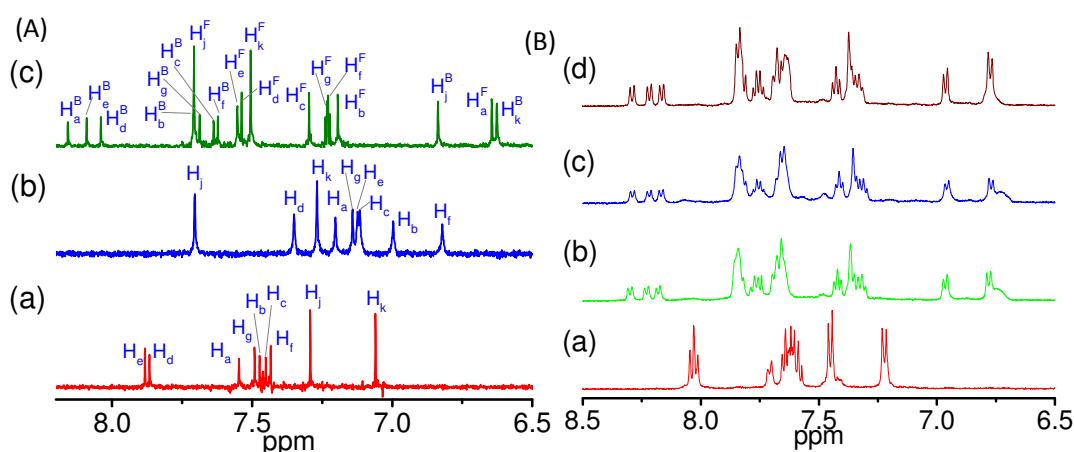


Figure 2.9: (A) Comparison of the 700 MHz pure shift ^1H NMR spectra of the aromatic region at 298 K for. (a) 1Cl_3 , (b) Inclusion complex of 1Cl_3 with CB[7] at mole ratio 1:4 and (c) Inclusion complex of 1Cl_3 with $\beta\text{-CD}$ at mole ratio 1:4, (B) Partial ^1H NMR spectra (700 MHz, D_2O , 298K) of 1Cl_3 ($1.64 \times 10^{-3}\text{M}$) with varying concentrations of $\beta\text{-CD}$ (a) 0.0 M (b) 1.0 M (c) 3.0 M and (d) 6.5 M.

The spectrum of the inclusion complex formed between 1Cl_3 and CB[7] show nine different types of 1Cl_3 protons while the spectrum of the complex formed between 1Cl_3 and $\beta\text{-CD}$ show as many as eighteen proton environments. The presence of well defined sharp signals implies that the additional signals could be due to the presence of bound and free 1Cl_3 which may be in slow exchange, or due to the inequivalence of the three arms in the complex formed between 1Cl_3 and $\beta\text{-CD}$. However, titration studies do not show any

Chapter 2

signals of free 1Cl_3 at $1\text{Cl}_3:\beta\text{-CD}$ ratios exceeding 1:1 (Figure 2.9B) indicating that the presence of free 1Cl_3 cannot account for the additional signals in the spectrum.

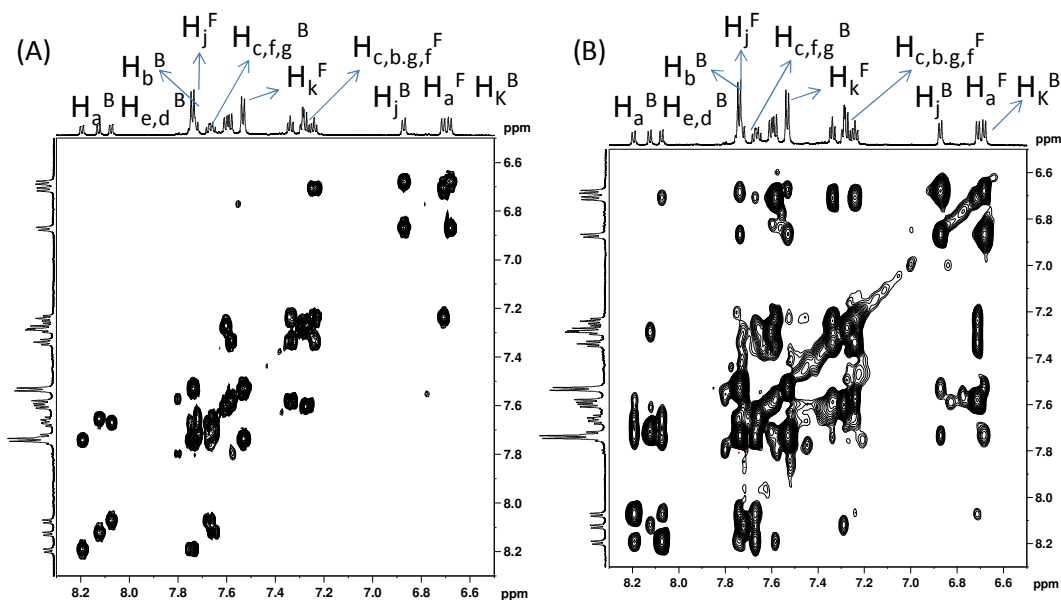
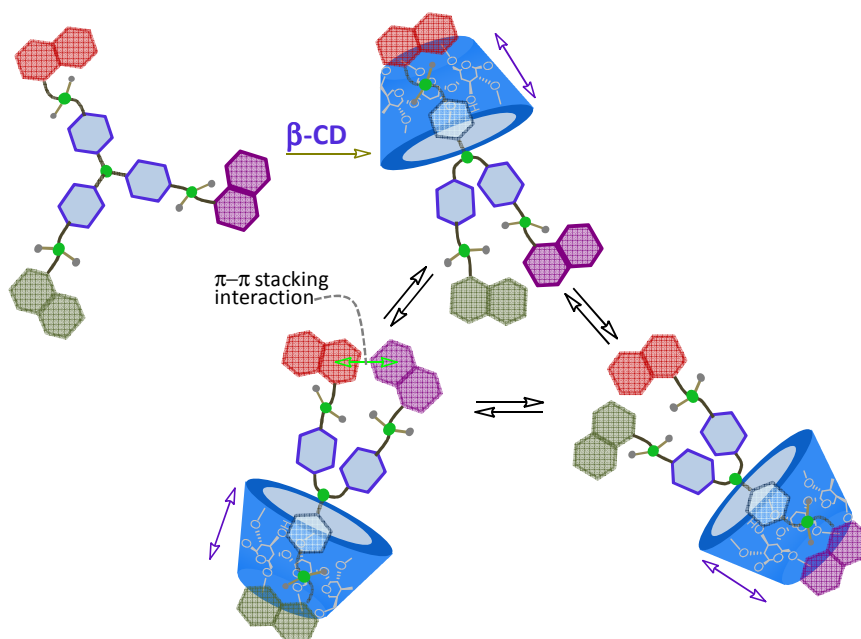


Figure 2.10: 700 MHz (A) COSY, (B) TOCSY spectrum of $[1\cdot\{\beta\text{-CD}\}]\text{Cl}_3$ at 298K. The spectrum was recorded in magnitude mode with $256 \times 2\text{K}$ points, relaxation delay of 2 s and 16 scans. The mixing time was set to 80ms for TOCSY spectrum.

In order to obtain the chemical shift assignments and explain the presence of additional signals of 1Cl_3 in the complex with $\beta\text{-CD}$, detailed 1D and 2D NMR investigations were carried out (Figure 2.10). These studies indicate that the signals of 1Cl_3 in the host-guest complex are doubled in number and occur with a ratio of 1:2. This suggests that one of the arms of 1Cl_3 behaves differently from the other two in the complex. Such a possibility can arise if only one of the three arms of 1Cl_3 is bound during complex formation with $\beta\text{-CD}$. For example, the spectra in Figure 2.8 shows that the H_j and H_k protons of the triphenylamine groups gives rise to two sets of signals in the complex with a ratio of 1:2. The signals with higher intensity are deshielded ($\text{H}_j = 7.53$ ppm, $\text{H}_k = 7.74$ ppm), while the lower intensity signals are shielded ($\text{H}_j = 6.87$ ppm, $\text{H}_k = 6.68$ ppm) with respect to those of neat 1Cl_3 ($\text{H}_j = 7.35$ ppm, $\text{H}_k = 7.11$ ppm). The observed intensity ratios suggest that the deshielded protons belong to the 'free' arms of 1Cl_3 and the shielded proton belongs to the arm 'bound' to $\beta\text{-CD}$. Similar behavior is observed for the methylene protons (H_h and H_i) of 1Cl_3 on complex formation (Figure 2.9). For 1Cl_3 , H_i and H_h protons appear as singlets at ~ 4.3 and ~ 4.6 ppm, respectively. On formation of the host-guest complex, signals of the H_h

Chapter 2

protons of the 'free' arms are shielded (singlet at 4.09 ppm), whereas the H_h proton of the 'bound' arm is deshielded and appear as an AB quartet (4.73 and 4.83 ppm, $J = 13.7$ Hz). Similarly, the H_i proton of the 'bound' arm experiences deshielding and occurs as an AB quartet (4.34 and 4.31 ppm, $J = 13.4$ Hz), while those of the 'free' arms show a deshielded AB quartet (4.01 and 3.85 ppm, $J = 13.2$ Hz).



Scheme 2.1. Cartoon representation of the 1:1 host-guest complex ($[1\cdot\beta\text{-CD}]\text{Cl}_3$) formed between 1Cl_3 and $\beta\text{-CD}$ molecule, in which only one arm of 1Cl_3 is bound at a time. The equivalence of the three arms results in a dynamic inclusion complex in which one $\beta\text{-CD}$ molecule may bind to any one of the three arms. The exchange equilibrium is indicated by using different colors for the naphthyl groups of the three arms.

Another striking feature of the ^1H NMR spectrum is the presence of a heavily shielded doublet at 6.71 ppm, assigned to the H_a proton of the naphthyl moiety (Figure 2.8). The chemical shift difference of H_a with respect to neat 1Cl_3 is ~ 0.9 ppm. The integrated peak area suggests that it originates from the two 'free' arms of 1Cl_3 . Interestingly, the H_a proton of the 'bound' arm of 1Cl_3 is considerably deshielded due to its interaction with the smaller rim of $\beta\text{-CD}$ and appears as a doublet at 8.19 ppm which is shifted by ~ 0.42 ppm with respect to neat 1Cl_3 . Upfield shift of aromatic protons on inclusion in the $\beta\text{-CD}$ cavity is not uncommon. However, the appreciable upfield shift of ~ 0.9 ppm for the two naphthyl H_a protons of the 'free' arms of 1Cl_3 on host-guest complex formation with $\beta\text{-CD}$ is rather unusual. The observed shielding of the H_a protons of the two 'free' arms can only be

Chapter 2

explained by considering an efficient π - π stacking interaction involving the naphthyl rings of the 'free' arms. This is possible if the two 'free' arms approach sufficiently close to each other to experience a π - π stacking interaction as indicated in Scheme 2.1. Influence of π - π stacking interaction in dictating the conformation in a host-guest complex has been reported.¹⁷ Even though most of the naphthyl protons of the 'free' arms of 1Cl_3 show upfield shifts and corresponding downfield shifts for the 'bound' arm, the magnitude of these shifts are less when compared to that seen for the H_a protons of the 'free' arms (Figure 2.8). These observations further corroborates the formation of a 1:1 host-guest complex ($[1\bullet\{\beta\text{-CD}\}]\text{Cl}_3$), in which the naphthyl moieties of the two unbound arms of 1Cl_3 approach close enough to induce a π - π stack interaction as shown in Scheme 2.1.

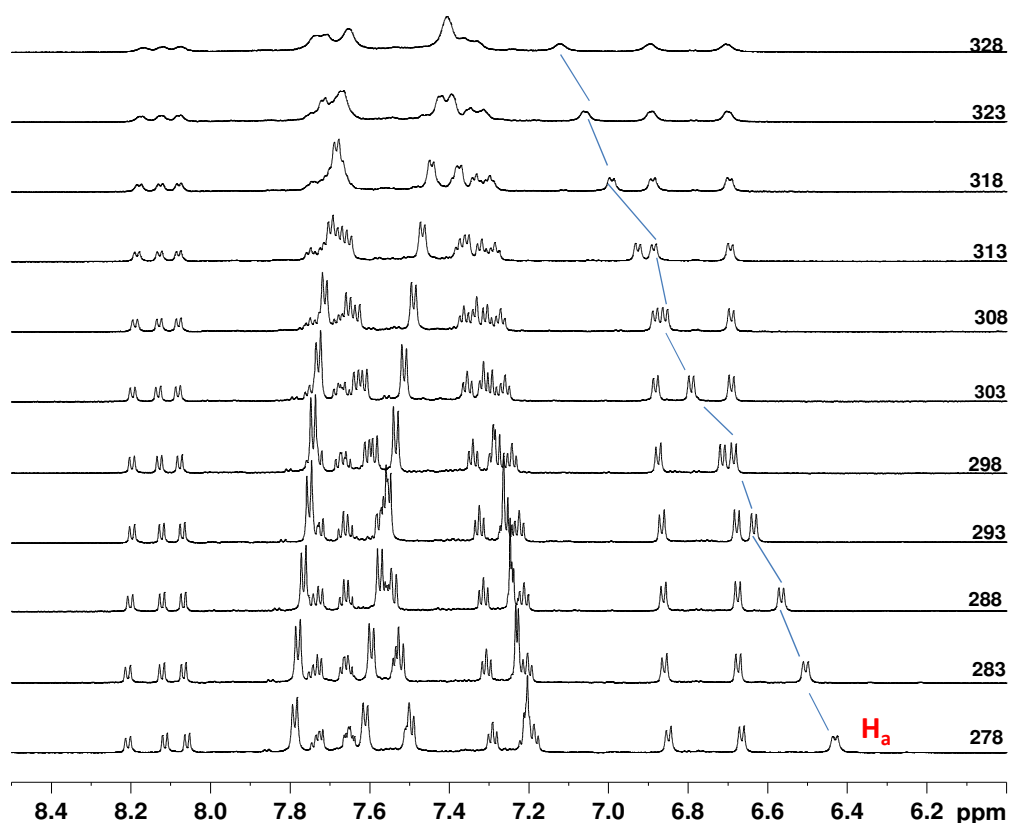


Figure 2.11: Aromatic region of the variable temperature ^1H NMR spectra (700 MHz) of the $[1\bullet\{\beta\text{-CD}\}]\text{Cl}_3$ complex with 1Cl_3 : $\beta\text{-CD}$ mole ratio of 1:4.

Variable temperature ^1H NMR spectra of $[1\bullet\{\beta\text{-CD}\}]\text{Cl}_3$ provides further evidence for the stacking interaction (Figure 2.11). The shielded H_a protons show substantial downfield shifts as the temperature increases. Enhanced molecular flexibility at higher temperatures

Chapter 2

is expected to reduce the possibility of π - π stack interactions thereby decreasing the shielding influence on the H_a proton.

In contrast, the H_k protons of the phenyl moiety of the 'free' arms, which are not under the influence of π - π stack interaction, show only a marginal upfield shift as temperature increases. Similar effects of the influence of temperature on the π - π stacking interaction is also seen for the H_h and H_i protons of the 'free' arms (Figure 2.12). The proton resonances of the host β -CD, are also split into two sets of unequal intensity providing further evidence for the formation of a 1:1 host-guest complex.

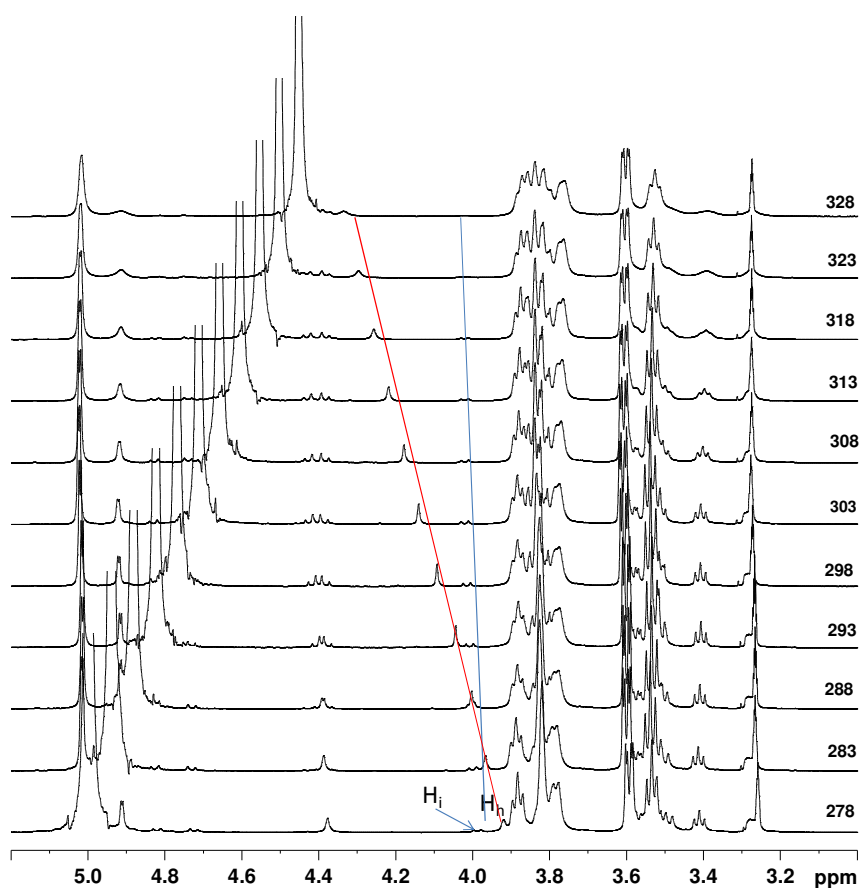


Figure 2.12: Aliphatic region of the variable temperature ^1H NMR spectra (700 MHz) of the $[1\cdot\{\beta\text{-CD}\}]\text{Cl}_3$ complex with $1\text{Cl}_3:\beta\text{-CD}$ mole ratio of 1:4.

The weaker signals arising from β -CD bound to 1Cl_3 are shielded while the stronger signals are unaffected compared to the ^1H NMR signals of unbound β -CD (Figure 2.13). Interestingly, the ratio of the area of a single aromatic proton of the 'bound' arm of 1Cl_3 to one of the weaker signals of β -CD, (for example, H_a of the 'bound' arm at 8.19 to H_i of

Chapter 2

bound β -CD at ~ 4.9 ppm) is 1:7. Since one molecule of β -CD has seven equivalent H_1 protons, the ratio of 1:7 is consistent with the formation of a 1:1 host-guest complex in which only one arm of $1Cl_3$ resides in the β -CD cavity. The results of ESI-MS studies and the mole ratio plot analysis also supports the formation of the proposed 1:1 host-guest complex ($[1\bullet\{\beta\text{-CD}\}]Cl_3$) depicted in scheme 2.1.

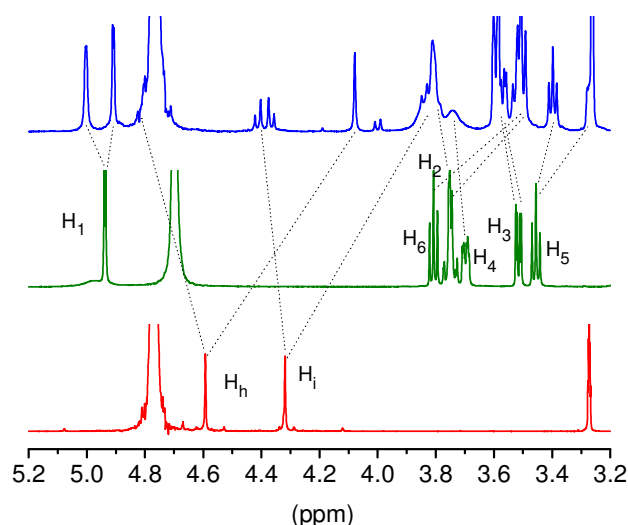


Figure 2.13: 700 MHz 1H NMR spectra of $1Cl_3$ (bottom), β -CD (center) and $[1\bullet\{\beta\text{-CD}\}]Cl_3$ complex at 1:4 mole ratio (top). Signals from the 'bound' and 'free' arms of $1Cl_3$ in the complex are indicated by 'B' and 'F' respectively.

The dynamic nature of the $[1\bullet\{\beta\text{-CD}\}]Cl_3$ complex is evident from the changes in the line widths of the $1Cl_3$ signals in the variable temperature 1H NMR spectra (Figures 2.11 and 2.12). The sharp signals observed at 298K broaden at temperatures above 323K, which implies that the exchange process shifts from slow to intermediate NMR time scales as temperature increases. The exchange between complexed and free $1Cl_3$ seems unlikely since the spectra do not show signals corresponding to free $1Cl_3$ in the presence of one or more mole equivalents of β -CD.

In order to obtain further insights into the exchange process we carried out NOESY experiments with a solution having $1Cl_3$: β -CD molar ratio of 1:4. The NOESY spectra show strong positive intermolecular cross peaks indicating complex formation (Figure 2.14). Interestingly, the protons of the 'free' and 'bound' arms of $1Cl_3$ show cross peaks between them (for example H_a^F at 6.71 to H_a^B at 8.19) and also to the protons of β -CD (Figure 2.14).

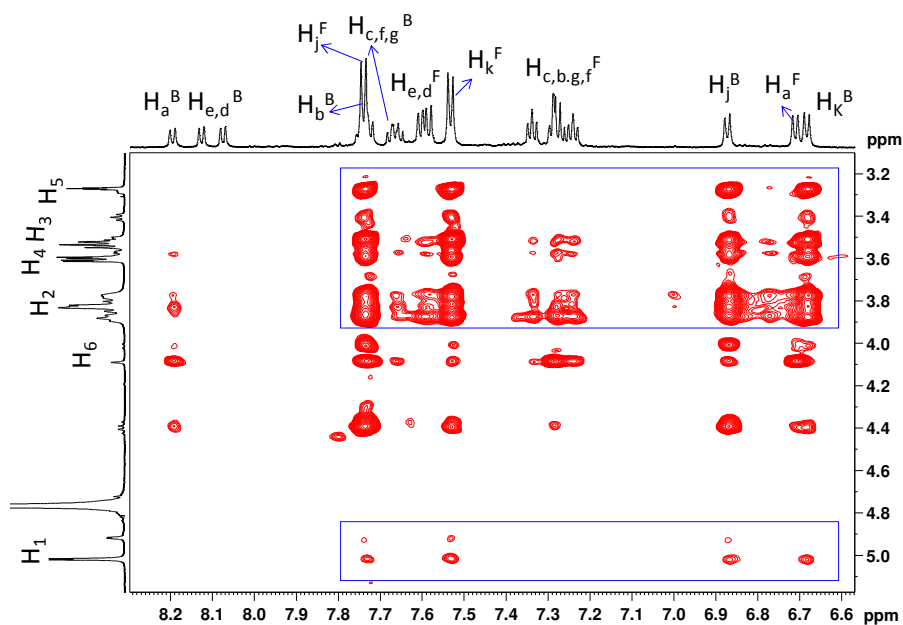


Figure 2.14: Part of the 700 MHz NOESY spectrum of $[1\cdot\{\beta\text{-CD}\}]\text{Cl}_3$ at 298 K. Cross peaks between bound and free $\beta\text{-CD}$ and aromatic protons of 1Cl_3 are indicated in boxes.

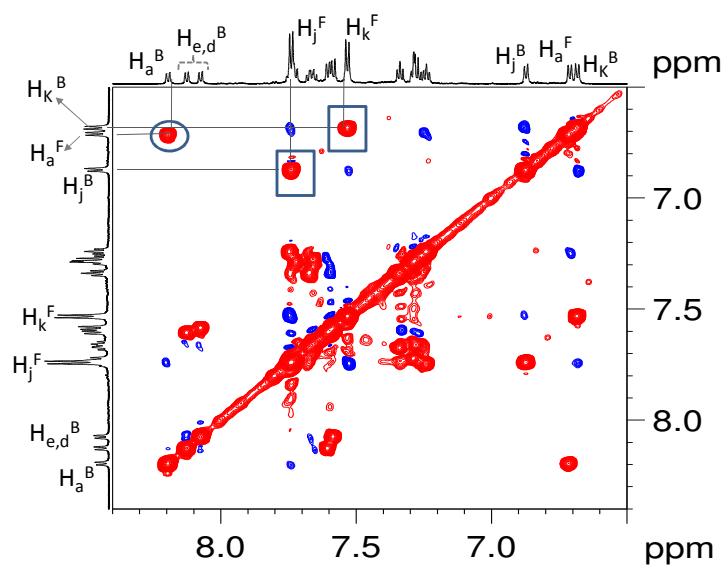


Figure 2.15: Partial ROESY spectrum of the $[1\cdot\{\beta\text{-CD}\}]\text{Cl}_3$ complex at mole ratio 1:4 obtained on a 700 MHz spectrometer at 298K. Exchange and NOE cross peaks are shown in red and blue, respectively. The exchange cross peak between the H_a protons of the 'bound' and 'free' arms are indicated by a circle while those corresponding to H_k and H_j protons are indicated by squares.

The cross peaks between the 'bound' and 'free' arms of 1Cl_3 implies an exchange equilibrium between them, mediated by $\beta\text{-CD}$ molecules in solution. A single arm of 1Cl_3 in

Chapter 2

the 1:1 host-guest complex is bound to a β -CD molecule at a given time. Since the three arms are equivalent, it is equally probable that another β -CD molecule from the bulk could bind to one of the two 'free' arms while releasing the arm which was initially bound. The nature of the exchange process was further substantiated by ROESY experiments (Figure 2.15) which showed two types of cross peaks; those arising from spatial proximity (negative cross peaks) and those due to chemical exchange (positive cross peaks).

The positive exchange cross peaks between the 'bound' and 'free' arms of 1Cl_3 (H_a protons at 6.71 and 8.19 ppm; H_j protons at 6.87 and 7.53 ppm; H_k , protons at 6.68 and 7.74 ppm,) provides clear evidence of the interchange of the 'bound' and 'free' status of the arms as discussed above. Also, temperature dependent ROESY spectra show the expected decrease in intensity of the exchange cross peaks at lower temperatures due to the reduced exchange rate (Figure 2.16).

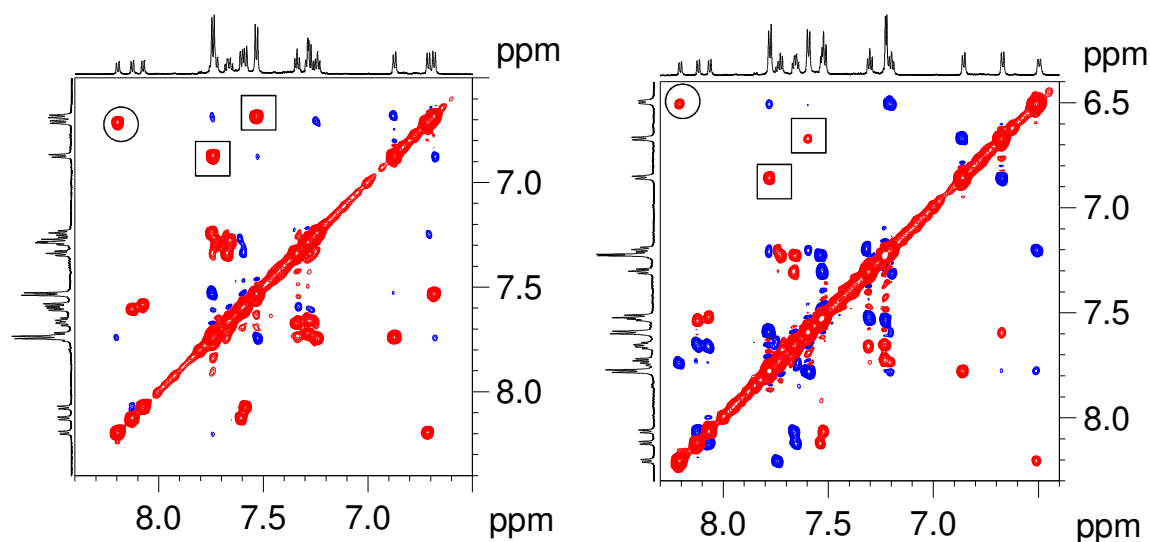


Figure 2.16: 700 MHz ROESY spectra of $[1\cdot\{\beta\text{-CD}\}]\text{Cl}_3$ at 298 K (left) and 283 K (right). Exchange cross peaks between the H_a protons of the 'bound' and 'free' arms of 1Cl_3 in the complex are indicated by circles and the corresponding pairs for the H_j and H_k protons are indicated by squares.

Examples of exchange between free and bound guest (or host) molecules during host-guest inclusion complex formation are common.¹⁸ However, a dynamic process involving inclusion of only one of the three equivalent arms of the guest molecule within the β -CD cavity at a given time as represented in Scheme 2.1 is rather uncommon.

Chapter 2

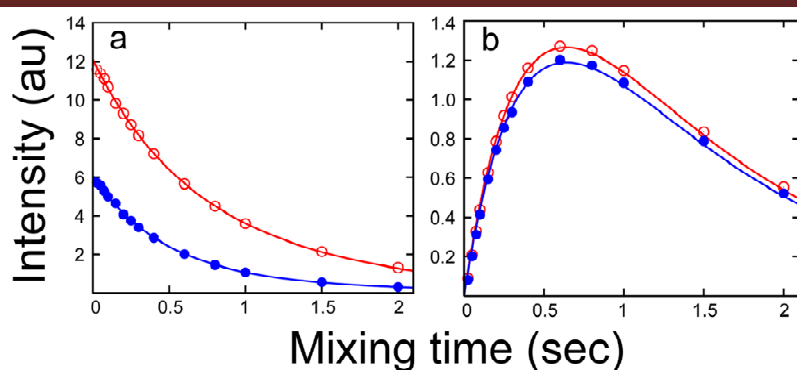


Figure 2.17: Fits of (a) decay and (b) build-up curves to experimental data for H_a protons of the naphthyl moiety (red: 'free' arm and blue: 'bound' arm) in $[1\bullet\{\beta\text{-CD}\}]\text{Cl}_3$ at 300K.

Attempts were also made to measure the exchange rates and evaluate the thermodynamic parameters for this exchange process by variable mixing time NOESY experiments at different temperatures. The exchange rates were evaluated by fitting the equations for cross peak build-up and diagonal peak decay to the experimental data (Figure. 2.17). At 300K, the exchange rate of the arms between the 'free' and 'bound' states was 1.32 s^{-1} . The thermodynamic parameters ($\Delta H \sim -13\text{ kJ}$ and $\Delta S \sim -0.3\text{ kJK}^{-1}$) for the exchange process were evaluated using Eyring plots (Figure. 2.18).

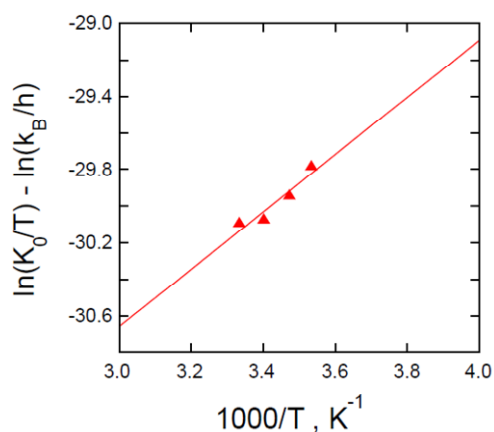


Figure 2.18: Eyring plot for estimation of ΔH and ΔS .

ROESY experiments also provide insights into the relative spatial orientation of 1Cl_3 in the $\beta\text{-CD}$ cavity through connectivity via negative NOE cross peaks (Figure 2.19). The "intra-arm" NOE cross peaks between protons of 1Cl_3 helps to distinguish the 'bound' and 'free' arms in $[1\bullet\{\beta\text{-CD}\}]\text{Cl}_3$. For example, cross peaks between H_i and H_j protons helps to

Chapter 2

assign the chemical shifts in the 'bound' (4.39 and 6.87 ppm) and 'free' (4.01 and 7.74 ppm) arms.

The protons of the 'bound' arm of 1Cl_3 show strong cross peaks to all β -CD protons except H_1 which is located outside the host cavity (Figure 2.19). The protons H_j and H_k of the 'bound' arm show NOE cross peaks to H_3 (3.51 ppm) and H_5 (3.28 ppm) of β -CD. In addition, H_j and H_k protons of the 'free' arms show unexpected NOE cross peaks to H_5 (3.28 ppm) and H_6 (3.56, 3.50 ppm) protons of β -CD. This can only arise if the bound β -CD molecule penetrates the bound arm of 1Cl_3 in such a way that the phenyl rings from the 'free' arms also come well within the NOE limits of 5\AA (Scheme 2.1). The NOE cross peaks between protons of β -CD and the arms of 1Cl_3 thus gives an indication of the extent to which the host molecule engulfs the guest molecule. Previous reports on host-guest complexes of dansyl derivatives with β -CD suggests the possibility of the inclusion of the naphthyl moiety via the narrow rim of β -CD.¹⁹

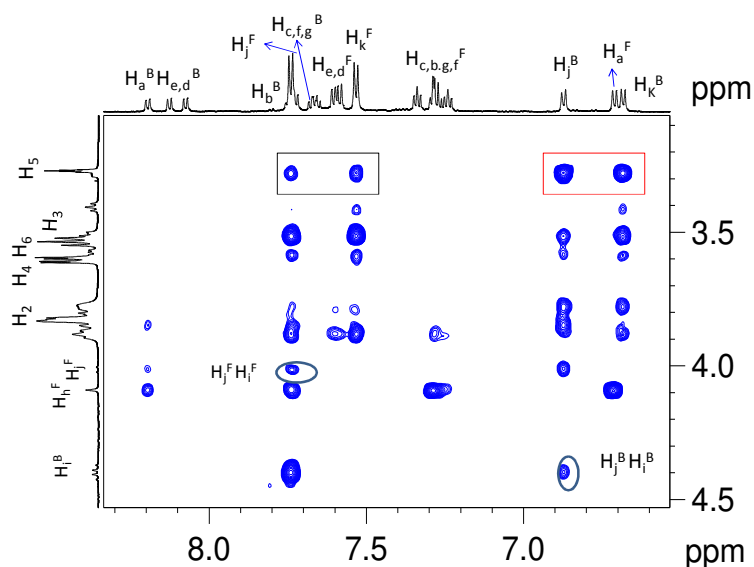


Figure 2.19: 700 MHz ROESY spectrum of $[1\cdot\{\beta\text{-CD}\}]\text{Cl}_3$ at 298 K. Expansion of the region showing intermolecular NOE contact (right). NOE cross peaks of H_j and H_k protons of 'free' and 'bound' arms of 1Cl_3 to H_5 proton of β -CD in the complex are highlighted by red and black boxes respectively. The intra-arm NOE cross peaks are shown in circles.

Inclusion complexes of β -CD with amine and secondary ammonium ion derivatives have been shown to be stabilized by hydrogen bonding between the primary $-\text{OH}$ group at the rim and amino group of the guest molecule.²¹ A similar situation involving weak H-bonding between the secondary $-\text{OH}$ group at the rim and the lone pair of electrons of the amine

Chapter 2

moiety could help in stabilizing the $[1\cdot\{\beta\text{-CD}\}]Cl_3$ complex since the wide rim of $\beta\text{-CD}$ is sufficiently close to the nitrogen atom of the tertiary amine. Thus the model of the 1:1 host-guest complex proposed on the basis of observations from ROESY and NOESY experiments, as indicated in Scheme 2.1 seems plausible.

Apart from chemical shifts, observed line widths of the ^1H NMR signals of $1Cl_3$ do not differ significantly on increasing the $1Cl_3$: $\beta\text{-CD}$ molar ratio from 1:1 to 1:4. This further confirms that only one of the three arms of the $1Cl_3$ is bound in the complex (Figure 2.9B). At mole ratios below 1:1, signals from uncomplexed $1Cl_3$ also appear in the ^1H spectrum and exchange cross peaks are observed between the protons of uncomplexed $1Cl_3$ and corresponding protons present in the 'bound' and 'free' arms of the complex (Figure 2.20). The uncomplexed $1Cl_3$ is present transiently during the exchange involving complexation of the different arms. As the concentration of $\beta\text{-CD}$ increases, these exchange peaks involving uncomplexed $1Cl_3$ tends to become weaker. In a solution with $1Cl_3$: $\beta\text{-CD}$ mole ratio 1:4, the population of the uncomplexed guest molecules is much lower, with very short life times making it impossible to detect the corresponding cross peaks in the exchange experiments.

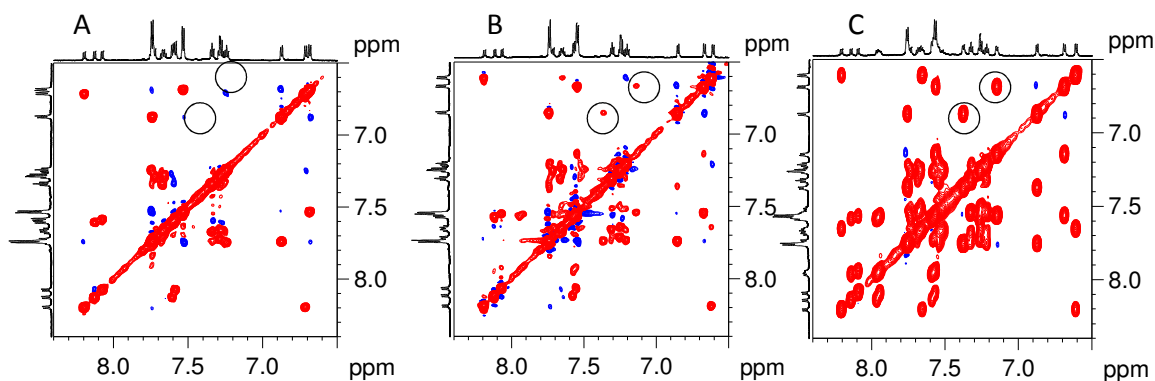


Figure 2.20: 700 MHz ROESY spectra of $[1\cdot\{\beta\text{-CD}\}]Cl_3$ at 298 K, for varying $1Cl_3$: $\beta\text{-CD}$ mole ratios, A) 1:4, B) 1:2 and C) 1:0.65. NOE and exchange cross peaks are shown in blue and red respectively. Intensity of the exchange cross peaks decreases with increase in $\beta\text{-CD}$ concentration due to the decrease in population and life time of uncomplexed $1Cl_3$.

The above discussion clearly reveals that $1Cl_3$ forms a 1:3 host-guest complex ($[1\cdot 3\{CB[7]\}]Cl_3$) with CB[7] and a dynamic 1:1 host-guest complex ($[1\cdot\{\beta\text{-CD}\}]Cl_3$) with $\beta\text{-CD}$. The difference in the complexes formed by CB[7] and $\beta\text{-CD}$ with $1Cl_3$ may be ascribed to the basic structural difference of the two host molecules. The CB[7] molecule has a

Chapter 2

pumpkin shape with symmetric portals, while β -CD has a tub shape with different portal sizes. The pumpkin structure of CB[7] helps to stabilise the guest molecule by the combined effect of two types of interactions, (i) ion-dipole interactions between the positive charges on the guest molecule and the carbonyl oxygens and (ii) the hydrophobic interactions between the guest molecule and the host cavity. The hydrophobic part of 1Cl_3 (naphthyl moiety) which resides within the CB[7] cavity and the cationic part of the guest located near the rim of the host helps to achieve strong binding. On the other hand, β -CD is composed of glucopyranose subunits with two cavity portals differing in size and the nature of the hydroxyl groups. The hydroxyl groups encircling the cavity entrances of β -CD helps to stabilize the guest molecule by hydrogen bonding interactions with the hydrophilic part of 1Cl_3 , while the hydrophobic interior of β -CD interacts with the hydrophobic part of the guest molecule. In the inclusion complex with β -CD, the wider rim of the host resides close to the phenyl rings of 1Cl_3 , hence steric effects would hinder the simultaneous approach of three β -CD molecules along the arms of 1Cl_3 .

2.3.3. Association Constant and Thermodynamic Parameters

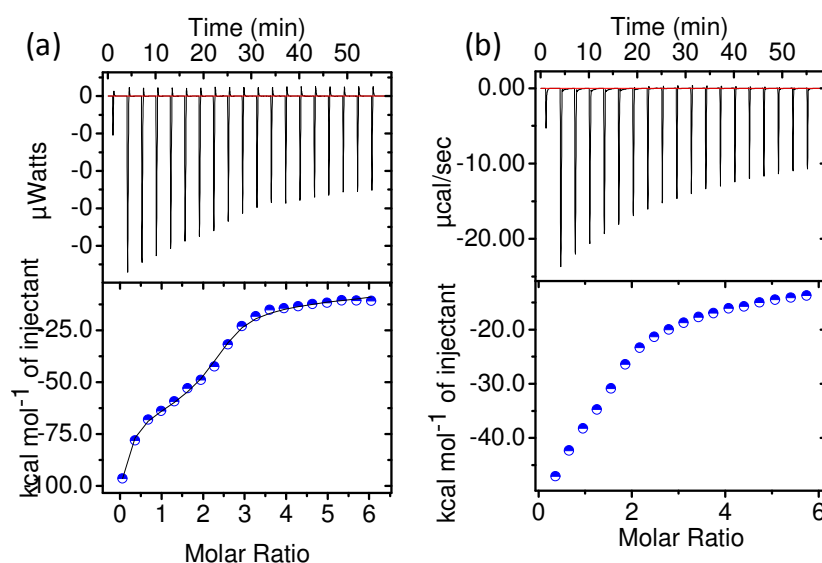


Figure 2.21: ITC profiles for the inclusion complex formation between (a) 1Cl_3 (0.116 mM) and CB[7] (3.42mM) and (b) 1Cl_3 (0.116 mM) and β -CD (3.55 mM). Raw data for the sequential injection of the hosts into 1Cl_3 in steps of 2 μL is shown in the top panel. Heat evolution on addition of the hosts is shown in the bottom panel.

Chapter 2

The host-guest complex formation between **1Cl₃** and CB[7] or β -CD and associated changes in thermodynamic parameters were investigated in aqueous solution at 298K by ITC measurements (Figure 2.21). ITC studies of the inclusion complex formation of **1Cl₃** with CB[7] and β -CD indicates binding stoichiometries of 1:3 and 1:1, respectively, which corroborates the results of NMR studies. The binding constants for the sequential binding (data was fitted to a more than one site of binding sites model) of three CB[7] molecules to **1Cl₃** determined by ITC are $K_1 = (8.3 \pm 0.16) \times 10^3 \text{ M}^{-1}$, $K_2 = (3.3 \pm 0.055) \times 10^4 \text{ M}^{-1}$ and $K_3 = (1.5 \pm 0.021) \times 10^3 \text{ M}^{-1}$ and the corresponding enthalpy changes are ($\Delta H_1 = -2.44$, $\Delta H_2 = 1.09$ and $\Delta H_3 = -1.72$) kcal/mol. Inclusion complex formation also results in a large entropic loss ($T\Delta S_1 = -11.02$, $T\Delta S_2 = -7.92$, $T\Delta S_3 = -5.99$) kcal/mol.

For host-guest complex formation between **1Cl₃** and β -CD, the fit for the one site binding model to the experimental data gives an association constant of $(1.44 \pm 0.7) \times 10^3 \text{ M}^{-1}$. The inclusion complex formation is accompanied by a large entropy loss ($T\Delta S = -8.07$ kcal/mol) and a large negative enthalpy change ($\Delta H = -7.56 \pm 0.7$ kcal/mol). The large entropy loss observed in both cases during inclusion complex formation is probably due to the release of a large number of water molecules from the host cavities. The contribution of the desolvation effect to the entropy change is expected to be more prominent compared to the effects of reduced molecular flexibility of **1Cl₃** on complex formation. The binding constant for complex formation of **1Cl₃** with CB[7] is higher than that for β -CD. NMR studies show that in [**1**•3{CB[7]}]Cl₃, the three arms of **1Cl₃** are bound by the host resulting in a fairly rigid complex, while in [**1**•{ β -CD}]Cl₃, the arms of **1Cl₃** exchange between 'bound' and 'free' states, hence the complex is not highly rigid. Binding stoichiometry and binding affinity of **1Cl₃** towards CB[7] and β -CD determined by ITC agree well with the conclusions drawn from NMR studies.

2.3.4. Photophysical studies

The UV-Visible and steady-state emission spectra of **1Cl₃** were recorded in aqueous solution and the spectral data are summarized in Table 2.1. The absorption spectrum of **1Cl₃** in water shows an intense absorption band ($\epsilon = 2.3 \times 10^5 \text{ Lmol}^{-1}\text{cm}^{-1}$) with a maximum (λ_{Max}) at 309 nm. The observed absorption band may be attributed to a π - π^* transition involving the triphenylamine and naphthyl moieties.

Chapter 2

The solvatochromic behavior of 1Cl_3 was examined in different solvents with varying polarities. As the solvent polarity increases from hexane to water, a red shift of 18 nm is observed in the absorption spectrum (Figure 2.22a). On the other hand, the emission spectrum of 1Cl_3 (λ_{Ext} of 309 nm) showed interesting changes with varying solvent polarities. In a nonpolar solvent such as hexane and others with low polarity indices (polarity index < 5.2), the emission maximum occurs at 363 nm and remains practically unchanged, whereas in more polar solvents (polarity index > 6.2), the emission maximum shifts linearly to longer wavelengths. The dependence of the emission maximum on polarity index of the solvent is indicated in Figure 2.23d. In addition, a distinctly new emission spectral pattern arises as the solvent polarity increases (Figure 2.22b). For example, emission spectra of 1Cl_3 in DMF and water show entirely new broad emission maxima at 440 and 483 nm respectively (Figure 2.23c). Earlier reports suggest that the naphthalene excimer fluorescence appears at ~ 425 nm.²²

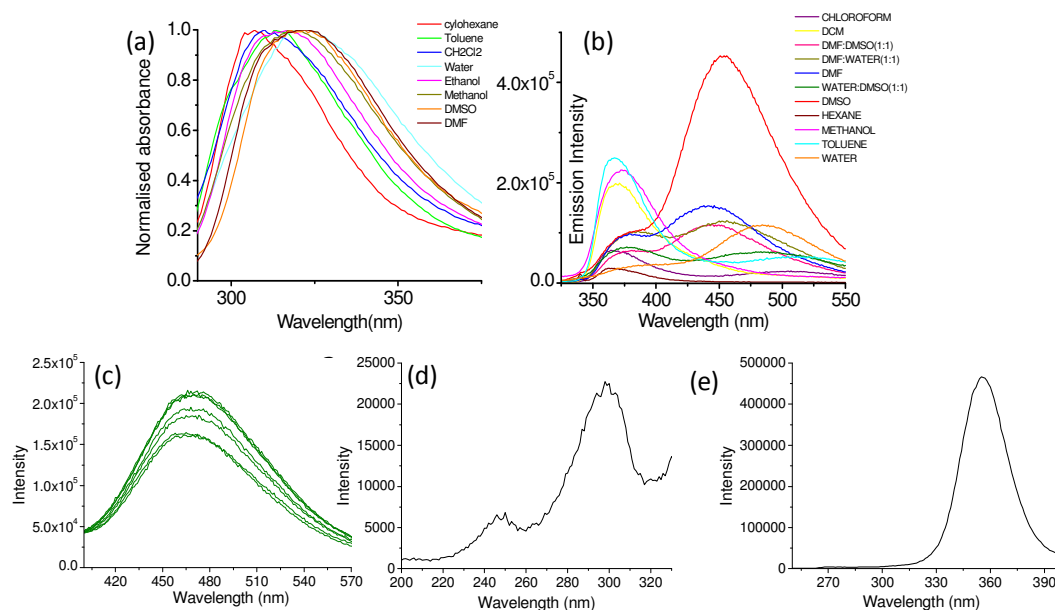


Figure 2.22: (a) Absorption spectra of 1Cl_3 in solvents of varying polarities, (b) Emission spectra of 1Cl_3 at $\lambda_{\text{ext}}=309$ nm in solvents of varying polarities. (c) Emission spectra of 1Cl_3 in aqueous solution with concentration ranging from 1.0×10^{-6} M to 1.0×10^{-4} M (d) Excitation spectra of 1Cl_3 in hexane and (e) water.

In order to verify the possibility that the new emission band observed at 483 nm arises from the naphthalene excimer fluorescence, we obtained emission spectra of 1Cl_3 in water at concentrations ranging from 1.0 – 100.0 μM (Figure 2.22). The lack of any significant

enhancement in emission intensity at ~ 480 nm implies that naphthalene excimer fluorescence cannot account for the band observed at 483 nm. Thus, the band at 363 nm arises from a locally excited (LE) state, while the additional longer wavelength emission band observed in polar solvents (483 nm in water and 454 nm in DMSO; Figure 2.22b) arises from an intramolecular charge transfer (ICT) process.²³ Excitation spectra recorded by using λ_{Ems} of 363 (in hexane) and 483 nm (in water) were distinctly different (Figure 2.22). This implies that the emitting states associated with the 363 and 483 nm emission maxima are different. The LE state is stabilized in solvents with polarity indices ≤ 5.2 , while the ICT state is stabilized in solvents with polarity indices ≥ 6.2 . The quantum yields at λ_{Ext} of 309 nm were determined for the two different emitting states of 1Cl_3 in two solvents of widely differing polarities; the observed quantum yield is 0.034 (Φ_{363}^{LE}) in hexane and 0.011 (Φ_{483}^{ICT}) in water. The decrease in the quantum yield with increase in solvent polarity has been described earlier for other analogous fluorophores.²⁴

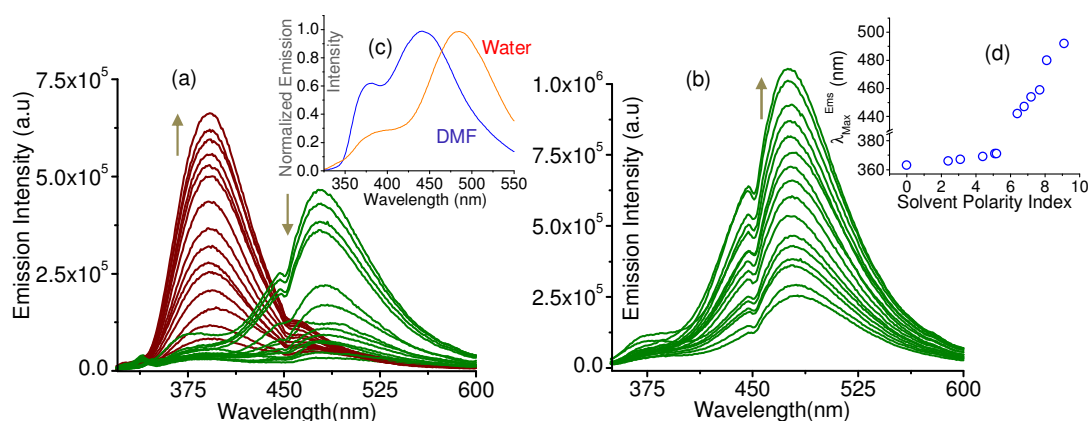


Figure 2.23: Changes in luminescence spectral pattern of 1Cl_3 on addition of increasing amounts of (a) CB[7] = 0 – 17.25×10^{-5} M and (b) $\beta\text{-CD}$ = 0 – 8.3×10^{-5} M. The 1Cl_3 concentrations are 2.08×10^{-5} M and 1.05×10^{-5} M. (c) Normalized emission spectra of 1Cl_3 in water and DMF depicting the dual emission bands and (d) plot of $\lambda_{\text{Ems}}^{\text{Max}}$ for 1Cl_3 in solvents with different polarity indices. λ_{Ext} of 309 nm was used for all measurements.

We also examined the effect of the addition of increasing amounts of CB[7] and $\beta\text{-CD}$ on the absorption and emission spectra of 1Cl_3 . On addition of three equivalents of CB[7] or $\beta\text{-CD}$, the absorption spectrum of 1Cl_3 shows distinct hyperchromic shifts, however the band maximum remains the same. On the other hand, significant differences in the emission spectral response are observed (Figures 2.23a and 2.23b). A decrease in the intensity of the emission band at 475 nm is observed on adding increasing amounts of

Chapter 2

CB[7] to an aqueous solution of 1Cl_3 . Figure 2.23a shows that for $1\text{Cl}_3:\text{CB}[7] \geq 0.12$, a new emission band appears at 388 nm, but with no further shift of the emission maximum. As discussed above, emission bands at lower wavelengths arising from LE states are observed for 1Cl_3 in solvents with polarity indices ≤ 5.2 . Literature reports have shown that the polarity of the cavity of CB[7] is similar to that of n-octanol (polarity index 3.2).²⁵ The disappearance of the emission band at 475 nm and the subsequent appearance of a new emission band at 388 nm as the concentration of CB[7] increases, confirms the inclusion of 1Cl_3 in the CB[7] cavity which has a polarity index similar to that of a non-polar solvent like n-octane thus leading to a LE state based emission. The greater rigidity of 1Cl_3 on forming the 1:3 host-guest complex ($[1\bullet 3\{\text{CB}[7]\}]\text{Cl}_3$) also favors the non-radiative pathway for the deactivation of the excited state and accounts for the increased quantum yield ($\Phi = 0.035$) for the emission band at 388 nm compared to 1Cl_3 (Table 2.1).

Table 2.1. Photo physical data of 1Cl_3 , $[1\bullet 3\{\text{CB}[7]\}]\text{Cl}_3$ and $[1\bullet\{\beta\text{-CD}\}]\text{Cl}_3$

Host-Guest Complex	λ_{abs} (nm)	λ_{em} (nm)	Φ (%)	τ av(ns) ^[e]
1Cl_3	309 ^[a]	475 ^[a]	1.1 ^[a] , 6.7 ^[b]	0.3 ^[d] , 1.43 ^[c]
$\{1\bullet 3\text{CB}[7]\} \text{Cl}_3$	305 ^[a]	388 ^[a]	3.5 ^[a]	0.80 ^[d]
$\{1\bullet\beta\text{-CD}\} \text{Cl}_3$	306 ^[a]	475 ^[a]	2.5 ^[a]	2.63 ^[c]

^[a]Measurements in water; ^[b]Measurements in glycerol; ^[c]Monitoring the emission maximum at 475 nm; ^[d]Monitoring the emission maximum at 388 nm; ^[e]Average lifetime of the excited state obtained from TCSPC studies using a nano-LED as an excitation source ($\lambda_{\text{Ext}} = 295$ nm) in water at 25°C. For all measurements $1 \leq \chi^2 \leq 1.3$.

In contrast, the emission responses of 1Cl_3 on addition of increasing amounts of $\beta\text{-CD}$ are significantly different. The intensity of the emission band at 475 nm is enhanced considerably with increasing concentration of $\beta\text{-CD}$ (Figure 2.23b). The polarity index of the cavity of $\beta\text{-CD}$ is much higher and is expected to favor an ICT process.²⁶ The emission quantum yield ($\Phi = 0.025$) in the complex with $\beta\text{-CD}$ is also higher compared to free 1Cl_3 (Table 2.1). Inclusion of even one of the three arms of 1Cl_3 by $\beta\text{-CD}$ imposes sufficient rigidity in 1Cl_3 as compared to free 1Cl_3 . This could account for the increased emission quantum yield in the $\beta\text{-CD}$ complex compared to free 1Cl_3 and the favoring of the radiative

Chapter 2

deactivation of the excited state. In order to explore this possibility further, we examined the emission behavior of 1Cl_3 in glycerol, a solvent with high polarity (polarity index 6.45) and viscosity. The high solvent viscosity is expected to decrease the molecular flexibility of 1Cl_3 significantly along with the associated non-radiative deactivation. A substantial increase in emission quantum yield ($\Phi = 0.067$) for the ICT based emission band is observed at 473 nm in glycerol when compared to that in water which is less viscous (Table 2.1).

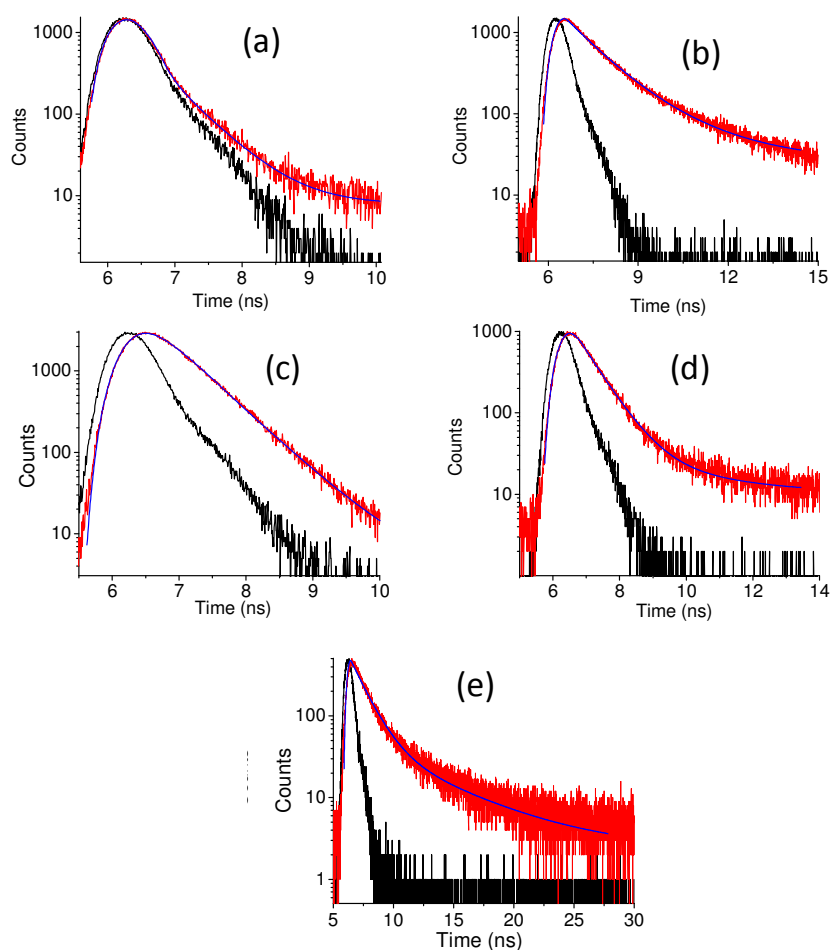


Figure 2.24: Time dependent fluorescent decay of (a) 1Cl_3 at 388 nm (b) 1Cl_3 at 475 nm (c) $1\text{Cl}_3 + \text{CB}[7]$ at 388 nm (d) $1\text{Cl}_3 + 3$ equivalents of $\text{CB}[7]$ at 475 nm (e) $1\text{Cl}_3 + 3$ equivalents of $\beta\text{-CD}$ at 475 nm.

Luminescence decay profiles following excitation at 295 nm were obtained for the excited state of 1Cl_3 in the free state and in the complexes with $\text{CB}[7]$ and $\beta\text{-CD}$ (Figure 2.24) by using time correlated single photon counting (TCSPC) technique. The decay time

Chapter 2

constants are included in Table 2.1. Both, the ICT based excited state monitored at 475 nm and the LE state monitored at 388 nm show multicomponent emission decays. This is probably due to the presence of equilibrium between different conformers in solution having slightly different emission decay time constants. In the Free State, $1Cl_3$ shows average excited state lifetimes of 0.3 (τ_{avg}^{388-LE}) and 1.43 ns ($\tau_{avg}^{475-ICT}$) at 388 and 475 nm, respectively. In the complex with CB[7] ($[1\bullet 3\{CB[7]\}]Cl_3$), the LE state at 388 nm shows τ_{avg}^{388-LE} of 0.8 ns which is higher than that observed in the free state of $1Cl_3$. On complexation with β -CD ($[1\bullet\{\beta-CD\}]Cl_3$), $\tau_{avg}^{475-ICT}$ of the ICT based excited state at 475 nm is enhanced to 2.63 ns. At 475 nm, the photon counts were too low for the $[1\bullet 3\{CB[7]\}]Cl_3$ complex, hence reliable measurements were not possible. Similarly photon counts were low for ($[1\bullet\{\beta-CD\}]Cl_3$) at 388nm. The formation of a 1:3 host-guest complex with CB[7] enhances the life time of the LE state while the 1:1 host-guest complex formation with β -CD enhances the lifetime of the ICT state with respect to that of free $1Cl_3$ along with corresponding increase in the emission quantum yield, Φ . This is in accordance with earlier reports of increase in quantum yield on inclusion complex formation.²⁷

The steady state emission studies clearly show that through appropriate choice of the host molecules (e.g. CB[7] or β -CD), it is possible to stabilize two completely different excited states in a TPA derivative in solution phase at room temperature following excitation at a particular wavelength. With CB[7], a 1:3 host-guest complex formation helps in stabilizing the LE state of $1Cl_3$ with an emission maximum at 388 nm, whereas a 1:1 host-guest complex formation with β -CD helps in stabilizing the ICT state of $1Cl_3$ with emission maximum at 475 nm. In the $[1\bullet 3\{CB[7]\}]Cl_3$ complex, all the three arms of $1Cl_3$ are trapped within host cavities of relatively low polarity, while in the $[1\bullet\{\beta-CD\}]Cl_3$ complex, a single arm of $1Cl_3$ is trapped at any given time within a host cavity of higher polarity. Thus, the differences in the mobility of $1Cl_3$ on complex formation with the two different host molecules having cavities of differing polarities, accounts for the different emission behavior observed in the two cases.

2.4. Conclusion

In this chapter we demonstrate a new TPA derivative ($1Cl_3$), which exhibits a rare dual emission property in solution at room temperature. The shorter wavelength emission band arises from a locally excited state while the longer wavelength emission band results from

Chapter 2

an intra molecular charge transfer process. Observation of dual emission from a single molecule at room temperature is rather uncommon. In presence of CB[7] and β -CD, the 1Cl_3 molecule forms inclusion complexes that are significantly different. NMR studies show that a 1:3 host-guest complex is formed on complexation with CB[7] ($[1\bullet 3\{\text{CB}[7]\}]\text{Cl}_3$), while a 1:1 host-guest complex is formed with β -CD ($[1\bullet\{\beta\text{-CD}\}]\text{Cl}_3$). The latter exists in a dynamic equilibrium in which only one of the three arms of 1Cl_3 is bound to a β -CD molecule at a given time. The two complexes also show very different emission behavior, with $[1\bullet 3\{\text{CB}[7]\}]\text{Cl}_3$ favoring emission from a locally excited state and $[1\bullet\{\beta\text{-CD}\}]\text{Cl}_3$ favoring an ICT-based excited state. The difference in the nature of complex formation and emission behavior of 1Cl_3 with the two host molecules was examined in detail by NMR, electronic and steady state fluorescence spectroscopic techniques. The differing shapes, electrostatic surface potentials of the host molecules and the differences in polarities of the two host cavities, account for the very different emission responses in the two cases.

Chapter 2

2.5. References

1. (a) Yasuda, Y.; Kamiyama, T.; Shirota, Y. *Electrochim. Acta.* **2000**, *45*, 1537; (b) Ostrauskaite, J.; Karickal, H. R.; Leopold, A.; Haarer, D.; Thelakkat, M. *J. Mater. Chem.* **2002**, *12*, 3469; (c) Zhao, L.; Lin, Y.; Liu, T.; Li, H.; Xiong, Y.; Yuan, W. Z.; Sung, H. H.-Y.; Williams, I. D.; Zhang, Y.; Tang, B. Z. *J. Mater. Chem. C.* **2015**, *3*, 4903.
2. (a) Chandra, B. P. *Indian J. Pure Appl. Phys.* **1980**, *18*, 743; (b) Wu, J.-H.; Liou, G.-S. *Adv. Funct. Mater.*, **2014**, *24*, 6422.
3. (a) Beaupré, S.; Dumas, J.; Leclerc, M. *Chem. Mater.* **2006**, *18*, 4011; (b) Shirota, Y.; Kageyama, H. *Chem. Rev.* **2007**, *107*, 953; (c) Friend, R. H.; Gymer, R. W.; Holmes, A. B.; Burroughes, J. H.; Marks, R. N.; Taliani, C.; Bradley, D. D. C.; Dos Santos, D. A.; Brédas, J. L. M.; Salaneck, W. R. *Nature.* **1999**, *397*, 121.
4. (a) Wei, P.; Bi, X. D.; Wu, Z.; Xu, Z. *Org. Lett.* **2005**, *7*, 3199; (b) Fang, Z.; Teo, T. L.; Cai, L.; Lai, Y. H.; Samoc, A.; Samoc, M. *Org. Lett.* **2009**, *11*, 1.
5. (a) Lueck, H. B.; McHale, J. L.; Edwards, W. D. *J. Am. Chem. Soc.* **1992**, *114*, 2342; (b) Meijer, G.; Berden, G.; Meerts, W. L.; Hunziker, H. E.; de Vries, M. S.; Wendt, H. R. *Chem. Phys.* **1992**, *163*, 209.
6. (a) Malagoli, M.; Bredas, J. L. *Chem. Phys. Lett.* **2000**, *327*, 13; (b) Reva, I.; Lapinski, L.; Chattopadhyay, N.; Fausto, R. *Phys. Chem. Chem. Phys.* **2003**, *5*, 3844.
7. Ranasinghe, M. I.; Varnavski, O. P.; Pawlas, J.; Hauck, S. L.; Louie, J.; Hartwig, J. F.; Goodson, T. *J. Am. Chem. Soc.* **2002**, *124*, 6520.
8. (a) Kobayashi, H.; Hama, Y.; Koyama, Y.; Barrett, T.; Regino, C. A. S.; Celeste, A.; Urano, Y. *Nano Lett.* **2007**, *7*, 1711; (b) Wang, L.; Zhao, W. J.; O' Donoghue, M. B.; Tan, W. H. *Bioconjugate Chem.* **2007**, *18*, 297.
9. (a) Browne, K. A.; Deheyn, D. D.; Brown, R. C.; Weeks, I. *Anal. Chem.* **2012**, *84*, 9222; (b) Wang, L.; Tan, W. *Nano Lett.* **2006**, *6*, 84.
10. (a) Nathani, R. I.; Moody, P.; Chudasama, V.; Smith, M. E. B.; Fitzmaurice, R. J.; Caddick, S. *Chem. Sci.* **2013**, *4*, 3455; (b) Rashidian, M.; Kumarapperuma, S. C.; Gabrielse, K.; Fegan, A.; Wagner, C. R.; Distefano, M. D. *J. Am. Chem. Soc.* **2013**, *135*, 16388.
11. (a) Xu, J.; Ma, L.; Guo, P.; Zhuang, X.; Zhu, X.; Hu, W.; Duan, X.; Pan, A. *J. Am. Chem. Soc.* **2012**, *134*, 12394; (b) Yao, L.; Zhang, S.; Wang, R.; Li, W.; Shen, F.; Yang, B.; Ma, Y. *Angew. Chem.* **2014**, *126*, 2151.

Chapter 2

12. (a) Muller, C. D.; Falcou, A.; Reckefuss, N.; Rojahn, M.; Widerhirn, V.; Rudati, P.; Frohne, H.; Nuyken, O.; Becker, H.; Meerholz, K. *Nature* **2003**, *421*, 6925, 829; (b) Zhao, Y. S.; Fu, H. B.; Hu, F. Q.; Peng, A. D.; Yao, J. N. *Adv. Mater.*, **2007**, *19*, 3554; (c) Lei, T.; Cao, Y.; Fan, Y.; Liu, C.-J.; Yuan, S.-C.; Pei, J. *J. Am. Chem. Soc.* **2011**, *133*, 6099.
 13. (a) Blakley, R. L.; DeArmond, M. K. *J. Am. Chem. Soc.* **1987**, *109*, 4895; (b) Suzuki, T.; Kuchiyama, T.; Kishi, S.; Kaizaki, S.; Takagi, H. D.; Kato, M. *Inorg. Chem.*, **2003**, *42*, 785.
 14. (a) Honda, K.; Fujishima, S. h; Ojida, A.; Hamachi, I. *ChemBioChem*. **2007**, *8*, 1370; (b) Chen, Q.; Zhang, X.; Sun, Y.; Ritt, M.; Sivaramakrishnan, S.; Fan, X. *Lab Chip*. **2013**, *13*, 2679.
 15. Sindelar, V.; Moon, K.; Kaifer, A. E. *Org. Lett.* **2004**, *6*, 2665.
 16. Foroozandeh, M.; Adams, R. W.; Meharry, N. J.; Jeannerat, D.; Nilsson, M.; Morris, G. A. *Angew. Chem. Int. Ed.* **2014**, *53*, 6990.
 17. (a) Gibson, H. W.; Yamaguchi, N.; Hamilton, L.; J. Jones, W. *J. Am. Chem. Soc.* **2002**, *124*, 4653; (b) Huang, F.; Jones J. W.; Gibson, H. W. *J. Org. Chem.* **2007**, *72*, 6573.
 18. (a) Ashton, P. R.; Baxter, I.; Fyfe, M. C. T.; Raymo, F. M.; Spencer, N.; Stoddart, J. F.; White, A. J. P.; Williams, D. J. *J. Am. Chem. Soc.* **1998**, *120*, 2297; (b) Affeld, A.; Hübner, G. M.; Seel, C.; Schalley, C. A.; *Eur. J. Org. Chem.* **2001**, 2877.
 19. (a) Zheng, B.; Klautzsch, F.; Xue. M.; Huang, F.; Schalley, C. A. *Org. Chem. Front.* **2014**, *1*, 532; (b) Cera, L.; Schalley, C. A. *Chem. Sci.* **2014**, *5*, 2560.
 20. (a) Nakashima, H.; Yoshida, N. *Org. Lett.* **2006**, *8*, 5997; (b) Corradini, R.; Dossena, A.; Galaverna, G.; Marchelli, R.; Panagia, A.; Sartor, G. *J. Org. Chem.* **1997**, *62*, 6283.
 21. (a) Rao, T. V. S. D.; Lawrence, S. *J. Am. Chem. Soc.* **1990**, *112*, 3614; (b) Catena, G. C.; Bright, F. V. *Anal. Chem.* **1989**, *61*, 905; (c) Nepal, D.; Samal, S.; Geckeler, K. E. *Macromolecules* **2003**, *36*, 3800.
 22. Chandross E. A.; Dempster, C. J. *J. Am. Chem. Soc.* **1970**, *92*, 704.
 23. (a) Diwu, Z.; Zhang, C.; Klaubert R. P.; Haughland, J. *J. Photochem. Photobiol. A* **2000**, *131*, 95; (b) Detert, H.; Schmidt, V. *J. Phys. Org. Chem.* **2004**, *17*, 1051.
 24. Woo, H. Y.; Liu, B.; Kohler, B.; Korystov, D.; Mikhailovsky, A.; Bazan, G. C. *J. Am. Chem. Soc.* **2005**, *127*, 14721.
 25. Nau, W. M.; Florea, M.; Assaf, K. I. *Isr. J. Chem.* **2011**, *51*, 559.
 26. (a) Cox, G. S.; Turro, N. J. *J. Am. Chem. Soc.*, **1984**, *106*, 422; (b) Heredia, A.; Requena, G.; Sanchez, F. G.; *J. Chem. Soc. Chem. Commun.*, **1985**, 1814.
-

Chapter 2

27. Berezin, M. Y.; Achilefu, S. *Chem. Rev.*, **2010**, *110*, 2641.

CHAPTER 3

[2]PSEUDOROTAXANE FORMATION WITH FRET- BASED LUMINESCENCE RESPONSE: DEMONSTRATION OF BOOLEAN OPERATIONS THROUGH SELF-SORTING ON SOLID SURFACE

Publication:
J. Org. Chem. 2016, 81, 8977–8987

3.1. Introduction

Supramolecular assembly formation relies on molecular recognition between groups that complement each other in terms of electrical charge and spatial orientation for driving the formation of supramolecular assemblies.¹ Thermodynamic stabilities of such assemblies are also aided by certain non-bonding interactions like [C-H...O]/[C-H...N_[NHR₁R₂]₊] and [C-H...π]/ [π-π].^{1b} Utilization of such recognition process for developing nanoscopic device has been the recent focus amongst researchers who are active in developing functional assemblies, pseudorotaxanes, rotaxanes and interlocked molecules.² Pseudorotaxanes with guest and/or host molecules, appropriately functionalized with photoactive unit(s), are found to have significance for molecular switches, logic gates, shafts, and machines.^{3,4} Assembly and de-assembly processes associated with such reversible pseudorotaxane formation from individual host and guest components could be achieved in presence of an external stimuli like media acidity/ polarity or in presence of certain ionic inputs. Formation of such threaded or inclusion complex induce controlled movement(s) of individual component(s) and achieving control in such inter-component movement(s) in a programmed fashion can actually help in mimicking the function of machines at molecular level. Further presence of an appropriate luminophore, suitably functionalized with host and/or guest fragment(s) offers the possibility of monitoring such processes based on change(s) in luminescence response(s). Förster resonance energy transfer (FRET) is a prevalent photophysical process which involves the transfer of excitation energy of an electronically excited donor molecule to an acceptor molecule at the ground state via non radiative process.⁵ Apart from this spectral overlap, distance of separation and relative spatial orientations of the donor and acceptor moieties are crucial in achieving such FRET based responses. Thus, host and or guest molecules with appropriately functionalized luminophores, that belong to a FRET pair, offers the option to monitor such pseudorotaxane formation by probing the FRET based luminescence responses. Importantly, time scale for luminescence process(es) for most organic fluorophores generally lies within nano- or pico-second time domain, which is relatively much faster than the time scales for the conformational transitions. However, use of the fluorescence based responses for monitoring the threaded complex or [2]pseudorotaxane formation as well as the associated conformational changes of the individual host or guest molecules on an supramolecular assembly formation are rather limited compared to other commonly used techniques like ¹H-NMR spectroscopy and single crystal X-ray crystallography.

Chapter 3

As an effective structural unit, at the active sites of various proteins, imidazole plays a vital role in their biological function in its protonated and non-protonated form. Crown-ether containing aromatic units offers possibilities of weak interactions like hydrogen bonding, π -stacking, cation- π and ion-dipole interactions. Use of imidazolium derivatives as a suitable guest for inclusion complex formation was demonstrated with macrocyclic hosts such as crown ether and cucurbituril derivatives.⁶

Separate studies with secondary ammonium ion derivative as guest and NO_6 -based azacrown derivatives as host, with host/guest molecules functionalized with appropriate FRET pair, reveal that the extent of an inclusion complex formation could be linked to the FRET based luminescence responses.⁷ An analysis of all these results leave us with an impression that perhaps the difference in the affinity constants for the inclusion complex formation as well as the functionalization of the guest fragments with suitable FRET pairs could help us in achieving self-sorting phenomena with different self-assembled inclusion complexes that show modified fluorescence responses for describing a Boolean logic operation.⁸ To the best of our knowledge demonstration such Logic Operation for pseudorotaxane formation is not common and only restricted to studies in solution phase.^{8,9} A variety of inclusion complexes have been explored by utilizing the synthetic self-sorting systems with binding motifs designed on the basis of hydrogen bonding, metal-ligand and π - π -stacking Interactions.¹⁰⁻¹²

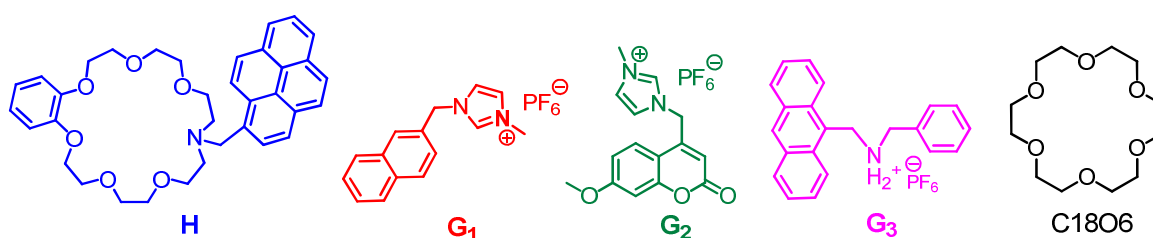


Figure 3.1: Schematic representation of the molecular components that are used for the formation of [2]pseudorotaxane.

In this chapter, we describe that the formation of two different [2]pseudorotaxane formation (**H.G₁** & **H.G₂**) in non-polar medium like dichloromethane between an NO_6 -aza crown ether derivative (**H**) as host with an appended pyrene moiety and imidazolium ion derivatives as guests being functionalized with naphthalene or coumarin moiety. Pyrene moiety is known to form FRET pairs with naphthalene as well as coumarin. This enabled us to achieve two different FRET based luminescence responses for two different inclusion complexes viz

H.G₁ & **H.G₂** (Figure 3.1). We have further utilized the higher affinity of the aza crown ether moiety (**H**) towards K⁺ for preferential formation of the coordination complex **H.K⁺** for achieving luminescence responses for demonstration of the Boolean logic operation on solid surface. To the best of our knowledge such an example is scarce in contemporary literature.

3.2. Experimental section

3.2.1. Materials

1-methyl imidazole and 2-bromo naphthalene, 4-bromomethyl-7-methoxycoumarin derivative, C18O6 were purchased and used without any further purification. All solvents were purchased from commercial suppliers and used without any further purification. Column chromatography was performed on silica gel 100-200 mesh. **H**, **G₁** and **G₃** were synthesized as per previous reported procedures.

3.2.2. Analytical Methods

Electrochemical measurements

Cyclic voltammograms were recorded using a three electrode system. A platinum electrode was used as the working electrode. A platinum wire served as the counter electrode and a saturate Ag/AgNO₃ as a reference electrode. A ferrocene/ferrocenium redox couple was used as the internal standard. All solutions were thoroughly purged with nitrogen gas prior to the electrochemical measurements.

ITC measurements

ITC experiments were performed at 25°C in dichloromethane. In each run 2 µl was injected with a stirring speed 1000 rpm into the solution of host. A control experiment was done to determine the heat of dilution by carrying the same experiment without host. Actual enthalpies were calculated by subtracting the control experiment enthalpy. All thermodynamic parameters were obtained by using one site binding model. Errors of binding constant are in the range of ±10%. Errors in ΔG amount to 0.4 kcal, while errors in ΔH and TΔS are higher due to uncertainties in the fitting procedure.

Spectral measurements

The absorption and emission spectra were acquired at room temperature (25 °C). All spectral measurements have been carried out with freshly prepared solutions in quartz cuvette of 1.0 cm path length. Fluorescence lifetimes were measured by time correlated single photon counting (TCSPC), using a nanosecond diode LED source 295 nm LED excitation source, 310 and 340 nm LASER as the light source to trigger the fluorescence decay. The decays were analysed on Data station-v6 decay analysis software. The acceptability of these fits was evaluated by χ^2 criteria and visual inspection of the residuals of the fitted function of the data. All NMR spectra were recorded with TMS as an internal standard on 500MHz FT NMR at room temperature (25 °C). Fluorescence Quantum yield (Φ_f) was determined using naphthalene and pyrene as a reference by employing the following equation,

$$\Phi_f = \Phi_f'(I_S/I_R)(A_R/A_S)(\eta_S^2/\eta_R^2)$$

in which I_i is the integrated area under the fluorescence curve, A_i denotes the absorption, η_i is the refractive index of the medium and Φ_i is the fluorescence quantum yield. The subscripts $i = S, R$ refers to the parameters corresponding to the sample and reference compound, respectively.

3.2.3. Synthesis

Synthetic procedure of 1: 1, 2-Dihydroxy benzene (3.00 g, 27.27 mmole) was dissolved in 70 ml of freshly dried DMF in two necks round bottom flask. To this solution K_2CO_3 powder (11.30 g, 81.81 mmole) was added. Then the reaction mixture turned from brown to violet colour, KI (13.60 g, 81.81 mmole) was added. This mixture was allowed to stir for 15 min, and 2-[2-(2-chloro-ethoxy)-ethoxy]-ethanol (9.10 g, 54.54 mmole) was added via a syringe at 60 °C. Then the temperature was raised up to 80 °C and allowed to stir for 5 days. The solvent was removed under reduced pressure and extracted three times with $CHCl_3$ and water. Organic layers were combined and dried over anhydrous sodium sulphate. Solvent was removed under reduced pressure to give crude product which was purified on a silica-gel column, using methanol:dichloromethane (2:98 v/v) as an eluent (**1**) as a sticky brown semisolid. 1H NMR (500 MHz, $CDCl_3$, δ ppm): 3.58 (4H, t, $J = 4.5$), 3.66 (4H, t, $J = 4.5$); 3.74–3.70 (8H, m), 3.86 (4H, t, $J = 4.5$), 4.15 (4H, t, $J = 4$), 6.89 (4H, s).

Chapter 3

Elemental analysis: Calculated for $C_{18}H_{30}O_8$: C 57.74, H 8.08; found: C, 57.67; H, 8.01. ESI-MS: calcd for $C_{18}H_{30}O_8$: 374.19, found: 397.41 $[M + Na]^+$.

Synthesis of 2: Compound (**1**) (5.40 g, 14.56 mmole) was dissolved in THF (40 ml) and 5 ml NaOH solution (10 M) was added to it at 0°C. *p*-Toluenesulfonyl chloride (9.70 g, 50.96 mmole) in 15 ml of THF was added drop wise over a period of 30 min to the reaction mixture at 0°C with vigorous stirring. The reaction was stopped after 5 days. The solvent was removed under reduced pressure and extracted three times with $CHCl_3$ and water. The organic layers were combined and dried over anhydrous sodium sulphate. Solvent was removed under reduced pressure to give crude product. This was purified on a silica-gel column, using $CH_3OH:CH_2Cl_2$ (2:98 v/v) as an eluent with the yield of (**2**) 7.75 g, 78.0%, as a sticky brown mass. 1H NMR (500 MHz, $CDCl_3$, δ ppm): 2.41 (6H, s), 3.59 (4H, t, $J = 4.0$), 3.69–3.63 (8H, m), 3.82 (4H, t, $J = 5.0$), 4.13 (4H, t, $J = 5.0$), 6.90 (4H, s), 7.31 (4H, d, $J = 8.0$), 7.79 (4H, d, $J = 8.5$). ^{13}C -NMR: 150.7, 147.0, 134.8, 131.8, 129.8, 128.0, 123.4, 116.2, 72.5, 71.5, 70.5, 23.3. Elemental analysis: Calculated for $C_{32}H_{42}O_{12}S_2$: C 56.29, H 6.20, S 9.39; found: C 56.18, H 6.14, S 9.31. ESI-MS: Calcd. For $C_{32}H_{42}O_{12}S_2$: 682.21, found: 683.40 $[M+H]^+$.

Synthesis of H: Compound (**2**) (1.00 g, 1.46 mmole) was dissolved in 5 ml of freshly distilled CH_3CN in two neck round bottom flask. Pyrene methyl amine hydrochloride (0.43 g, 1.60 mmole) was added followed by five drops of triethylamine to get a clear solution. To this stirred solution K_2CO_3 (2.20 g, 16.00 mmole), KI (0.40 mg, 2.40 mmole) and total 30 ml of solvent was added. The reaction mixture was refluxed for 18 hr. Solvent was removed under reduced pressure and extracted three times with $CHCl_3$. Combined organic layer were dried over anhydrous sodium sulphate. The crude product was purified by passing through alumina column using hexane: $CHCl_3$ (2:8 v/v) as an eluent, to yield (**H**) as a sticky brown mass. Yield : 490 mg (60%) Sticky brown mass. 1H NMR (500 MHz, $CDCl_3$, δ ppm): 2.73 (4H, t, $J = 5.5$ Hz), 3.43–3.49 (8H, m), 3.57-3.62 (4H, m), 3.71 (4H, t, $J = 4.5$ Hz), 3.95-4.00 (4H, m), 4.15 (2H, s), 6.76 (4H, d, $J = 4.8$ Hz), 7.76-7.87 (4H, m), 7.90-7.93 (2H, m), 7.95-8.01 (2H, m), 8.48 (1H, d, $J = 9$ Hz). ^{13}C NMR (125 MHz, $CDCl_3$, ppm): 149.1, 131.3, 130.9, 130.7, 129.9, 128.3, 127.5, 127.1, 127.1, 125.8, 125.0, 124.9, 124.8, 124.4, 121.6, 114.6, 71.1, 70.6, 69.9, 69.6, 69.3, 58.3, 54.2. HRMS (ESI-TOF) m/z : $[M + H]^+$ calculated for $C_{35}H_{40}NO_6$ 570.2811; Found 570.2850.

Chapter 3

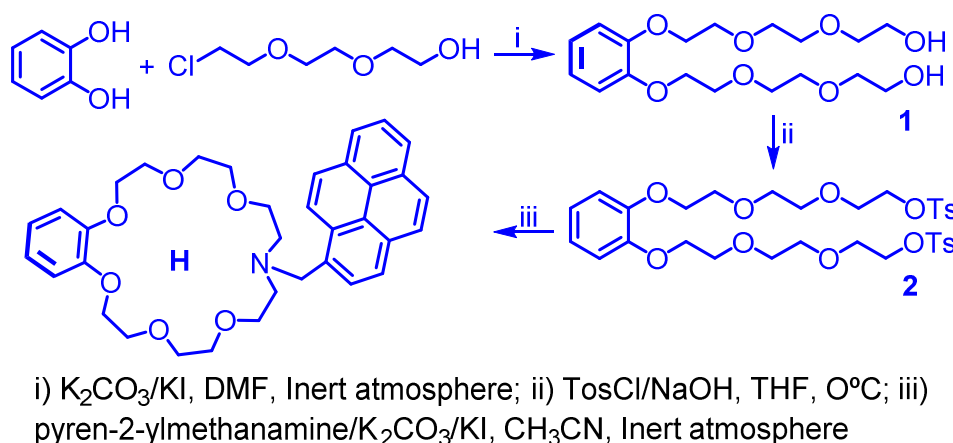
Synthetic procedure of G₁: The methodology adopted for the synthesis of G₁ was followed from earlier literature.¹³ (500 mg, 2.26 mmol) of bromomethyl naphthalene and (185 g, 2.26 mmole) of 1-methyl imidazole was dissolved in 30 ml of dry toluene and refluxed for 24 hr. Then the reaction mixture was cooled. The white sticky solid which was settled in the bottom was separated out and washed several times with cold toluene to give the bromide salt. Finally anion exchange in water using NH₄PF₆ gave the desired PF₆⁻ salt of G₁. White powder solid. Yield: 670 mg (80%). ¹H NMR (500 MHz, CD₃CN, δ ppm): 3.84 (3H, s), 5.50 (2H, s), 7.39 (1H, s), 7.45 (1H, s), 7.47 (1H, d, J = 5Hz), 7.60-7.62 (2H, m), 7.93-8.00 (4H, m), 8.52 (1H, s). ¹³C NMR (125 MHz, CD₃CN, ppm): 36.0, 53.0, 122.4, 124.0, 125.6, 127.0, 127.1, 127.8, 128.0, 128.2, 129.1, 131.2, 133.2, 133.3, 136.2. HRMS (ESI-TOF) m/z : [M - PF₆]⁺ calculated for C₁₅H₁₅N₂⁺, 223.1235; Found 223.1230. Melting point - 85 °C.

Synthetic procedure of G₂: A solution of 1-methyl imidazole (184 mg, 2.22 mmol) and 4-(bromomethyl)-7-methoxy-2H-chromen-2-one (600 mg, 2.22 mmol) in 50 mL of toluene was refluxed until a large amount of insoluble product occurred. The insoluble compound was isolated and washed with toluene. Then the insoluble residue was treated with aqueous solution of NH₄PF₆. White precipitate appeared after overnight stirring. Precipitate was washed with cold water. Yield: 760 mg (82%). ¹H NMR (500 MHz, CD₃CN, δ ppm): 3.88 (3H, s), 3.95 (3H, s), 5.55 (2H, s), 5.78 (1H, s), 6.89 (1H, s), 6.94 (1H, d, J = 10 Hz), 7.40 (2H, d, J = 5 Hz), 7.50 (1H, d, J = 10 Hz), 8.66 (1H, s). ¹³C NMR (125 MHz, CD₃CN, ppm): 36.3, 48.9, 55.9, 101.4, 110.9, 112.5, 117.4, 123.1, 124.5, 125.1, 137.0, 148.2, 155.6, 160.1, 163.5. HRMS (ESI-TOF) m/z: [M - PF₆]⁺ calculated for C₁₅H₁₅N₂O₃⁺, 271.1083; Found 271.1078. Melting point - 182 °C.

Synthetic procedure of G₃: Benzylamine (0.50 g, 5.20 mmol) was added to anthracene-9-carbaldehyde (1.07 g, 5.20 mmol) dissolved in dry methanol (30 ml), and the reaction mixture was stirred vigorously at room temperature. After 24 h, the reaction mixture was cooled to 0°C. NaBH₄ was added portionwise to the stirred cooled reaction mixture and was allowed to reach the room temperature, stirred for 2 h. The solvent was removed under reduced pressure, the residue was extracted three times with CHCl₃ and water, and the organic layers were combined and dried over anhydrous sodium sulphate. The solvent was removed under reduced pressure to give the crude product, which was purified on a column chromatography with CH₃OH/CHCl₃ (4:96, v/v) as the eluent. The compound was isolated as a sticky brown solid and acidified with HCl in acetone (20 ml) and stirred for 2

Chapter 3

h. Finally anion exchange in water using NH_4PF_6 gave the desired PF_6^- salt of **G**₃. Yield : 450 mg (60%). Light yellow crystalline solid. ^1H NMR (500 MHz, DMSO-*d*₆, δ ppm): 9.62 (2H, broad signal), 8.77 (1H, s), 8.25 (2H, d, $J = 10.0$ Hz), 8.17 (2H, d, $J = 10.0$ Hz), 7.70-7.69 (2H, m), 7.60 (4H, t, $J = 8.0$ Hz), 7.51-7.50 (3H, m), 5.12 (2H, s), 4.50 (2H, s). ^{13}C NMR (125 MHz, DMSO-*d*₆, ppm): 42.0, 51.3, 123.5, 124.6, 125.9, 127.4, 129.2, 129.5, 129.6, 130.2, 131.0, 131.3, 132.4. HRMS (ESI-TOF) m/z : $[\text{M} - \text{PF}_6^-]^+$ calculated for $\text{C}_{22}\text{H}_{20}\text{N}^+$, 298.1590; Found: 298.1573. Melting point - 185 °C.



Scheme 3.1: Schematic representation of synthesis of **H**.

3.3. Results and Discussions

The inclusion complex formation between **H** and **G**₁ or **G**₂ was examined in details by ^1H & ^{13}C NMR spectroscopy. Thermodynamic parameters for the binding processes of inclusion complex formation were evaluated from data obtained from ITC studies. The luminescence properties of the individual host, guest and inclusion complexes were investigated by steady state and time resolved emission studies. Energies of the highest and lowest occupied energy levels were evaluated from their respective ground state redox potential and spectroscopic data.

3.3.1. Photophysical studies

The absorption spectrum of **G**₁ in dichloromethane showed an intense absorption band ($\epsilon = 2.4 \times 10^4 \text{ Lmol}^{-1}\text{cm}^{-1}$) with a maximum at 280 nm (Figure 3.2a). The absorption spectrum of **H** was also recorded in dichloromethane and this revealed three maxima at 314 ($\epsilon = 1.14 \times 10^4 \text{ Lmol}^{-1}\text{cm}^{-1}$), 328 ($\epsilon = 2.65 \times 10^4 \text{ Lmol}^{-1}\text{cm}^{-1}$) and 344 nm ($\epsilon = 3.89 \times 10^4 \text{ Lmol}^{-1}\text{cm}^{-1}$).

Chapter 3

$^1\text{cm}^{-1}$) (Figure 3.2b). The absorption spectrum recorded for a 1:1 mixture of **H** and **G₁** in dichloromethane medium was basically a summation of the individual spectrum of **H** and **G₁** (Figure 3.2c). This suggests that there was no significant interaction between host and guest molecule in the ground electronic state on an assembly formation. The host molecule **H** showed a very weak emission ($\Phi = 0.009$) bands at 378, 397, 416 nm, which are characteristic of the pyrene moiety on excitation at any one of these three (314, 328, and 344 nm). Relative emission quantum yields were evaluated using pyrene as the standard. Low emission intensity of **H** is attributed to the photo induced electron transfer (PET) process involving the lone pairs of electrons of the tertiary N_{Amine} -atom the NO_6 -aza crown ether moiety as the donor to the π system of the photo-excited pyrene unit.^{12a,17} Fluorescence spectrum was recorded for **G₁** in CH_2Cl_2 medium shows a band at 340 nm ($\Phi = 0.229$; $\lambda_{\text{Ext}} = 277$ nm; naphthalene was used as reference).

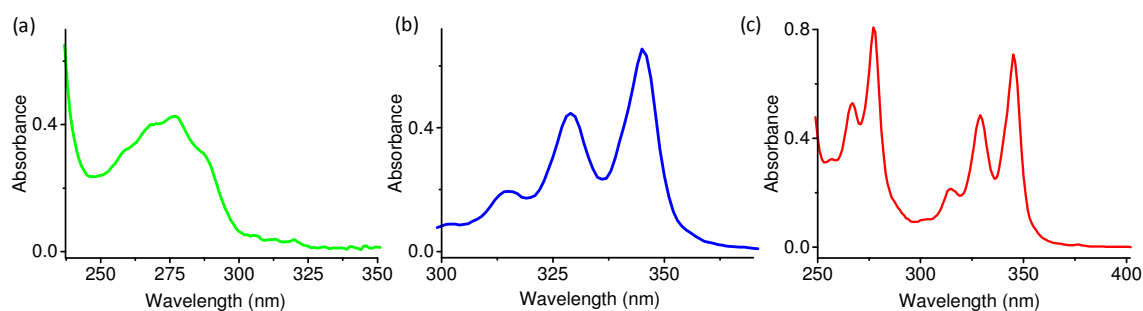


Figure 3.2: UV-Vis spectra of (a) **G₁** (1.68×10^{-5} M), (b) **H** (1.68×10^{-5} M), (c) **H**:**G₁** at mole ratio of 1:1 in dichloromethane solution at room temperature. Concentrations used (1.68×10^{-5} M).

Interestingly, emission spectrum of **G₁** has a substantial spectral overlap with the electronic spectrum of **H** (Figure 3.4b), which is one of the essential prerequisite for an efficient FRET process between two interacting fluorophores. Other factors for an efficient FRET process being the favourable distance between the donor and acceptor ($10\text{\AA} - 100\text{\AA}$) and their suitable spatial orientation for achieving the appropriate orientation of the transition dipole of the donor and acceptor fluorophores.^{5b}

In order to check the possibility of any inclusion complex formation between **H** and **G₁** and any plausible FRET based emission response involving the donor (naphthalene in **G₁**) and acceptor (pyrene in **H**) fluorophores, equimolar mixture of two molecular components (**G₁** and **H**) were allowed to mix in CH_2Cl_2 medium. This solution on excitation with 277 nm (naphthalene absorbed predominantly at this wavelength) showed distinct pyrene based emission bands in the region 378 to 420 nm, which could only be explained on the basis of

Chapter 3

a FRET-based energy transfer. Control experiment performed with equimolar mixture of **H** and unsubstituted naphthalene did not show any such FRET based emission response under identical experimental conditions.(Figure 3.3).

This tends to suggest a host-guest adduct formation with favorable spatial orientation that favors the FERT process. 1,3-disubstituted imidazolium salt is known to form an inclusion complex with DBC24O8 or its derivatives through intermolecular H-bond formation.^{14,15} Observed FRET-based emission response also supported the formation of such an inclusion complex, as H-bonding interactions that were important for inclusion complex formation was expected to engage the lone pairs of electron of the tertiary nitrogen of the aza-crown ether moiety with effective interruption of the PET process that was initially responsible for the low emission quantum yield of the pyrene moiety in **H**. Interestingly, a substantially low emission quantum yield was observed for naphthalene moiety ($\Phi = 0.04$; $\lambda_{\text{Ext}} = 277$ nm) when **G**₁:**H** molar ratio was $\sim 1:20$. Thus, the emission of the donor naphthalene moiety of **G**₁ in inclusion complex (**H.G**₁) was substantially low as compared to that for **G**₁ alone. Systematic emission titration in CH₂Cl₂ medium ($\lambda_{\text{Ext}} = 277$ nm) revealed that for increasing [**H**], a gradual decrease in naphthalene based emission with concomitant increase in pyrene based emission was observed.

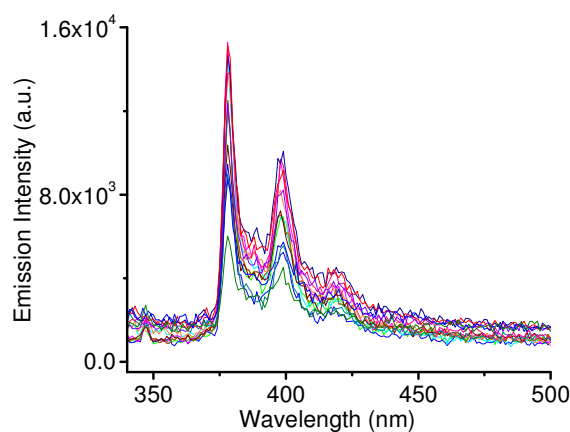


Figure 3.3: Control experiment performed with equimolar mixture of **H** and unsubstituted naphthalene under identical experimental conditions λ_{ext} at 277 nm. Concentrations used of **H** 1.75×10^{-6} M and unsubstituted naphthalene imidazolium (0 - 7.75×10^{-4} M).

This further corroborated our presumption about the FRET process for the possible inclusion complex **H.G**₁. Sensitized emission of the acceptor fluorophore (pyrene) with increased quantum yield ($\Phi = 0.059$; $\lambda_{\text{Ext}} = 277$ nm) confirmed an efficient FRET process

Chapter 3

involving naphthalene (in \mathbf{G}_1) as donor and pyrene (in \mathbf{H}) as acceptor on formation of a host-guest adduct ($\mathbf{H.G}_1$) formation (Figure 3.4a). Absence of any FRET based emission response for control experiments confirm that the H-bonding interactions in $\mathbf{H.G}_1$ not only stabilize adducts formation, but also favors the appropriate spatial orientation of the donor acceptors fluorophore for an efficient FRET process. Emission spectra for \mathbf{H} alone in CH_2Cl_2 were also recorded using $\lambda_{\text{Ext}} = 277 \text{ nm}$, which showed a much weaker emission as compared to that was observed for $\mathbf{H.G}_1$ for any comparable concentration of \mathbf{H} (Figure 3.5).

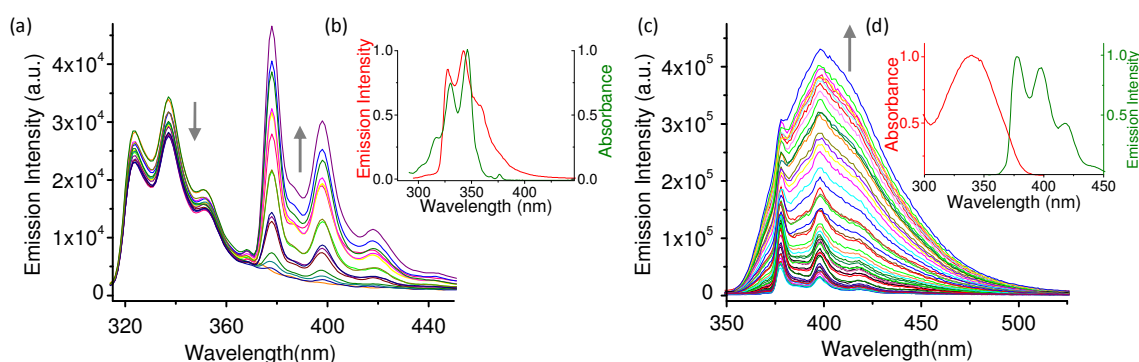


Figure 3.4: (a) Fluorescence spectra of \mathbf{G}_1 ($2.0 \times 10^{-7} \text{ M}$), in dichloromethane upon addition of increasing concentration of \mathbf{H} ($0 - 8.3 \times 10^{-5} \text{ M}$), $\lambda_{\text{Ext}} = 277 \text{ nm}$, slit-1/1, (b) Overlap spectra for the emission spectrum of \mathbf{G}_1 (red) and absorption spectrum of \mathbf{H} (green), (c) Changes in luminescence spectral pattern of \mathbf{H} ($1.68 \times 10^{-6} \text{ M}$) on addition of increasing amounts of \mathbf{G}_2 ($0 - 8.3 \times 10^{-5} \text{ M}$). $\lambda_{\text{Ext}} = 314 \text{ nm}$, slit-1/1, (d) Overlap spectra for the emission spectrum of \mathbf{H} (green) and absorption spectrum of \mathbf{G}_2 (red).

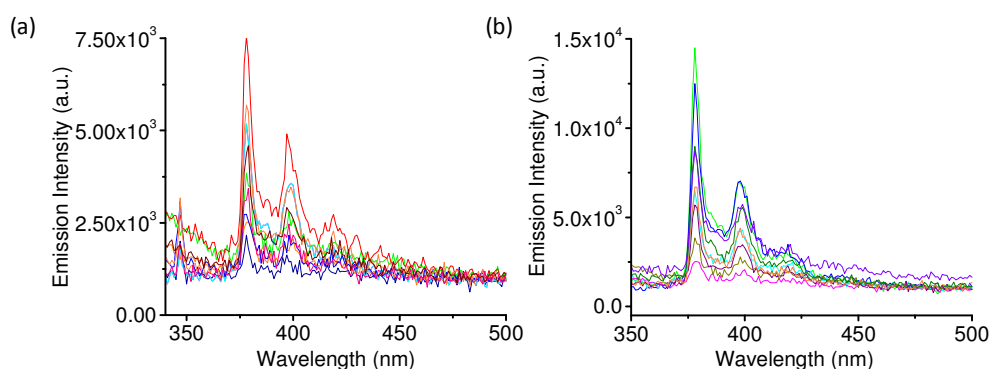


Figure 3.5: Emission spectra for \mathbf{H} alone in CH_2Cl_2 λ_{ext} at (a) 277 nm (b) 314 nm . Concentrations used for \mathbf{H} ($1.75 \times 10^{-6} \text{ M} - 1.75 \times 10^{-4} \text{ M}$).

Chapter 3

Optical spectral studies with **G**₂ revealed absorption and emission band with maxima at 340 and 400 nm (λ_{Ext} of 340 nm), (Figure 3.6a), respectively, and absorption band showed a definite spectral overlap with the emission spectrum of **H** which was appropriate for a FRET based emission responses on formation of a possible host-guest adduct **H.G**₂ (Figure 3.4d). Analogous studies, as it was performed with **G**₁, were performed with **H** as host and **G**₂ as guest molecules in identical experimental conditions. Emission titrations were performed in CH₂Cl₂ medium maintaining [**H**] as 1.68×10^{-6} M and varying [**G**₂] ($0 - 8.3 \times 10^{-5}$ M) and these showed a steady growth in emission intensity with a maximum at 400 nm ($\lambda_{\text{Ext}} = 314$ nm) on gradual increase in [**G**₂]. It is worth mentioning that at 314 nm, pyrene moiety is predominantly excited. Emission spectra recorded for pure **G**₂ in CH₂Cl₂ solution (using $\lambda_{\text{Ext}} = 314$ nm) for any comparable concentration of **G**₂ were much weaker. Further, the possible decrease in the emission band for donor pyrene moiety in **H.G**₂ was masked by the more prominent increase in the emission band of the coumarin moiety (Figure 3.4c).

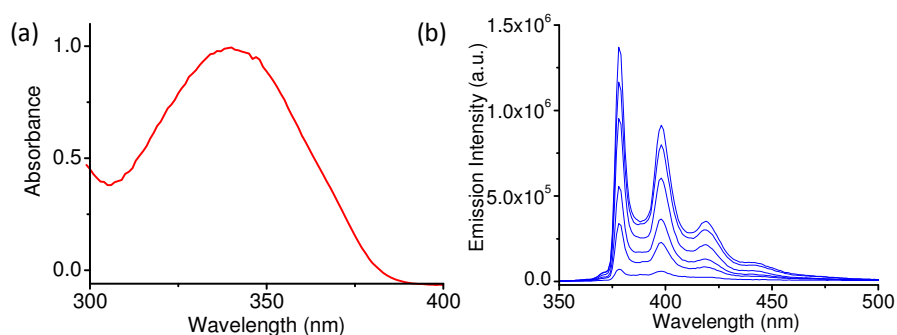


Figure 3.6: UV-Vis spectra of (a) **G**₂ (6.67×10^{-5} M) in dichloromethane at room temperature, (b) Control experiment performed with of **H** and increasing concentration of unsubstituted coumarin under identical experimental conditions λ_{ext} at 314 nm.

Figure 3.4d clearly reveals that the coumarin moiety in **G**₂ has no significant absorption at 314 nm. All these data and the observed enhancement in coumarin-based emission ($\Phi = 0.21$) (compared to that for pure **G**₂, $\Phi = 0.076$) on excitation of the pyrene fragment at 314 nm in the hydrogen-bonded adduct **H.G**₂, signify an efficient FRET-based process involving the donor pyrene fragment and the acceptor coumarin unit. Control experiments in CH₂Cl₂ solution having equimolar mixture of **H** and unsubstituted coumarin were performed using λ_{Ext} of 314 nm and no such increase in coumarin based emission was observed (Figure 3.6b). This confirmed the effective FRET based process between pyrene

as donor to coumarin as acceptor in **H.G₂** adduct. The excitation spectra monitored on the emission band of 1:1 complex for **H:G₁** (378 nm) and 1:1 complex for **H:G₂** (400 nm) showed the shape of the excitation spectra matching with its corresponding donor absorption spectra, suggesting that energy transfer takes place to the acceptors from the donor chromophore in both of the system and proves the excitation energy transfer mechanistic pathway (Figure 3.7).

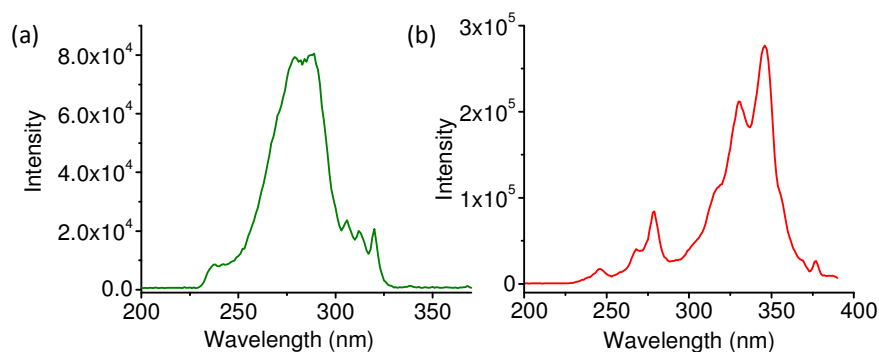


Figure 3.7: Excitation spectra recorded of 1:1 molar mixture of (a) **H.G₁** and (b) **H.G₂** in dichloromethane at room temperature.

3.3.2. Time resolved emission studies

Time correlated single photon counting (TCSPC) studies were performed for individual components as well as for the host-guest assembly in the CH₂Cl₂ solution for developing a better insight about the FRET processes. The fluorescence lifetimes of the individual components (**H**, **G₁** and **G₂**) and corresponding host-guest adducts (**H.G₁** and **H.G₂**) are provided in the table 3.1. On excitation at 295 nm (LED) a bi-exponential decay profile was observed for **G₁**, $\tau_1 = 4.7 \pm 0.08$ ns (18.3 %) and $\tau_2 = 10.54 \pm 0.04$ ns (81.7%). The 10.54 ns component was anticipated for the naphthalene moiety. Similar bi-exponential decay profile was also observed for **H**, $\tau_1 = 6.29 \pm 0.01$ ns (12.75%) and $\tau_2 = 28.54 \pm 0.003$ ns (87.25%). Emission decay profile for 1:1 mixture of **H** and **G₁** was monitored at 340 nm following excitation at 295 nm (λ_{Max} for naphthalene moiety). (Figure 3.8). Data presented in table 3.1 clearly reveal that on predominant excitation of the donor (naphthalene) moiety, there is a distinct decrease in the donor component with a substantial increase component for the acceptor lifetime in the overall emission decay profile. This further supports the FRET based ET from naphthalene moiety to pyrene moiety in the host-guest adduct (**H.G₁**). We failed to resolve if there had been any rise time component in the

Chapter 3

overall decay profile for **H.G₁**, which could be due to a much faster ET transfer than the fluorescent decays of both the donor and the acceptor.

Table 1. Summary of time resolved lifetime details. Measurements are done in dichloromethane. In case of **H + G₁/G₂** (1:1) molar mixture are used and for all measurements $1 \leq \chi^2 \leq 1.2$.

System	λ_{Ext} (nm)	λ_{Mon} (nm)	τ (ns)
H	310	378	$\tau_1 = 6.3 \pm 0.01$ (12.75%); $\tau_2 = 28.54 \pm 0.003$ (87.25%)
G₁	295	340	$\tau_1 = 4.7 \pm 0.08$ (18.28%); $\tau_2 = 10.54 \pm 0.04$ (81.72%)
G₂	340	410	$\tau_1 = 0.596 \pm 0.007$ (86.84%); $\tau_2 = 4.46 \pm 0.04$ (13.16 %)
H + G₁	295	378	$\tau_1 = 6.4 \pm 0.1$ (8.09%); $\tau_2 = 30.0 \pm 0.04$ (91.91%)
H + G₂	310	410	$\tau_1 = 1.35 \pm 0.08$ (66.32 %); $\tau_2 = 21.54 \pm 0.05$ (33.68 %)

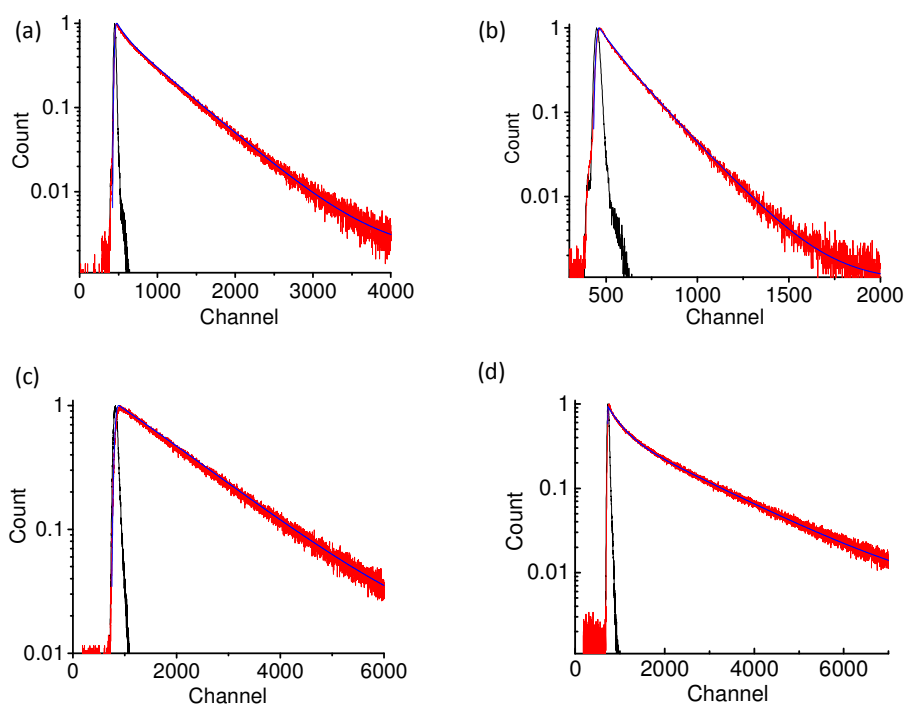


Figure 3.8: Time dependent fluorescent decay of (a) **H** monitored at 378 nm, using 310 nm excitation (b) **G₁** monitored at 340 nm, using 295 nm excitation (c) (1:1) molar mixture of **H + G₁** at 378 and (d) (1:1) molar mixture of **H + G₁** at 340 nm using 295 nm excitation.

Chapter 3

Data presented in table 3.1 clearly reveal that on predominant excitation of the donor (naphthalene) moiety, there is a distinct decrease in the donor component with a substantial increase component for the acceptor lifetime in the overall emission decay profile. This further supports the FRET based ET from naphthalene moiety to pyrene moiety in the host-guest adduct (**H.G₁**). We failed to resolve if there had been any rise time component in the overall decay profile for **H.G₁**, which could be due to a much faster ET transfer than the fluorescent decays of both the donor and the acceptor. Energy transfer efficiency was evaluated to be 52.25%, while Förster distance (R_0) was evaluated as 30.2Å for **H.G₁** solution. Similar studies were also performed with a solution of **G₂** and data were compared with that recorded for an equimolar mixture of **H** and **G₂** in CH₂Cl₂ medium ($\lambda_{\text{Ext}} = 310$ nm; $\lambda_{\text{Mon}} = 410$ nm) (Table 3.1). On excitation at 310 nm (pyrene absorbs predominantly) for equimolar mixture **H.G₂** solution, a substantial decrease in the donor (pyrene) component with subsequent increase in the acceptor (coumarin) component was observed for λ_{Mon} at 410 nm (Figure 3.9).

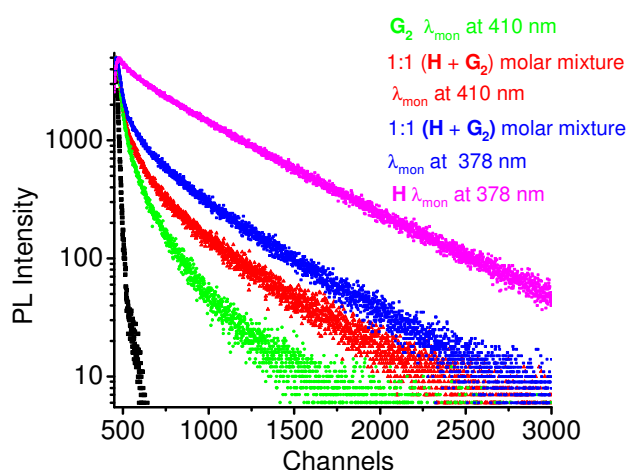


Figure 3.9: Time dependent fluorescent decay in dichloromethane of **H** monitored at 378 nm (pink) using 310 nm excitation, **G₂** monitored at 410 nm (green) using 340 nm excitation, (1:1) molar mixture of **H** + **G₂** monitored at 378 nm (blue) using 310 nm excitation and (1:1) molar mixture of **H** + **G₂** monitored at 410 nm (red) using 310 nm excitation.

Based on the time-resolved emission data, energy transfer efficiency and Förster distance (R_0) were evaluated as 69.37% and 14.12Å, respectively. Data derived from the emission decay profile also enabled us to evaluate the ET rates, which were found to be 1.2×10^8 s⁻¹ for **H.G₁** and 8.81×10^7 s⁻¹ for **H.G₂**. FRET based energy transfer for the host-guest adducts (**H.G₁** and **H.G₂**) ensures that donor and acceptor fluorophores are within the

Chapter 3

interacting distances with favorable transitional dipole moments for respective donor/acceptor fluorophore. Also, the calculated interchromophoric distances between naphthalene and pyrene in **H**:**G**₁ complex is found to be 30.10 Å, whereas the interchromophoric value for **H**:**G**₂ complex was found to be 10.6 Å. Considering the fact the FRET mechanism is effective only when the interchromophoric distances are above 10 Å. Therefore we believe that in our proposed system FRET mechanisms prevail.

3.3.3. NMR studies

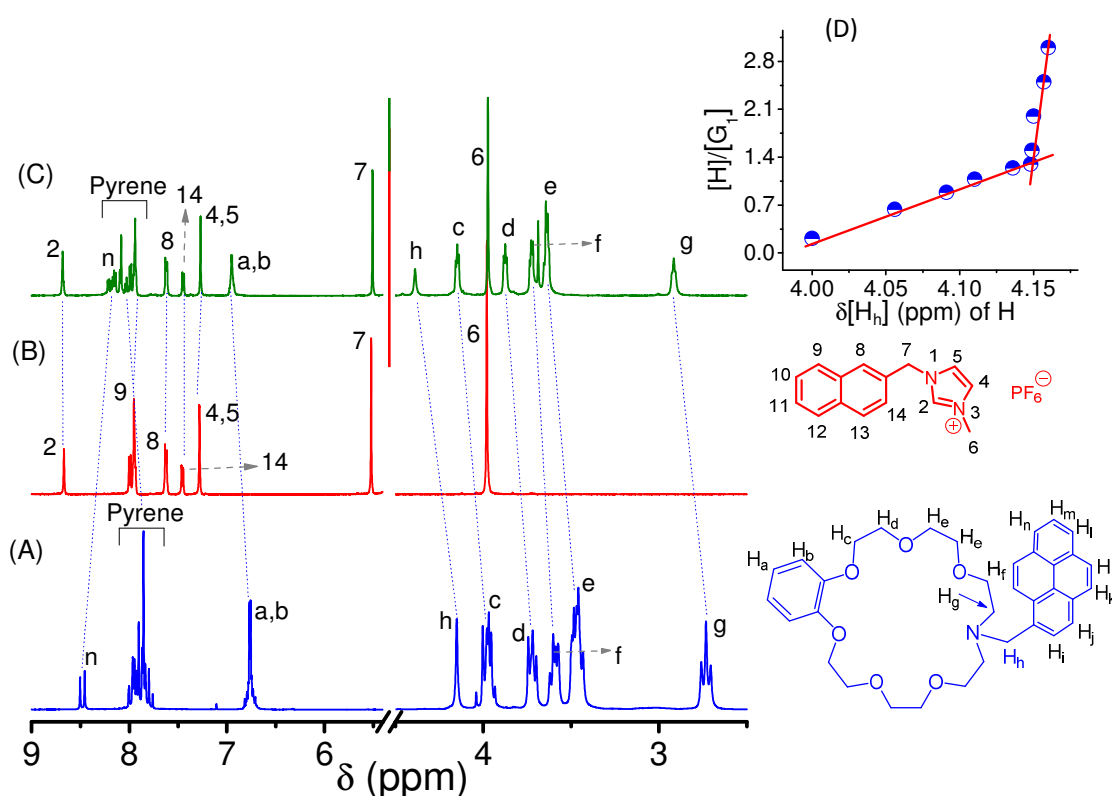


Figure 3.10: Partial ¹H NMR spectra of (A) 5.27 × 10⁻³ M of **H**, (B) 5.27 × 10⁻³ M **G**₁, (C) equimolar mixture of **H** and **G**₁ in CD₂Cl₂ (500 MHz) and (D) mole ratio plot for the complexation of **H** with **G**₁ using Δδ (ppm) for the H_n proton in **H**.

The complexation of aza crown-based host (**H**) with two different imidazolium based guest molecules (**G**₁ and **G**₂) in CD₂Cl₂ were studied in details using ¹H NMR spectroscopic studies. It is well documented that derivatives of imidazolium cation can form inclusion complexes with macrocyclic host molecules like derivatives of DB24CO8 via H-bonding.¹⁶ Analogous binding constants ($K_a \sim 10^3 \text{ M}^{-1}$ in acetonitrile at 25°C) are reported for bis(benzimidazolium)ethane and dibenzylammonium cations,¹⁷ towards DBC24O8. In our

Chapter 3

earlier studies we have established that NO₆-based aza-crown ether derivative, specifically **H**, formed stable inclusion complexes with secondary ammonium ion.⁷ It is also well documented that dilute solution of imidazolium ions exist as highly dissociated naked ions in solution.^{16,17} In 1,3-disubstituted imidazolium salts, all protons on the imidazolium ring are quite acidic due to an effective delocalization of the positive charge over the entire imidazolium ring. These acidic hydrogen atoms also participate in H-bond [(C-H)_{imidazolium}...O_{Crown}] formation involving the lone pair of electrons of the oxygen/nitrogen atoms on the azacrown moiety and this accounts for the stability of the adduct formed.

Let us first discuss the results of ¹H NMR spectral studies involving **H** and **G**₁. ¹H NMR spectra of **G**₁ (5.27 × 10⁻³ M) were recorded in CD₂Cl₂ in absence and presence of varying concentration of **H** (0 – 15.07 × 10⁻³ M). At room temperature, only one set of signals were observed in the ¹H NMR spectrum of the solution having equimolar amount of **H** and **G**₁ (Figure 3.10C), which implied that the equilibrium kinetics were fast and rapid exchange between complexed and uncomplexed species happened within the NMR timescale. No further change was observed when addition **H** was added (even for [**H**]:[**G**₁] ≥ 1:2). This confirmed that the equilibrium was achieved at these concentrations for **H** and **G**₁. For **H**, majority protons show downfield shifts (Δδ_{Ha,b} = 0.21 ppm, Δδ_{Hc} = 0.18 ppm, Δδ_{Hd} = 0.15 ppm, Δδ_{He} = 0.18 ppm, Δδ_{Hg} = 0.20 ppm, Δδ_{Hf} = 0.14 ppm and Δδ_{Hh} = 0.27 ppm) on formation of the adduct **H.G**₁. In case of **G**₁, the signal for the H₈ proton experiences a marginal upfield shift (Δδ_{H8} = -0.01) in **H.G**₁ compared to free compound **G**₁. Relatively higher downfield shifts are evident for H_h and H_g and these supports H-bond/electrostatic interaction between the lone pair of electrons of N_{Amine}^H and the imidazolium ion on **H.G**₁ adduct formation.

Presumably, H₈ proton lies little in the shielded environment due to its proximity and the ring current of the pyrene ring in **H**. H₂ proton of the imidazolium moiety is acidic and expected to be downfield shifted on formation of (H₂)_{imidazolium}...O/N_{Crown} H-bonding. As anticipated, a downfield shift of 0.03 ppm for H₂ proton is observed. Relatively smaller shift is presumably due to a weak H-bond interaction. Similarly, a weak H-bond interaction is also observed for H₇ (Δδ_{H7} = 0.03) proton. Most other naphthalene ring protons in **H.G**₁ have appeared in the same region as that for most pyrene protons and thus, it is difficult to assign the shift for any such individual protons. Little but definite upfield shifts are observed for H₉ (Δδ = -0.04) and H₁₄ (Δδ = -0.02) protons. All these tend to suggest a π-π stacking interaction involving **H**_{Pyrene} moiety and **G**_{Naphthalene} moieties. Interestingly, π-π

Chapter 3

stacking interactions are operational over a distance that also favours the FRET process, as it is observed in steady state emission studies. Downfield shifts for H₂ proton suggest the formation of a threaded complex for **H**.**G**₁. Nonetheless, ¹H NMR studies enabled us to understand the relative orientation of the guest molecule (**G**₁) in **H**.**G**₁ adduct.

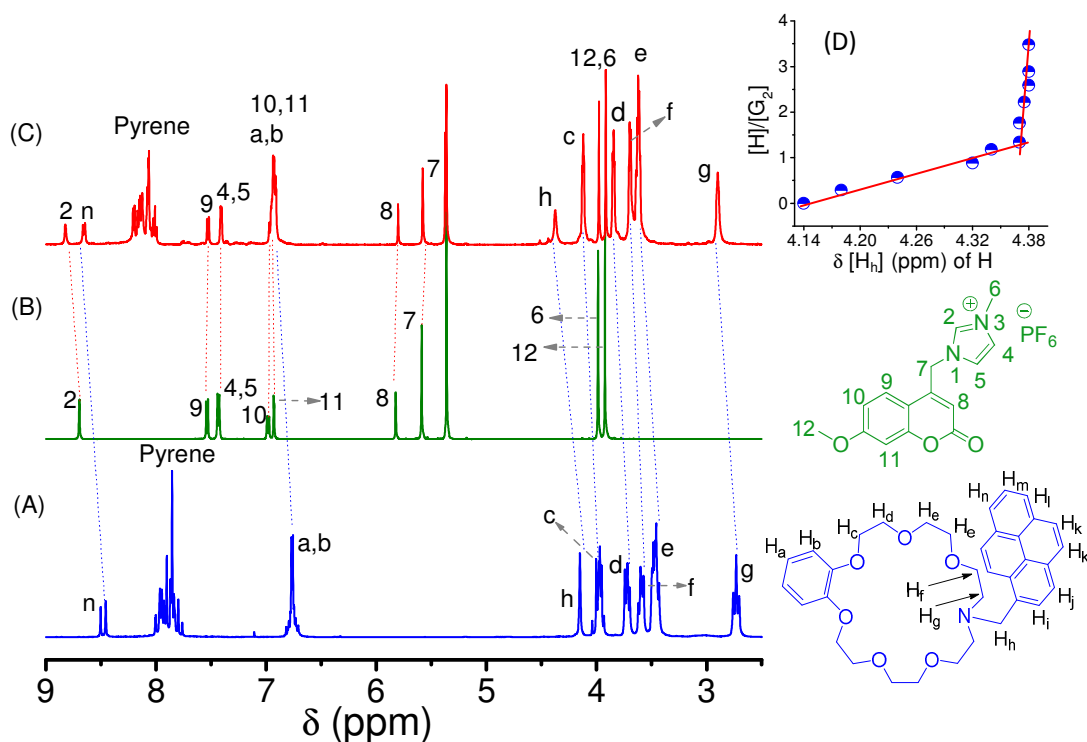


Figure 3.11: Partial ¹H NMR spectra of (A) 4.42×10^{-3} M of **H**, (B) 4.42×10^{-3} M of **G**₂, (C) the equimolar mixture of **H** and **G**₂ in CD₂Cl₂ (500 MHz) and (D) mole ratio plot for the complexation of **H** with **G**₂ using $\Delta\delta$ (ppm) for the H_h proton in **H**.

As most prominent shift is observed for H_h of the host (**H**), systematic changes in the $\Delta\delta_{H_h}$ is plotted as a function of varying **[H]:[G**₁**]** with systematic changes in **[H]** (Figure 3.10D). A clear breakpoint appears at **[H]:[G**₁**]** = 1.31, which further suggests a 1:1 inclusion complex formation. After validating the 1:1 binding stoichiometry the formation constant was evaluated as $(1.82 \pm 0.03) \times 10^3 \text{ M}^{-1}$ by analyzing the sequential changes in chemical shift value of H_h at various concentrations of **H** and this is indicative of the moderate affinity towards imidazolium ions.

Systematic ¹H NMR titrations were also carried out for another guest **G**₂. As it is observed for **G**₁, only one set of proton NMR signals is observed (Figure 3.11C) and this confirms a fast exchange process within the NMR time scale. Most prominent down filed shifts are

Chapter 3

observed for H_n ($\Delta\delta_{Hn} = 0.22$ ppm) and H_g ($\Delta\delta_{Hg} = 0.17$ ppm). Ethylene glycol chain protons show a little downfield shift in the presence of G_2 , $\Delta\delta_{Hc} = 0.15$ ppm, $\Delta\delta_{Hd} = 0.10$ ppm, $\Delta\delta_{He} = 0.16$ ppm, $\Delta\delta_{Hf} = 0.12$ ppm, $\Delta\delta_{Hg} = 0.17$ ppm, $\Delta\delta_{Hh} = 0.24$ ppm. As anticipated, downfield shift ($\Delta\delta_{H2} = 0.12$ ppm) is observed also for H_2 ($\Delta\delta_{H2} = 0.12$ ppm), which confirms H-bonding interaction between O_{Crown} and acidic H_2 proton on imidazolium ring. Appreciable downfield shift was observed for H_n ($\Delta\delta_{Hn} = 0.20$ ppm), $H_{a,b}$ ($\Delta\delta_{Ha,b} = 0.18$ ppm), proton. Binding stoichiometry of 1:1 was evaluated from the plot of systematic changes in the $\Delta\delta_{Hh}$ with changes in $[H]:[G_2]$ with systematic changes in $[G_2]$ (Figure 3.11D), while formation constant for $H.G_2$ is evaluated as $(1.17 \pm 0.03) \times 10^3 M^{-1}$ from the Benesi-Hildebrand (B-H) plot (Figure 3.12b). Changes for all other protons for H and G_2 in $H.G_2$ are almost similar as it is observed in case of $H.G_1$. This justifies almost similar formation constant for two respective inclusion complexes, $H.G_1$ and $H.G_2$.

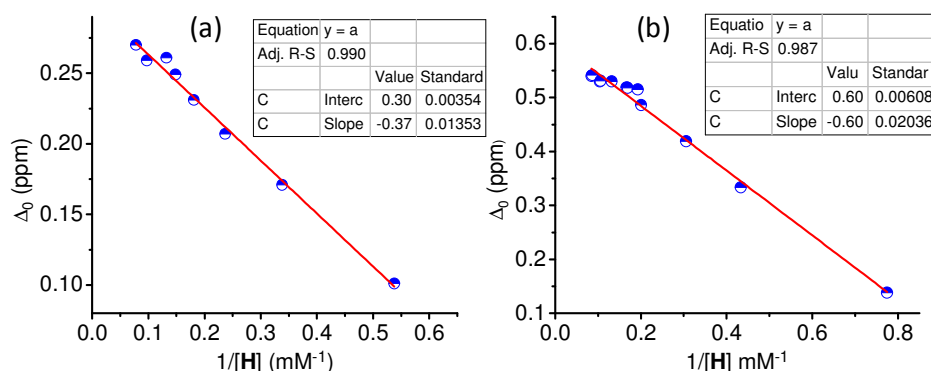


Figure 3.12: B-H plot for (1:1) molar mixture of (a) H and G_1 (b) H and G_2 from NMR.

To gain insight into the molecular interactions and the spatial orientations of the individual components in the host-guest assembly, we performed 2D NMR studies. NOESY experiments are generally well suited for this purpose, even though the COSY peaks are more intense at the concentrations used. In NOESY spectrum recorded for equimolar mixture of H and G_1 , the spatial distance between interacting protons must be less than 5 \AA to observe cross peaks. The NOESY spectrum of an equimolar mixture of H and G_1 in CD_2Cl_2 gave an intense cross peaks between the H_7 proton of G_1 and the pyrene protons of H (Figure 3.13A). These cross peaks are evidence for the inclusion complex between H and G_1 .

Chapter 3

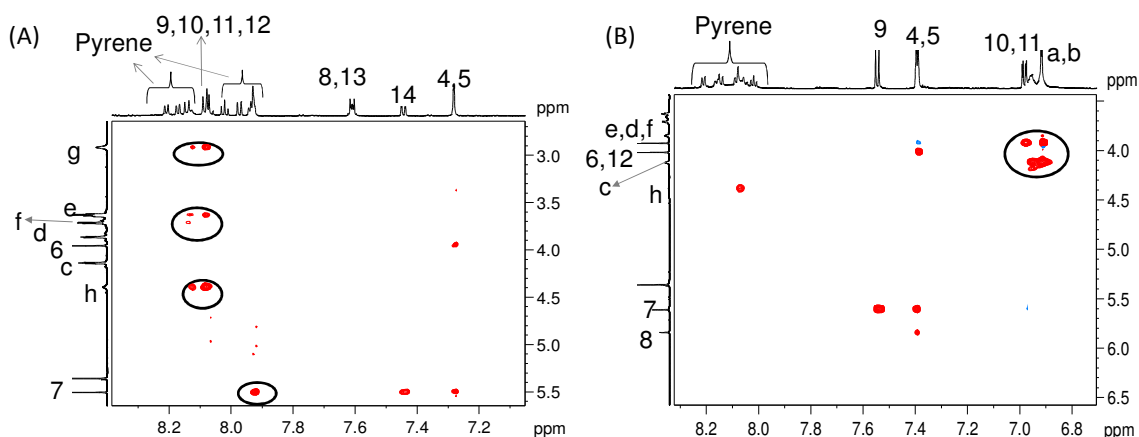
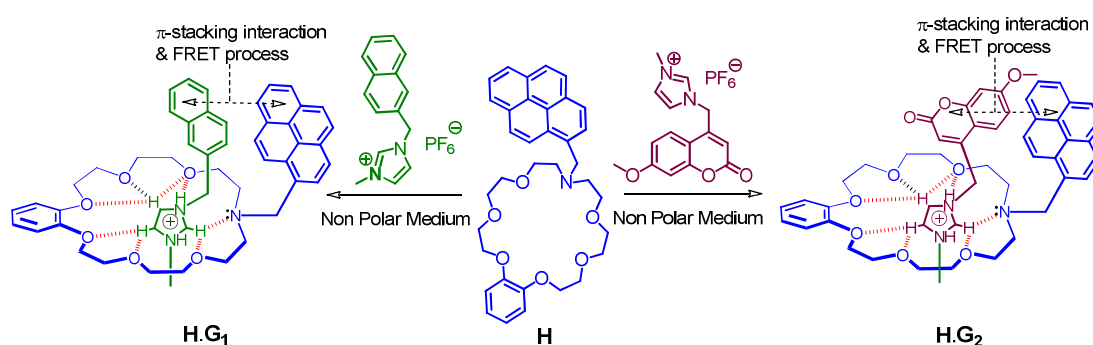


Figure 3.13: Correlation of the aromatic protons of imidazolium units with the ethylenoxy protons of the **H** unit in the NOESY spectrum in CD_2Cl_2 with (A) **G**₁, (B) **G**₂.

Moreover, the presence of cross peaks of $\text{H}_{9,10,11,12}$ of **G**₁ with H_g of **H** (ethylenoxy protons) clearly shows the interactions between **G**₁ and **H**. Again, strong correlation was observed between $\text{H}_{9,10,11,12}$ protons of **G**₁ with H_h of **H**. Weak cross peaks are also observed between $\text{H}_{9,10,11,12}$ of **G**₁ and certain protons ($\text{H}_{e,f}$) of the crown ether moiety (Figure 3.13A). These data clearly establish the formation of a threaded complex for the host-guest adduct **H.G**₁. The NOESY spectrum of equimolar mixture of **H** and **G**₂ also shows intense cross peaks between $\text{H}_{a,b}$ of **H** and $\text{H}_{6,12}$ of the imidazolium residue of **G**₂. Cross peaks are also observed between $\text{H}_{10,11}$ of the imidazolium residue and the H_c protons of the **H** (Figure 3.13B). This observation can be interpreted as a spatial proximity of the crown ether cavity with the imidazolium residue (Scheme 3.2).



Scheme 3.2: Proposed molecular structure for **H.G**₁ and **H.G**₂ with spatial proximity between two FRET pairs, namely naphthalene-pyrene and pyrene-coumarin in **H.G**₁ and **H.G**₂, respectively.

ESI-mass spectra of complexes confirm the formation of 1:1 complex. Mass spectrum recorded for **H** and **G**₁ (with $[\text{H}]:[\text{G}_1]$ is 1:2) showed a signal for m/z of 791, which could be

attributed to ($\mathbf{H} + \mathbf{G}_1 - \text{PF}_6^+$) while that for \mathbf{H} and \mathbf{G}_2 appeared at 985 for ($\mathbf{H} + \mathbf{G}_2 + \text{H}^+$). Thus, mass spectral data also corroborated our findings of fluorescence and ^1H NMR spectral studies.

3.3.4. Electrochemical studies

In order to check the thermodynamic feasibility of the FRET process, HOMO and LUMO energy levels of respective fluorophores were evaluated from the data available from electrochemical studies along with the information derived from absorption/emission spectra.

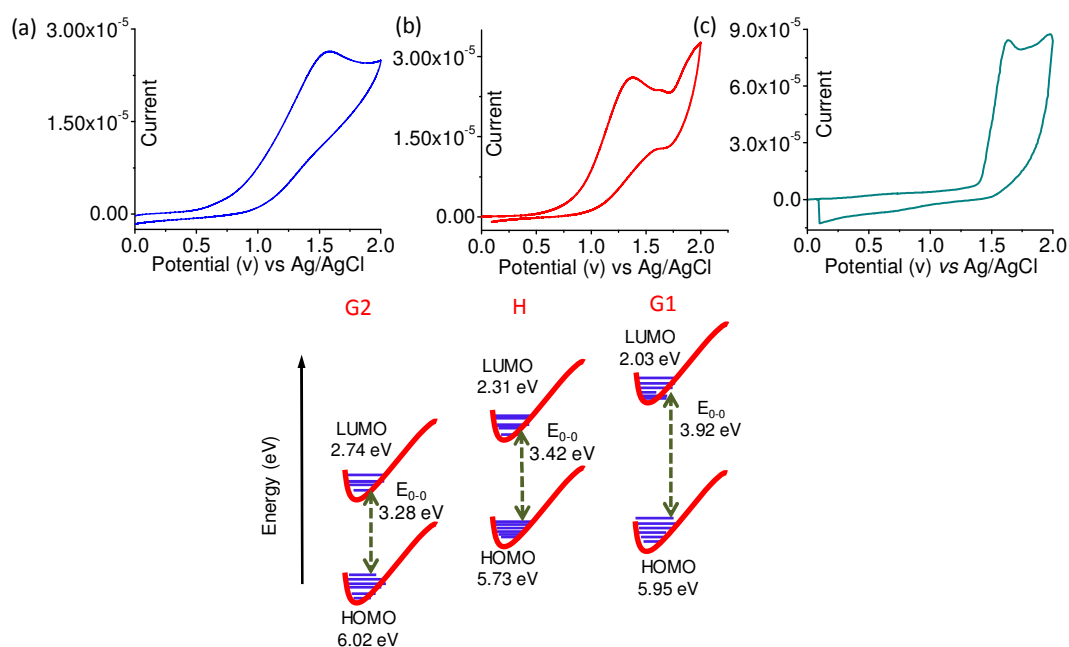


Figure 3.14: The cyclic voltammograms of (a) \mathbf{H} (blue), (b) \mathbf{G}_1 (red), (c) \mathbf{G}_2 (cyan blue) measured in $\text{CH}_2\text{Cl}_2/\text{Bu}_4\text{NPF}_6$ using a three electrode cell system with a Pt micro disc as the working electrode with 100 mV s^{-1} scan rate. Schematic representation of the electrochemical energy levels of \mathbf{H} , \mathbf{G}_1 , \mathbf{G}_2 and the feasibility of intramolecular energy transfer between \mathbf{G}_1 to \mathbf{H} and \mathbf{H} to \mathbf{G}_2 .

The intersection of the absorption and emission spectra for each fluorophore in \mathbf{H} , \mathbf{G}_1 and \mathbf{G}_2 was used for calculating the ΔE_{0-0} value for the respective fluorophore. Oxidation potential data for \mathbf{H} , \mathbf{G}_1 and \mathbf{G}_2 were evaluated from electrochemical studies of respective species and these are linked to HOMO levels of the acceptor fluorophores. Oxidation potential for \mathbf{G}_1 , \mathbf{H} and \mathbf{G}_2 are found to be 1.56 V, 1.34 V and 1.634 V, respectively (Figure 3.14). E_{0-0} value for three respective chromophores could be used for evaluating HOMO-LUMO energy gap and these values, 3.92 (\mathbf{G}_1), 3.42 (\mathbf{H}) and 3.28 (\mathbf{G}_2) eV (Figure 3.14).

Chapter 3

Subsequently, HOMO-LUMO energy gap and $E_{0,0}$ value for the respective luminophore are used for estimating the LUMO energy for the three chromophores (Figure 3.14). These values clearly confirm the thermodynamic feasibility of the energy transfer process involving naphthalene as donor and pyrene as acceptor in **H.G₁** and pyrene as donor and coumarin as acceptor in **H.G₂**.

3.3.5. Isothermal Titration Calorimetry studies

Binding constants and thermodynamic data for the inclusion complex formation were evaluated from ITC studies. In a typical ITC experiment, a solution of the host (**H**) is placed in the sample cell and is treated stepwise with small amounts of a solution of the guest **G₁** or **G₂**. The titrations were performed at 298 K in CH_2Cl_2 (Figure 3.15). Experimental data confirmed formation of 1:1 binding stoichiometry for both complexes. A control experiment was carried out in each run to determine the heat of dilution by injecting a solution of host or guest into CH_2Cl_2 containing no guest or host molecules, respectively. The heat of dilution evaluated in the control experiment was subtracted from the apparent heat of the reaction measured in the titration experiments for calculating the net reaction heat. As anticipated, the heat of reaction was found to decrease after each injection of the host molecules. The binding constants for the formation of **H.G₁** and **H.G₂** were $(2.61 \pm 0.015) \times 10^3 \text{ M}^{-1}$ ($K_{\text{H.G}_1}$) and $(1.27 \pm 0.16) \times 10^3 \text{ M}^{-1}$ ($K_{\text{H.G}_2}$), respectively. Binding processes were governed by negative enthalpy changes: $\Delta H^\circ = -14.48 \pm 0.032 \text{ kcal mol}^{-1}$ for **H.G₁** and $\Delta H^\circ = -12.91 \pm 0.059 \text{ kcal mol}^{-1}$ for **H.G₂**. Entropy changes were observed for the formation of both inclusion complexes ($T\Delta S = -10.22 \text{ kcal/mole}$ for **H.G₁**, $T\Delta S = -7.92 \text{ kcal/mole}$ for **H.G₂**). Calculated binding free energies are $-4.258 \text{ kcal mol}^{-1}$ and $-4.983 \text{ kcal mol}^{-1}$ for **H.G₁** and **H.G₂** respectively. It is well-known that the association process arising from conformational freedom and the desolvation effect is entropically favoured ($T\Delta S < 0$). Whereas, the negative enthalpy contributions ($\Delta H < 0$) arise mainly from the electrostatic, hydrogen-bonding, π - π , and Van der Waals interactions upon complexation.¹⁸ Binding constants obtained from ITC experiments agreed well with the data evaluated from ^1H NMR titration data in CD_2Cl_2 . Stoichiometry and binding constants values obtained from these methods closely resembled each other. The ^1H NMR titration data gave a relatively low binding constant value, compared to the value obtained from ITC measurements.

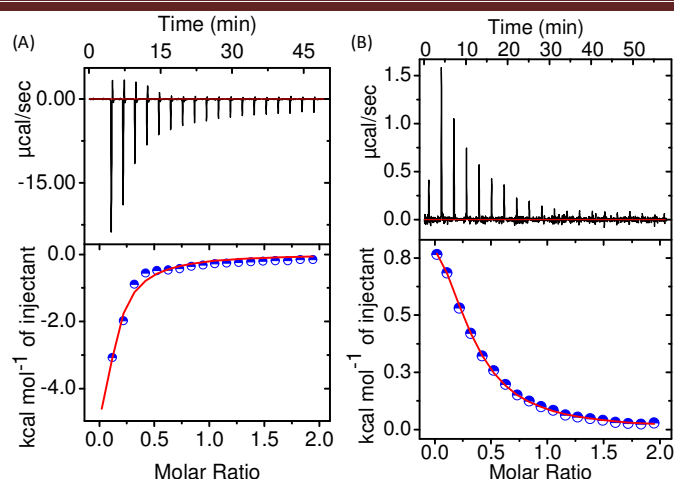


Figure 3.15: ITC titration profiles for the inclusion complex formation between (A) **H** (5 mM) and **G₁** (51.08 mM) and (B) **H** (7 mM) and **G₂** (71.09 mM) in dichloromethane (298K). Raw data for the sequential injection of the hosts into **G₁**, **G₂** in steps of 2 μL is shown in the top panel. Heat evolutions on addition of the hosts are shown in the bottom panel.

3.3.6. Self-sorting

Nature efficiently uses the principle of self-sorting phenomena to generate complex, functional architectures.¹⁹ In the past decades, this has been effectively utilized for achieving a varieties of supramolecular systems and the self-organization of nano structures.^{19a,d,20a} Various factors such as recognition motifs, size, shape, thermodynamic and kinetic binding parameters, stoichiometry are responsible for self-discrimination.^{20,19c} It is well documented that K^+ forms strong complexes with crown ether and its derivatives.²¹ Binding constant for **H.K⁺** ($K_{H,K^+} = (7.2 \pm 0.07) \times 10^4 M^{-1}$) was evaluated by fluorescence titration and this was higher by an order of magnitude compared to those for **H.G₁** and **H.G₂**. Taking advantages of the differences in the binding affinities of **G₁/G₂** and K^+ towards **H**, the higher binding affinity of K^+ towards **C1806** ($K_a = 1.3 \times 10^6 M^{-1}$) in methanol at 25 °C)^{21a} as compared to **H** (*vide infra*) and reversible formation of host-guest complexes, associated luminescence responses could be correlated for demonstrating the Boolean operations.⁹ Emission spectra of **H** was recorded in presence of K^+ , $K^+ + \mathbf{C1806}$ or Cl^- (in given sequence) following excitation at 314 nm (λ_{Ext}^{Pyrene}). Spectra recorded for **H** in presence of K^+ showed strong pyrene based emission on formation of K^+H , as coordination to K^+ would have interrupt the PET process. As anticipated, spectra recorded on further addition of **C1806** or Cl^- to the solution of K^+H showed complete quenching of the pyrene based luminescence; as both **C1806** or Cl^- was expected to bind preferentially

to K^+ and caused the complete decomplexation with simultaneous generation of free **H** (Figure 3.16).

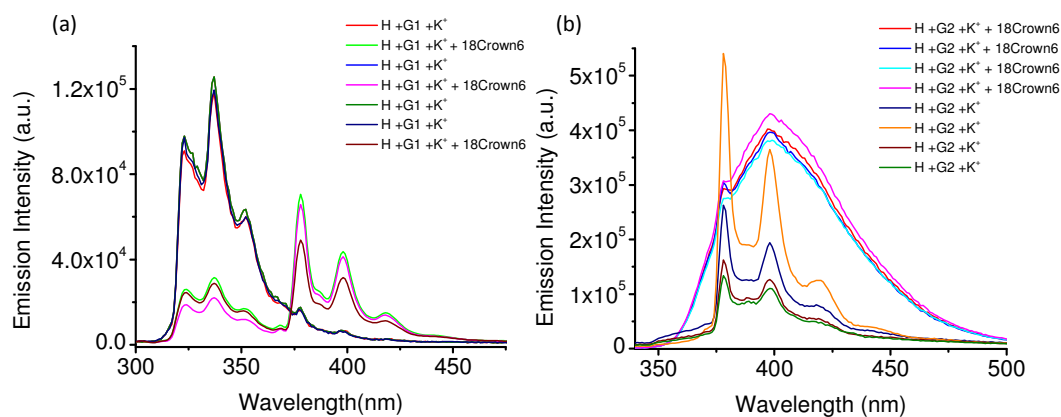


Figure 3.16: Fluorescence spectra for reversible complexation of (a) **H** and **G₁** λ_{ext} at 277 nm, (b) **H** and **G₂** λ_{ext} at 314 nm.

As discussed earlier, **H.G₁** (1:2 mole equivalence) solution on excitation at 277 nm (predominantly naphthalene-based excitation) shows a FRET based fluorescence response that is characteristic for the pyrene moiety of **H** (Figure 3.17a). Binding affinity of K^+ towards **H** is much higher as compared to **G₁** and this led to the dethreading of **H.G₁** with concomitant formation of **HK⁺** and free **H**. This results a complete quenching of the pyrene based emission (Figure 3.17a), which is understandable if we consider that **HK⁺** has insignificant absorbance at 277 nm. Identical emission responses were anticipated and observed when K^+ was added to the solution of **H.G₂**, as this also led to the formation of **HK⁺** and free **G₂** (Figure 3.17b). For both these instances, pyrene based emission could only be observed when 314 nm ($\lambda_{\text{Ext}}^{\text{Pyrene}}$) was used as excitation wavelength (Figure 3.17b).

Earlier discussions (*vide infra*) have established that K^+ has a higher affinity towards **C18O6** as compared to that for **H**. A solution having **H + G₁ + K⁺** showed emission spectra that is characteristic for **G₁**, a typical naphthalene based emission as λ_{Ext} of 277 nm ($\lambda_{\text{Ext}}^{\text{Naphthalene}}$) was used as excitation wavelength. However, on addition of **C18O6**, formation of **C18O6K⁺** prevailed and this led to generation of free **H** for **G₁** to form a threaded complex **H.G₁** with a FRET-based emission response that is characteristic for pyrene moiety for λ_{Ext} of 277 nm. This fluorescence response clearly helped in demonstrating the self-sorting phenomenon. Similar observation was also observed when

Chapter 3

Cl^- was used instead of **C18O6**, as Cl^- formed a tight ion-pair with K^+ and this led to the de-complexation of the K^+ from K^+H with complete quenching of pyrene based emission (λ_{Ext} of 277 nm; Figure 3.17c). ESI mass spectra obtained for a 1:1:1 mixture of **H**, **G₁** or **G₂** and K^+ showed m/z signal at 608, which signified the formation of HK^+ and clarified that K^+ could actually replace **G₁** or **G₂** from the complex **H.G₁** and **H.G₂** respectively.

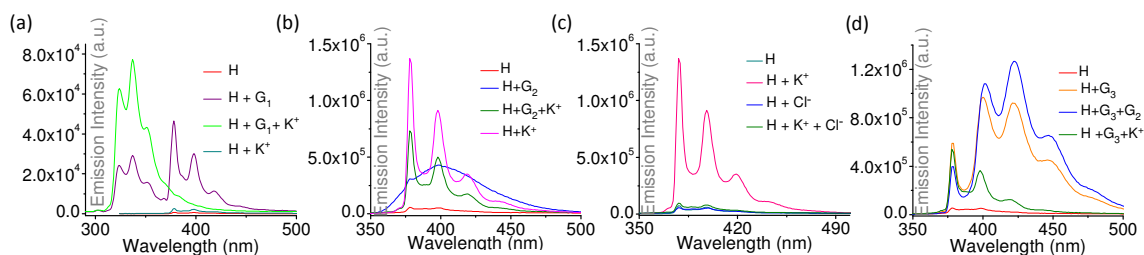


Figure 3.17: Fluorescence spectral responses recorded in CH_2Cl_2 at 25 °C for **H** with (a) **G₁**, **G₁** + KPF_6 and KPF_6 ; (b) **G₂**, **G₂** + KPF_6 and KPF_6 ; (c) KPF_6 , Cl^- and Cl^- + KPF_6 and (d) **G₃**, **G₃**+**G₂**, KPF_6 , **G₃**+ KPF_6 . λ_{Ext} used are (a) 277 nm, (b) 314 nm, (c) 314 nm and (d) 314 nm respectively.

For demonstration the self-sorting phenomena further, binding process with another guest molecule (**G₃**) is utilized. Earlier studies reveal that secondary ammonium ion derivative forms a stronger inclusion complex than the imidazolium ion with NO_6 -based azacrown ether.⁷ Accordingly, we have utilized a previous reported guest molecule **G₃** (as hexafluoro phosphate salt).⁷ Absorption spectra of anthracene has a strong spectral overlap with the emission spectra of pyrene and this is the primary reason for choosing anthracene fluorophore **G₃**. To take the advantage of the higher binding affinity of **G₃** towards **H**, **G₃** was added to a solution that predominantly had **H.G₂** in equilibrium. By virtue of its higher affinity, **G₃** replaced **G₂** from **H.G₂** and on excitation at 314 nm ($\lambda_{\text{Ext}}^{\text{Pyrene}}$) a distinct anthracene based emission was observed (Figure 3.17d). This was attributed to the formation of the threaded complex **H.G₃** with associated FRET based response from the anthracene fragment (Figure 3.17d).⁷ Further on addition of KPF_6 to this CH_2Cl_2 solution, HK^+ was formed with subsequent generation of free **G₃** and this accounted for only pyrene based emission on excitation at 314 nm. However, the process was reversed on subsequent addition of **C18O6**. As mentioned above, 18-Crown-6 does not interact with **G₁**/**G₂**/**G₃**, but forms a strong complex with the K^+ and helps **H** to form a threaded complex (**H.G₃**) with **G₃** (Figure 3.17d). These results clearly revealed that the formation of the crown ether based pseudorotaxanes can be switched *off* and *on* in a controllable manner

Chapter 3

simply by utilizing the differences in affinities of different guests towards different host molecules.

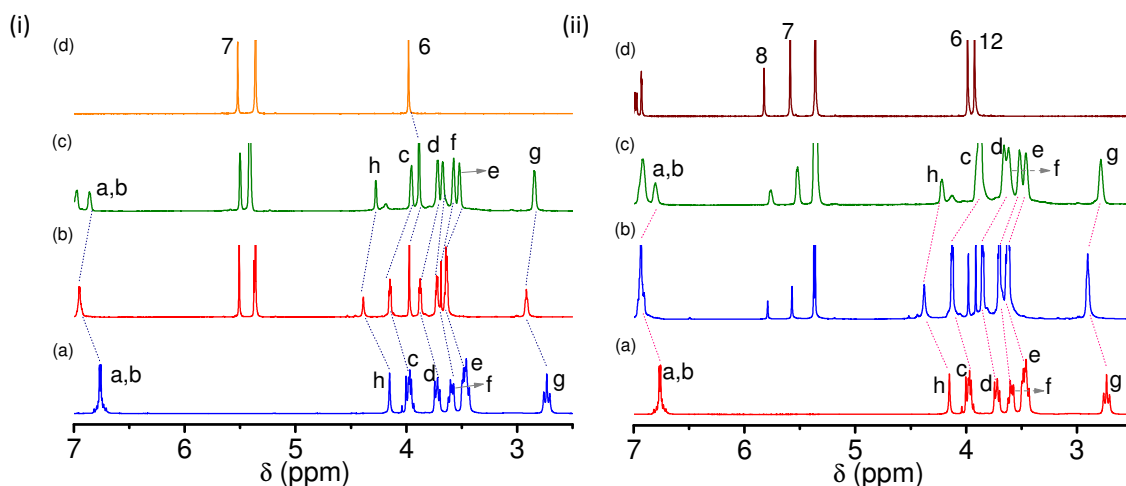


Figure 3.18: (i) Partial ^1H NMR spectra (500 MHz, 298 K) recorded in (4:1 (v/v), $\text{CD}_2\text{Cl}_2:\text{CD}_3\text{CN}$) for (a) 3.5 mM **H**; (b) 3.5 mM **H** with 3.5 mM **G**₁; (c) 3.5 mM **H** with 3.5 mM **G**₁ and then 3.5 mM KPF_6 ; (d) 3.5 mM **G**₁; (ii) (a) 2.7 mM **H**; (b) 2.7 mM **H** with 2.7 mM **G**₂; (c) 2.7 mM **H** with 2.7 mM **G**₂ and then 2.7 mM KPF_6 ; (d) 2.7 mM **G**₂.

Results of the ^1H NMR studies also demonstrated this self-sorting process. When one mole equivalent of KPF_6 is added to a solution having one mole equivalent of **H** + **G**₁ in CD_2Cl_2 , a distinct reversible change in ^1H NMR spectra was observed. In presence of K^+ , **H.G**₁ dissociates and formation of **HK**⁺ prevailed and these were evident in the ^1H NMR spectral changes (Figure 3.18i). The spectral shifts induced by the complexation of **H** and **G**₁ disappeared on formation of **HK**⁺. Analogous changes were also observed when similar studies were repeated for **G**₂ (Figure 3.18ii). All these data confirmed that K^+ can actually replace the imidazolium-based guests from the host (**H**) cavity.

3.3.7. Photophysical properties in film and construction of Logic gates

Demonstration of optical responses on solid surface is preferred for developing any optoelectronic devices. To explore such a possibility, modified silica films were obtained by drop casting host/guest/ K^+ solution ($[\text{H}] = 1.68 \times 10^{-6}$ M in CH_2Cl_2 solution and equimolar amount of other inputs were used for studies) onto silica plates (layer thickness 0.2 mm) and air dried at 35°C prior to our use. Initially, spectra were recorded (λ_{Ext} of 277 nm) for silica surface modified with only **H**. Then these plates were exposed to different sets of guest/host and/or K^+ ions and luminescence spectra were recorded accordingly (Figure

Chapter 3

3.19). Our main focus is to demonstrate the logic operation by monitoring the emission response of **H** in presence of different inputs on solid surface.

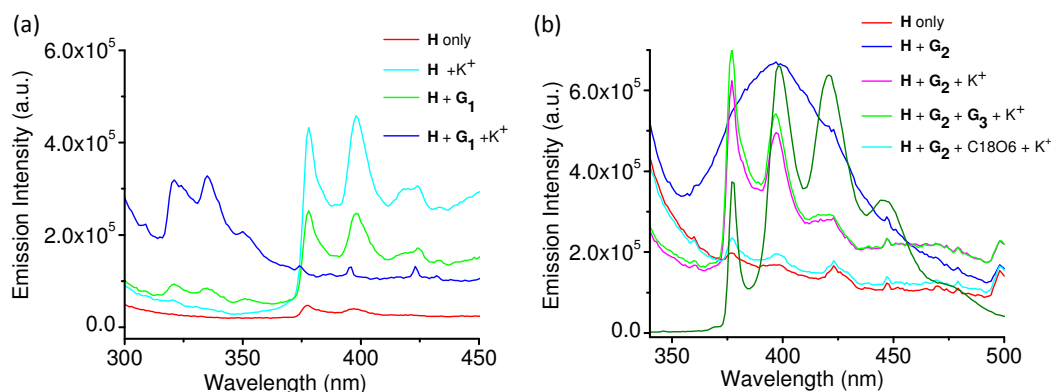


Figure 3.19: Solid state emission spectra on silica surface modified with (a) **H** and exposed to **G₁** and KPF₆, (b) **H** and exposed to **G₂**, **G₃** and KPF₆.

Possibility of reconfiguring the optical output of the photoactive molecules in presence of certain molecular or ionic inputs has special relevance for developing molecular logic gates. We have taken the advantages of the difference on the relative affinities of **G₁/G₂** and **G₃** or K⁺ towards **H**, as well as the preferential binding of K⁺ to C18O6 as compared to **H** for achieving different luminescence responses. Interestingly, such luminescence responses in presence of various ionic (**G₁**, **G₂**, **G₃**, K⁺ used either alone or in different combinations) inputs, either in solution or on silica-based thin film of the host (**H**), could be correlated for demonstrating Boolean operations.

By taking appropriate threshold values and a logic convention, the physicochemical input and output emission signals could be used to encode binary information. For demonstrating this, emission intensities were monitored at 340 and 378 nm ($\lambda_{\text{Ext}} = 277$ nm) using threshold emission intensity value of 3.0×10^4 . Emission intensities above and below this threshold value are considered as “1” and “0”, respectively. In absence of any ionic input (**G₁**: input 1 or K⁺: input 2), output is “0”, be it monitored at 378 or 340 nm (Figure 3.20).

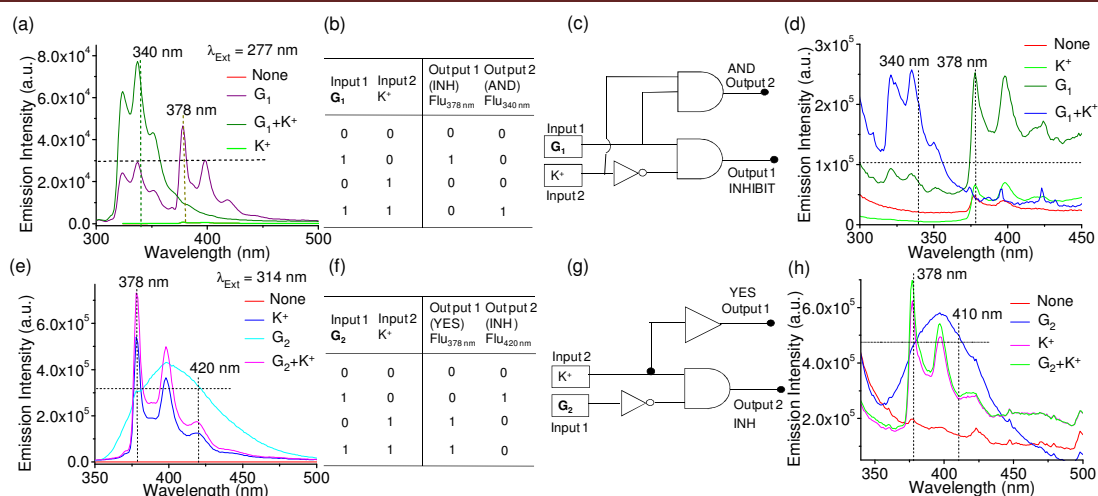


Figure 3.20: Fluorescence spectra of **H** under different input conditions in solution state and then treated with (a) G_1 and K^+ , (e) G_2 and K^+ ; in solid state using silica surface and then treated with (d) G_1 and K^+ , (h) G_2 and K^+ . Truth table corresponds to the inputs (b) G_1 and K^+ , (f) G_2 and K^+ . In this study (a) $[H] = 7.75 \times 10^{-7}$ M and (e) $[H] = 1.68 \times 10^{-5}$ M was used; $H:G_1 = 1:1$, $H:K^+ = 1:1$, $H:G_1:K^+ = 1:1:1$ molar ratio were used. The combinatorial logic schemes are shown in (c) G_1 and K^+ and (g) G_2 and K^+ . The horizontal dashed line marks the threshold value. λ_{Ext} was used for (a) 277 nm, (d) 314 nm.

First, we examined the luminescence responses of **H** either in solution or on silica surface in absence/presence of either one or both of the ionic inputs (G_1 and K^+ ; Figures 3.20a-d). Threshold values for emission intensities were used as 3.0×10^4 and 1.0×10^5 for studies with solution and silica surface, respectively. In presence of inputs (1, 0), output at 378 and 340 nm are “1” and “0”, respectively. In presence of inputs (0,1), outputs are “0” and “0”, respectively, at 378 and 340 nm. In presence of both inputs (1, 1), formation of HK^+ would prevail in solution, which accounted for output “0” and “1” at 378 and 340 nm, respectively. Thus an active output “1” is obtained at 378 nm only when G_1 (1,0) is present as inputs (Truth table in figure 3.20b) and this could be correlated to inhibit (**INH**) logic function, as output is ‘1’ obtained only when one particular input (G_1) is present (1). Luminescence response at 340 nm could be correlated to an “**AND**” (Figure 3.20a) logic operation, as an output signal “1” is achievable only when two inputs (1, 1) are present.²²

Next we examined the luminescence responses of **H** either in solution or on silica surface in absence/presence of either one or both of the ionic inputs G_2 and K^+ (Figures 3.20e-h) following excitation at 314 nm and using threshold intensity value of 3.2×10^5 and 4.75×10^5 for solution and solid surface, respectively. Emission responses below (“0”) and above (“1”) this threshold value in absence/presence of ionic inputs like G_2 and K^+ are

Chapter 3

summarized in truth table (Figure 3.20f). For monitoring wavelength of 410 nm, as output 2 responses could be correlated to an **INH** logic operator. While fluorescence responses monitored at 378 nm, as output 1 were found to be consistent with a **YES** logic operator. YES gate transforms one input signal to output neglecting another input signal.

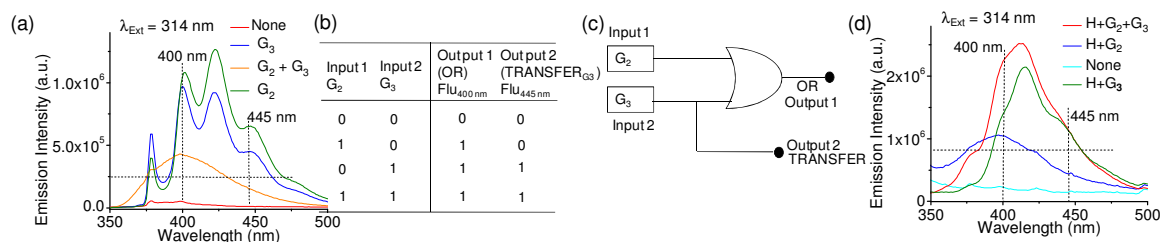


Figure 3.21: Fluorescence spectral response of **H** with different input added in sequence (a) in solution with **G₂** and **G₃** and (d) in silica surface with **G₂** and **G₃**, (b) Truth table corresponds to the input **G₂** and **G₃** in sequence and (c) the combinatorial logic scheme for inputs **G₂** and **G₃**. The horizontal line marks the threshold value for emission intensity. For this study [**H**] of 1.68×10^{-5} M, **H**:**G₃** = 1:1.1 molar equivalent, **H**:**G₂** is 1:1 molar ratio and **H**:**G₂**:**G₃** is 1:1:1 molar ratio were used.

Taking advantage of the preferential binding of **H** with **G₃** even in presence of other guest molecule like **G₂** luminescence responses could be correlated for demonstrating more complicated logic operation. For this **G₂** (input 1) and **G₃** (input 2) were used as two ionic inputs, while emission intensity of 2.4×10^5 was used as the threshold value for monitoring at 400 or 445 nm. Figure 3.21a reveals that in absence of chemical input **G₂** (input 1) and **G₃** (input 2), the emission intensities at 400 nm were very low. In the presence of either **G₂** or **G₃** or both, emission response at 400 nm was higher due to the effective interruption of the PET process. Among different guest fragments, **G₃** having higher preference towards **H** than that of **G₂**, would displace **G₂** from **H**:**G₂** to form **H**:**G₃** with an associated emission response that is typical for anthracene moiety, which could be attributed to the FRET process between pyrene_H donor and anthracene_{G₃} as acceptor. Emission responses at 445 nm in presence of two inputs **G₂** (input 1) and **G₃** (input 2) were correlated for constructing a truth table that could describe a binary logic operation like **TRANSFER_{G₃}** and this could be extended for solution responses of **H** on silica surfaces (Figures 3.21a-d). In turn the fluorescence output at 445 nm mimicked **TRANSFER_{G₃}** being only 1 when **G₃** is present. While emission responses at 400 nm could be used to describe a two input OR gate (Figures 3.21). The change of luminescence intensity at 400 nm was monitored as output by using **G₂** (input 1) and **G₃** (input 2). The OR gate is generally switched on when either one or both inputs are present.

3.4. Conclusion

In summary, we have studied in details the inclusion complex formation of an aza-macrocyclic host **H** with different two guest molecules (**G**₁, **G**₂) having a pendent imidazolium ion. ¹H NMR studies have helped in establishing the relative spatial orientation/conformation of the individual host and guest moieties in the supramolecular assemblies (**H.G**₁ and **H.G**₂). These studies have also confirmed a distinct π - π stacking interactions between the pyrene of the host molecule and naphthalene (for **G**₁) or coumarin (for **G**₂) of two individual guest molecule in **H.G**₁ or **H.G**₂. This has further corroborated the FRET based luminescence responses that are being observed for **H.G**₁ or **H.G**₂. FRET based energy transfer is also confirmed from the results of the time resolved emission studies. Thermodynamic feasibility for such energy transfer is ascertained from data obtained from steady state redox potential and the evaluation of the E_{0-0} value for the respective molecule. Binding stoichiometry and association constant for each inclusion complexes are evaluated by fluorescence or/and ITC studies. Differences in the affinity of the respective guest molecules (**G**₁, **G**₂, **G**₃ and C18O6) and K⁺ towards **H** as well as the differences in affinities for K⁺ towards **H** and C18O6 have been utilized in demonstrating the self-sorting phenomena with distinctly different luminescence responses, which could be correlated in describing certain simple as well as complicated binary logic operations. Interestingly, such logic operations could be demonstrated based on the luminescence responses of the silica surfaces modified with **H** in presence of various inputs. Thus, results described in the present study may provide a perspective for designing molecular devices for performing complicated logic functions. Such example for supramolecular assembly on solid surface is scarce in the contemporary literature.

3.5. References

1. (a) Whitesides, G. M.; Boncheva, M. *Proc. Natl. Acad. Sci. U S A.* **2002**, *99*, 4769; (b) Biedermann, F.; Schneider, H.-J. *Chem. Rev.* **2016**, *116*, 5216; (c) Peng, H.-Q.; Niu, L.-Y.; Chen, Y.-Z.; Wu, L.-Z.; Tung, C.-H.; Yang, Q.-Z. *Chem. Rev.* **2015**, *115*, 7502; (d) Hernandez, J. V.; Kay, E. R.; Leigh, D. A. *Science* **2004**, *306*, 1532.
2. (a) Ashton, P. R.; Chrystal, E. J. T.; Glink, P. T.; Menzer, S.; Schiavo, C.; Spencer, N.; Stoddart, J. F.; Tasker, P. A.; White, A. J. P.; Williams, D. J. *Chem. Eur. J.* **1996**, *2*, 709; (b) Huang, F.; Gibson, H. W. *Prog. Polym. Sci.* **2005**, *30*, 982; (c) Xue, M.; Yang, Y.; Chi, X.; Yan, X.; Huang, F. *Chem. Rev.* **2015**, *115*, 7398.
3. (a) Fahrenbach, A. C.; Zhu, Z. X.; Cao, D.; Liu, W. G.; Li, H.; Dey, S. K.; Basu, S.; Trabolsi, A.; Botros, Y. Y.; Goddard III, W. A.; Stoddart, J. F. *J. Am. Chem. Soc.* **2012**, *134*, 16275; (b) Saha, S.; Flood, A. H.; Stoddart, J. F.; Impellizzeri, S.; Silvi, S.; Venturi, M.; Credi, A. *J. Am. Chem. Soc.* **2007**, *129*, 12159; (c) Zhang, H.; Wang, Q.; Liu, M.; Ma, X.; Tian, H. *Org. Lett.* **2009**, *11*, 3234.
4. (a) Balzani, V.; Credi, A.; Langford, S. J.; Stoddart, J. F. *J. Am. Chem. Soc.* **1997**, *119*, 2679; (b) Jiang, W.; Han, M.; Zhang, H.Y.; Zhang, Z. J.; Liu, Y. *Chem.-Eur. J.* **2009**, *15*, 9938; (c) Semeraro, M.; Credi, A. *J. Phys. Chem. C* **2010**, *114*, 3209; (d) Rogez, G.; Ribera, B.F.; Credi, A.; Ballardini, R.; Gandolfi, M. T.; Balzani, V.; Liu, Y.; Northrop, B. H.; Stoddart, J. F. *J. Am. Chem. Soc.* **2007**, *129*, 4633.
5. (a) Webber, S. E. *Chem. Rev.* **1990**, *90*, 1469; (b) Fox, M. A. *Acc. Chem. Res.* **1992**, *25*, 569; (c) Heilemann, M.; Tinnefeld, P.; Mosteiro, G. S.; Parajo, M. G.; Van Hulst, N. F.; Sauer, M. *J. Am. Chem. Soc.* **2004**, *126*, 6514.
6. Mandal, A. K.; Gangopadhyay, M.; Das, A. *Chem. Soc. Rev.* **2015**, *44*, 663.
7. Mandal, A. K.; Suresh, M.; Kesharwani, M. K.; Gangopadhyay, M.; Agrawal, M.; Boricha, V. P.; Ganguly, B.; Das, A. *J. Org. Chem.* **2013**, *78*, 9004.
8. Mandal, A. K.; Das, P.; Mahato, P.; Acharya, S.; Das, A. *J. Org. Chem.* **2012**, *77*, 6789.
9. (a) Kompa, K.L.; Levine, R. D. *Proc. Natl. Acad. Sci.* **2001**, *98*, 410; (b) de Silva, A. P.; McClenaghan, N. D. *Chem. Eur. J.* **2004**, *10*, 574; (c) Szacilowski, K.; Macyk, W.; Stochel, G. *J. Am. Chem. Soc.* **2006**, *128*, 4550.
10. (a) Barrett, E. S.; Dale T. J.; Rebek Jr., J. *J. Am. Chem. Soc.* **2008**, *130*, 2344; (b) Rudzevich, Y.; Rudzevich, V.; Klautzsch, F.; Schalley, C. A.; Böhmer, V. *Angew. Chem., Int. Ed.* **2009**, *48*, 3867.

Chapter 3

11. (a) Yamauchi, Y.; Yoshizawa, M.; Akita, M.; Fujita, M. *J. Am. Chem. Soc.* **2010**, *132*, 960; (b) Schmittel, M.; Mahata, K. *Chem. Commun.* **2010**, *46*, 4163.
12. (a) Shaller, A. D.; Wang, W.; Gan, H.; Li, A. D. Q. *Angew. Chem., Int. Ed.* **2008**, *47*, 7705; (b) Ghosh, S.; Wu, A.; Fettingner, J. C.; Zavalij, P. Y.; Isaacs, L. *J. Org. Chem.* **2008**, *73*, 5915–; (c) Safont-Sempere, M. M.; Osswald, P.; Stolte, M.; Grüne, M.; Renz, M.; Kaupp, M.; Radacki, K.; Braunschweig, H.; Würthner, F. *J. Am. Chem. Soc.* **2011**, *133*, 9580.
13. Mandal, A. K.; Suresh, M.; Das, A. *Org. Biomol. Chem.* **2011**, *9*, 4811.
14. (a) Noujeim, N.; Leclercq, L.; Schmitzer, A. R. *J. Org. Chem.* **2008**, *73*, 3784-3790; (b) Yao, Y.; Chi, X.; Zhou, Y.; Huang, F. *Chem. Sci.* **2014**, *5*, 2778; (c) Zhou, Y. J.; Yao, Y.; Xue, M. *Chem. Commun.* **2014**, *50*, 8040.
15. Kiviniemi, S.; Sillanpaa, A.; Nissinen, M.; Rissanene, K.; Lamsa, M. T.; Pursiainen, J. *Chem. Commun.* **1999**, 897.
16. Stolwijk, T. B.; Sudhoelter, E. J. R.; Reinhoudt, D. N.; Van Eerden, J.; Harkema, S. *J. Org. Chem.* **1989**, *54*, 1001.
17. (a) Castillo, D.; Astudillo, P.; Mares, J.; Gonzalez, F. J.; Vela, A.; Tiburcio, J. *Org. Biomol. Chem.* **2007**, *5*, 2252-2256; (b) Li, L.; Clarkson, G. J. *Org. Lett.* **2007**, *9*, 497.
18. (a) Chen, L.; Zhang, Y. M.; Liu, Y. *J. Phys. Chem. B* **2012**, *116*, 9500; (b) Chen, L.; Zhang, H. Y.; Liu, Y. *J. Org. Chem.* **2012**, *77*, 9766.
19. (a) Whitesides, G. M.; Mathias, J. P.; Seto, C. T. *Science* **1991**, *254*, 1312; (b) Wu, A.; Isaacs, L. *J. Am. Chem. Soc.* **2003**, *125*, 4831; (c) Mukhopadhyay, P.; Wu, A.; Isaacs, L. *J. Org. Chem.* **2004**, *69*, 6157; (d) He, Z.; Jiang, W.; Schalley, C. A. *Chem. Soc. Rev.*, **2015**, *44*, 779; (e) Jiang, W.; Schalley, C. A. *Proc. Natl. Acad. Sci. U.S.A.* **2009**, *106*, 10425; (f) Wang, F.; Han, C.; He, C.; Zhou, Q.; Zhang, J.; Wang, C.; Li, N.; Huang F. *J. Am. Chem. Soc.* **2008**, *130*, 11254.
20. (a) Safont-Sempere, M. M.; Fernández, G.; Würthner, F. *Chem. Rev.* **2011**, *111*, 5784–5814; (b) Saha, M. L.; Schmittel, M. *Org. Biomol. Chem.* **2012**, *10*, 4651; (c) Mukhopadhyay, P.; Zavalij, P. Y.; Isaacs, L. *J. Am. Chem. Soc.* **2006**, *128*, 14093.
21. (a) Frensdorff, H. K. *J. Am. Chem. Soc.* **1971**, *93*, 600-606; (b) Jiang, W.; Schalley, C. A. *Beilstein J. Org. Chem.* **2010**, *6*, 14.
22. Lee, M.; Niu, Z.; Schoonover, D. V.; Slebodnick, C.; Gibson, H. W. *Tetrahedron* **2010**, *66*, 7077.

CHAPTER 4

CHIRAL DISCRIMINATION THROUGH FRET BASED PROCESS IN SUPRAMOLECULAR ASSEMBLIES

Publication:
To be communicated

4.1. Introduction

Chirality plays an essential role in nature as well as in chemical and biological sciences. Chiral recognition is one of the most significant processes in a variety of physical, chemical, and biological phenomena including purification and resolution of enantiomers, asymmetric catalysis reactions, antibody-antigen interactions, biocatalysis and for optoelectronic applications.¹⁻³ More recently, chiral recognition is being exploited for sensing crucial optically active isomers.⁴ Biological activities of many chiral substances depends solely on the stereochemistry. Therefore, detection of chirality, and interactions between chiral species, is an important area of research. Enantiomeric recognition is a special case of molecular recognition that involves discrimination between enantiomers of the guest molecules by a chiral host molecule. Such a process is crucial if it involves a chiral molecule or ion that has biological significance, for example various derivatives of ammonium ion are frequently involved in physiological processes. Earlier reports reveal that secondary ammonium ions forms threaded [2]pseudorotaxane complexes with crown ether or aza-crown ether derivatives⁵. Such reports also suggest that stability and relative conformation of host and/or guest molecules in such assemblies are governed by H-bonding interactions as well as π - π stacking interactions. Therefore, chiral macrocyclic ligands capable of selective recognition of other species have been of great interest in investigations of catalysis, separations, enzyme mimics and other areas involving chiral molecular recognition.⁶ The enantiomeric recognition of amines and corresponding ammonium ion derivatives are of great interest, as these compounds are effective structural units of many biologically active compounds. Recognition between groups that are both electronically and geometrically complementary to each other actually drives the formation of various supramolecular assemblies. Studies on supramolecular architecture derived from enantiomerically pure host and guest molecules provide better insight in understanding the role of complementarity in optical activity in the formation of such [2]pseudorotaxane or supramolecular architecture. Such insights are crucial in understanding various interactions that are common in nature.⁷ Few recent reports reveal that artificial chiral receptors have been utilized for studying enantiomeric recognition with binding motif(s) that is/are integral part of the receptor molecule. Various non-bonding interactions like electrostatic interactions, H-bonding, cation- π interactions, hydrophobic interactions, π - π stacking and structural complementarity have been exploited for such recognition process.^{6d,8,9,10}

Chapter 4

Various spectroscopic (UV–Vis,¹¹ fluorescence,¹² NMR,^{13a} circular dichroism,^{13b,c}) methods as well as methods based on polarimetric, liquid chromatographic and electrochemical techniques have been utilized for determining enantiomeric recognition by chiral macrocyclic hosts.^{14,2} More recently, Nau and coworkers have utilized self-assembled ternary complex formation between the macrocyclic hosts cucurbit[8]uril, dicationic dyes, and chiral aromatic analytes for recognition of certain chiral amino acids/peptides by probing changes in induced circular dichroism signals.¹⁵ Among various possibilities, fluorescence-based enantioselective sensors allow rapid analysis of the enantiomeric composition of chiral compounds. The relative ease of detection, high sensitivity and real time analysis using multi-signalling modes provide an obvious edge over other detection processes.^{16,1b} Steric effects of the host have been recognised as an important factor in enantiomeric recognition process.¹⁷ Cram *et al.* first reported the use of binaphthyl based chiral crowns for enantioselective recognition of chiral ammonium salts.¹⁸ Since then, 1,1'-bi-2-naphthol (BINOL) and its derivatives have been extensively used in chiral recognition and exhibited excellent chiral induction in many processes.^{19,20,21} There are literature reports on the use of different chiral macrocyclic hosts for enantiomeric discrimination.^{22,23}

In this chapter, the possibility of using a crown ether-based chiral host molecule (R-H or S-H), derived from the BINOL moiety, for delineating optically active secondary ammonium ion with an associated luminescence ON response were discussed (Figure 4.1). Functionalization of the guest molecules (R-G or S-G) with appropriate fluorophore allows us to probe the specific recognition of an optically pure enantiomer by an enantiomerically pure host molecule with FRET based luminescence response. Interestingly, such response also offers a way to predict the relative orientation of the individual host and/or guest molecule in the supramolecular assembly.

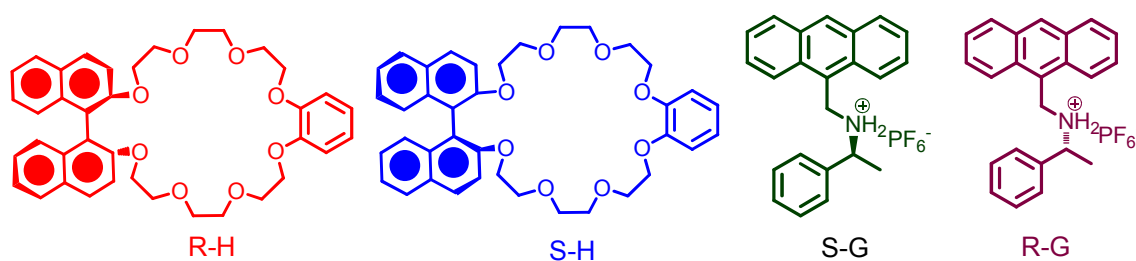


Figure 4.1: Schematic representation of the molecular components for the formation of a chiral supramolecular assembly.

4.2. Experimental section

4.2.1. Materials

9-anthracenecarboxaldehyde, (S)-(-)- α -Methylbenzylamine, (R)-(+)- α -Methylbenzylamine chemicals were purchased and used as received. All organic solvents were freshly distilled under vacuum over a suitable drying agent. Column chromatography was performed on silica gel 100-200 mesh.

4.2.2. Analytical Methods

Spectral measurements

^1H NMR and ^{13}C NMR spectra were obtained on a 700 MHz spectrometer, using TMS an internal standard. HRMS was performed on a Q-ToF mass spectrometer. MALDI-TOF mass spectra were recorded on a Bruker BIFLEX III or AUTOFLEX III time-of-flight (TOF) mass spectrometer (Bruker Daltonics, Billerica, MA, USA) using a 337 nm nitrogen laser with DHB as matrix. Absorption spectra were recorded on a PerkinElmer Lambda 950 Scan UV/vis-NIR. PL spectra were recorded on a PTI-QM 400 Luminescence spectrofluorimeter at room temperature. CD spectra were measured with a JASCO J-810 spectrometer. Fluorescence lifetimes were measured by time correlated single photon counting (TCSPC), on Horiba-Jovin Yvon Luminescence spectrofluorimeter using a 295 nm LED nanosecond diode LED source, 340 nm LASER as excitation source. Fluorescence Quantum yield (Φ_f) was determined using quinine hemisulphate as the reference.

ITC measurements

A thermo stated and fully computer operated isothermal titration calorimetry was used for all the microcalorimetric experiments. The ITC experiments were performed at 25°C In DCM solvent. In each run, a solution of guest in a 2.0 μL syringe was sequentially injected with stirring at 1000 rpm into a solution of host in the sample cell. A control experiment was done to determine the heat of dilution was carried out for each run by performing the same number of injections with the same concentration of host compound as used in the titration experiments into a same solution without the guest compound. To obtain the net reaction heat dilution enthalpies determined in control experiments were subtracted from the

Chapter 4

enthalpies measured in the titration experiments. 'One set of binding sites' model were used to measure all the thermodynamic parameters reported in this work.

Electrochemical measurements

Cyclic voltammetry was carried out with a three compartment cell. The working electrode was a freshly polished Platinum electrode. Potentials were measured versus a nonaqueous Ag/Ag⁺ reference electrode (10 mM AgNO₃ in acetonitrile) counter electrode was a platinum wire. Solutions were prepared from dry DCM containing 1 mM of the analyte and 0.1 M tetrabutylammonium hexafluorophosphate as supporting electrolyte.

4.2.3. Synthesis

Synthetic procedure of R-H: The methodology adopted for the synthesis of R-H was followed from literature.²⁴ Characterization details are provided in the appendix. Yield: 560 mg (82%). ¹H NMR (700 MHz, CD₂Cl₂, ppm) 7.96 (2H, d, J = 9.0 Hz), 7.89 (2H,d, J = 8.2 Hz), 7.51 (2H,d, J = 9.0 Hz), 7.35 (2H,t, J = 7.5 Hz), 7.23 (2H,t, J = 7.6 Hz), 7.09 (2H,d, J = 8.5 Hz), 6.95 (4H,d, J = 7.4 Hz), 4.23 (2H, ddd, J = 10.5, 6.7, 3.6 Hz), 4.15 – 4.12 (4H, m), 4.11 – 4.08 (2H, m), 3.82 – 3.79 (2H, m), 3.64 – 3.60 (2H, m), 3.55 (4H, t, J = 5.9 Hz), 3.52 – 3.49 (2H, m), 3.41 – 3.36 (4H, m). ¹³C NMR (175 MHz, CD₂Cl₂, ppm): 154.5, 149.5, 134.0, 129.3, 129.2, 127.8, 126.1, 125.1, 123.5, 121.3, 120.2, 115.9, 114.2, 70.7, 70.6, 69.7, 69.6, 69.0, 30.5. HRMS (ESI–TOF) m/z : [M + H⁺]⁺ calculated for C₃₈H₄₀O₈,625.2801; Found 625.2796.

Synthetic procedure of S-H: The methodology adopted for the synthesis of S-H was followed from literature.²⁴ Characterization details are provided in the appendix. Yield: 543 mg (79%). ¹H NMR (700 MHz, CD₂Cl₂, ppm) 7.96 (2H, d, J = 9.0 Hz), 7.89 (2H, d, J = 8.2 Hz), 7.51 (2H, d, J = 9.0 Hz), 7.36 (2H, t, J = 7.5 Hz), 7.23 (2H,t, J = 7.6 Hz), 7.09 (2H,d, J = 8.5 Hz), 6.95 (4H, dt, J = 9.5, 4.8 Hz), 4.25 – 4.22 (2H, m), 4.13 (dd, J = 5.9, 3.2 Hz), 4.11 – 4.08 (2H,m), 3.81 – 3.79 (2H,m), 3.62 (2H, ddd, J = 11.2, 5.3, 3.7 Hz), 3.56 – 3.54 (4H, m), 3.51 (2H, d, J = 4.0 Hz), 3.41 – 3.36 (4H, m). ¹³C NMR (175 MHz, CD₂Cl₂, ppm): 154.5, 149.5, 134.0, 129.3, 129.2, 127.8, 126.1, 125.1, 123.5, 121.3, 120.2, 115.9, 114.2, 70.7, 70.6, 69.7, 69.6, 69.0, 30.5. HRMS (ESI–TOF) m/z: [M + H⁺]⁺ calculated for C₃₈H₄₀O₈,625.2801; Found 625.2796.

Synthetic procedure of Achiral Crown: The methodology adopted for the synthesis of achiral crown was followed from literature.²⁴ Characterization details are provided in the

Chapter 4

appendix. Yield: 543 mg (79%). NMR (500 MHz, CD₂Cl₂, ppm) δ 7.86 (2H, d, J = 9.0 Hz), 7.79 (2H, d, J = 8.0 Hz), 7.44 (2H, d, J = 8.9 Hz), 7.28 (2H, s), 7.17 (2H, t, J = 7.4 Hz), 7.11 (2H, d, J = 8.4 Hz), 6.88 (4H, d, J = 4.4 Hz), 4.17 (2H, s), 4.10 (4H, dd, J = 7.9, 3.7 Hz), 4.02 – 3.98 (2H, m), 3.79 (4H, s), 3.58 (2H, d, J = 11.4 Hz), 3.52 (4H, s), 3.43 (2H, d, J = 5.2 Hz), 3.34 (2H, d, J = 4.8 Hz), 3.29 (2H, d, J = 4.9 Hz). ¹³C NMR (125 MHz, CDCl₃, ppm): 164.2, 162.5, 154.4, 148.8, 134.0, 129.4, 129.2, 127.8, 126.2, 125.3, 123.6, 121.4, 120.5, 116.1, 114.1, 70.7, 70.6, 69.9, 69.8, 69.6, 68.9, 38.5, 36.4, 31.3. HRMS (ESI–TOF) m/z : [M + H]⁺ calculated for C₃₈H₄₀O₈, 625.2801; Found 625.2796.

Synthetic procedure of S-G: 9-anthracenecarboxaldehyde (1.0 g, 4.85 mmol) and (S)-(–)- α -Methylbenzylamine (0.675 g, 5.75 mmol) were dissolved in 50 ml EtOH/THF (3:2,v/v). The mixture was kept for reflux for 7 hrs. The mixture was then cooled to room temperature and solvent was evaporated under vacuum. The reaction mixture was dissolved in 50 ml EtOH/THF (1:1,v/v) and temperature was reduced to 0°C. NaBH₄ was added gradually to the cooled reaction mixture. The reaction mixture was allowed to reach room temperature and stirred for overnight. Solvent was removed under reduced pressure and extracted with DCM and water. Crude product was purified on a silica gel column using DCM:Pet Ether (2:5, by volume) as an eluent. A solution of concentrated HCl (0.5ml) in methanol was added drop wise and stirred for 24 hrs. After solvent evaporation insoluble residue was treated with aqueous solution of NH₄PF₆. Light yellow precipitate appeared after overnight stirring. Precipitate was washed with cold water. Yield: 810mg (%). ¹H NMR (700 MHz, CD₂Cl₂, ppm) 8.63 (1H,s), 8.11 (2H,d, J = 8.4 Hz), 7.81 (2H,d, J = 8.4 Hz), 7.64 – 7.61 (2H,m), 7.58 (5H,t, J = 6.7 Hz), 7.46 (2H,d, J = 7.9 Hz), 5.21 (1H,d, J = 14.3 Hz), 5.12 (1H,d, J = 14.4 Hz), 4.55 (q, J = 6.9 Hz), 1.79 (2H,d, J = 7.0 Hz). ¹³C NMR (175 MHz, CD₂Cl₂, ppm): δ 134.7, 131.2, 130.6, 130.4, 129.8, 129.7, 128.3, 127.5, 125.6, 121.8, 119.5, 60.1, 42.3, 30.5, 19.5. HRMS (ESI–TOF) m/z : [M – PF₆]⁺ calculated for C₂₃H₂₂N⁺, 312.1752; Found 312.1747.

Synthetic procedure of R-G: 9-anthracenecarboxaldehyde (1.0g, 4.85 mmol) and (R)-(+)- α -Methylbenzylamine (0.675 g, 5.75 mmol) were dissolved in 50 ml EtOH/THF (3:2,v/v) and kept for 8hrs reflux. The mixture was then cooled down to room temperature and solvent was evaporated under reduced pressure to give imine as a yellowish sticky solid. The solid was dissolved in MeOH and NaBH₄ was added portion wise at 0°C until the reduction was finished. The reaction mixture was then allowed to stir for overnight. After evaporation of the solvent residue was extracted with DCM and water an which was

Chapter 4

purified on a silica gel column by DCM:Pet Ether (2:5, by volume) as an eluent. Concentrated HCl was added drop wise. The hydrochloride salt was then suspended in an aqueous solution of NH_4PF_6 resulting a deep yellow solid. Yield: 780 mg (%). ^1H NMR (700 MHz, CD_2Cl_2 , ppm) 8.66 (s), 8.13 (d, $J = 8.4$ Hz), 7.81 (s), 7.67 – 7.64 (m), 7.61 – 7.55 (m), 7.41 (d, $J = 6.8$ Hz), 5.28 (d, $J = 14.4$ Hz), 5.22 (d, $J = 14.4$ Hz), 4.56 (q, $J = 6.7$ Hz), 1.80 (d, $J = 6.9$ Hz). ^{13}C NMR (175 MHz, CD_2Cl_2 , ppm): 134.7, 131.3, 131.2, 130.6, 130.4, 129.9, 129.8, 128.4, 127.5, 125.6, 121.8, 119.6, 60.2, 42.3, 30.6, 19.5. HRMS (ESI-TOF) m/z : $[\text{M} - \text{PF}_6]^{+}$ calculated for $\text{C}_{23}\text{H}_{22}\text{N}^{+}$, 312.1752; Found 312.1747.

4.3. Results and Discussions

The methodology adapted for chiral crown synthesis was followed from the literature.²⁴ Various guest molecules with different chirality were synthesized by reducing the product of the Schiff base reaction between appropriate amine and aldehyde derivatives. These amine derivatives were protonated and eventually isolated as the desired hexafluorophosphate salts. Synthetic procedure and all relevant characterization details of these host and guest molecules are provided in the appendix.

4.3.1. Photophysical studies

The binaphthol based crown ether derivatives (R-H and S-H) and ammonium-ion based chiral guests (R-G and S-G) are readily soluble in dichloromethane and steady state absorption and luminescence studies as well as time resolved emission studies were carried out in this low polar solvent which is also conducive for favoring the formation of inclusion complexes between them.⁵

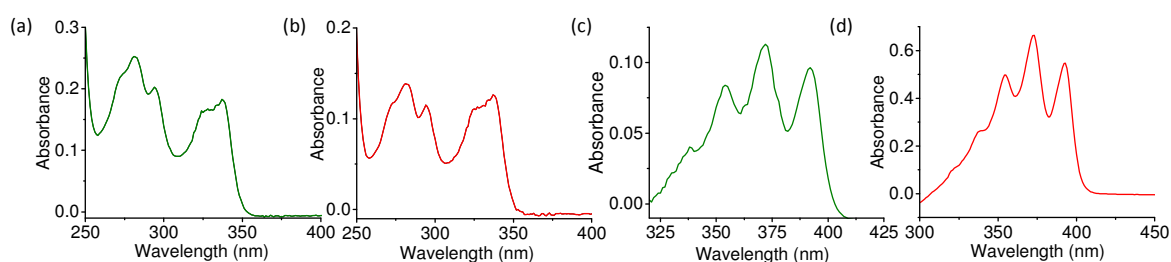


Figure 4.2. UV-Vis spectra of (a) R-H, (b) S-H, (c) R-G, (d) R-G in dichloromethane at room temperature

The absorption spectrum recorded for R-H in dichloromethane showed maxima at 282 ($\epsilon = 3.7 \times 10^4 \text{ Lmol}^{-1}\text{cm}^{-1}$), 294 ($\epsilon = 2.14 \times 10^4 \text{ Lmol}^{-1}\text{cm}^{-1}$) and 336 ($\epsilon = 1.14 \times 10^4 \text{ Lmol}^{-1}\text{cm}^{-1}$)

nm (Figure 4.2a). Analogous absorption spectrum was observed for S-H with maxima at 282 ($\epsilon = 4 \times 10^4 \text{ Lmol}^{-1}\text{cm}^{-1}$), 294 ($\epsilon = 2.56 \times 10^4 \text{ Lmol}^{-1}\text{cm}^{-1}$) and 336 ($\epsilon = 1.14 \times 10^4 \text{ Lmol}^{-1}\text{cm}^{-1}$) nm. (Figure 4.2b). The spectra of R-G and S-G were dominated by the absorption band of the anthracene moiety with maxima at 354, 372, 392 nm and 353, 373, 393 nm, respectively (Figure 4.2c,d). The absorption spectra recorded for 1:1 host:guest mixtures (R-H:S-G, S-H:S-G, S-H:R-G and S-H:S-G) in dichloromethane are basically a sum of the individual spectra of the host and guest (Figure 4.3a-d).

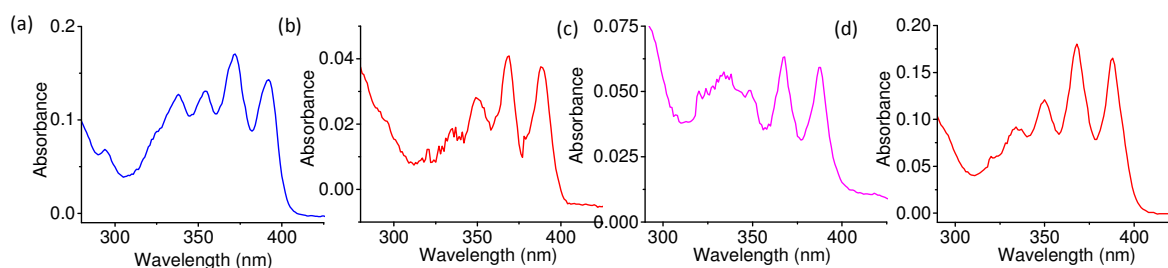


Figure 4.3: UV-Vis spectra of (a) R-H:R-G, (b) R-H:S-G, (a) S-H:S-G, (a) S-H:R-G at mole ratio of 1:1 in dichloromethane solution at room temperature. Concentrations used ($1.68 \times 10^{-5} \text{ M}$).

Absorption spectra monitored systematically during titrations of R-H with R-G or S-G did not show any detectable change from the sum of the spectra of individual components. This confirmed that there was no significant ground state electronic interaction between the host (R-H) and guest (R-G or S-G) molecule in solution. Similar results were observed for titration of S-H with R-G or S-G. Enantiomerically pure host molecules, R-H and S-H showed emission bands at 365 nm which is characteristic of the binaphhtol moiety on excitation at any one of the three absorption band maxima (282, 292, 336 nm). Relative quantum yields of $\Phi_{\text{R-H}} = 0.57$ and $\Phi_{\text{S-H}} = 0.61$ were estimated for R-H and S-H respectively by employing quinine hemisulphate as a standard. Interestingly, the emission spectra of the chiral hosts (R-H or S-H) showed substantial spectral overlap with the absorption spectra of the guests (R-G or S-G), which is one of the prerequisites for Förster resonance energy transfer (FRET) between the two interacting fluorophores^{25a} (Figure 4.4). Initially, R-H was employed for chiral recognition studies with two enantiomerically pure guest molecules, R-G and S-G. Luminescence titration experiments were performed ($\lambda_{\text{Ext}} = 292 \text{ nm}$) at a fixed concentration of R-H ($1.0 \times 10^{-7} \text{ M}$) while varying the concentration of R-G or S-G systematically in the range ($0 - 3.5 \times 10^{-5} \text{ M}$).

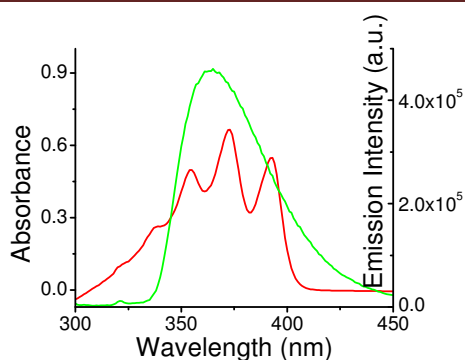


Figure 4.4: Overlap spectra for the emission spectrum of R-H/S-H (green) and absorption spectrum of R-G/S-G (red).

Interestingly, a gradual decrease in the characteristic luminescence intensity of the binaphthol moiety (~ 365 nm) was observed along with a concomitant increase in luminescence intensity at 400, 419 and 444 nm upon addition of R-G (Figure 4.5a) or S-G (Figure 4.5c) to R-H. Even though, luminescence band maxima at 400, 419 and 444 nm are characteristic of the anthracenyl moiety. The above results and (Figure 4.4) clearly reveals that the anthracene moiety in the guest does not absorb at 292 nm, thus the observed enhancement in anthracene-based emission at 400, 419 and 444 nm in the hydrogen-bonded adduct R-H·R-G implies an efficient FRET-based process involving the donor binaphthol fragment and the acceptor anthracene unit in the assembly.

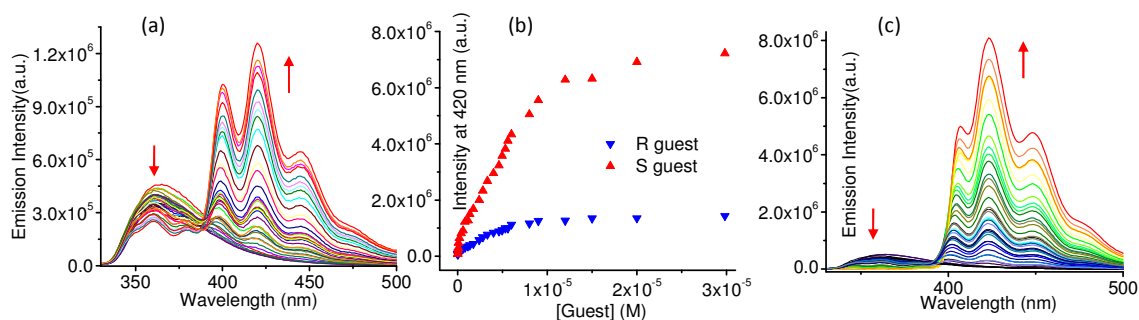


Figure 4.5: Changes in luminescence spectral pattern of R-H (1.0×10^{-7} M), in dichloromethane upon addition of increasing concentration of (a) R-G = $0 - 3.0 \times 10^{-5}$ M, (b) Fluorescence enhancement of R-H (1.0×10^{-7} M) vs concentration of (R)- and (S)- Guest, (c) S-G = $0 - 3.5 \times 10^{-5}$ M. Excitation wavelength = 292 nm, slit-1/1.

Literature reports suggest that secondary ammonium ion derivatives form a reasonably stable threaded complex with $C_{18}O_8$ -crown ether derivatives^{25b}. Thus, results from luminescence studies tend to suggest the formation of [2]pseudorotaxane complexes

Chapter 4

(R-H•R-G and R-H•S-G) with an appropriate head-on orientation which favors an efficient FRET based energy transfer between the binaphthol and anthracene moieties.

However, there is a distinct difference in the extent of the FRET based luminescence response observed with the two guests R-G and S-G. The relative luminescence quantum yield evaluated for 3.5×10^{-5} M solutions of R-G and S-G are $\Phi^{[R-H \cdot R-G]} = 0.40$ and $\Phi^{[R-H \cdot S-G]} = 0.56$ respectively. In order to quantify the energy transfer (ET) efficiency, we compared the fluorescence quantum yields of the donor (binaphthol moiety) in the presence and absence of acceptor. The ET quantum yield calculated for R-H•R-G and R-H•S-G are 74% and 83% respectively with corresponding ET rates $5.43 \times 10^8 \text{ s}^{-1}$ (R-H•R-G) and $9.35 \times 10^8 \text{ s}^{-1}$ (R-H•S-G). The high ET rates and efficiencies can be ascribed to the large spectral overlap and presumably a relatively short distance between the donor and the acceptor fluorophores. It is evident from Figure 4.5b that the emission enhancement of the acceptor fluorophore (anthracene moiety) is much higher in the inclusion complex formed between R-H and S-G. The measured intensity ratio at 420 nm ($I_{420}^{[R-G]} / I_{420}^{[S-G]}$) was 6.45, while the enantioselective fluorescence enhancement ratio was 6.68. [$ef = (I^{[S-G]} - I_0) / (I^{[R-G]} - I_0)$]. This clearly reveals the ability of R-H in delineating two different enantiomers R-G and S-G. Ideally this should also be reflected in the difference in the association constants for the formation of R-H•R-G and R-H•S-G.

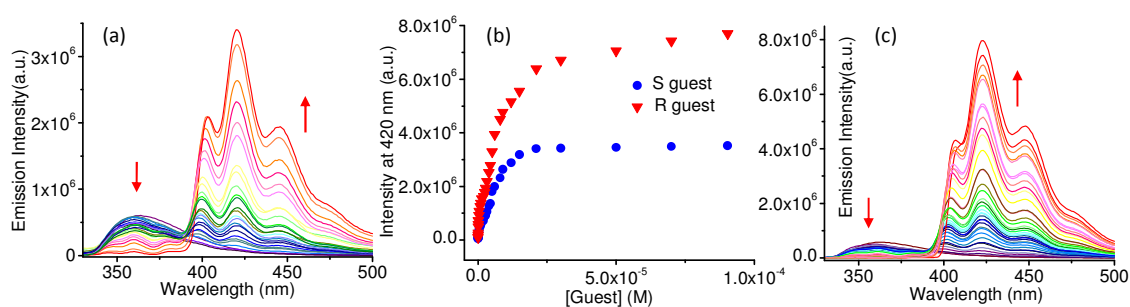


Figure 4.6: Changes in luminescence spectral pattern of S-H (1.0×10^{-7} M), in dichloromethane upon addition of increasing concentration of (a) S-G = 0 – 1.0×10^{-4} M, (b) Fluorescence enhancement of S-H (1.0×10^{-7} M), in dichloromethane) vs concentration of (R)- and (S)- Guest, (c) R-G = 0 – 1.0×10^{-4} M. Excitation wavelength = 292 nm, slit-1/1.

In these two diastereomeric complexes, the attractive interactions are mainly the hydrogen bonding interactions involving the lone pair of electrons of the ethelenoxy oxygen and $H_{NH_2^+}/CH_2$. The observation of an efficient FRET-based ET process confirms the proximity of the two interacting fluorophores. Earlier reports also reveal that π - π interactions may

Chapter 4

contribute favourably to enantiomeric recognition.^{25c} Clearly, in the diastereomeric complex R-H•S-G, the guest molecule (S-G) adopts an orientation that favours a better proximity of the two interacting fluorophores when compared to the other enantiomeric guest molecule R-G resulting in a more efficient ET efficiency as well as ET rate for R-H•S-G.

As in the case of R-H, absorption spectra of a 1:1 mixture of S-H and R-G or S-G also correspond to a sum of the spectra of individual components suggesting a lack of any ground state interaction between two fluorophores (Figure 4.3c-d). Systematic luminescence titrations were performed using fixed [S-H] (1.0×10^{-7} M) and varying concentrations of R-G or S-G ($0 - 1.0 \times 10^{-4}$ M) in dichloromethane. The trend in FRET-based luminescence changes is similar to that observed for R-G (Figure 4.6). The quantum yield of binaphthol unit was found to decrease from 0.61 to 0.09 ($\Phi_{365}^{[S-H \cdot S-G]}$) and 0.05 ($\Phi_{365}^{[S-H \cdot R-G]}$) in [S-H•S-G] and [S-H•R-G], respectively. Concomitant gains in quantum yield evaluated for anthracenyl-based emission ($\lambda = 420$ nm) are 0.29 and 0.39 for S-H•S-G and S-H•R-G respectively, showing FRET based ET efficiencies of 85% and 91%. The corresponding ET rates are 1.08×10^9 s⁻¹ for S-H•S-G and 1.92×10^9 s⁻¹ for S-H•R-G.

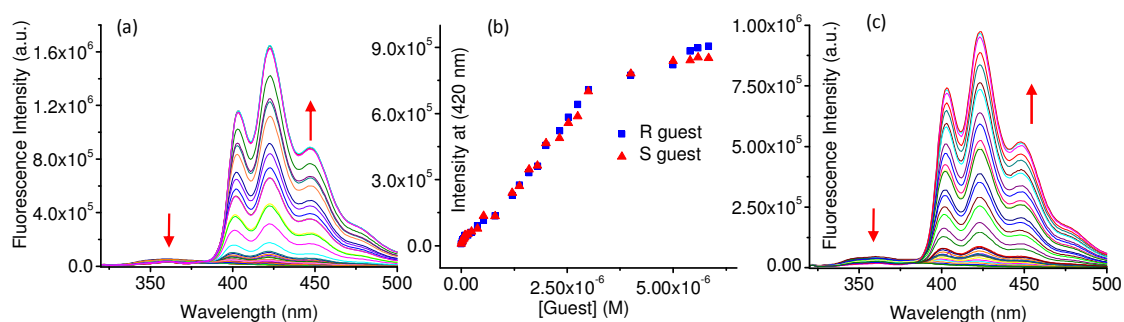


Figure 4.7: Changes in luminescence spectral pattern of Achiral host (1.0×10^{-7} M), in dichloromethane upon addition of increasing concentration of (a) S-G = $0 - 8.3 \times 10^{-6}$ M, (c) Fluorescence enhancement of Achiral crown (1.0×10^{-7} M), in dichloromethane) vs concentration of (R)- and (S)-Guest, (b) R-G = $0 - 8.3 \times 10^{-6}$ M. Excitation wavelength = 292 nm, slit-1/1

Importantly, control experiments did not show any obvious enantioselectivity when luminescence titrations were performed with the achiral crown molecule and the two enantiomeric guests R-G and S-G (Figure 4.7). This confirms that the chiral environment of the chiral host molecule is an important factor in determining enantioselectivity in the

interaction with the two guest molecules, R-G or S-G. The observed selectivity is analogous to the enantiomeric differentiation which originates from different conformations of binding pockets, as seen in the stereo control of an enzyme pocket in an enzymatic reaction.²⁷ In the present study, the confinement of the host (R-H/S-H) creates a more discriminating chiral environment for the guests, leading to different levels of emission enhancement for the acceptor chromophore.

We also explored the possibility of developing a modified silica surface for use in chiral recognition, as optical responses on a solid surface is preferable for developing optoelectronic devices. Modified thin silica films (layer thickness 0.2 μm) for luminescence measurements were obtained by drop casting a solution of R-H or S-H (1.0×10^{-7} M) onto silica plates and air drying at 35°C prior to further use. These plates were then exposed to chiral guests (R-G or S-G) and luminescence spectra were recorded (Figure 4.8). In the luminescence spectrum, the extent of energy transfer is different for different chiral guests.

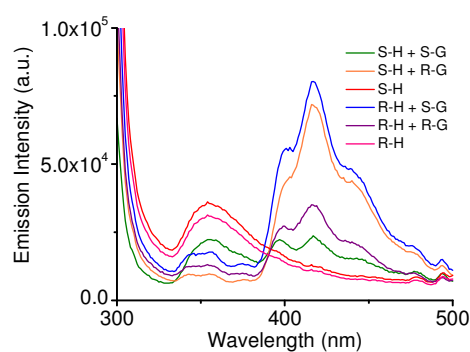


Figure 4.8: Solid state emission spectra on silica surface modified with R-H/S-H and exposed to R-G/S-G.

4.3.2. Time resolved emission studies

Time correlated single photon counting (TCSPC) experiments were performed for the individual components and the host-guest assemblies in air saturated dichloromethane solution (Figure 4.9, 4.10). On excitation at 295 nm (LED), R-H shows a bi-exponential decay with time constants of $\tau_1 = 0.37 \pm 0.01$ (1.12%) and $\tau_2 = 5.30 \pm 0.08$ (98.99%) ns. In analogous studies with S-H the time constants were found to be $\tau_1 = 2.90 \pm 0.04$ (4.05%) and $\tau_2 = 5.36 \pm 0.05$ (95.95%) ns. The longer and major component (~ 5.3 ns) typically matches with the lifetime of the binaphthol unit.^{1b}

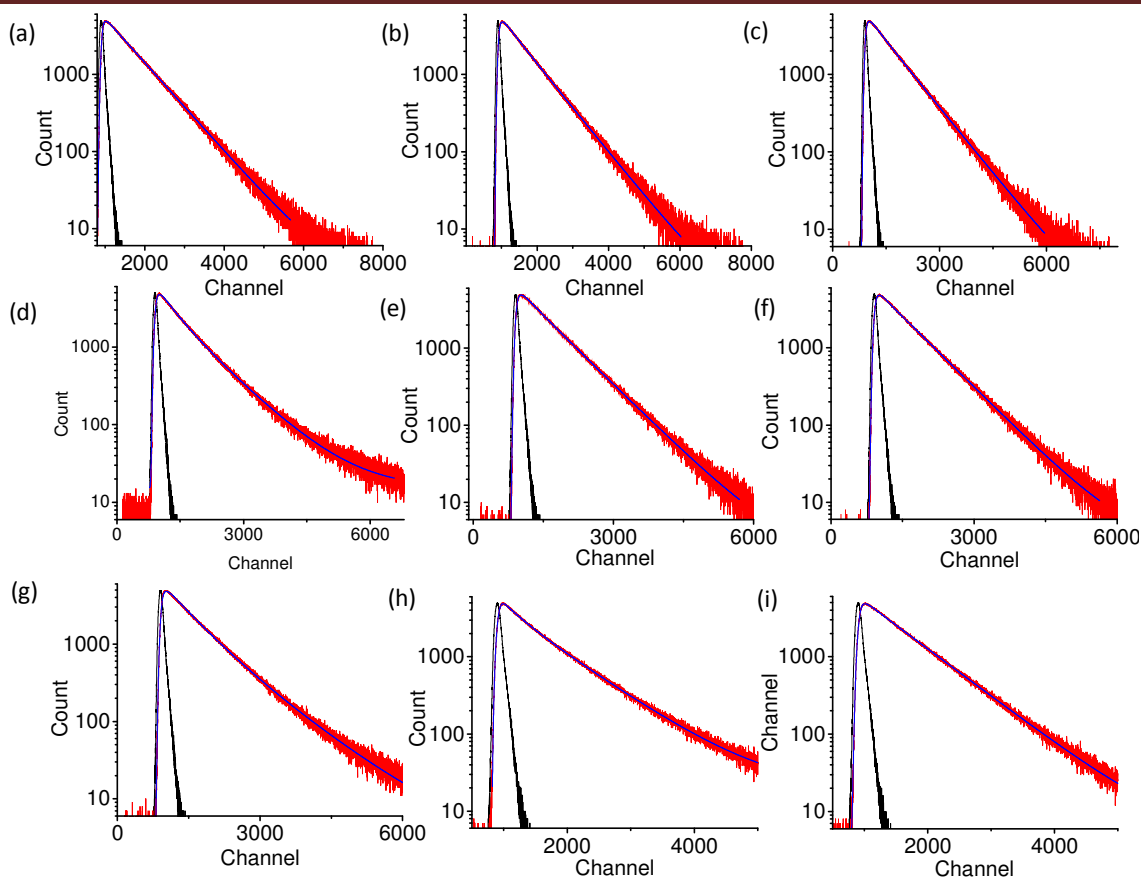


Figure 4.9: Time dependent fluorescent decay of (a) R-H monitored at 365 nm, (b) S-H monitored at 365 nm, (c) Achiral crown monitored at 365 nm, using 295 nm excitation, (d) (1:1) molar mixture of R-H + R-G at 365nm, (e) (1:1) molar mixture of R-H + S-G at 365 nm (f) (1:1) molar mixture of S-H + S-G at 365 nm using 295 nm excitation, (g) (1:1) molar mixture of S-H + R-G at 365 nm, (h) (1:1) molar mixture of Achiral crown + R-G at 365 nm, (i) (1:1) molar mixture of Achiral crown + S-G at 365 nm.

Similarly, bi-exponential decay profiles were also observed for R-G, ($\tau_1 = 2.16 \pm 0.02$ (3.19 %) and $\tau_2 = 8.89 \pm 0.04$ (96.81%) ns and S-G, ($\tau_1 = 2.04 \pm 0.03$ (2.20 %) and $\tau_2 = 9.94 \pm 0.01$ (97.80%) ns upon excitation with a 340 nm laser source. Larger and major components in the decay profiles of R-G and S-G are typical of the anthracene moiety.²⁶ The emission decay profile of a 1:1 mixture of host and guest (R-H + R-G) when monitored at 365 nm showed a biexponential decay with the time constants $\tau_1 = 2.76 \pm 0.04$ (26.40%) and $\tau_2 = 4.07 \pm 0.02$ (73.60%) ns. A decrease in the lifetime of the donor (binaphthol) moiety is evident. However, the decrease is even more substantial ($\tau_1 = 2.50 \pm 0.02$ ns, (4.75 %) and $\tau_2 = 4.17 \pm 0.07$ ns, (95.25%); $\lambda_{\text{Mon}} = 365$ nm) for analogous studies with a 1:1 mixture of R-H and S-G. Also emission decay profile of a 1:1 mixture of host and guest

Chapter 4

(S-H + S-G) when monitored at 365 nm showed a biexponential decay with the time constants $\tau_1 = 0.68 \pm 0.03$ (1.65 %) and $\tau_2 = 3.99 \pm 0.05$ (98.35%) ns. Apart from spectral overlap, the efficiency of the FRET process depends on other factors such as the distance between the donor and acceptor moieties and their relative orientation which influences the transition dipole of the donor and acceptor fluorophores.^{25a} There could be a subtle difference in relative distance and transition dipoles for donor and acceptor fluorophores in diastereomeric supramolecular assemblies of R-H•R-G and R-H•S-G and these could account for the observed differences in the ET efficiencies.

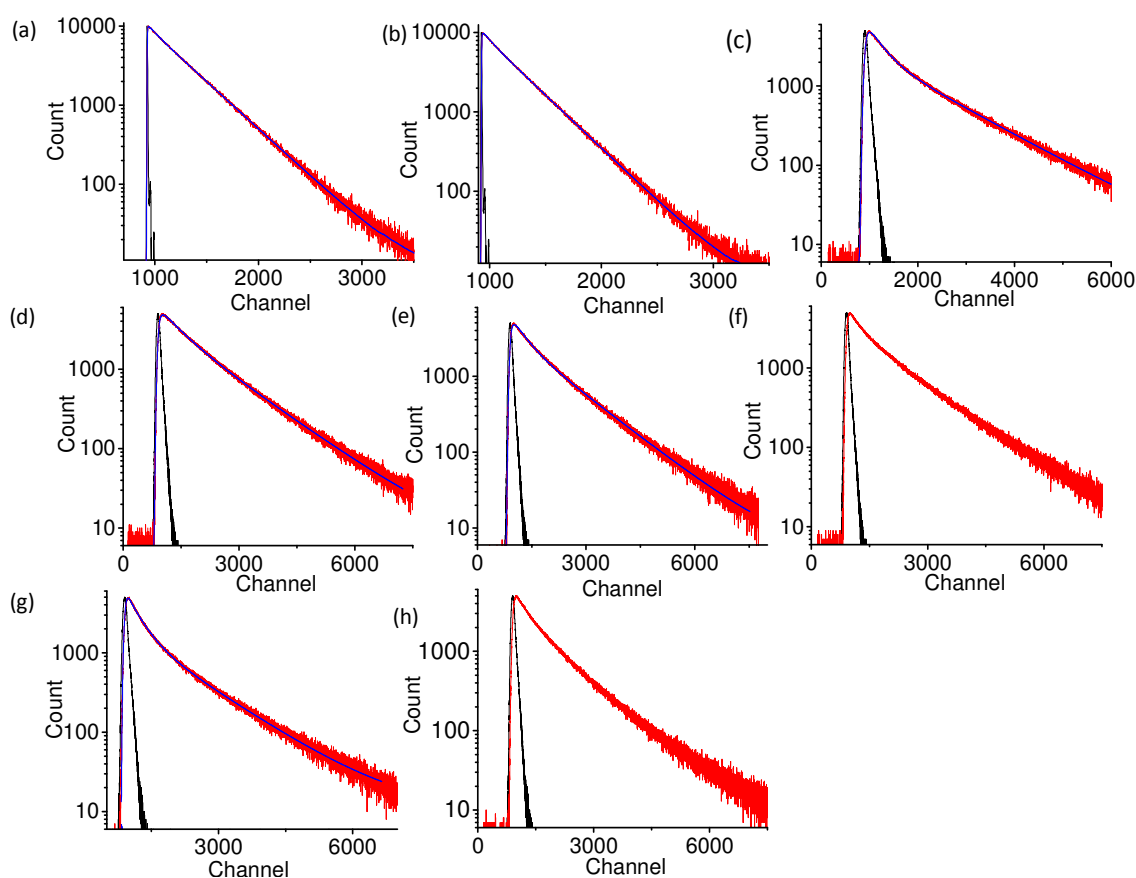


Figure 4.10: Time dependent fluorescent decay of (a) R-G monitored at 420 nm, (b) S-G monitored at 420 nm, using 340 nm excitation, (c) (1:1) molar mixture of R-H + R-G at 420 nm, (d) (1:1) molar mixture of R-H + S-G at 420 nm (e) (1:1) molar mixture of S-H + S-G at 420 nm (f) (1:1) molar mixture of S-H + R-G at 420 nm, (g) (1:1) molar mixture of Achiral crown + R-G at 420 nm, (h) (1:1) molar mixture of Achiral crown + S-G at 420 nm using 295 nm excitation.

The data clearly indicates that on excitation of the donor (binaphthol) moiety, a distinct decrease in the donor lifetime and a substantial increase in the acceptor lifetime is observed. The data for the 1:1 mixture of S-H and S-G further corroborate the assumption

Chapter 4

that enantiomeric recognition causes subtle changes in the relative distance and orientation of the donor and acceptor fluorophore thereby influencing the ET efficiencies as well as ET rates among diastereomeric assemblies of S-H•S-G and S-H•R-G. The decrease in the fluorescence lifetimes of R-H/S-H correlates well with the decrease in their fluorescence quantum yields. The Forster distance (R_0) evaluated by introducing the steady-state and time-resolved emission data in the standard equation is 32.34 Å and 29.12 Å for R-H•R-G and R-H•S-G respectively. In the case of host-guest complexes of opposite chirality the estimated Förster distance (R_0) is 29.55 and 31.50 Å for S-H•R-G and S-H•S-G respectively.

4.3.3. Electrochemical studies

In order to obtain insights into the relative energy levels of the frontier orbitals, oxidation/reduction potentials of the host and guest molecules were measured by cyclic voltammetry (Figure 4.11). The relative HOMO energy levels (E_{HOMO}) of the different fluorophores could be predicted from their oxidation potential values. The band gap energy (E_{0-0}) of each fluorophore was evaluated from the intersection of the corresponding excitation and emission spectra. Redox potentials are reported with respect to ferrocene/ferrocenium as the internal standard.²⁸ The measured oxidation potential values of the chromophores are 1.53 V (anthracene) and 1.75 V (binaphthol). The HOMO-LUMO transition energy was evaluated based on the E_{0-0} values of the chromophores. The transition energies are 3.19 eV and 3.63 eV for the guest (R-G/S-G) and host (R-H/S-H) molecules respectively (Figure 4.11). The estimated energy levels of the frontier orbitals indicates that energy transfer from the binaphthol fragment to the anthracenyl moiety is thermodynamically favourable.

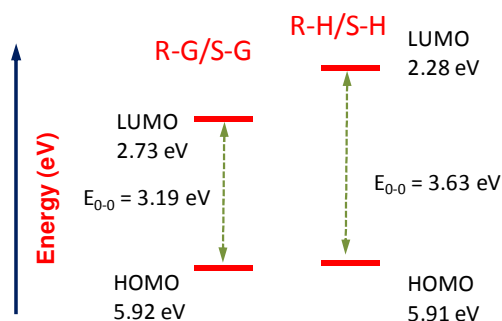


Figure 4.11: Schematic representation of the HOMO-LUMO energy levels for R-G/S-G and R-H/S-H.

4.3.4. Isothermal Titration Calorimetry studies

Intermolecular interactions and changes in thermodynamic parameters associated with complex formation between the different chiral host (R-H or S-H) and guest (R-G or S-G) molecules were investigated in CH_2Cl_2 by isothermal titration calorimetric (ITC) measurements (Figure 4.1) at 298K. The heat of reaction corrected for dilution effects was found to decrease during each injection of host into a solution of the guest molecule. The experimental data indicates a binding stoichiometry of 1:1 for the different [2]pseudorotaxanes. Heat of dilution was evaluated by injecting a solution of individual guest into pure CH_2Cl_2 and this was subtracted from the apparent heat of the reaction measured in the titration experiments for calculating the net reaction heat which was found to decrease after each injection of the host molecules. The calculated binding constants and thermodynamic parameters are shown in Table 4.1.

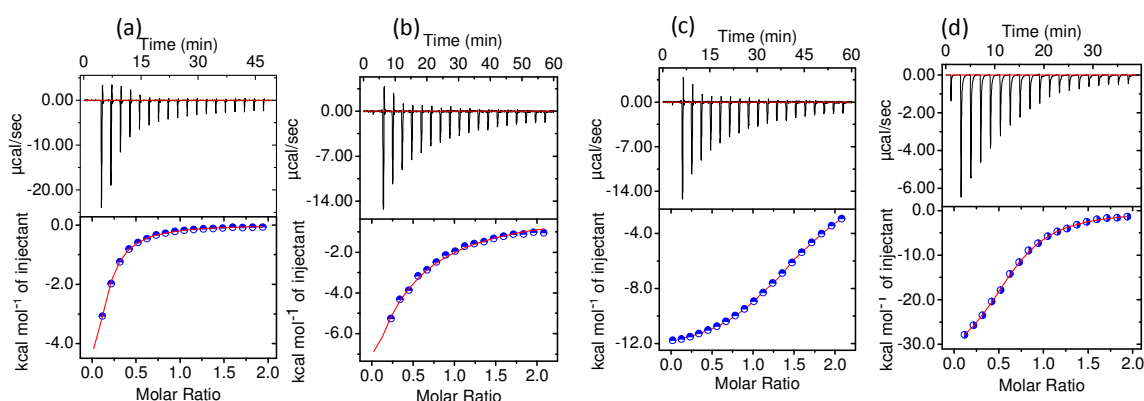


Figure 4.12: ITC profiles for the binding of (a) R-H with R-G, (b) R-H with S-G, (c) S-H with S-G, (d) S-H with R-G at 25°C in CH_2Cl_2 . Top: Raw data for the sequential 2 μl injection of the respective guests into corresponding hosts. Bottom: Plot of the heat evolved (Kcal) per mole of guests added. The data (filled circle) were fitted to a single set binding model and the solid line represented the best fit.

The formation of [2]pseudorotaxane complexes is accompanied by negative enthalpy changes. Presumably this arises from the electrostatic, H bonding, π -stacking, and Van der-waal's interactions upon complexation of host and guest.²⁹ The associated entropy changes are negative and this could be attributed to the conformational rigidity and/or desolvation of host molecule/guest ions.^{29,5} The Gibbs free energy for the formation of the different diastereomeric [2]pseudorotaxane complexes are appreciably negative, indicating that spontaneous formation of these inclusion complexes are thermodynamically

Chapter 4

favourable. The association constants estimated for the four inclusion complexes are comparable (Table 4.1).

This together with the 1:1 binding stoichiometry agrees well with the results of the ^1H NMR titrations. In general, macrocycles with a chiral centre exhibits a preference for binding the same enantiomer of the guest.³⁰ Results of ITC studies (Table 4.1) suggest that the formation of R-H•R-G and S-H•S-G complexes are thermodynamically somewhat more favourable compared to R-H•S-G and S-H•R-G. However, results of the luminescence studies reveal much higher ET efficiencies for R-H•S-G and S-H•R-G compared to R-H•R-G and S-H•S-G. This implies that the relative orientation of the host and guest molecules in the complex is more significant in determining the energy transfer efficiency, rather than the stability of the complex itself. [2]pseudorotaxane complex that allow donor and acceptor fluorophores to come to close to each other, which favours a more efficient energy transfer.

Table 4.1: Thermodynamic data and association constant obtained from the ITC measurements with chiral inclusion complexes formed from hosts R-H, S-H and guests R-G, S-G. ITC measurements were performed in dichloromethane at room temperature.

Host-Guest Complex	Association constant \mathbf{K} (M^{-1})	$\Delta\mathbf{H}$ (kcal.mol^{-1})	$\mathbf{T}\Delta\mathbf{S}$ (kcal.mol^{-1})	$\Delta\mathbf{G}$ (kcal.mol^{-1})
R-H : R-G	$(2.76 \pm 0.19) \times 10^3$	-1.91	-0.122	-1.78
R-H : S-G	$(1.05 \pm .20) \times 10^3$	-1.83	-0.063	-1.76
S-H : S-G	$(3.56 \pm 0.28) \times 10^3$	-1.97	-0.111	-1.86
S-H : R-G	$(2.23 \pm 0.24) \times 10^3$	-1.34	-0.090	-1.25

4.3.5. Circular Dichroism

Circular Dichroism (CD) spectra were recorded for each enantiomerically pure host and guest molecule in dichloromethane. In all cases CD spectra which are mirror images were obtained for the R and S enantiomers of the respective host or guest molecules. As expected, achiral crown ether host is found to be CD silent. A positive CD maximum is observed for the R-binaphthol host (R-H) while the opposite is true for S-H. Guests containing a single chiral centre show a positive couplet for the R enantiomer (R-G) and a negative CD response at 420 nm for the S enantiomer. Although the chiral ammonium group containing guests show CD cotton effect around 350-390 nm, the amplitude is very

Chapter 4

weak. CD spectrum recorded for the inclusion complex R-H•R-G in dichloromethane solution exhibit intense signals with positive cotton effects which is essentially a sum of the cotton effect of the two individual components. In order to evaluate the chiral discriminative effect of R-H in a mixture of R-G and S-G, we recorded CD spectra of R-H in presence of varying molar compositions of R-G and S-G. The most prominent change in cotton effect was observed in a mixture containing 70% S-G and 30% R-G. Analogous experiments were performed using S-H instead of R-H and the most prominent change occurs in a solution having 70% R-G and 30% S-G (Figure 4.13).

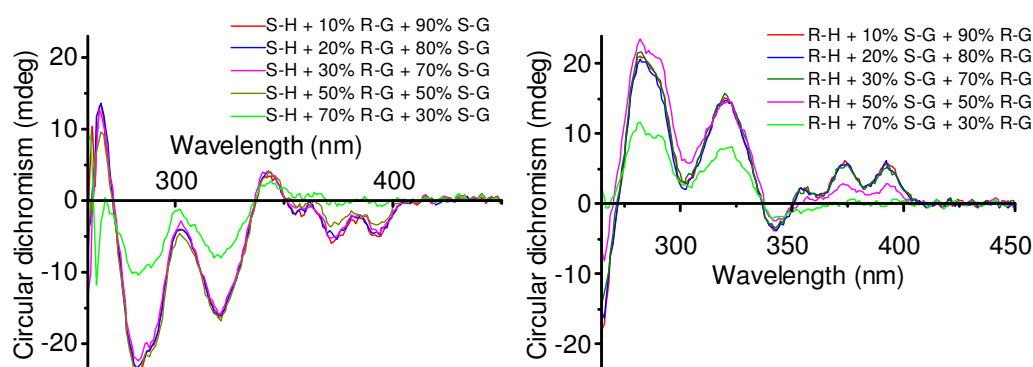


Figure 4.13: CD spectra of (a) R-H in presence of various composition of R-G & S-G; (b) S-H in presence of various composition of R-G & S-G. All studies were performed with dichloromethane solution at 298K.

4.3.6. NMR studies

Appropriately sized crown ethers and its derivatives are known to form hydrogen bonded adducts with secondary ammonium ions ($\text{RNH}_2^+\text{-CH}_2\text{R}'$, R and R' being alkyl or phenyl group) involving by hydrogen bonding ($\text{N}^+\text{-H}\cdots\text{O}$ and $((\text{RNH}_2)^+\text{-CH}_2)\text{C-H}\cdots\text{O}$) interactions. Such binding motif has been used by the researcher for secondary ammonium ions ($\text{RNH}_2^+\text{-CH}_2\text{R}'$) to thread through the cavities of crown ether derivatives to afford interwoven complexes. Earlier reports reveal that chiral crown ether derivatives are used for stereo specific recognition of amino acids and secondary amines.³¹

The formation of host-guest complexes between the chiral host (R-H, S-H) and guest (R-G, S-G) molecules in dichloromethane were examined in more detail by NMR spectroscopy. Most of the signals were readily assigned except for some with heavily overlapped multiplets. The ^1H NMR spectra show broad lines at 298 K hence all

Chapter 4

experiments for obtaining assignments were performed at 278K. The aromatic region of the ^1H NMR spectra of R-H, R-G and a 1:1 mixture of R-H and R-G are shown in Figure 4.14. The addition of one molar equivalent of R-G to R-H results in significant changes in the spectrum. The binding stoichiometry of 1:1 for the formation of the host-guest complex R-H•R-G was determined from the inflection point in the mole ratio plot obtained from titration studies (Figure 4.14D). On complex formation, the signals of R-G double in number while there are three signals corresponding to the R-H protons. In addition there are significant chemical shift changes for several of the guest and host signals, the shifts being more prominent in the latter. The two sets of signals of R-G correspond to the free and bound forms, the latter being shifted with respect to the signals of the free form. In case of R-H, interaction with the guest breaks the molecular symmetry thereby making the two halves of R-H inequivalent in the complex. Thus R-H•R-G spectrum shows two sets of R-H signals in the bound state in addition to the free R-H signals (Figure 4.14, 4.15).

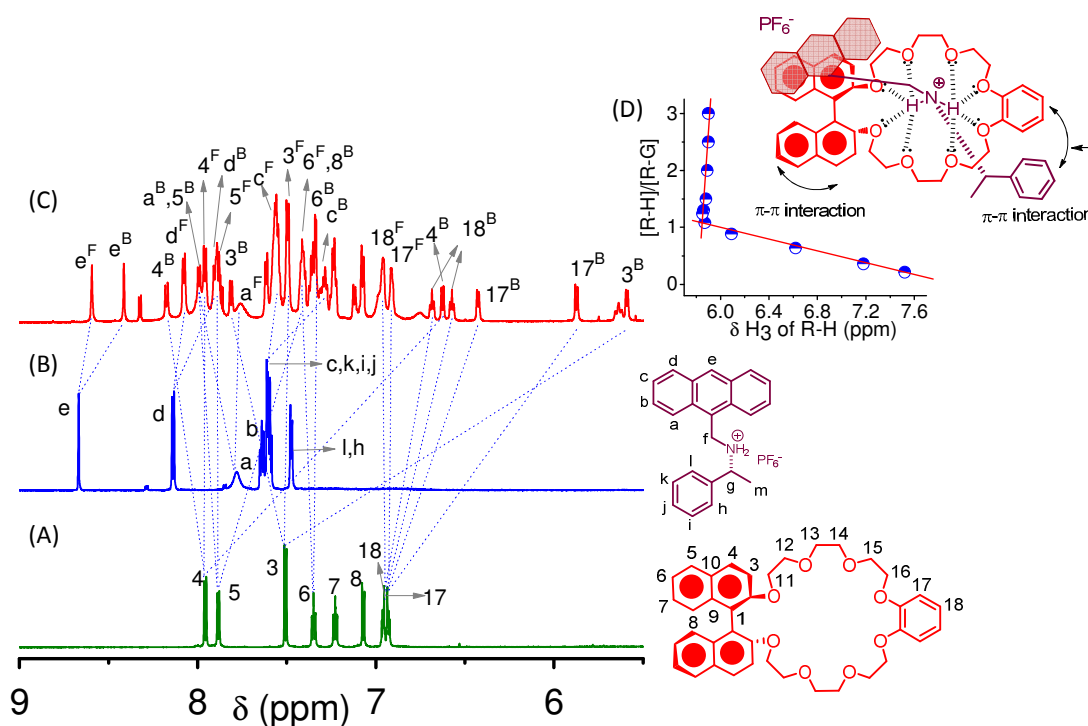


Figure 4.14: Partial ^1H NMR spectra (aromatic region) of (A) 3.85×10^{-3} M of R-H, (B) 3.85×10^{-3} M R-G, (C) equimolar mixture of R-H and R-G in CD_2Cl_2 (700 MHz) at 278K and (D) mole ratio plot for the complexation of R-H with R-G using $\Delta\delta$ (ppm) for the H_3 proton in R-H.

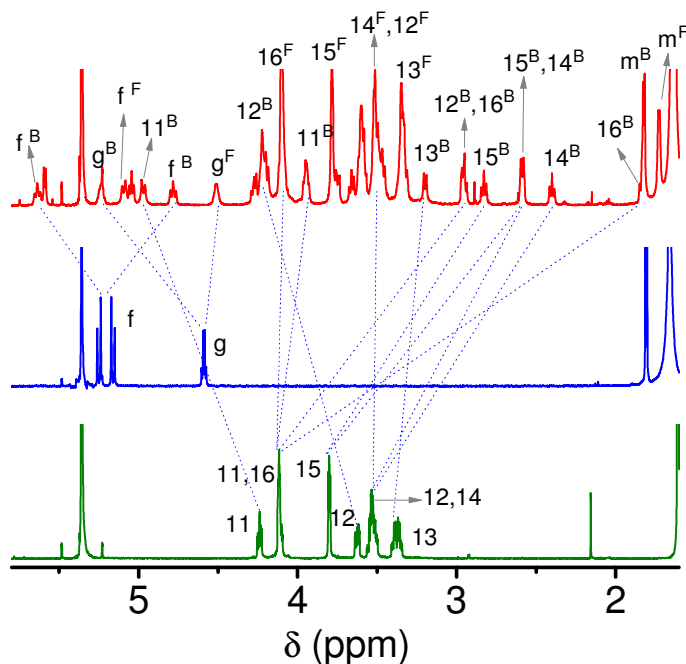


Figure 4.15: Partial ^1H NMR spectra (aliphatic region) of (A) 3.85×10^{-3} M of R-H, (B) 3.85×10^{-3} M R-G, (C) equimolar mixture of R-H and R-G in CD_2Cl_2 (700 MHz) at 278K and (D) mole ratio plot for the complexation of R-H with R-G using $\Delta\delta$ (ppm) for the H_3 proton in R-H.

The chemical shift changes observed for the protons of the anthracenyl moiety of R-G in the 1:1 complex, H_a ($\Delta\delta_{\text{H}} = 0.21\text{ppm}$), H_d ($\Delta\delta_{\text{H}} = -0.23\text{ppm}$), H_c ($\Delta\delta_{\text{H}} = -0.33\text{ppm}$) and H_e ($\Delta\delta_{\text{H}} = -0.26\text{ppm}$) suggests strong π - π stacking interactions with the binaphthol moiety of the R-H. The presence of a chiral carbon adjacent to the NH_2^+ group makes the two CH_2 -protons (H_f) magnetically inequivalent, giving rise to AB quartet in the R-G spectrum which is broad due to weak coupling to the protons of the adjacent positively charged NH_2^+ group (Figure 4.15). Stabilization of the inclusion complex architecture occurs principally via a combination of C-H...O and N⁺-H...O hydrogen bonds involving the NH_2^+ center and the crown ether oxygens. This observation further confirms the [2]pseudororaxane formation.^{32,5} Spectral changes show that the crown ether binds with the NH_2^+ center since the H_f resonance of R-G at 5.09 ppm undergoes a downfield shift to 5.64 ppm ($\Delta\delta_{\text{H}} = 0.55$) while the doublet at 4.97 undergoes an upfield shift to 4.78ppm ($\Delta\delta_{\text{H}} = -0.19$) (Figure 4.15). Also, these shifted signals are sharper and show an additional splitting of the H_f protons in the bound state due to J coupling with the NH_2^+ protons. The chiral methine proton H_g undergoes a downfield shift ($\Delta\delta_{\text{H}} = 0.72\text{ppm}$), which also reflects the interaction of NH_2^+ with the lone pair of electrons on the crown ether oxygens.

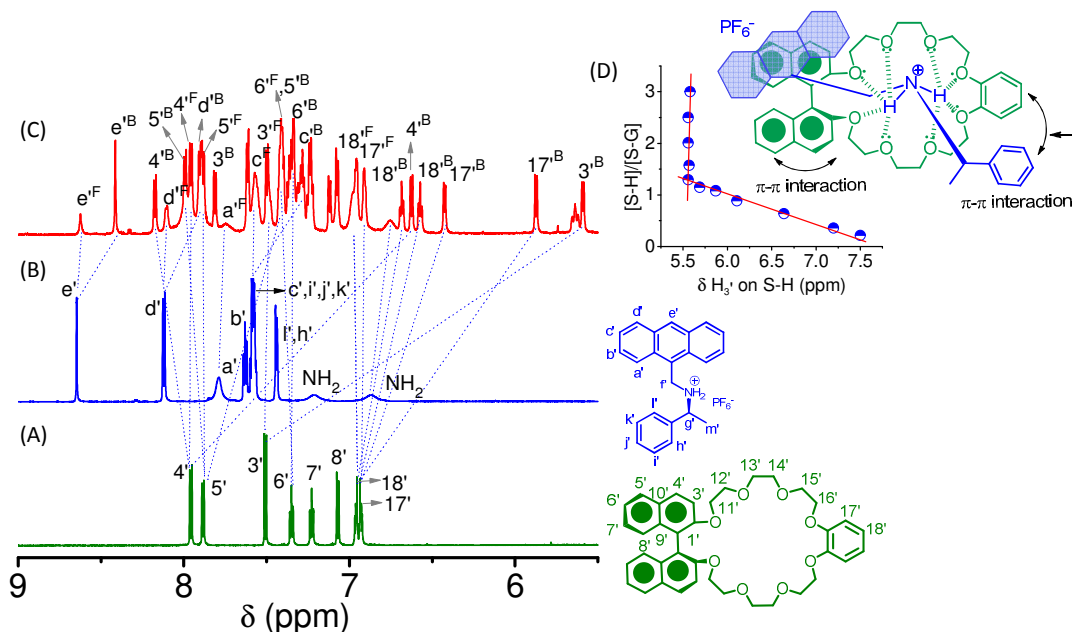


Figure 4.16: Partial ^1H NMR spectra (aromatic region) of (A) 3.30×10^{-3} M of S-H, (B) 3.30×10^{-3} M S-G, (C) equimolar mixture of S-H and S-G in CD_2Cl_2 (700 MHz) at 278 K and (D) mole ratio plot for the complexation of S-H with S-G using $\Delta\delta$ (ppm) for the $\text{H}_{3'}$ proton in S-H.

Significant chemical shift changes were also observed for the signals of the aromatic protons of the binaphthol unit. The doublets of H_3 , H_4 and H_5 undergo significant upfield and downfield shifts corresponding to the two inequivalent halves of the binaphthol unit in the complex. The upfield shifts ($\Delta\delta_3 = -1.94\text{ppm}$, $\Delta\delta_4 = -1.33\text{ppm}$, $\Delta\delta_5 = -0.49\text{ ppm}$) are considerably higher than the downfield shifts ($\Delta\delta_3 = 0.31\text{ppm}$, $\Delta\delta_4 = 0.22\text{ppm}$, $\Delta\delta_5 = 0.11\text{ ppm}$). These chemical shift changes result from the π - π stacking interactions with the anthracenyl moiety of R-G. Clearly, the anthracenyl moiety should be positioned close to the one of the "naphthyls" of the binaphthol unit which experiences shielding in the complex. The other half (other "naphthyl" unit) of the binaphthol being positioned laterally with respect to the anthracenyl group, experiences deshielding. The phenyl ring protons of R-H also show chemical shift changes in the complex. The H_{17} protons of R-H become inequivalent in the complex and shifts upfield, resonating at 6.42 ppm ($\Delta\delta_{\text{H}} = -0.48\text{ppm}$) and 5.86 ppm ($\Delta\delta_{\text{H}} = -1.32\text{ ppm}$). Similarly the adjacent H_{18} protons become inequivalent with upfield shifts of $\Delta\delta_{\text{H}} = -0.39\text{ ppm}$ and $\Delta\delta_{\text{H}} = -0.28\text{ ppm}$. In the free state, the H_{17} and H_{18} protons form a AA'BB' type spin system and has broad signals but the inequivalence of the two halves of the host on binding to the guest, makes the phenyl ring protons of R-H into an AMKX type spin system which gives sharp doublets for H_{17} and sharp triplets for

Chapter 4

H_{18} in the complex. Large changes are also observed for the oxy-methylene protons adjacent to the phenyl group of R-H. The H_{16} protons becomes inequivalent and undergoes large upfield shifts in the complex, $\Delta\delta_H = -1.14\text{ppm}$ and $\Delta\delta_H = -2.27\text{ppm}$. Similarly the adjacent H_{15} protons show shifts of $\Delta\delta_H = -0.95\text{ppm}$ and $\Delta\delta_H = -1.19\text{ppm}$. In the complex, the guest molecule threads through the crown with the phenyl ring of the guest being positioned adjacent to the phenyl ring of the host. Thus the phenyl ring protons H_{17} , H_{18} and adjacent oxy-methylene protons H_{15} and H_{16} experience shielding effects due to the proximity to the R-G phenyl ring. The guest molecule is not positioned exactly along the center hence the distance of the R-G phenyl ring to the oxy-methylene units on either side of the crown is different resulting in greater or lesser shielding effects (Figure 4.14,4.15). The protons of the oxy-methylene units close to the binaphthol moiety of the host (H_{11} , H_{12}) also shows shielding and deshielding effects depending on the proximity and orientation with respect to the anthracenyl moiety of R-G. For example, in the complex, H_{11} protons on one side of the crown is shielded ($\Delta\delta_H = -0.32\text{ppm}$) while those on the other side is deshielded ($\Delta\delta_H = 0.77\text{ppm}$).

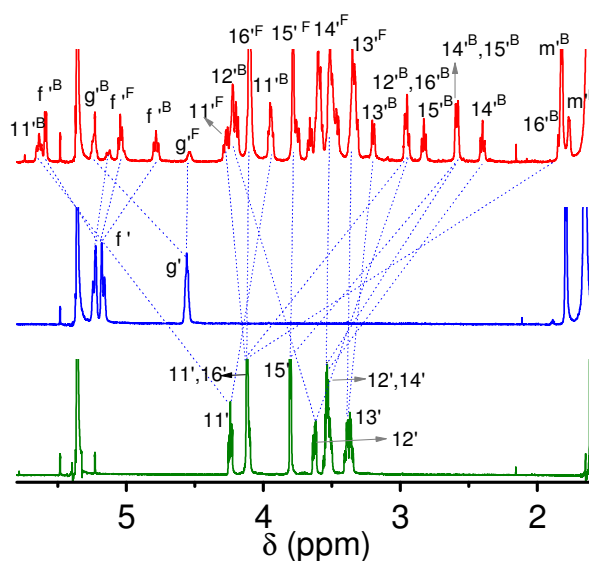


Figure 4.17: Partial ^1H NMR spectra (aliphatic region) of (A) 3.30×10^{-3} M of S-H, (B) 3.30×10^{-3} M S-G, (C) equimolar mixture of S-H and S-G in CD_2Cl_2 (700 MHz) at 278 K and (D) mole ratio plot for the complexation of S-H with S-G using $\Delta\delta$ (ppm) for the $H_{3'}$ proton in S-H.

Host-guest complex formation between S-H and S-G also has a 1:1 binding stoichiometry and the changes in the NMR spectrum as a result of the host-guest interaction is similar to that observed in the case of R-H•R-G (Figure 4.16, 4.17). The spectral changes

accompanying complex formation is readily seen in the 2D HSQC spectrum shown in Figure 4.17. Spectra of both R-H•R-G and S-H•S-G show sharp signals for the free and bound forms indicating that the host, guest and complex are in a slow exchange equilibrium.

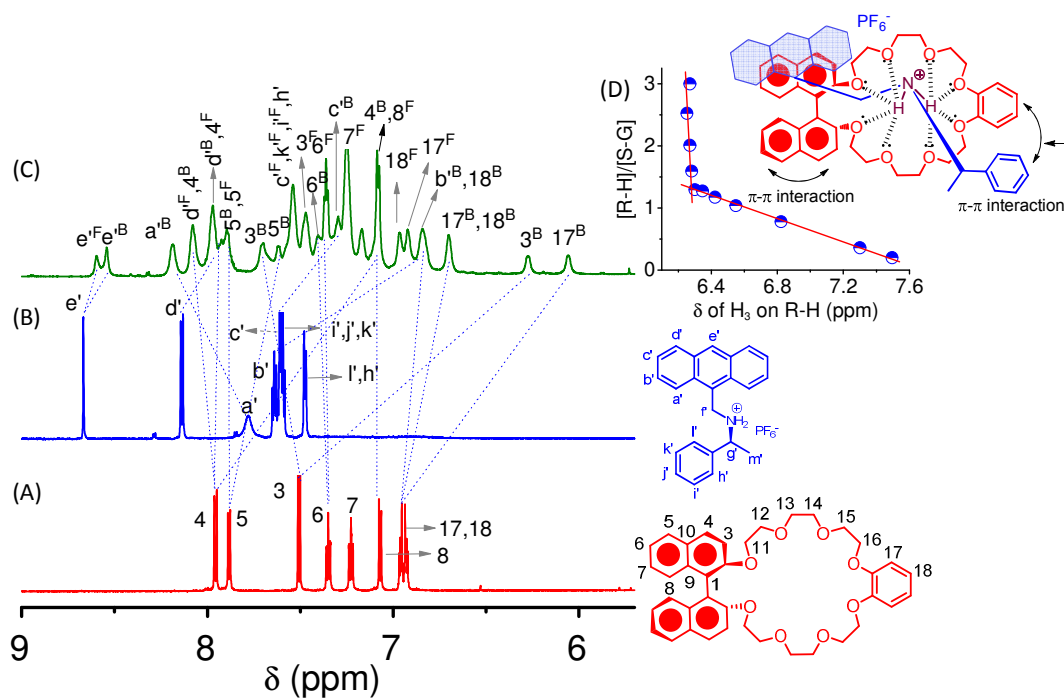


Figure 4.18: Partial ^1H NMR spectra (aromatic region) of (A) 3.85×10^{-3} M of R-H, (B) 3.85×10^{-3} M S-G, (C) equimolar mixture of R-H and S-G in CD_2Cl_2 (700 MHz) at 268K and (D) mole ratio plot for the complexation of R-H with S-G using $\Delta\delta$ (ppm) for the H_3 proton in R-H.

Compared to the interaction between host and guest molecules of the same chirality, complex formation between partners of opposite chirality shows several differences. Figure 4.18 shows the aromatic region of the ^1H NMR spectra of R-H, S-G and a 1:1 mixture of R-H and S-G. The mole-ratio plot again indicates a 1:1 binding stoichiometry for the formation of R-H•S-G. In the complex, R-H shows three sets of signals while S-G shows two sets of signals analogous to what is observed in complexes between hosts and guests of same chirality. However the spectral lines of the complex are significantly broader compared to that of R-H•R-G and S-H•S-G. Also, the chemical shift changes accompanying complex formation are considerably lower as seen in Figure 4.18 and 4.19. The anthracenyl protons of S-G, namely H_a , H_d , H_c and H_e undergo chemical shift changes of $\Delta\delta_{\text{H}} = 0.50$, $\Delta\delta_{\text{H}} = -0.11$, $\Delta\delta_{\text{H}} = -0.25$ and $\Delta\delta_{\text{H}} = -0.05$ ppm respectively. While the deshielding of H_a increases, the shielding of the other aromatic protons decrease relative

Chapter 4

to that in R-H•R-G and S-H•S-G. Similarly, there is a decrease in the chemical shift changes of the methylene, H_f ($\Delta\delta_{\text{H}} = 0.51$ ppm) and methine protons, H_g ($\Delta\delta_{\text{H}} = 0.34$ ppm) of S-G. Clearly, there is a change in the extent of π - π stacking interactions in complexes formed between host and guest of opposite chirality, which is also reflected in the chemical shift changes of the host R-H in the R-H•S-G complex.

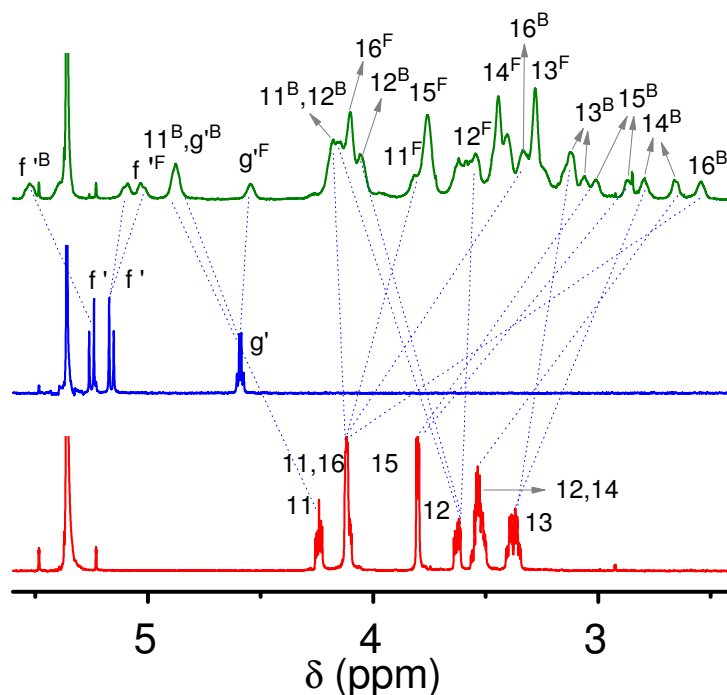


Figure 4.19: Partial ¹H NMR spectra (aliphatic region) of (A) 3.85×10^{-3} M of R-H, (B) 3.85×10^{-3} M S-G, (C) equimolar mixture of R-H and S-G in CD₂Cl₂ (700 MHz) at 268K and (D) mole ratio plot for the complexation of R-H with S-G using $\Delta\delta$ (ppm) for the H₃ proton in R-H.

The two sets of protons H₃, H₄ and H₅ of the binaphthol unit in R-H are inequivalent in R-H•S-G and shows changes due to shielding as well as deshielding. Protons on one of the naphthyl units show shielding, ($\Delta\delta_3 = -1.2$ ppm, $\Delta\delta_4 = -0.88$ ppm, $\Delta\delta_5 = -0.28$ ppm) while those on the other are deshielded ($\Delta\delta_3 = 0.23$ ppm, $\Delta\delta_4 = 0.1$ ppm, $\Delta\delta_5 = 0.03$ ppm). The magnitude of the chemical shift changes is much reduced in comparison to those in R-H•R-G and S-H•S-G. This is also the case for the phenyl ring protons and adjacent oxy-methylene groups. The shielding induced changes for the H₁₇ protons are $\Delta\delta_{\text{H}} = -0.86$ ppm and $\Delta\delta_{\text{H}} = -0.22$ ppm while those of H₁₈ are $\Delta\delta_{\text{H}} = -0.26$ ppm and $\Delta\delta_{\text{H}} = -0.14$ ppm. The oxy-methylene protons on each half of the crown show inequivalent shifts; H₁₆ ($\Delta\delta_{\text{H}} = -0.69$ ppm and $\Delta\delta_{\text{H}} = -1.55$ ppm), H₁₅ ($\Delta\delta_{\text{H}} = -0.74$ ppm and $\Delta\delta_{\text{H}} = -0.89$ ppm) and H₁₄ $\Delta\delta_{\text{H}} = -$

Chapter 4

0.64ppm and $\Delta\delta_H = -0.78$ ppm. The trends observed for the S-H•R-G complex is very similar to that of R-H•S-G (Figure 4.20,4.21).

The NMR results indicate that the orientation of the guest molecule with respect to the host is different in R-H•R-G / S-H•S-G and R-H•S-G / S-H•R-G. In addition, the line shapes clearly shows that the exchange equilibrium is different in the two cases with the free and bound forms in a slow exchange on the NMR time scale in case of R-H•R-G / S-H•S-G and intermediate exchange in R-H•S-G / S-H•R-G. Temperature dependent NMR spectra clearly shows that the signals in R-H•S-G and S-H•R-G reveal multiplets only at much lower temperatures compared to R-H•R-G / S-H•S-G complexes.

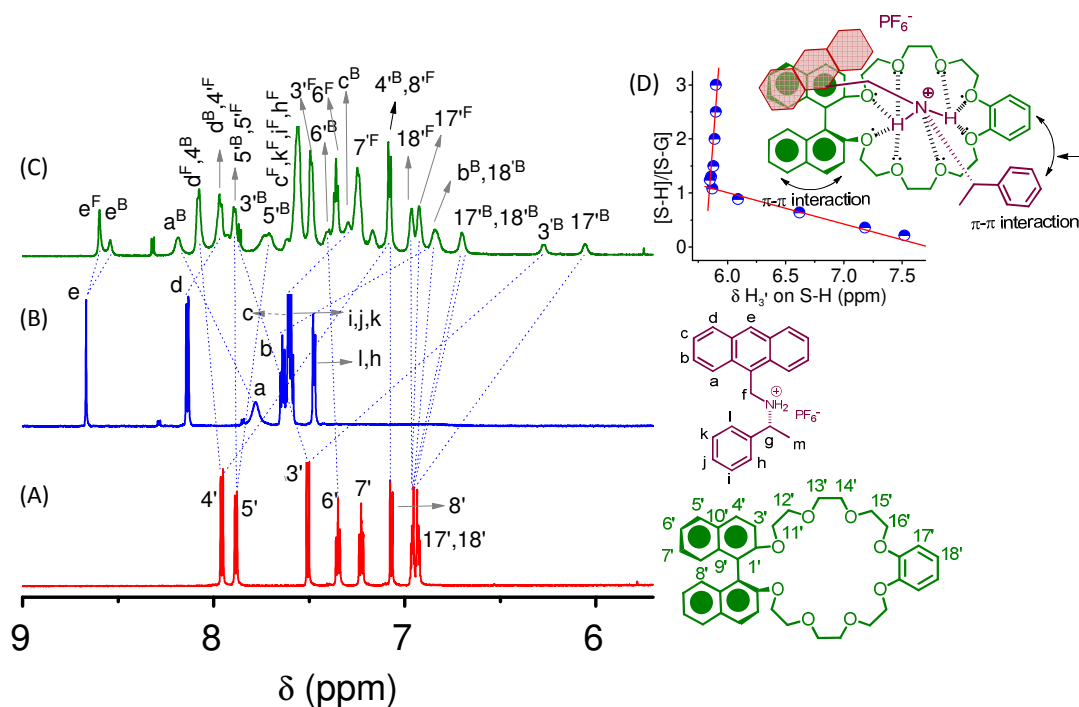


Figure 4.20: Partial ^1H NMR spectra of (A) 3.27×10^{-3} M of S-H, (B) 3.27×10^{-3} M R-G, (C) equimolar mixture of S-H and R-G in CD_2Cl_2 (700 MHz) and at 268K (D) mole ratio plot for the complexation of S-H with R-G using $\Delta\delta$ (ppm) for the H_3 proton in S-H.

In order to quantify the exchange process, NOESY experiments were carried out on the four different complexes at different mixing times. Initially, the exchange kinetics was analyzed by monitoring the well separated H_e proton signals of the guest molecule corresponding to the bound and free forms (Figure 4.22).

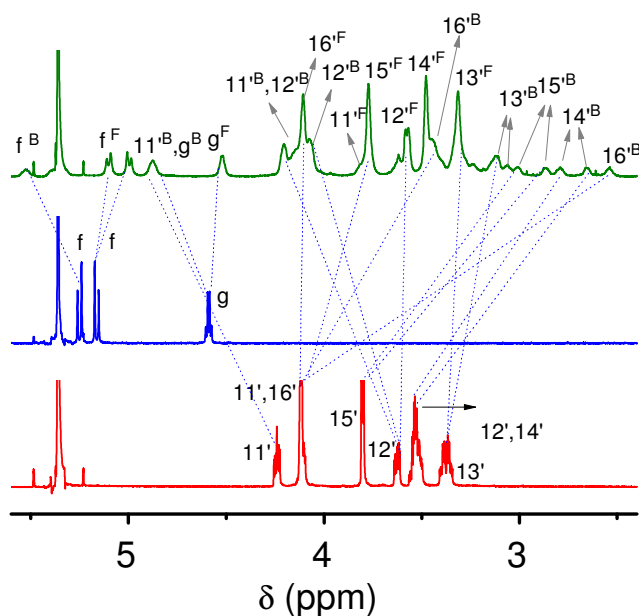


Figure 4.21: Partial ^1H NMR spectra of (A) 3.27×10^{-3} M of S-H, (B) 3.27×10^{-3} M R-G, (C) equimolar mixture of S-H and R-G in CD_2Cl_2 (700 MHz) and at 268K (D) mole ratio plot for the complexation of S-H with R-G using $\Delta\delta$ (ppm) for the H_3 proton in S-H.

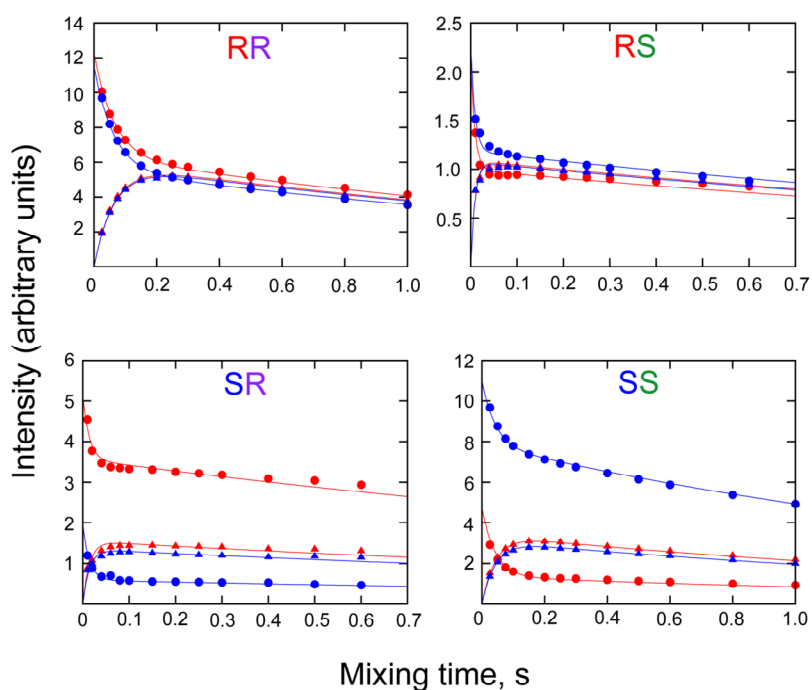
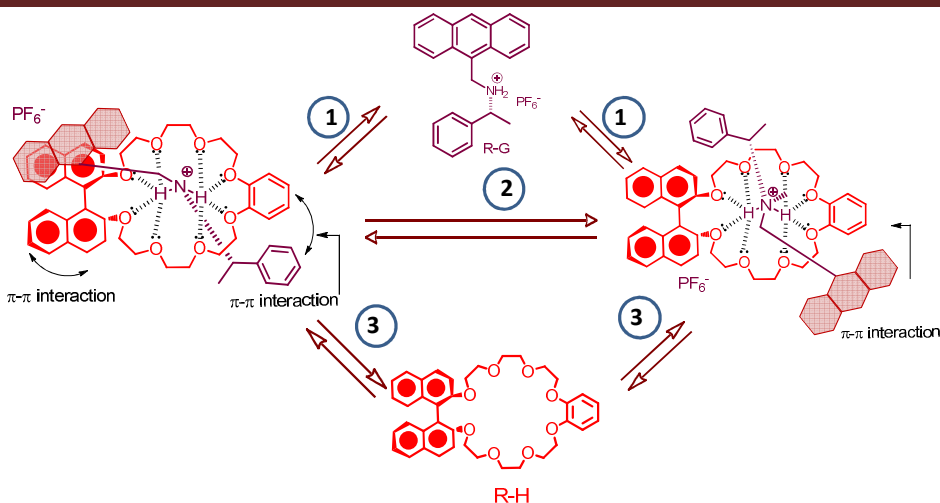


Figure 4.22: Fits of decay and build-up curves for H_e proton of the guest molecule exchanging between free and bound forms.

Chapter 4

The apparent exchange rates were determined by fitting the equations for cross peak build-up and diagonal peak decay to the experimental data. At 278K, the exchange rates evaluated based on a two site exchange model are 15.4, 23.5, 110.0 and 71.0 s⁻¹ for R-H•R-G, S-H•S-G, R-H•S-G and S-H•S-G respectively. Even though the rates are different for the four complexes, the much higher exchange rates observed for complexes with host and guest molecules of opposite chirality, clearly indicate that R-H•S-G / S-H•R-G are less stable compared to R-H•R-G / S-H•S-G. This is in agreement with the results from ITC experiments which also reveal that R-H•R-G / S-H•S-G complexes are thermodynamically more favorable. Even though the guest molecule shows only two sets of signals corresponding to free and bound forms, the host molecules show three sets of signals of which two are from bound forms. The protons of the guest molecule, have the same chemical shift in the two bound forms, hence the two cannot be distinguished based on the signals from the guest. The host signals in the much better resolved NOESY spectra of R-H•R-G and S-H•S-G, clearly show exchange cross peaks between the two bound forms of the complex, in addition to the exchange cross peaks with the free form. This implies that there are two possible ways in which the guest molecule can be aligned with respect to the host molecule in the complex. In both these cases, the environment of the guest protons remain the same, however the two halves of the host which are inequivalent in the complex, are reversed for each possible orientation of the guest molecule. Exchange equilibrium in a benzo-naphtho-24-crown-8 complex with dipyridinium ion based guests have been reported previously.³³ The exchange was explained in terms of two possible orientations in which the dipyridinium unit maybe aligned with the naphtho or benzo end of the crown ether. In the present case a similar exchange model would mean that the guest molecule could be bound with the anthracenyl unit towards the binaphthol end or the phenyl end of the host. This would imply that the guest would show signals corresponding to two different bound environments, since chemical shift perturbations could be quite different depending on whether the anthracenyl unit is stacked on the binaphthol or phenyl group. However, we do not observe signals corresponding to two bound environments for the guest molecule, hence the exchange might involve guest orientations in which the anthracenyl group maybe aligned with either of the "naphthyl" units in binaphthol as represented in Scheme 4.1.

Chapter 4



Scheme 4.1: Cartoon representation of exchange equilibrium mediated by corresponding guest and host. (1) Guest exchanges between bound and free form (quantified from NOESY mixing time dependence), (2) bound signal of host exchanges with another bound form, (3) bound signal of host exchanges with free form of host.

The environment of the guest molecule would remain the same for both these orientations but the two halves of the host molecule would show different sets of signals in the complex. We analyzed the exchange equilibrium by monitoring the H₄ proton signals of the host in R-H•R-G and S-H•S-G at 278K.

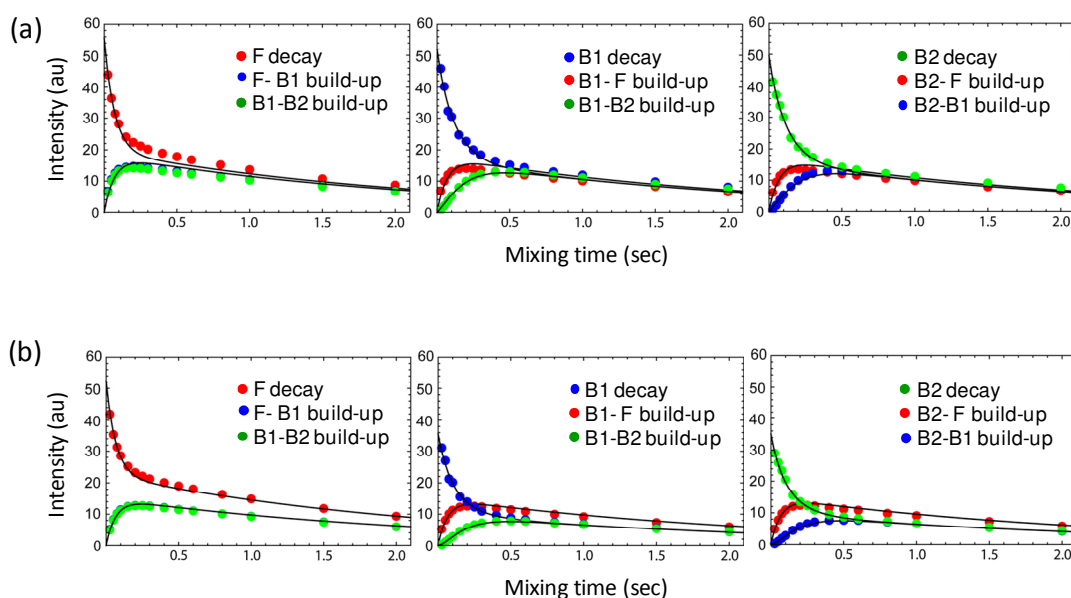


Figure 4.23: Fits of decay and build-up curves for H₄ proton of the host molecule exchanging between free and bound forms.

Chapter 4

The build-up of cross peaks and decay of the diagonal peaks were fit to a three site exchange model represented schematically in figure 4.23. The build-up of the cross peak intensity corresponding to the exchange between free and bound states is faster while the cross peaks connecting the two bound states build up slower. The exchange rates from 'bound to free' and 'free to bound' are defined as k_{12} and k_{21} respectively, without any distinction between the two bound states. The exchange between the two bound states is defined as k_{23} . The rates estimated from the fits to the experimental data are $k_{12} = 4.54 \text{ s}^{-1}$, $k_{21} = 4.77 \text{ s}^{-1}$, $k_{23} = 0.93 \text{ s}^{-1}$ for R-H•R-G and $k_{12} = 4.22 \text{ s}^{-1}$, $k_{21} = 6.22 \text{ s}^{-1}$, $k_{23} = 0.25 \text{ s}^{-1}$ for S-H•S-G. On the basis of the higher 'free to bound' exchange rate and lower exchange rate between bound states, the S-H•S-G complex seems to be somewhat more stable compared to R-H•R-G. This observation also agrees with the slightly higher association constant estimated for S-H•S-G from ITC experiments. Similar three site exchange analysis could not be carried out for the R-H•S-G and S-H•R-G complexes due to much broader spectral lines causing considerable overlap of signals. Even though the broadening of spectral lines, and large chemical shift changes induced on mixing the host and guest molecules in 1:1 ratio clearly indicates intermolecular interaction and complex formation, the complexes are very dynamic. Even at very low temperatures (248 K), the exchange persists and ROESY spectra show positive cross peaks due to exchange between free and bound forms. Interestingly, the benzo-naphtho-24-crown-8 complex with dipyrindinium ion based guests was also reported to show rapid chemical exchange even at temperatures as low as 195K in CD_2Cl_2 .³³ While the negative intramolecular NOE cross peaks became more visible due to slowing down of exchange at lower temperature, intermolecular cross peaks between host and guest could not be observed since the exchange dynamics makes it a loosely bound complex. Hence the relative orientation of the host and guest molecules in the complex can only be inferred on the basis of the chemical shift differences resulting from π - π stacking interactions and difference in exchange dynamics.

Results of NMR and ITC experiments clearly show that R-H•R-G and S-H•S-G complexes are more stable compared to R-H•S-G and S-H•R-G. However, optical measurements show that FRET is more efficient in R-H•S-G and S-H•R-G which undergoes faster exchange. The time scale of the exchange between bound and free forms is of the order of milliseconds while the FRET process occurs on a time scale that is shorter by several orders of magnitude. NMR results clearly show that the orientation of the guest with

Chapter 4

respect to the host is different in R-H•R-G / S-H•S-G and R-H•S-G / S-H•R-G, the latter pair probably being more favorable for FRET.

4.4. Conclusion

In this chapter it was shown that chiral crown ethers with binaphthol chromophore units are efficient sensing materials for the discrimination of enantiomer amine pairs through FRET mechanism. The remarkable chiral recognition of the guests with impressive enantioselectivity may result from their different orientations in the host cavity. Complexes having host and guest of opposite chirality was found to give a more efficient FRET transfer compared to complexes with host and guest of same chirality. In general there is a tendency for chiral hosts to include guests with the same absolute configuration. This was confirmed by ITC experiments which show higher thermodynamic stability for R-H.R-G and S-H.S-G compared to R-H.S-G and S-H.R-G. Also the exchange rates determined by NMR are lower for R-H.R-G and S-H.S-G, implying greater stability for these complexes. NMR studies reveal that the shielding and deshielding effects on complexation is significantly different when a host binds a guest of same or opposite chirality implying that the relative orientation of the guest in the host cavity changes. In R-H.S-G and S-H.R-G, the relative orientation and distance of the fluorophores is more favorable for FRET compared to that in R-H.R-G and S-H.S-G, thus providing a basis for discrimination of enantiomers.

4.5. References

1. (a) Tanaka, H.; Matile, S. *Chirality* **2008**, *20*, 307–312; (b) Pu, L. *Chem. Rev.* **2004**, *104*, 1687.
2. (a) Moberg, C. *Angew. Chem., Int. Ed.* **1998**, *37*, 248; (b) Davis, A. P.; Wareham, R. S. *Angew. Chem., Int. Ed.* **1999**, *38*, 2978; (c) Wei, J. J.; Schafmeister, C.; Bird, G.; Paul, A.; Naaman, R.; Waldeck, D. H. *J. Phys. Chem. B* **2006**, *110*, 1301; (d) Hazen, R. M.; Sholl, D. S. *Nat. Mater.* **2003**, *2*, 367.
3. (a) Horvath, J. D.; Koritnik, A.; Kamakoti, P.; Sholl, D. S.; Gellman, A. J. *J. Am. Chem. Soc.* **2004**, *126*, 14988; (b) Horvath, J. D.; Gellman, A. J. *J. Am. Chem. Soc.* **2002**, *124*, 2384; (c) Talma, A.G.; Jouin, P.; Vries, J.G. D.; Troostwijk, C.B.; Buning, G.H. W.; Waninge, J.K.; Visscher, J.; Kellogg R.M. *J. Am. Chem. Soc.* **1985**, *107*, 3981; (d) Hembury, G. A.; Borovkov, V. V.; Inoue, Y. *Chem. Rev.* **2008**, *108*, 1.
4. (a) Jiao, J.; Wei, G.; Li, F.; Mao, X.; Cheng Y.; Zhu C. *RSC Adv.*, **2014**, *4*, 5887; (b) Huang, Z.; Yu, S.; Zhao, X.; Wen, K.; Xu, Y.; Yu, X.; Xu, Y.; Pu, L. *Chem. Eur. J.* **2014**, *20*, 16458; (c) Cheng, C.; Cai, Z.; Peng, X.-S.; Wong, H. N. C. *J. Org. Chem.* **2013**, *78*, 8562.
5. Mandal, A. K.; Suresh, M.; Kesharwani, M. K.; Gangopadhyay, M.; Agrawal, M.; Boricha, V. P.; Ganguly, B.; Das, A. *J. Org. Chem.* **2013**, *78*, 9004.
6. (a) Grove, J.T.; Viski, P. *J. Org. Chem.* **1990**, *55*, 3628; (b) Malley, S. O.; Kodadek, T. *Organometallics* **1992**, *11*, 2299; (c) Misiti, G. D.; Borchardt, A.; Burger, M.T.; Still, W.C. *J. Org. Chem.* **1995**, *60*, 4314; (d) Helgeson, R.C.; Koga, K.; Timko, J.M.; Cram, J. *J. Am. Chem. Soc.* **1973**, *95*, 3021; (e) Webb, T.H.; Suh, H.; Wilcox C.S. *J. Am. Chem. Soc.* **1991**, *113*, 8554.
7. Zhang, X. X.; Bradshaw, J. S.; Izatt, R. M. *Chem. Rev.* **1997**, *97*, 3313.
8. Chao, Y.; Cram, D. J. *J. Am. Chem. Soc.* **1976**, *98*, 1015.
9. (a) Cram, D. J.; Trueblood, K. N. *Springer*, Berlin, **1981**, *2*, 43; (b) Chin, J. K.; Lee, K. J.; Park, S.; Kim, D. H. *Nature* **1999**, *401*, 254.
10. (a) Ghosn, M. W.; Wolf, C. *J. Am. Chem. Soc.* **2009**, *131*, 16360; (b) Liu, H. L.; Peng, Q.; Wu, Y. D.; Chen, D.; Hou, X. L.; Sabat, M.; Pu, L. *Angew. Chem., Int. Ed.* **2010**, *49*, 602; (c) Wong, W. L.; Huang, K. H.; Teng, P. F.; Lee, C. S.; Kwong, H. L. *Chem. Commun.* **2004**, 384; (d) Yang, D.; Li, X.; Fan, Y. F.; Zhang, D. W. *J. Am. Chem. Soc.* **2005**, *127*, 7996.

Chapter 4

11. (a) Kubo, Y., Maeda, S., Tokita, S. Kubo, M. *Nature* **1996**, *382*, 522; (b) Zhu, L. & Anslyn, E. V. *J. Am. Chem. Soc.* **2004**, *126*, 3676; (c) Tsubaki, K., Nuruzzaman, M., Kusumoto, T., Hayashi, N., Bin-Gui, W., Fuji K. *Org. Lett.* **2001**, *3*, 4071.
12. (a) Matsushita, M., Yoshida, K., Yamamoto, N., Wirsching, P., Lerner, R. A., Janda, K. D., *Angew. Chem. Int. Ed* **2003**, *42*, 5984; (b) Yu, S.; Pu, L. *J. Am. Chem. Soc.* **2010**, *132*, 17698; (c) James, T.D.; Sandanayake, K.R.A.S.; Shinkai, S. *Nature* **1995**, *374*, 345.
13. (a) Labuta, J.; Ishihara, S.; S̆ikorsky', T.; Futera, Z.; Shundo, A.; Hanykova, L.; Burda, J. V.; Ariga, K.; Hill, J. P. *Nat. Commun.* **2013**, doi: 10.1038/ncomms3188; (b) Mizuno, Y., Aida, T. Yamaguchi, K.. *J. Am. Chem. Soc.* **2000**, *122*, 5278; (c) Nieto, S., Lynch, V. M., Anslyn, E. V., Kim, H. & Chin, J. *J. Am. Chem. Soc.* **2008**, *130*, 9232.
14. Mirri, G.; Bull, S. D.; Horton, P. N.; James, T. D.; Male L.; Tucker, J. H. R.; *J. Am. Chem. Soc.* **2010**, *132*, 8903; (b) Huszthy, P.; Oue, M.; Bradshaw, J. S.; Zhu, C. Y.; Wang, T.; Dalley, N. K.; Curtis, J. C.; Izatt, R. M. *J. Org. Chem.* **1992**, *57*, 5383.
15. Biedermann, F.; Nau, W. M. *Angew. Chem., Int. Ed.*, **2014**, *53*, 5694.
16. (a) Leung, D., Kang, S. O., Anslyn, E. V. *Chem. Soc. Rev.* **2012**, *41*, 448; (b) Accetta, A., Corradini, R., Marchelli, R., *Top. Curr. Chem.* **2010**, *300*, 175; (c) Zhang, X., Yin, J., Yoon, J. *Chem. Rev.* **2014**, *114*, 4918; (d) Yu, G.; Jie, K.; Huang, F. *Chem. Rev.* **2015**, *115*, 7240.
17. Izatt, R. M.; Wang, T.; Hathaway, J. K.; Zhang, X. X.; Curtis, J. C.; Bradshaw, J. S.; Zhu, C. Y. *J. Inclusion Phenom. Mol. Recognit. Chem.* **1994**, *17*, 157.
18. (a) Kyba, E. P.; Siegel, M. G.; Sousa, L. R.; Sogah, G. D. Y.; Cram, D. J. *J. Am. Chem. Soc.* **1973**, *95*, 2691; (b) Kyba, E. P.; Koga, K.; Sousa, L. R.; Siegel, M. G.; Cram, D. J. *J. Am. Chem. Soc.* **1973**, *95*, 2692.
19. Pu, L. *Chem. Rev.* **1998**, *98*, 2405.
20. (a) Upadhyay, S. P.; Karnik, A. V. *Tetrahedron Lett.* **2007**, *48*, 317; (b) Karnik, A. V.; Upadhyay, S. P.; Gangrade, M. G. *Tetrahedron: Asymmetry* **2006**, *17*, 1275.
21. Yu, S. S.; Plunkett, W.; Kim, M.; Pu, L. *J. Am. Chem. Soc.*, **2012**, *134*, 20282.
22. Zhang, X. X.; Bradshaw, J. S.; Izatt, R. M. *Chem. Rev.* **1997**, *97*, 3313.
23. Lee, C.-S.; Teng, P.-F.; Wong, W.-L.; Kwonga, H.-L.; Chan, A. S. C. *Tetrahedron* **2005**, *61*, 7924.
24. Ishiwari, F.; Fukasawa, K.; Sato, T.; Nakazono, K.; Takata, Y. K. T. *Chem.–Eur. J.*, **2011**, *17*, 12067.

Chapter 4

25. (a) Fox, M. A. *Acc. Chem. Res.* **1992**, *25*, 569; (b) Mandal, A. K.; Gangopadhyay, M.; Das, A. *Chem. Soc. Rev.* **2015**, *44*, 663; (c) Prodi, L.; Bolletta, F.; Montalti, M.; Zaccheroni, N.; Huszthy, P.; Samu, E.; Borba, V. *New J. Chem.*, **2000**, *24*, 781.
26. Okada, T.; Fujita, T.; Kubota, M.; Masaki, S.; Mataga, N.; Ide, R., Sakata Y.; Mlsuiw, S. *Chem. Phys. Lett.* **1972**, *14*, 563.
27. (a) A. J. Kirby, *Angew. Chem.* **1996**, *108*, 770; (b) G. A. E. Oxford, D. Dubbeldam, L. J. Broadbelt, R. Q. Snurr, *J. Mol. Catal. A* **2011**, *334*, 89.
28. Mandal, A. K.; Das, P.; Mahato, P.; Acharya, S.; Das, A. *J. Org. Chem.* **2012**, *77*, 6789.
29. (a) Bonal, C.; Israëli, Y.; Morel J. P.; Morel-Desrosiers, N.; *J. Chem. Soc., Perkin Trans 2*, **2001**, 1075; (b) Liu, Y.; Guo, D. S.; Zhang, H. Y.; Ma, Y. H.; Yang, E. C. *J. Phys. Chem. B* **2006**, *110*, 3428; (c) Rekharsky, M.; Inoue, Y. *J. Am. Chem. Soc.*, **2000**, *122*, 4418–4435; (d) Chen, L.; Zhang, H. Y.; Liu, Y.; *J. Org. Chem.* **2012**, *77*, 9766.
30. Pandey, A. D.; Mohammed, H.; Pissurlenkar, R. R. S.; Karnik. A. V. *ChemPlusChem* **2015**, *80*, 475.
31. Tsubaki, K.; Tanaka, H.; Kinoshita, T.; Fuji, K. *Tetrahedron* **2002**, *58*, 167.
32. Gangopadhyay, M.; Maity, A.; Dey, A.; Das, A. *J. Org. Chem.* **2016**, *81*, 8977.
33. Loeb, S. J.; Tiburcio, J.; Vella, S. J. *Chem. Commun.* **2006**, 1598.

CHAPTER 5

TUNING OF MONOMER/EXCIMER EMISSION OF A BIS-CROWN ETHER BY DI-CATIONIC AMMONIUM GUESTS

Publication:
To Be Communicated

5.1. Introduction

There is a considerable interest among the researchers active in the area of supramolecular chemistry, material scientists and chemists for achieving the desired control on the tenability of the photophysical properties for a supramolecular assembly or architecture through a manipulation of the various non-covalent interactions that are generally operational in such structures. Apart from this, a molecule that exhibits molecular movements in response to an applied stimulus is of considerable interest. As such a smart molecule could be used for achieving the programmed molecular movements.¹ For the constructions of well-defined supramolecular structures having different length scales, choice of appropriate molecular building blocks are crucial for proper utilization of physical interactions like hydrogen bonding, π - π stacking, hydrophobic interactions and electrostatic interactions.² In biology, individual molecule or an assembly of molecules as part of a complex molecular network, constitute a complex system for performing some special biological function.³ Inspired by nature, a variety of non-covalent strategies have been explored to realize the spontaneous and selective formation of highly stable and complex artificial supramolecular architectures with specific structures and properties.⁴ Many biological systems can be considered as complex molecular machines operated by chemical or physical stimuli.⁵ Previously Schalley *et al.* reported heteropseudo[3]rotaxane bearing two similar crown ethers (dibenzo[24]crown-8 and benzo-[21]crown-7) in a specific sequence by asymmetrical dicationic guests.⁶ Further they also reported that binary pseudorotaxanes, which are based on two different secondary ammonium/crown ether binding motifs and biscrown ethers as host.⁷ Self-sorting has also been utilized in the construction of a hetero[3]rotaxane, which is based on two similar crown ethers and a diammonium alkyl axle containing two different binding sites.⁸

Use of non-covalent interactions in conformationally flexible aromatic system for developing supramolecular architecture that shows excimer emissions has received considerable attention for developing new organic light emitting devices.⁹ In this context, recent efforts are centered around development of self-assembled supramolecular structures that allows the On or OFF state in terms of excimer emission of aromatic luminophores.¹⁰ Many systems have been developed which shows monomer to excimer fluorescence switching upon substrate binding and this is primarily induced by the conformational change(s) adopted by the individual host and/or guest molecule(s) in that assembly.¹¹ Luminophores like naphthalene and pyrene are important in this regard due to

Chapter 5

their unique property of excimer fluorescence.^{10b,11} Host or guest molecule, having more than one pyrene or naphthalene moiety participating in an efficient π - π stacking interaction generally exhibits excimer emission from of the rings in the free state or due to the interaction of excited state fluorophore with ground state. Formation of a host-guest assembly could allow a conformational change with subsequent change(s) in excimer luminescence. For crown ether based host molecules, attention for designing of such host-guest assemblies is generally focused towards the influence of binding motif that allows a stable adduct formation as well as the cavity size of the respective crown ether derivatives that allows the threading of the axel type guest molecules.¹² Here, we describe a supramolecular system involving a divalent crown ether as host and divalent secondary ammonium ion derivatives as guest. We could successfully demonstrate that a crown-ether derivative having a bis-naphthalene based molecule that exhibits a change in excimer emission upon guest complexation. Ammonium based guests are well known to form inclusion complexes with crown ethers.^{13a} In the present report we have discussed how subtle changes in structures of the guest molecules could influence the host-guest complexation with subsequent changes in the excimer emission as the optical output.

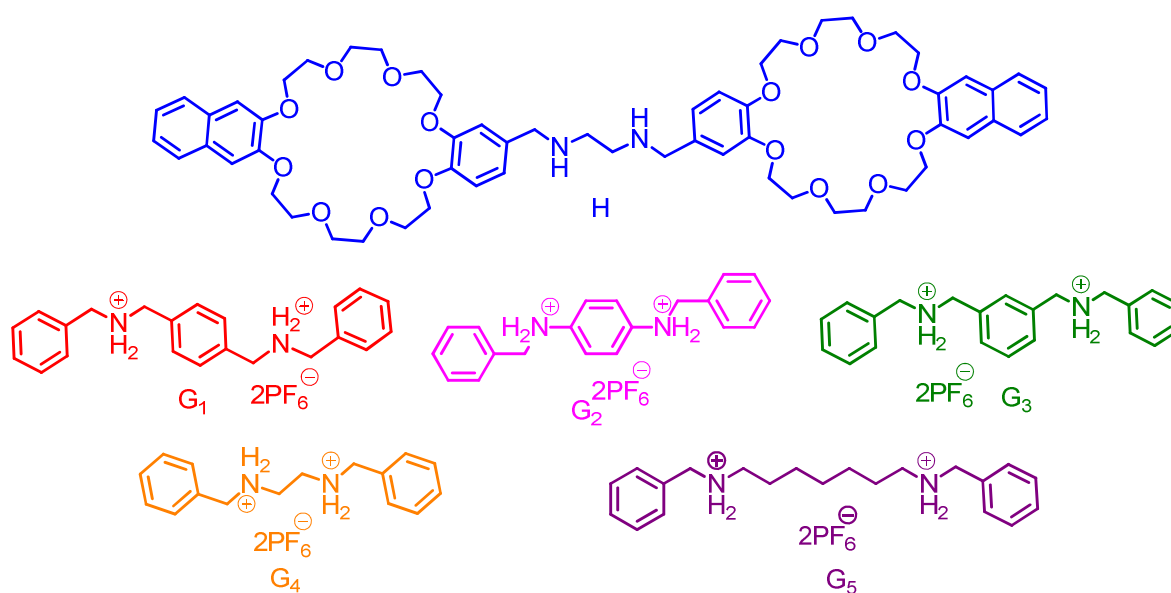


Figure 5.1: Schematic representation of the molecular components that are used for the formation of self-assembly.

5.2. Experimental section

5.2.1. Materials

Ethylenediamine, 1,4-phenylenedimethanamine and benzaldehyde derivative were purchased from Sigma-Aldrich and were used without any further purification. Solvents used in this study are of AR grade and were used without any further purification. All intermediate and new compounds were purified using column chromatographic technique using silica gel (100-200 mesh) as the stationary phase.

5.2.2. Analytical Methods

The absorption and emission spectra were acquired on Cary 500 Scan UV-vis-NIR spectrometer and PTI-QM 400 Luminescence spectrofluorimeter at room temperature (25°C). All spectral measurements were carried out with freshly prepared solutions in quartz cuvette having 1.0 cm path-length. Fluorescence lifetimes were measured by time correlated single photon counting (TCSPC) using Horiba-Jovin Yvon Luminescence spectrofluorimeter utilizing a nanosecond diode LED source (280 nm LED excitation source) and 340 nm LASER as the light source to trigger the fluorescence decay. Decay profiles were deconvoluted on Data station-v 6 decay analysis software. The acceptability of these fits were evaluated by χ^2 criteria and visual inspection of the residuals of the fitted function of the data. All NMR spectra were recorded with TMS as an internal standard on Bruker 500MHz FT NMR Advance-DPX 500 spectrometer at room temperature (25°C).

5.2.3. Synthesis

Synthetic procedure of 1: 1.0 g (6.2 mmol) of 2,3-dihydroxynaphthalene was dissolved in 50 mL of freshly dried DMF in two neck round bottom flask. To this solution K_2CO_3 powder (2.5 g, 18.6 mmol) was added and the reaction mixture turned from brown to violet colour and then KI (3 g, 18.6 mmole) was added. This mixture was allowed to heat (~60°C) and stir for 15 min. Finally 2-[2-(2-chloro-ethoxy)-ethoxy]-ethanol (2 ml, 12.4 mmole) in 20 ml of dry DMF was added dropwise via a syringe at 60°C. Then temperature was raised upto 80°C and allowed to stir for 5 days. The solvent was removed under reduced pressure and extracted three times with $CHCl_3$ and water. All organic layers were combined and dried over anhydrous sodium sulphate. Solvent was removed under reduced pressure to give crude product, which was purified on silica gel column using methanol:chloroform (1:99;

Chapter 5

v/v) as an eluent to yield **A** (1.4 g, 53.0%) as a sticky dark brown solid. $^1\text{H-NMR}$ (200 MHz, CD_2Cl_2 , δ ppm): 7.67 (2H, m), 7.32 (2H, m), 7.15 (2H, s), 4.25 (4H, m), 3.92 (4H, m), 3.74 (4H, m), 3.66 (8H, m), 3.56 (4H, m). Elemental analysis ($\text{C}_{22}\text{H}_{32}\text{O}_8$): Cal. C, 62.25; H, 7.60 and Expt. C, 62.48; H, 7.53. ESI-MS ($\text{C}_{22}\text{H}_{32}\text{O}_8$): calc. 424.48; Expt. 447.24 $[\text{M} + \text{Na}]^+$.

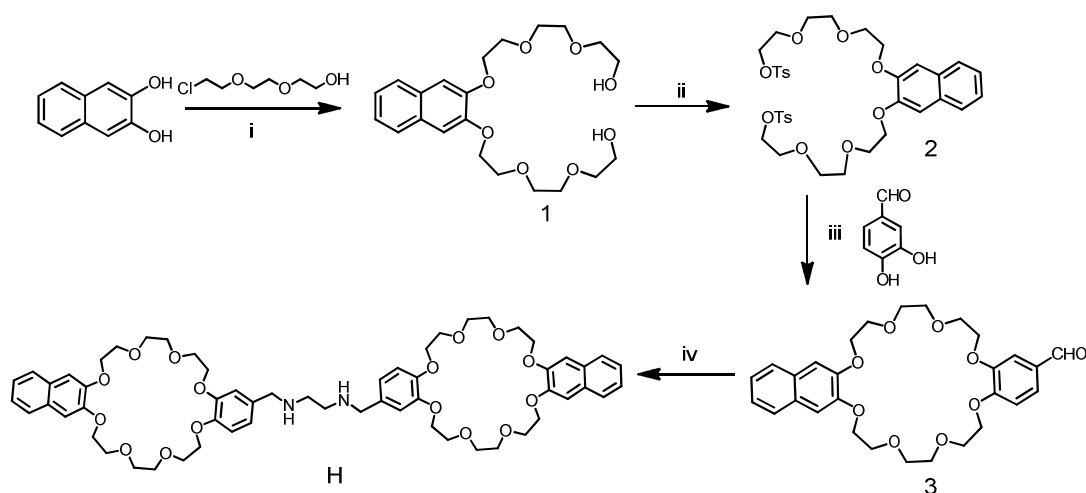
Synthetic procedure of 2: Compound **1** (1.4 g, 3.3 mmole) was dissolved in THF (20 ml) and it was kept in ice bath. To this solution, 10 mL NaOH solution (1.7 mol) was added to it at 0°C and this reaction mixture was allowed to stir for 10 min. Finally, p-Toluene sulfonyl chloride (1.8 g, 9.4 mmol) in 25 mL of dry THF was added drop-wise over a period of 1 hr to the reaction mixture at 0°C with vigorous stirring. After 5 days, solvent was removed under reduced pressure and extracted three times with CHCl_3 and water. Organic layers were combined and dried over anhydrous sodium sulphate. Solvent was removed under reduced pressure to give crude product. This was purified using silica-gel as stationary phase and CHCl_3 as an eluent to yield **2** (2.0 g, 82%), as a sticky brown mass. $^1\text{H-NMR}$ (500 MHz, CD_2Cl_2 , δ ppm): 7.75 (4H, dd), 7.66 (2H, m), 7.30 (6H, s), 7.14 (2H, s), 4.20 (4H, t, $J = 4.5$), 4.09 (4H, t, $J = 4.5$), 3.85 (4H, t, $J = 4.5$), 3.63 (8H, m), 3.56 (4H, t, $J = 4.5$), 2.36 (6H, s). $^{13}\text{C-NMR}$ (125 MHz, CD_2Cl_2 , δ ppm): 148.9, 144.8, 132.9, 129.8, 127.8, 126.3, 124.2, 108.3, 70.7, 69.4, 68.6, 68.3, 29.6. Elemental analysis (for $\text{C}_{36}\text{H}_{44}\text{O}_{12}\text{S}_2$): Cal. C, 59.00; H, 6.05; S, 8.75, Exp. C, 59.16; H, 6.00, S, 8.70. ESI-MS (for $\text{C}_{36}\text{H}_{44}\text{O}_{12}\text{S}_2$): Cal. 732.86, Exp. 755.14 $[\text{M} + \text{Na}]^+$.

Synthetic procedure of 3: 3,4-Dihydroxybenzaldehyde (0.38 g, 2.8 mmol) was dissolved in 40 mL of freshly dried DMF. To this solution K_2CO_3 powder (1.3 g, 9.6 mmole) was added and stirred for 15 min, and then compound **2** (2.0 g, 2.7 mmol) dissolved in 50 ml of dry DMF, was added in a dropwise manner over 2 h at 60°C . Temperature was raised to 80°C and the mixture was allowed to stir for 5 days. The solvent was removed under reduced pressure; the residue was extracted 3 times with CHCl_3 and water. The organic layers were combined and dried over anhydrous sodium sulphate. Removal of the solvent under vacuum gave crude product, which was purified on a silica-gel column using $\text{CHCl}_3:\text{CH}_3\text{OH}$ (98:2, v/v) as eluent to yield pure **3** (0.90 g, 62%), as a brown solid (mp: $80^\circ\text{C} - 85^\circ\text{C}$). $^1\text{H-NMR}$ (200 MHz, CDCl_3 , δ ppm): 9.78 (1H, s), 7.64 - 7.63 (2H, m); 7.38 - 7.35 (2H, m), 7.32 - 7.30 (2H, m), 7.08 (2H, s), 6.91 (1H, s), 4.25 (4H, broad s), 4.22 - 4.20 (4H, broad m), 4.00 - 3.99 (4H, broad m), 3.97 - 3.93 (4H, broad m), 3.89 - 3.86 (8H, broad m). $^{13}\text{C-NMR}$ (CDCl_3): 190.9, 162.6, 148.9, 130.1, 129.2, 126.8, 126.2, 124.2, 111.8,

Chapter 5

110.9, 107.8, 71.5, 69.5, 69.0. Elemental analysis (for $C_{29}H_{34}O_9$): Cal. C, 66.15; H, 6.51 and Exp. C, 65.93; H, 6.48. ESI-MS (for $C_{29}H_{34}O_9$): cal. 526.22, Exp. 549.39 $[M + Na]^+$.

Synthetic procedure of H: Compound **3** (373mg, 0.7 mmol) was dissolved in 60 ml dry ethanol. To this solution, 21mg (0.354 mmol) of ethylenediamine was added. Then the reaction mixture was stirred for 24 hrs. After a day white precipitate appeared which was filtered through a G3 crucible and was washed thrice with cold ethanol. The precipitate was made soluble in methanol and $NaBH_4$ was added portion wise to the stirred cool reaction mixture. The reaction mixture was stirred for overnight. The solvent was removed under reduced pressure, the residue was extracted three times with CH_2Cl_2 and water, and the organic layers were combined and dried over anhydrous sodium sulfate. The solvent was removed under reduced pressure to give the crude product. Crude product was precipitated out in cold diethyl ether. White precipitate came and washed with cold diethyl ether repeatedly and dried. Yield: 760 mg (82%). 1H NMR (700 MHz, $CDCl_3$, ppm): δ 7.64 (4H, dd, $J = 6.1, 3.3$ Hz), 7.29 (4H, dd, $J = 6.1, 3.2$ Hz), 7.10 (4H, s), 6.92 (2H, s), 6.79 (4H, d, $J = 1.7$ Hz), 4.22 (8H, dd, $J = 7.3, 3.6$ Hz), 4.11 (8H, d, $J = 14.1$ Hz), 3.96 - 3.93 (9H, m), 3.88 - 3.85 (9H, m), 3.83 - 3.81 (8H, m), 3.79 (8H, dd, $J = 5.7, 2.8$ Hz), 3.69 (4H, s), 2.77 (2H, s). ^{13}C NMR ($CDCl_3$, 100 MHz, ppm): δ 149.00, 129.29, 126.30, 124.17, 113.77, 107.86, 71.49, 71.32, 69.94, 69.74, 69.56, 69.21.



i. K_2CO_3 , KI, DMF; ii. TsCl, NaOH, THF/ H_2O ; iii. K_2CO_3 , KI, DMF; iv. Ethylenediamine, EtOH; v. $NaBH_4$, MeOH.

Scheme 5.1: Schematic representation of synthesis of **H**.

Synthetic procedure of G₁: 1,4-phenylenedimethanamine (300 mg, 2.2 mmol) and benzaldehyde (467mg, 4.41 mmol) was added and dissolved in 30 ml of dry ethanol. The

Chapter 5

reaction mixture was refluxed for 24 hrs and the solvent mixture was evaporated under reduced pressure. Methanol was added to the reaction mixture and the temperature was reduced to 0°C. To this chilled reaction mixture, NaBH₄ (0.6 g) was added portion wise. The reaction mixture was allowed to attain room temperature and stirred for 6 hrs. Reaction mixture was dried under reduced pressure and the desired product was extracted from this residue in CHCl₃ layer using CHCl₃-water partition. The organic layers were collected and dried with anhydrous sodium sulphate. Further, solvent was removed under reduced pressure a white solid as the crude product was collected. To this, 0.2 ml of concentrated HCl in 20 ml of methanol was added drop wise and stirred for 24 hrs. Finally, anion exchange in water using NH₄PF₆ resulted precipitation of the desired product (**G**₁) as PF₆⁻ salt. Yield: 0.48 g, 35.0%. ¹H NMR (400 MHz, CD₃CN, ppm): δ 7.56 (4H s), 7.51 (10H s), 4.29 (4H, d, *J* = 3.8 Hz). ¹³C NMR (100 MHz, ppm): δ 131.93, 130.81, 130.26, 130.18, 129.90, 129.14, 51.66, 50.82. HRMS: *m/z* calculated 463.1738 for C₂₂H₂₆N₂PF₆⁺, found 463.1722 [M - PF₆⁻]⁺.

Synthetic procedure of G₂: The desired PF₆⁻ salt of **G**₂ was obtained by following a similar experimental procedure as it was mentioned for **G**₁, as a brown solid (Yield: 0.55 g, 58.0%). ¹H NMR (400 MHz, CD₃CN, ppm): δ 7.51 (10,H s), 6.88 (4H, s), 4.23 (4H, s). HRMS: *m/z* calculated 435.1425 for C₂₀H₂₂N₂PF₆⁺, found 435.1419 [M - PF₆⁻]⁺.

Synthetic procedure of G₃: The desired PF₆⁻ salt of **G**₃ was obtained as a brown solid by following a similar experimental procedure as it was mentioned for **G**₁ (Yield: 0.6 g, 65.0%). ¹H NMR (400 MHz, CD₃CN, ppm): δ 7.59 (6H, t, *J* = 7.2 Hz), 7.49 (1H, d, *J* = 7.6 Hz), 7.41 (7H, s), 4.13 (8H,s). ¹³C NMR (101 MHz, CD₃CN): δ 132.76, 132.61, 131.02, 130.57, 129.29, 129.05, 50.22, 50.05, 40.58, 40.37, 40.16, 39.95, 39.74, 39.54, 39.33. HRMS: *m/z* calculated 463.1738 for C₂₂H₂₆N₂PF₆⁺, found 463.1725 [M - PF₆⁻]⁺.

Synthetic procedure of G₄: The desired PF₆⁻ salt of **G**₄ was obtained as a brown solid by following a similar experimental procedure as it was mentioned for **G**₁ (Yield: 0.8 g, 58.0%). ¹H NMR (200 MHz, CD₃CN, ppm): δ 9.40 (4H s), 7.53 (10H d, *J* = 14.2 Hz), 4.24 (4H, s). ¹³C NMR (101 MHz, CD₃CN, ppm): δ 196.51, 174.00, 157.81, 149.60, 148.96, 148.13, 123.66, 116.40, 108.00, 105.03, 74.57, 72.73, 72.37, 71.84, 71.44, 71.04, 45.79, 44.48. HRMS: *m/z* calculated 531.0983 for (C₁₆H₂₂N₂P₂F₁₂⁻ H)⁻, found 531.0991 [M - H⁺]⁻.

Synthetic procedure of G₅: The desired PF₆⁻ salt of **G**₅ were obtained by following a similar experimental procedure as it was mentioned for **G**₁, as a brown solid (Yield: 0.40 g,

42.0%). ^1H NMR (400 MHz, CDCl_3 , ppm): δ 7.56 (4H, d, $J = 7.9$ Hz), 7.44 (6H, d, $J = 12.9$ Hz), 4.42 (4H, d, $J = 5.6$ Hz), 2.06 (s), 1.86 (6H, d, $J = 6.9$ Hz), 1.42 (8H, s). ^{13}C NMR (126 MHz, δ ppm): 130.85, 130.55, 129.77, 117.33, 51.53, 51.43, 47.81, 47.73, 27.91, 27.72, 25.68.

5.3. Results and Discussions

Synthesis of guest ammonium derivatives and host (Scheme 5.1) are described in the experimental section. Desired purity of **H**, **G**₁, **G**₂, **G**₃, **G**₄, **G**₅ were ensured based on various analytical and spectroscopic data, which are provided either in the experimental section. The luminescence properties of the individual host, guest and inclusion complexes were investigated by steady state and time resolved emission studies.

5.3.1. Spectroscopic studies

All the spectroscopic studies are carried out dichloromethane solvent. Host **H** display an intense absorption bands at 272 nm. ($\epsilon = 1.9 \times 10^4 \text{ Lmol}^{-1}\text{cm}^{-1}$), which probably arise from $\pi \rightarrow \pi^*$ transitions (Figure 5.2). When irradiated at 272 nm, the biscrown ether host (**H**) gives rise to only monomer emission at 340 nm. Based on both the spectral profile and the observed lifetime the emission is assigned as fluorescence from naphthalene.^{13b} The absorption spectrum recorded for a mixture of **H** and **G**₁ in dichloromethane medium gives no change in the spectral pattern suggesting no significant interaction between host and guest in the ground state (Figure 5.2).

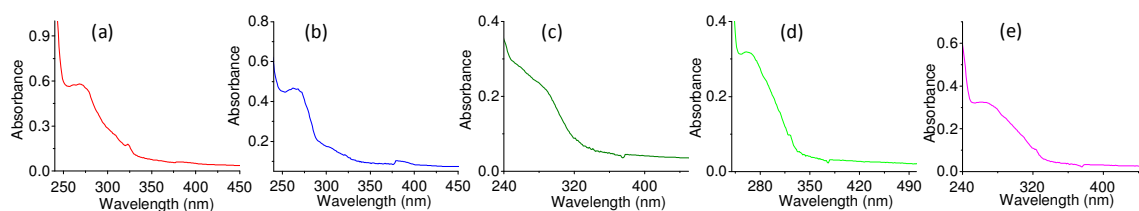


Figure 5.2: UV-vis spectra of (a) **H** (9.0×10^{-7} M), (b) **H** (9.0×10^{-7} M), with **G**₁ (1.1×10^{-5} M), (c) **H** (9.0×10^{-7} M), with **G**₂ (1.2×10^{-5} M), (d) **H** (9.0×10^{-7} M), with **G**₃ (1.7×10^{-5} M), (e) **H** (9.0×10^{-7} M), with **G**₄ (1.5×10^{-5} M). All spectra were recorded in CH_2Cl_2 at 25°C .

Emission spectrum of **H** was recorded in CH_2Cl_2 medium following excitation at 272 nm. Relative quantum yield (Φ_{H}) of 0.15 was estimated for **H**, by employing naphthalene as a standard. Low quantum yield of **H** was attributed to the flexible nature of crown ether. A significant change in emission spectrum for **H** was observed when such a spectrum was

Chapter 5

recorded in presence of \mathbf{G}_1 . On subsequent increase in concentration of \mathbf{G}_1 , the intensity for the emission band maximum of \mathbf{H} at 343 nm was found to increase. Subsequently, a new and broad emission band maximum at 420 nm reaching appeared. The increase in band intensity at 420 nm reached a maximum for 12.5 mole equiv. of \mathbf{G}_1 . Emission band having a band maximum at 343 nm was assigned to a naphthalene based $\pi-\pi^*$ transition, while the broad red shifted emission band at 420 nm was assigned to a characteristics excimer emission that is reported for naphthalene based systems.¹⁴ The spectrum is significantly broaden on the low energy portion of the emission envelop. The spectra also show a slight, but steady increase in the emission peaks at 343 nm, which was attributed to the enhanced emission form naphthalene monomer on formation of inclusion complex. The changing pattern of the emission spectra of \mathbf{H} with increasing concentration of \mathbf{G}_1 in dichloromethane is presented in figure 5.3. In earlier chapters, we have successfully demonstrated that secondary ammonium ion derivatives form a threaded inclusion complex with crown ether derivatives having appropriate cavity size.

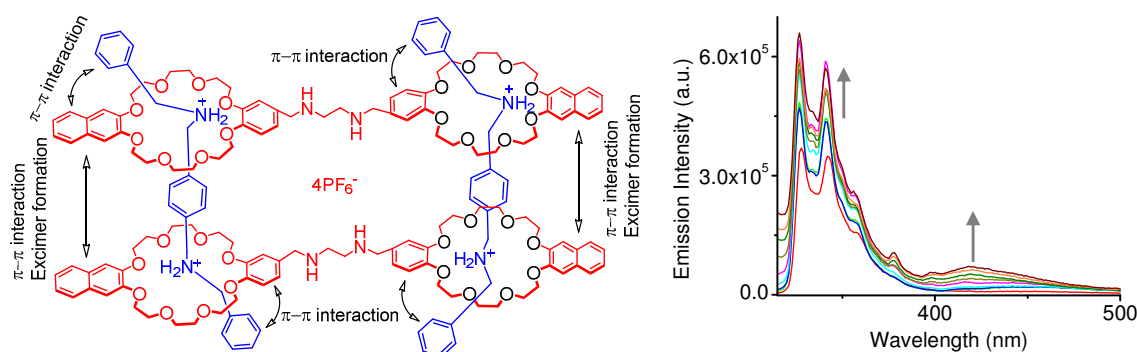


Figure 5.3: Proposed molecular structure for $2\mathbf{H}\cdot 2\mathbf{G}_1$. Fluorescence spectra of \mathbf{H} (9.0×10^{-7} M), in dichloromethane upon addition of increasing concentration of $\mathbf{G}_1 = (0 - 1.1 \times 10^{-5})$ M, $\lambda_{\text{Ext}} = 272$ nm, slit-1/1.

Derivatives of dibenzo-24-crown-8 (DB24C8) are known to form stable inclusion complexes with secondary ammonium ion derivatives.^{13a} Thus, formation of a [2]pseudorotaxane complex is typically anticipated between each naphthalene functionalized fragment of DB24C8 in \mathbf{H} with an individual \mathbf{G}_1 (Figure 5.3). Results discussed in the previous chapters have also revealed that $\pi-\pi$ stacking interaction also plays a crucial role in determining the stability of the inclusion complexes as well as determining the conformation of the individual host and/or guest molecules in the supramolecular assembly. Results also reveal that there is no indication for interaction

Chapter 5

between the naphthalene nuclei in the ground state. Thus, the increase of monomer emission after guest addition is attributed to the inclusion complex formation between the guest with the host. In the absence of guest molecule, two naphthalene units in **H** exhibit typically show strong naphthalene monomer-based emission at ~ 343 nm. The emission band that appeared on formation of inclusion complex at ~ 430 is attributed to two naphthalene units in an intermolecular π - π stacked arrangement.

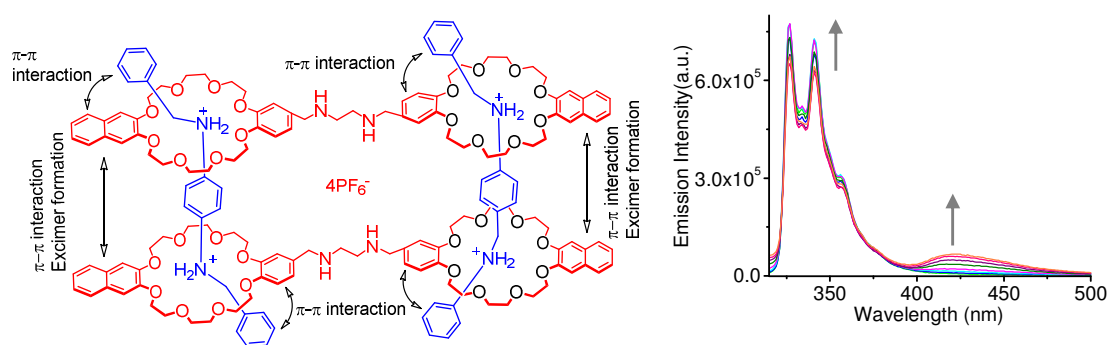


Figure 5.4: Fluorescence spectra of **H** (9.0×10^{-7} M), in dichloromethane upon addition of increasing concentration of **G**₂ = ($0 - 1.2 \times 10^{-5}$ M), $\lambda_{\text{Ext}} = 272$ nm, slit-1/1. Proposed molecular structure for $2\mathbf{H} \cdot 2\mathbf{G}_2$.

To elucidate the role of linkers of the guests the fluorescence properties of the inclusion complexes with varying linker length of di-cationic guests in CH_2Cl_2 were compared. We also recorded the emission spectra of **H** in the presence of three other guest molecules (**G**₂, **G**₃, and **G**₄) to study the complexation process in CH_2Cl_2 medium following excitation at 277 nm. The observed trend in the changes in the emission spectral pattern for **H** on formation of the respective inclusion complex ($2\mathbf{H} \cdot 2\mathbf{G}_2$, $2\mathbf{H} \cdot 2\mathbf{G}_3$, $2\mathbf{H} \cdot 2\mathbf{G}_4$) with **G**₂, **G**₃ and **G**₄ was similar to that found for the complexation with **G**₁. For **G**₄, the monomer intensity ($\Phi_{\text{H}} = 0.62$) was found to be more than that was observed for **G**₁. Inclusion of **G**₄ allows formation of $2\mathbf{H} \cdot 2\mathbf{G}_4$ with two naphthalene to come even closer than that was the case for [4]pseudorotaxane of $2\mathbf{H} \cdot 2\mathbf{G}_1$. As the length of the linker was almost identical for **G**₁ and **G**₃, similar emission response was observed. Upon the addition of progressively higher concentration of **G**₃, an emission peak ~ 420 nm appeared, which suggested that **G**₃ bind to **H** and form excimer (Figure 5.5). Relative quantum yields of inclusion complexes were $\Phi_{\text{H.G}_1} = 0.34$, $\Phi_{\text{H.G}_2} = 0.41$ and $\Phi_{\text{H.G}_3} = 0.36$ were estimated for **H.G**₁, **H.G**₂, **H.G**₃, respectively. Relative emission quantum yield was evaluated using naphthalene as a standard. Quantum yield value indicates that the short distance between two ammonium

Chapter 5

centres in the guest (\mathbf{G}_4) allows two pairs of naphthalene units to come close to each other and this favours the π - π stacking interaction to form excimer between two naphthalene pairs. The degree of structural change highly depends on the kind of guest molecules, mainly the length in between of the two ammonium centres. This is further substantiated when the distance of separation between two secondary ammonium units in a particular guest molecule was evaluated. This distance for various linkers are as follows: 3.9Å (\mathbf{G}_4), 5.7 Å (\mathbf{G}_2), 6.6Å (\mathbf{G}_3), 7.4Å (\mathbf{G}_1) and 10Å (\mathbf{G}_5).

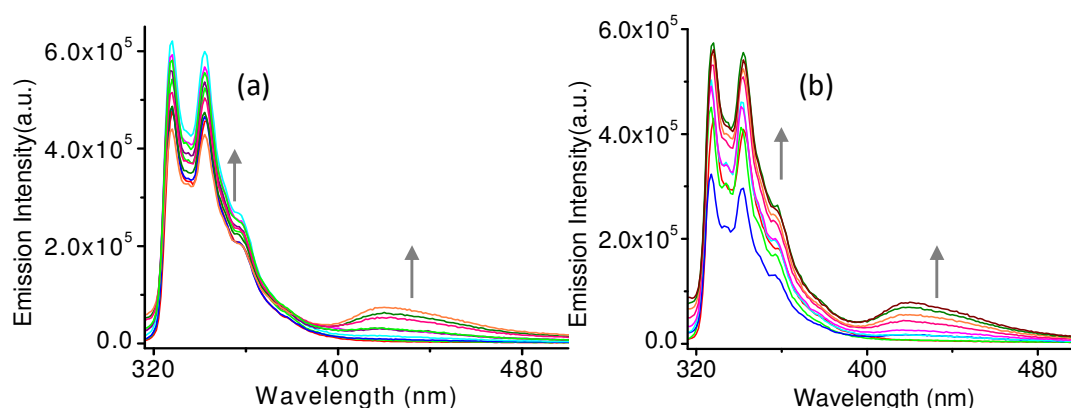


Figure 5.5: (a) Fluorescence spectra of \mathbf{H} (9.0×10^{-7} M), in dichloromethane upon addition of increasing concentration of $\mathbf{G}_3 = (0 - 2.0 \times 10^{-5})$ M, (b) $\mathbf{G}_4 = (0 - 1.8 \times 10^{-5})$ M, $\lambda_{\text{Ext}} = 272$ nm, slit-1/1.

The existence of an excimer is usually observed when there occurs a restriction of geometries that hinder the mobility of naphthalene fluorophore present in the crown ring, which helps in stacking of two naphthalene moieties. Fluorescent spectra confirm the aromatic-aromatic interaction between naphthalene groups.

An examination of the linker lengths in respective guests ($\mathbf{G}_1 - \mathbf{G}_5$) and the emission properties reveals that the length of the linker indeed has a crucial role on the excimer formation. We envisioned that moderately long alkyl chains for example heptyl moiety in \mathbf{G}_5 either allows conformational flexibility in the ground and excited states or the eventual distance of separation between two naphthalene moieties in each set of pairs are just too far to induce any π - π interaction leading to excimer complex formation. This could be attributed to the absence of any observed emission band at ~ 420 nm for \mathbf{G}_5 (Figure 5.6).

In order to avoid intramolecular excimer formation of \mathbf{H} , photoluminescence experiments are conducted in diluted conditions, as the excimer formation is highly dependent on the concentration of the respective fluorophore.¹⁵ The macrocyclic molecule \mathbf{H} , on formation of

Chapter 5

the pseudorotaxane complex assumes a favourable conformation that allows a better π -stacking interaction. Pseudorotaxane formation also helps in attaining the structural rigidity, which is also expected to favour the π -stacking interaction and favours pre-organization in the ground state that subsequently helps in populating the stacked conformations that readily undergo excimer formation in the excited state. In such assemblies, neighbouring chromophores that are in close proximity give rise to strong electronic communication between them in excited states.

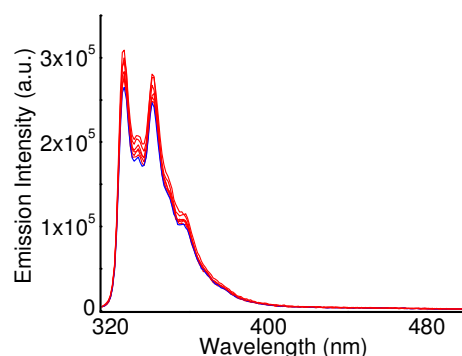


Figure 5.6: Fluorescence spectra of **H** (9.0×10^{-7} M), in dichloromethane upon addition of increasing concentration of **G₅** = ($0 - 2.0 \times 10^{-5}$ M), λ_{Exc} = 272 nm, slit-1/1.

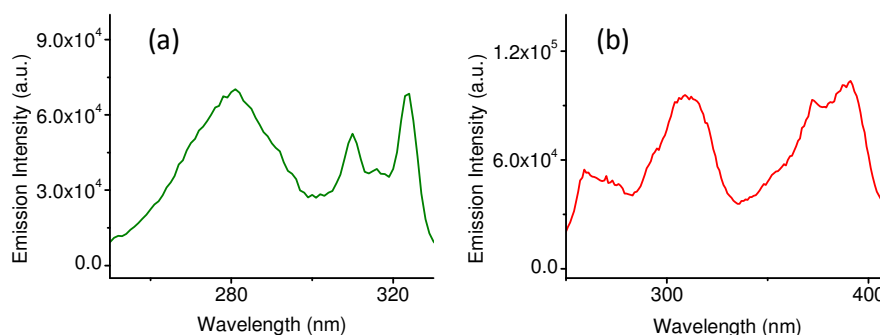


Figure 5.7: (a) Excitation spectra of **H.G₁** in CH_2Cl_2 solution (a) monitored at 343 nm, (b) monitored at 420 nm, slit-1/1.

To investigate this excimer emission in inclusion complexes, the excitation spectrum of **2H.2G₁** was monitored using 343 and 420 nm as the excitation wavelength (Figure 5.7). There are distinct differences and this clearly reveal that final emitting states associated

Chapter 5

with these two excitation processes are different. The spectroscopic data are also useful to elucidate the mechanism of excimer formation.¹⁶ Similar, with the UV-spectra, the excitation spectra of the **2H.2G**₁, showed a distinct spectral broadening when the emission wavelength was set at 420nm (Figure 5.2). Since the excitation spectra of **H** with **G**₁ monitored at 420 nm (structure less emission) was not identical to that monitored at 343 nm indicating two excited states are existing in the inclusion complex (Figure 5.7).

For control experiments, we measured the concentration-dependent absorption and luminescence spectra of the host molecule (**H**). As shown in Figure 5.8, no appreciable change in the shape and position of the band maximum was observed when the concentration of **H** was increased from 1.0×10^{-6} to 5.0×10^{-4} M. To ensure that the observed emission band at ~ 420 was not due to an intermolecular aggregation of **H** only, higher limit for the [**H**] used for this control study was 100 times larger than the concentration used for the other experiments (Figure 5.3 and 5.4).¹⁵ This also excluded the possibility of intermolecular excimer formation at 420 nm for naphthalene. No change was registered in the fluorescence spectra with the variation of concentration of **H** or with time (keeping [**H**] constant). Thus, the observed excimer luminescence is not an intramolecular excimer or luminescence that has arisen from ground state aggregate. Rather, this could be attributed to the excimer emission of two naphthalene moiety of two **H** molecules, which adopts a favourable orientation and conformation for attaining the favourable distance that allows the excimer process to happen.¹⁷

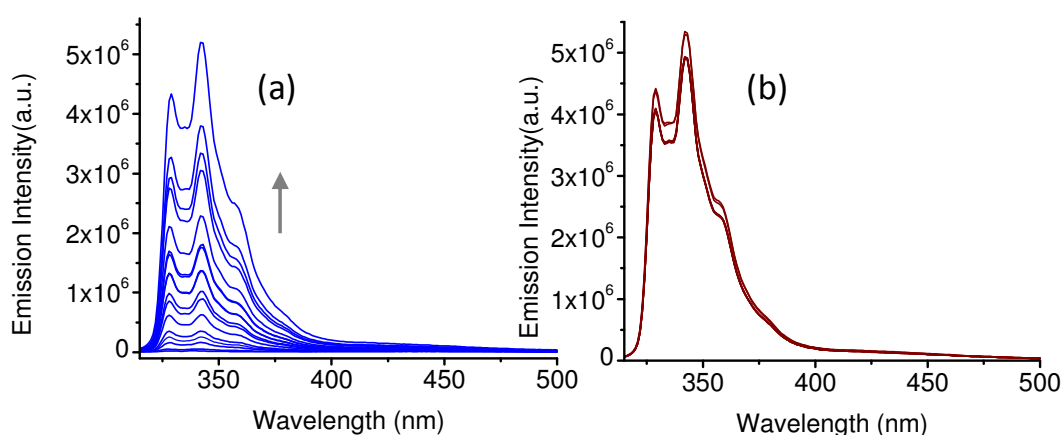


Figure 5.8: (a) Emission spectra of **H** in CH_2Cl_2 solution with concentration ranging from 1.0×10^{-6} M to 1.0×10^{-4} M, (a) time dependent spectra of **H** (1.0×10^{-6} M) recorded for 2 hrs. $\lambda_{\text{Exc}} = 277$ nm, slit-1/1.

5.3.2. Temperature dependent fluorescence studies

Steady state emission spectra were also recorded at varying temperature. Changes in luminescence spectra with temperature for inclusion complexes ($2\text{H}\cdot\text{G}_1$, $2\text{H}\cdot 2\text{G}_2$, $2\text{H}\cdot 2\text{G}_3$ & $2\text{H}\cdot 2\text{G}_4$) are shown in Figures 5.9 and 5.10, which reveal that a decrease of the excimer fluorescence intensity with increase in temperature. Increase in the temperature not only adversely influences the π - π stacking and H-bonding interaction, but also the rigidity of the inclusion complexes ($2\text{H}\cdot\text{G}_1$, $2\text{H}\cdot 2\text{G}_2$, $2\text{H}\cdot 2\text{G}_3$ & $2\text{H}\cdot 2\text{G}_4$). This accounts for the observed decrease in excimer luminescence with increase in temperature.

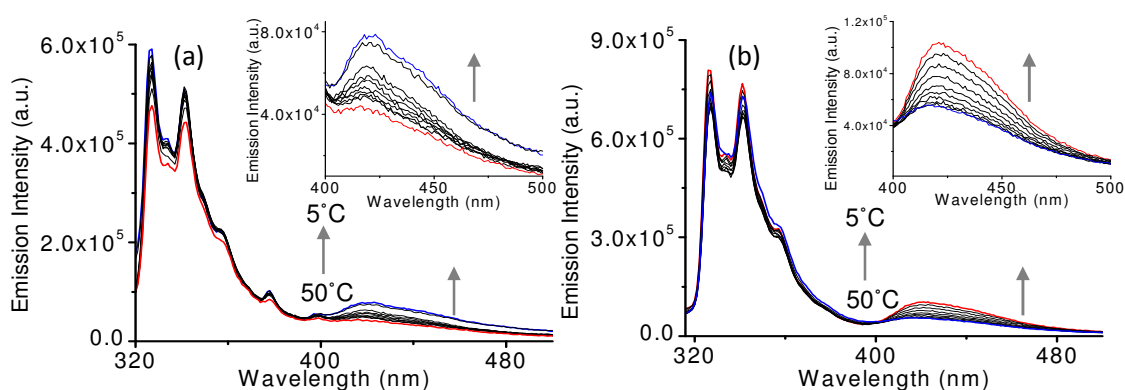


Figure 5.9: Temperature dependence of the fluorescence emission spectra for compound **H** ($9.0 \times 10^{-7}\text{M}$), with (a) **G**₁ ($1.2 \times 10^{-5}\text{M}$), and (b) **G**₂ ($1.0 \times 10^{-5}\text{M}$), $\lambda_{\text{Ext}} = 277\text{ nm}$, slit-1/1.

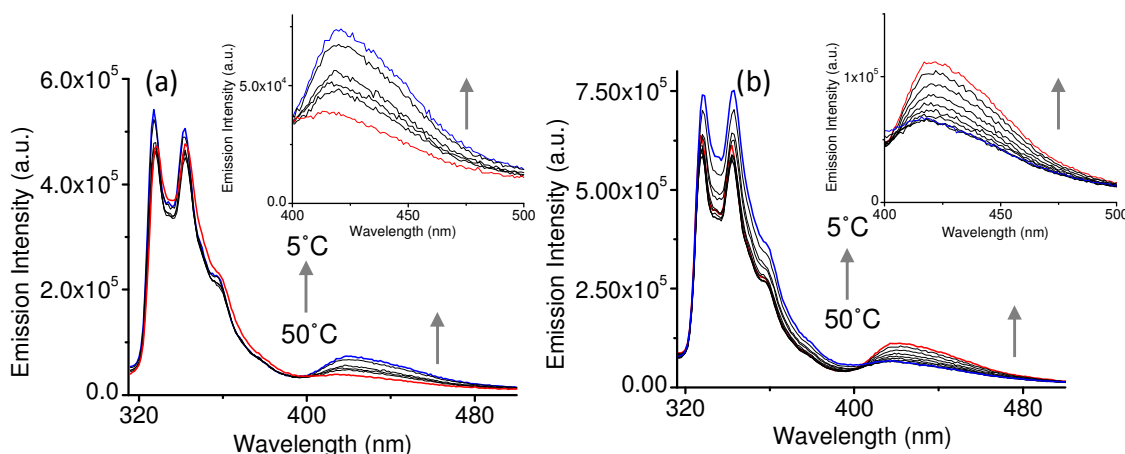


Figure 5.10: (a) Temperature dependence of the fluorescence emission spectra for compound **H** ($9.0 \times 10^{-7}\text{M}$), with (a) **G**₃ ($2.0 \times 10^{-5}\text{M}$), and (b) **G**₄ ($1.0 \times 10^{-5}\text{M}$), $\lambda_{\text{Ext}} = 277\text{ nm}$, slit-1/1.

This could be explained if we consider that with the decrease in the temperature of the

Chapter 5

medium, mobility of the fluorophores decreases and this enhances the chance of two naphthalene rings to adopt a favourable orientation for interactions. Temperature dependent emission spectra for **H** (Figure 5.11) were also recorded and it did not show any luminescence band at around 420 nm. This further nullifies the possibility of generating any 420 nm emission band owing to the intramolecular excimer process.

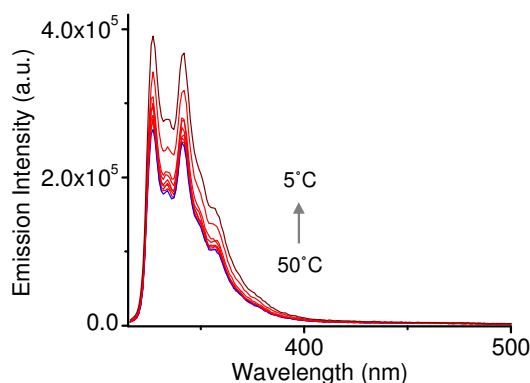


Figure 5.11: Temperature dependence of the fluorescence emission spectra for compound **H** (9.0×10^{-7} M), $\lambda_{\text{Ext}} = 277$ nm, slit-1/1.

5.3.3. Time resolved emission studies

To get better insight of excited states which are involved in the process, we carried out Time Correlated Single Photon Counting (TCSPC) experiment for individual component and the host guest assembly in the dichloromethane solution. The fluorescence decay profiles of the individual component and the inclusion complexes of the crown and the respective guests are shown in the figure 5.11. On excitation at 280 nm (LED), a biexponential decay profile is observed for **H** ($\tau_1 = 4.56 \pm 0.08$ (14.06%) ns and $\tau_2 = 10.10 \pm 0.04$ (85.94%) ns). Major component is typically the lifetime of naphthalene monomer excited state.¹⁸ Importantly the time resolved fluorescence for **H** monitored at 420 nm in CH_2Cl_2 is best described by a bi exponential decay ($\tau_1 = 5.49 \pm 0.08$ (14.06%) and $\tau_2 = 10.49 \pm 0.05$ (95.02%). Interestingly, τ_1 and τ_2 value are identical for both excitation processes ($\lambda_{\text{Mon}} = 343$ and 420 nm). However, preexponential factors are not identical.¹⁹ The emission decay profile of 1:1 mixture of host–guest (**H+G₁**) when monitored at 343 nm showed single exponential decay with the time constant of $\tau_1 = 11.73$ ns but when monitored at 420 nm it shows biexponential decay ($\tau_1 = 1.44 \pm 0.08$ (68.64%) and $\tau_2 = 10.14 \pm 0.05$ (31.36%).

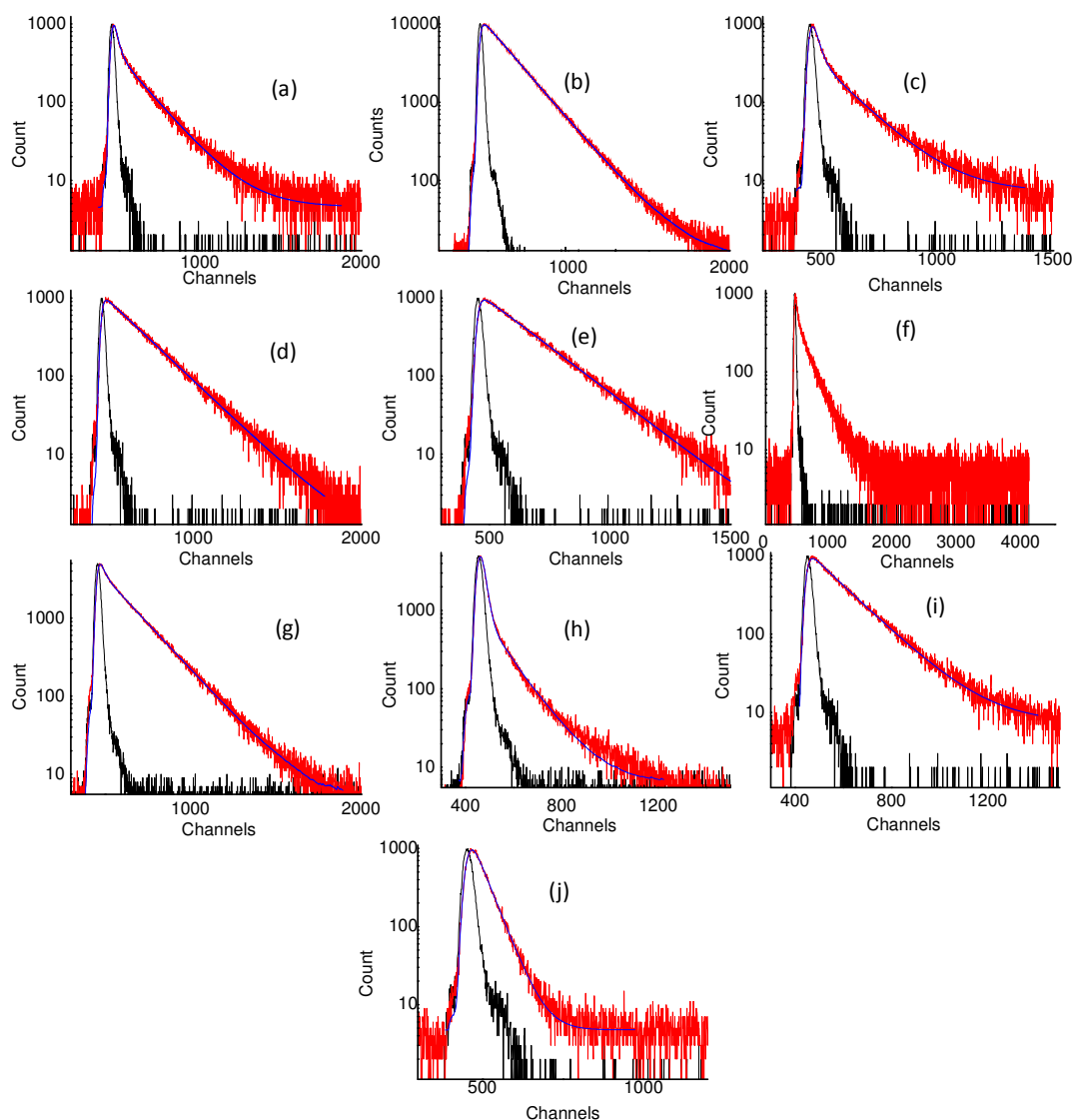


Figure 5.12: Time dependent fluorescent decay of (a) **H** monitored at 343 nm, (b) **H** monitored at 420 nm, (c) **H + G₁** at 343 nm, (d) **H + G₁** at 420 nm, (e) **H + G₂** at 343 nm, (f) **H + G₂** at 420 nm, (g) **H + G₃** at 343 nm, (h) **H + G₃** at 420 nm, (i) **H + G₄** at 343 nm, (j) **H + G₄** at 420 nm.

The emission decay profile of 1:1 mixture of host-guest (**H+G₂**) when monitored at 343 nm showed biexponential decay with the time constant of ($\tau_1 = 1.12 \pm 0.08$ (6.07%) and $\tau_2 = 10.17 \pm 0.03$ (93.93%) ns but when monitored at 420 nm it shows biexponential decay ($\tau_1 = 8.74 \pm 0.08$ (-43.26%) and $\tau_2 = 9.73 \pm 0.05$ (143.26%)). At the excimer emission region a negative pre-exponential factor with shorter decay time is generally observed.²⁰ This interpretation was clearly proven by time-resolved fluorescence with the appearance of double exponential decays with a rise time observed at the excimer emission

Chapter 5

wavelength.²⁰ This is observed for $H \cdot G_2$ and this also further corroborates the excimer complex formation in excited state. Emission decay profile for 1:1 mixture of host and guest (**H** and **G₃**), when monitored at 343 nm, showed biexponential decay with the time constant of ($\tau_1 = 0.52 \pm 0.03$ ns (77.74%) and $\tau_2 = 5.31 \pm 0.03$ ns (22.53%) and it shows biexponential decay ($\tau_1 = 0.64 \pm 0.08$ ns (69.19%) and $\tau_2 = 5.63 \pm 0.05$ ns (30.81%)) when monitored at 420 nm. The emission decay profile **H** and **G₄**, when monitored at 343 nm, showed bi exponential decay with the time constant of ($\tau_1 = 0.87 \pm 0.08$ ns (14.57%) and $\tau_2 = 9.82 \pm 0.03$ ns (85.43%) ns, but a biexponential decay with time constants $\tau_1 = 0.63 \pm 0.08$ ns (53.59%) and $\tau_2 = 10.08 \pm 0.05$ ns (46.41%) were observed when monitored at 420 nm.

Moreover, pseudorotaxane formations were also confirmed by ESI Mass spectroscopy. A solution of **H** and **G₁** at a molar ratio 1:1 in CH_2Cl_2 showed prominent peaks at $m/z = 699.59$ were observed. This peak corresponds to $[2H + 2G_1 - 4PF_6^-]^{4+}$, which confirms the 2:2 inclusion complex formation between **H** and **G₁**. Similar ESI-mass spectra of complexes confirm the formation of 2:2 complex for **H** and **G₂**. A signal for m/z of 1370, which could be attributed to $(2H + 2G_2 - 2PF_6^-)^{2+}$. Mass spectrum recorded for **H** and **G₃** (with $[H]:[G_3]$) also confirmed formation of a 2:2 inclusion complex, which showed a signal for m/z of 1398. This could be attributed to $(2H + 2G_3 - 2PF_6^-)^{2+}$, while that for **H** and **G₃** appeared at 1398 for $(2H + 2G_3 - 2PF_6^-)^{2+}$. The most intense peak at m/z 1468 in the ESI mass spectrum of the 1:1 mixture in CH_2Cl_2 corresponds to doubly charged $[2H + 2G_4 - 4PF_6^-]^{4+}$.

5.4. Conclusion

We have demonstrated that the intramolecular monomer/excimer inter-conversion in supramolecular assembly could be tuned based on the length of the appropriate linkers of the bivalent guest molecules. Upon inclusion of di-cationic guest excimer emission response comes from bis crown ether derivative functionalized with naphthalene moiety. The molecular organization of bis crown ether can enhance the possibility for the naphthalene rings to encounter each other and provides an excimer to monomer emission ratio. Our studies confirm that pseudorotaxane formation as well as with the lowering of temperature, structural rigidity of the supramolecular architecture favour the excimer emission.

5.5. References

1. (a) Ballardini, R.; Balzani, V.; Clemente-Leon, M.; Credi, A.; Gandolfi, M. T.; Ishow, E.; Perkins, J.; Stoddart, J. F.; Tseng, H. R.; Wenger, S. *J. Am. Chem. Soc.* **2002**, *124*, 12786; (b) Balzani, V.; Credi, A.; Venturi, M. *Proc. Natl. Acad. Sci. U.S.A.* **2002**, *99*, 4814; (c) Balzani, V.; Credi, A.; Venturi, M. *Chem.-Eur. J.* **2002**, *8*, 5524; (d) G. Pace, V. Ferri, C. Grave, M. Elbing, C. v. Hañnisc, M. Zharnikov, M. Mayor, M. A. Rampi, P. Samori *Proc. Natl. Acad. Sci.*, **2007**, *104*, 9937.
2. Schmittel, M.; Mahata, K. *Angew. Chem., Int. Ed.*, **2008**, *47*, 5284.
3. W. Wang, Y. Zhang, B. Sun, L.-J. Chen, X.-D. Xu, M. Wang, X. Li, Y. Yu, W. Jiang, H.-B. Yang *Chem. Sci.*, **2014**, *5*, 4554.
4. (a) Chichak, K. S.; Cantrill, S. J.; Pease, A. R.; Chiu, S.-H.; Cave, G. W. V.; Atwood, J. L.; Stoddart, J. F. *Science*, **2004**, *304*, 1308; (b) Forgan, R. S.; Sauvage, J.-P.; Stoddart, J. F. *Chem. Rev.*, **2011**, *111*, 5434.
5. (a) Boyer, P. D. *Angew. Chem., Int. Ed.*, **1998**, *37*, 2296; (b) Walker, J. E. *Angew. Chem., Int. Ed.*, **1998**, *37*, 2308; (c) Junge, W. *Proc. Natl. Acad. Sci. USA*, **1999**, *96*, 4735.
6. Jiang, W.; H. D. F. Winkler, C. A. Schalley, *J. Am. Chem. Soc.* **2008**, *130*, 13852.
7. Jiang, W.; Schäfer, A.; Mohr, P. C.; Schalley, C. A. *J. Am. Chem. Soc.* **2010**, *132*, 2309.
8. Celtek, G.; Artar, M.; Scherman, O. A.; Tuncel, D. *Chem. Eur. J.* **2009**, *15*, 10360.
9. (a) Hu, J.-Y.; Pu, Y.-J.; Nakata, G.; Kawata, S.; Sasabe, H.; Kido, J. *Chem. Commun.*, **2012**, *48*, 8434; (b) Hu, J.-Y.; Pu, Y.-J.; Yamashita, Y.; Satoh, F.; Kawata, S.; Katagiri, H.; Sasabe, H.; Kido, J. *J. Mater. Chem. C*, **2013**, *1*, 3871.
10. (a) Shafikov, M. Z.; Suleymanova, A. F.; Kozhevnikov, D. N.; König, B. *Inorg. Chem.*, **2017**, *56*, 4885; (b) Farhangi, S.; Casier, R.; Li, L.; Thoma, J. L.; Duhamel, J. *Macromolecules* **2016**, *49*, 9597;
11. Fujii, A.; Sekiguchi, Y.; Matsumura, H.; Inoue, T.; Chung, W.-S.; Hirota, S.; Matsuo, T. *Bioconjugate Chem.* **2015**, *26*, 537;
12. Jiang, W.; Sattler, D.; Rissanen, K.; Schalley, C. A. *Organic Letters* **2011**, *13*, 4502.
13. (a) Mandal, A. K.; Gangopadhyay, M.; Das, A. *Chem. Soc. Rev.* **2015**, *44*, 663; (b) Beriman, I. B. *Handbook of Fluorescence Spectra of Aromatic Molecules*, 2nd ed.; Academic Press: New York, 1971.

Chapter 5

14. (a) Albelda, M. T.; Bernardo, M. A.; Díaz, P.; García-Espana, E.; Seixas de Melo, J.; Pina, F.; Soriano, C.; Santiago, V. L. E. *Chem. Commun.* **2001**, 1520; (b) Seixas de Melo, J.; Albelda, M. T.; Díaz, P.; García -Espana, E.; Lodeiro, C.; Alves, S.; Lima, J. C.; Pina, F.; Soriano, C. J. *Chem. Soc., Perkin Trans.* **2002**, 998.
15. Chandross E. A.; Dempster, C. J. *J. Am. Chem. Soc.* **1970**, *92*, 704.
16. Winnik, F. M. *Chem. Rev.* **1993**, *93*, 587.
17. Zhang, Q.-W.; Li, D.; Li, X.; White, P. B.; Mecinović, J.; Ma, X.; Ågren, H.; Nolte, R. J.M.; Tian, H. *J. Am. Chem. Soc.* **2016**, *138*, 13541.
18. Gangopadhyay, M.; Maity, A.; Dey, A.; Das, A. *J. Org. Chem.* **2016**, *81*, 8977.
19. Valeur, B. *Molecular Fluorescence: Principles and Applications*, Wiley-VCH Verlag GmbH, **2001**, 95.
20. (a) Melo, J. S. d.; Pina, J. *J. Phys. Chem. A* **2003**, *107*, 11307; (b) Cao, T.; Zhang, X.; Qian, R. *Polymer Journal*, **1989**, *21*, 489.

Conclusion

Conclusion of the Thesis

The thesis entitled “*Design and Synthesis of Supramolecular Assemblies and their Photophysical studies*” describes, how attempt has been made to demonstrate these non-bonded interactions could be used in our favour to achieve a desired host-guest structures that are capable of demonstrating either some useful function or help us in achieving the control in probing the molecular conformations in an assembly simply by looking into the spectral responses of the appropriately substituted host or guest components. The thesis contains overall five chapters. The first chapter is the introductory chapter, which describes supramolecular structures are the result of not only additive but also cooperative interactions, including various non-bonding interactions like, π - π interaction, hydrogen bonding, hydrophobic and van der Waals interactions. Selectivity can arise from a number of different factors, such as complementarity of the host and guest binding sites, preorganisation of the host conformation, or co-operativity and multivalency of the binding groups. The aim of the thesis is to design stimuli dependent change of optical response mainly fluorescence have been used for probing the conformational change associated with inclusion complex formation.

In the chapter 2 we could demonstrate a TPA derivative (**1**Cl₃) that exhibited a rare dual emission property at room temperature. Shorter wavelength emission band was assigned to locally excited states and longer wavelength emission band was attributed to an intra molecular charge transfer process. Such example of dual emission from a single molecule at room temperature is not common. This TPA derivative formed a [4]pseudorotaxane complex ([**1**•3{CB[7]}]Cl₃) with CB[7]. Presumably, widely different electrostatic potential of the β -CD, as compared to that for CB[7], helped in stabilizing a completely different inclusion complex. For β -CD, a dynamic [2]pseudorotaxane complex formation took place with β -CD hopping between the three equivalent arms of **1**Cl₃ in [**1**•{ β -CD}]Cl₃, choosing only one at a given moment. For [**1**•3{CB[7]}]Cl₃, LE state was favoured, while ICT state was favoured for [**1**•{ β -CD}]Cl₃. Observed results were rationalized based on the results obtained from detailed NMR and steady/excited state emission studies.

In the chapter 3 we could demonstrate the complexation behaviour of **H** with two imidazolium ion based guest molecules (**G**₁, **G**₂). Detail luminescence studies help us to understand the energy transfer mechanism. The energy levels calculated on the basis of electrochemical data and E₀₋₀ value for the respective molecule also agrees well with

Conclusion

spectral responses for different energy transfer processes. From the investigation of the influence of small addition of KPF_6 and 18C6 on the complexation of either of the guests to H, we found that the addition of KPF_6 could dissociate the complexes completely and subsequent addition of 18C6 could reform the inclusion complexes completely. This reversible control makes H and imidazolium derivatives good candidate components for constructing molecular machines driven by adding small molecules. It is noteworthy that the PET process could be reversibly controlled by binding and release of the cationic guests and metal ion. Consequently, these obtained results may provide a perspective for the design of molecular machines based on inclusion complex formation with controlled photophysical behaviors. The self-sorting phenomena can be monitored by NMR spectroscopy and ESI mass spectrometry and show the expected self-sorting behaviour.

In the chapter 4 we have shown that chiral crown ethers with binaphthol chromophore units are efficient sensing materials for the discrimination of enantiomer amine pairs through FRET mechanism. The remarkable chiral recognition of the guests with impressive enantioselectivity may result from their different orientations in the host cavity. Complexes having host and guest of opposite chirality was found to give a more efficient FRET transfer compared to complexes with host and guest of same chirality. This was confirmed by ITC experiments which show higher thermodynamic stability for R-H.R-G and S-H.S-G compared to R-H.S-G and S-H.R-G. Also the exchange rates determined by NMR are lower for R-H.R-G and S-H.S-G, implying greater stability for these complexes. In R-H.S-G and S-H.R-G, the relative orientation and distance of the fluorophores is more favorable for FRET compared to that in R-H.R-G and S-H.S-G, thus providing a basis for discrimination of enantiomers.

In the chapter 5 we could demonstrate the monomer/excimer interconversion of systems consisting of a polyamine chain, end-terminated by two naphthyl units upon inclusion of di cationic guests excimer emission response comes from bis crown ether. The molecular organization of Bis crown ether can enhance the possibility for the naphthalene rings to encounter each other and provides an excimer to monomer emission ratio. This would be analogous to intermolecular excimer formation. Moreover from the result of temperature dependent fluorescence studies, as temperature decreases excimer emission is favored.

Appendix

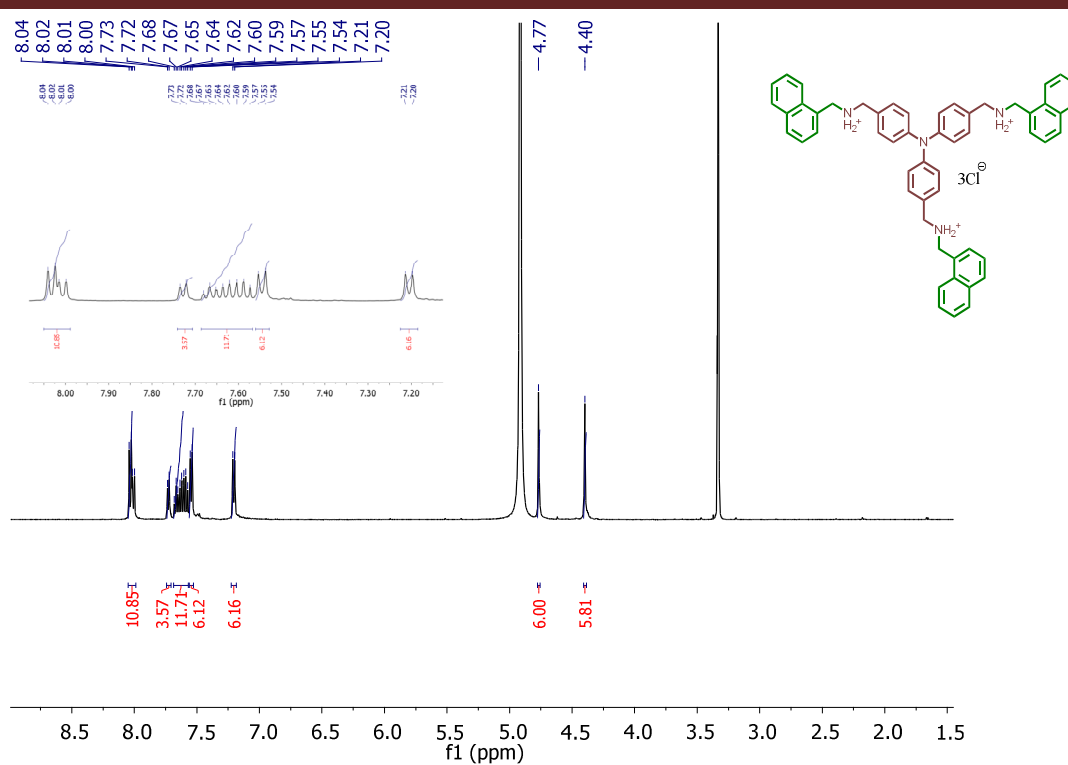


Figure 1. ^1H NMR spectra recorded in CD_3OD at room temperature.

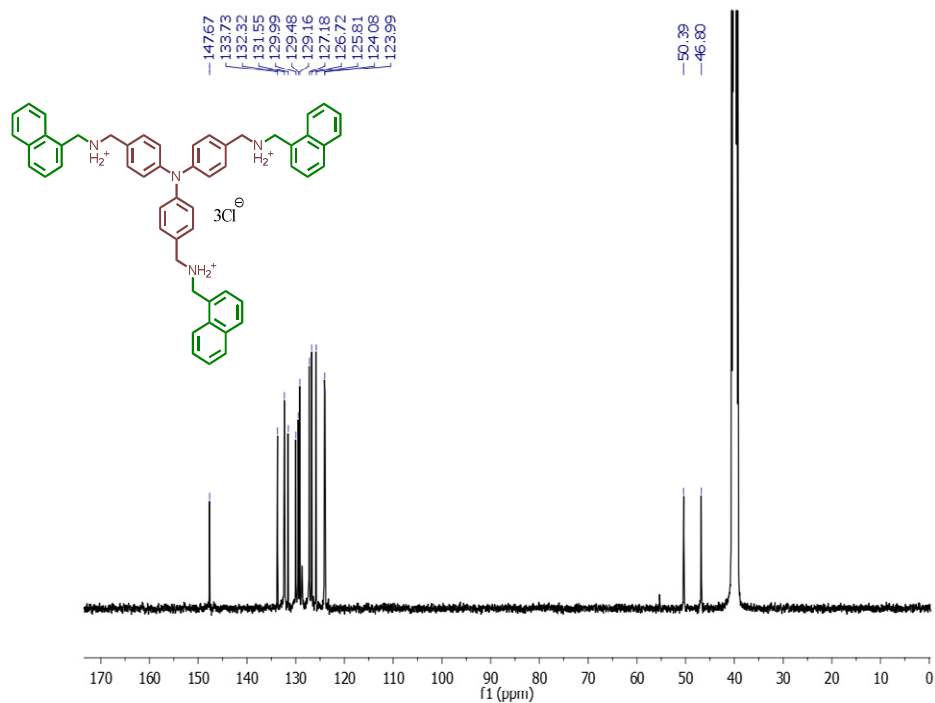


Figure 2. ^{13}C NMR spectra recorded in DMSO-d_6 at room temperature.

Appendix

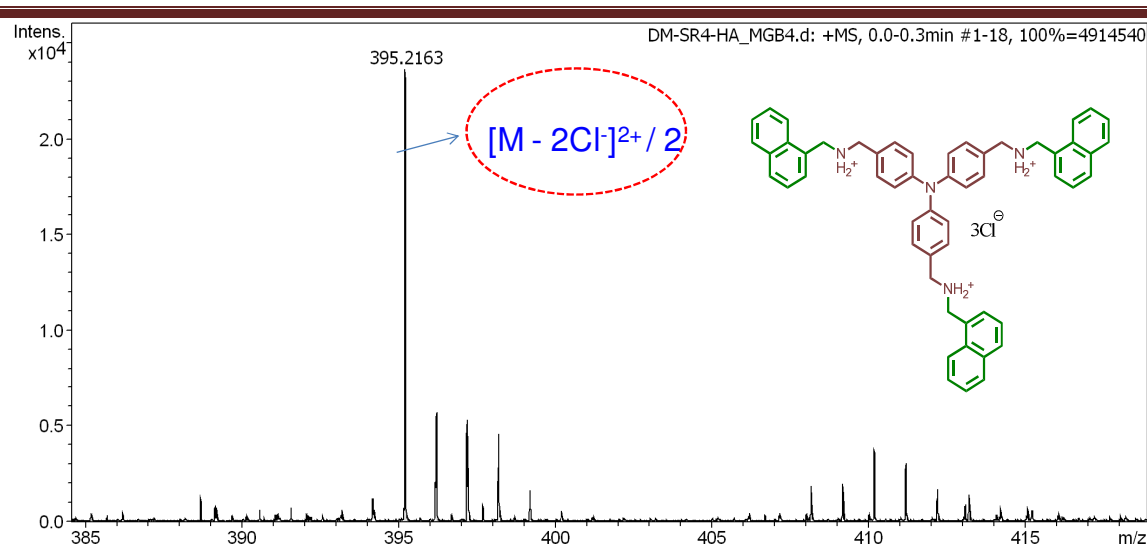


Figure 3. ESI-MS spectra recorded in positive ion mode in MeOH.

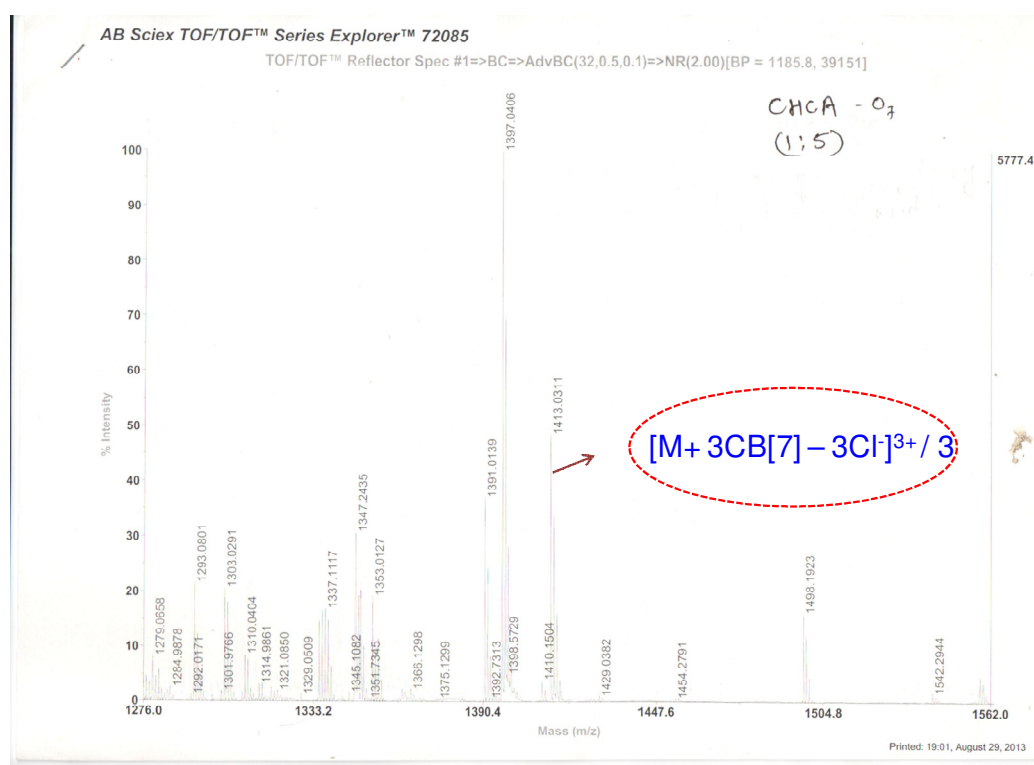


Figure 4. MALDI-TOF Mass spectrum for $1\text{Cl}_3 \cdot 3\text{CB}[7]$ recorded in H_2O at room temperature by using α -cyano hydroxy benzoic acid as matrix spectra.

Appendix

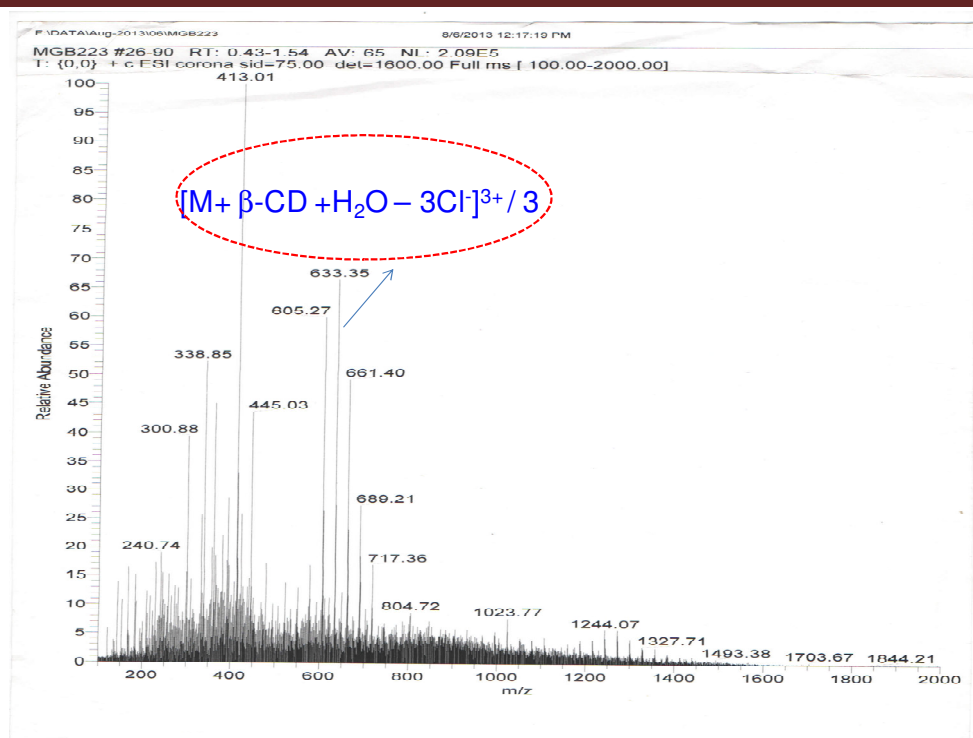


Figure 5. ESI-MS spectrum $\{1Cl_3.\beta\text{-CD}\}$ recorded in water in positive ion mode at room temperature.

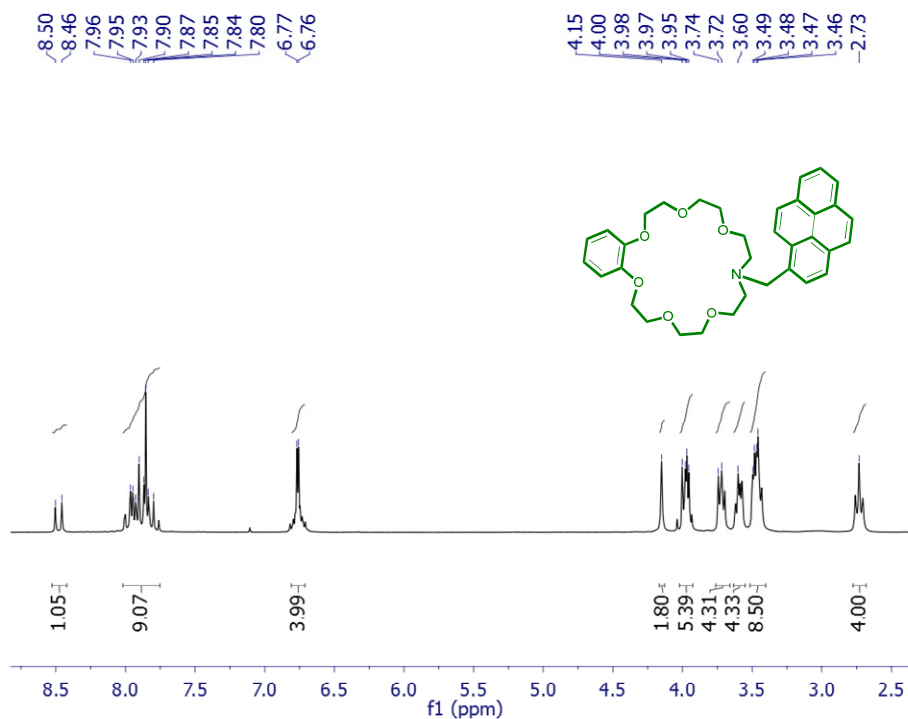


Figure 6. $^1\text{H-NMR}$ spectrum in CDCl_3 at 298K.

Appendix

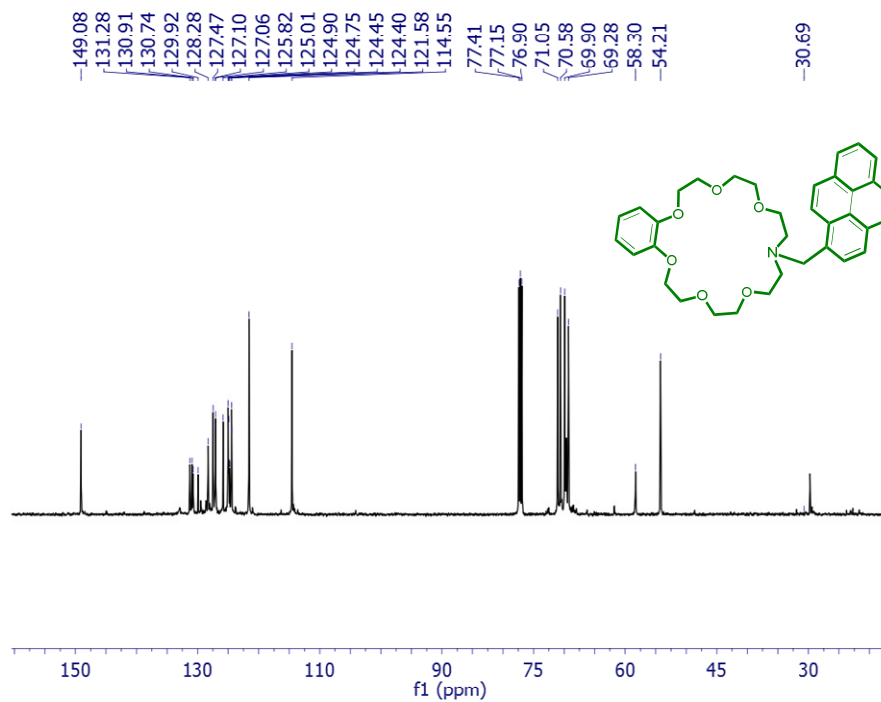


Figure 7. ^{13}C -NMR spectrum in CDCl_3 at 298K

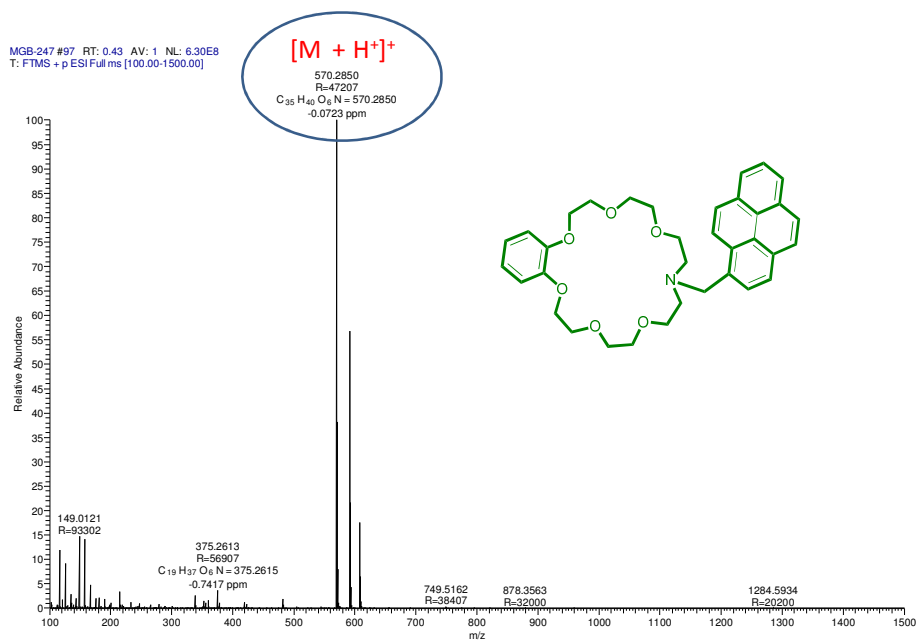


Figure 8. HRMS spectrum in CH_3OH at 298K spectra.

Appendix

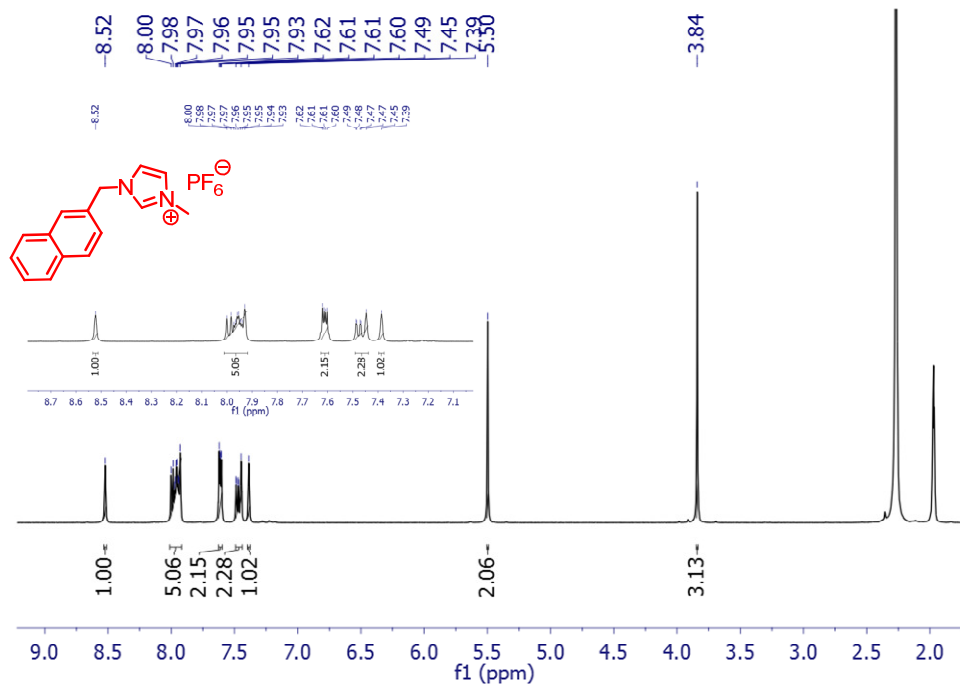


Figure 9. $^1\text{H-NMR}$ spectrum in CD_3CN at 298K.

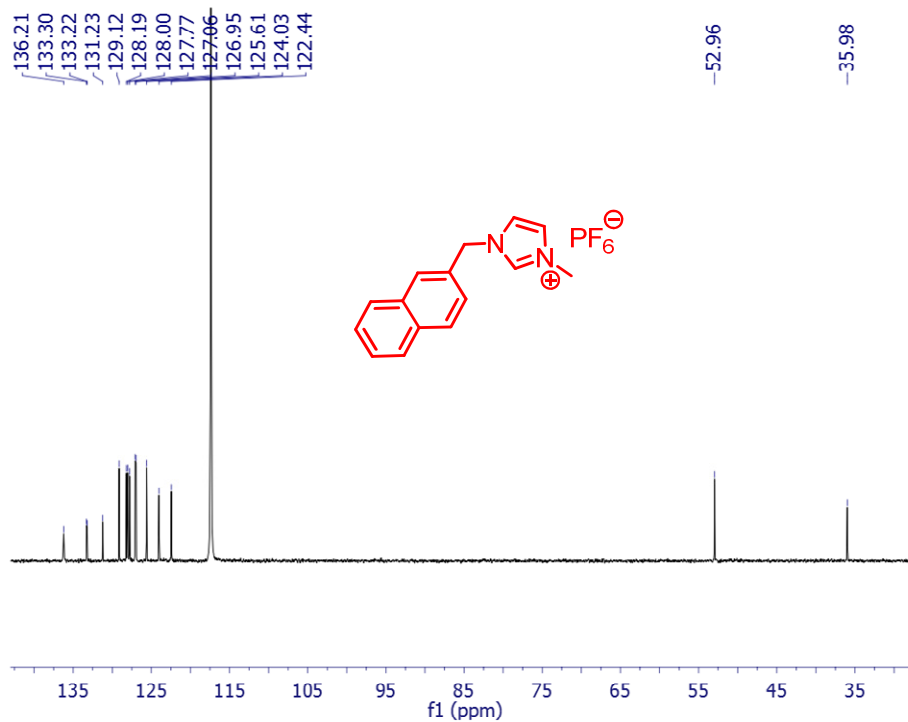


Figure 10. $^{13}\text{C-NMR}$ spectrum in CD_3CN at 298K.

Appendix

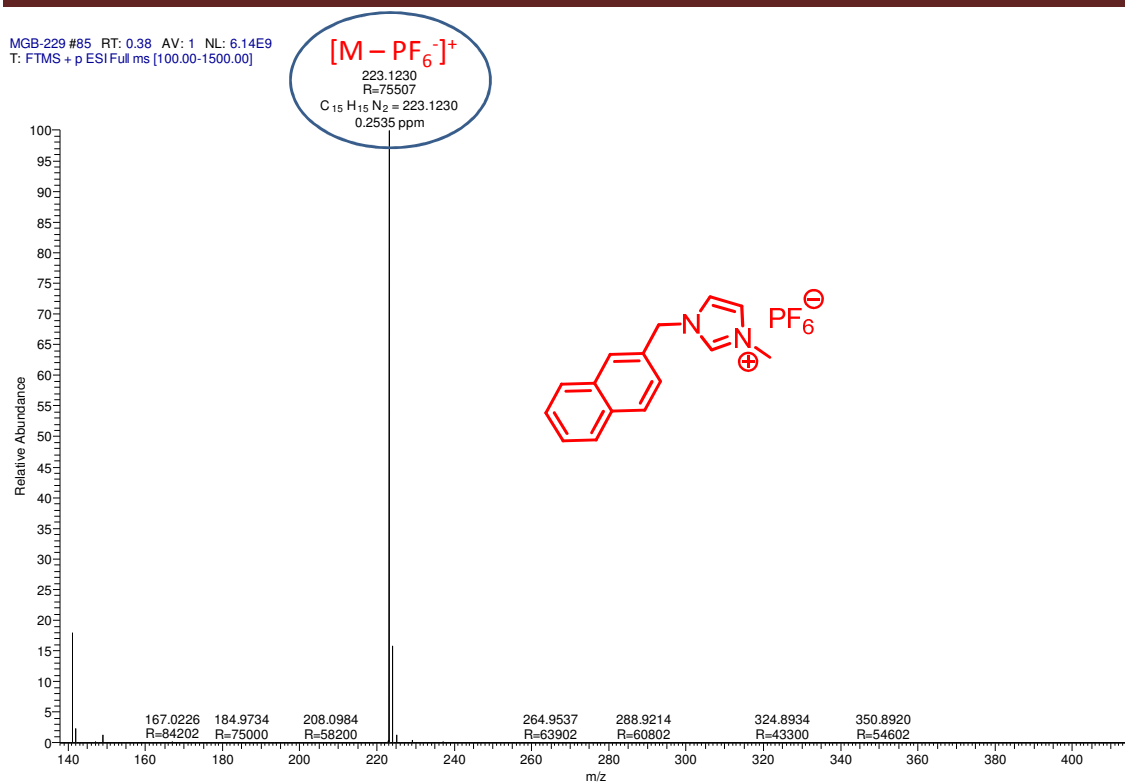


Figure 11. HRMS spectrum in CH₃OH at 298K.

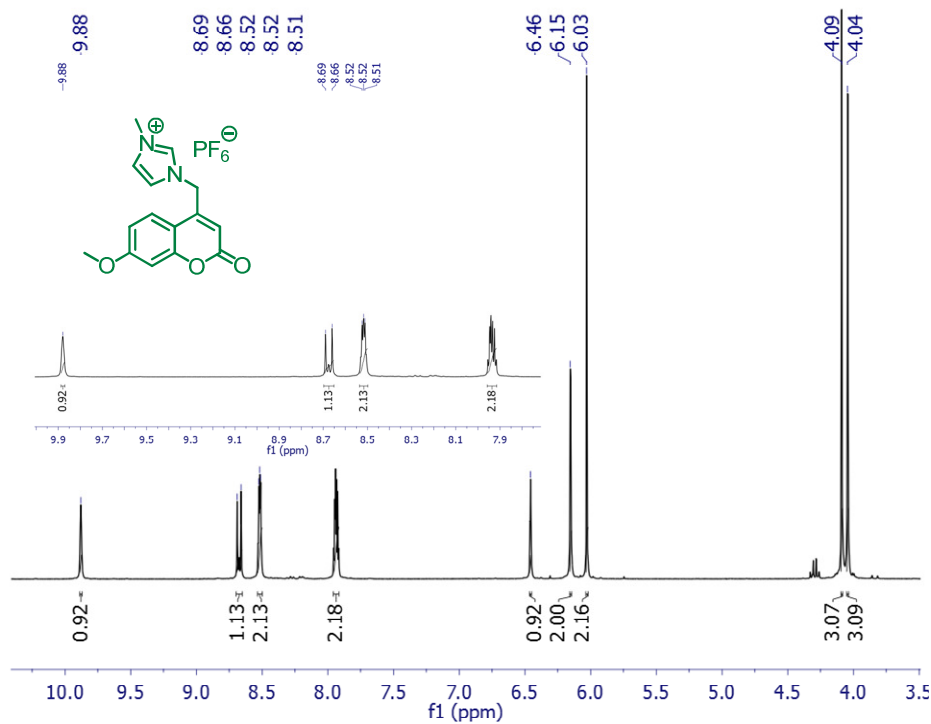


Figure 12. ¹H-NMR spectrum in CD₃CN at 298K.

Appendix

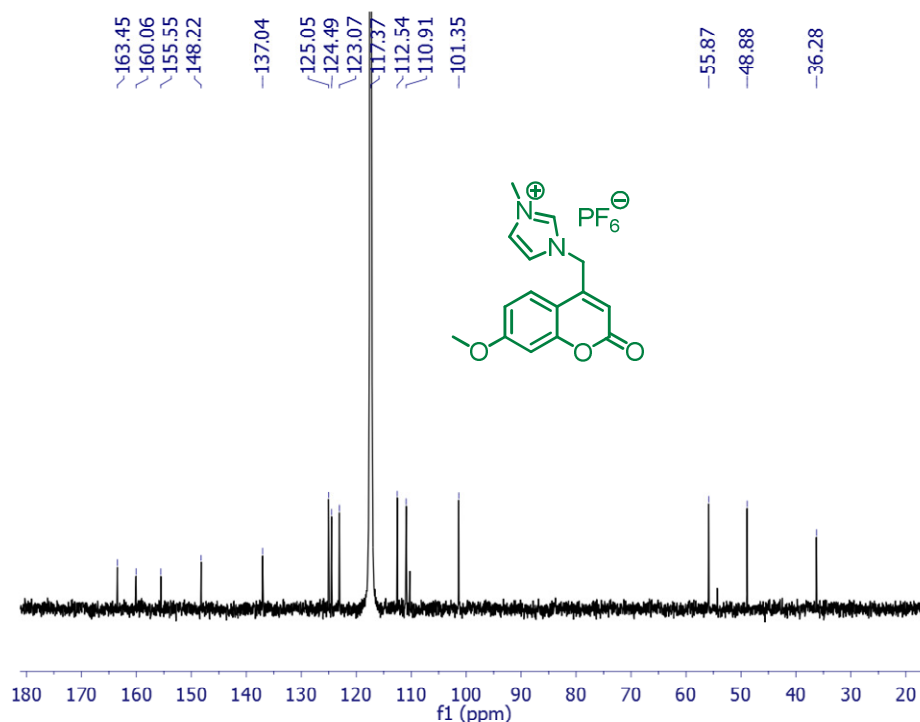
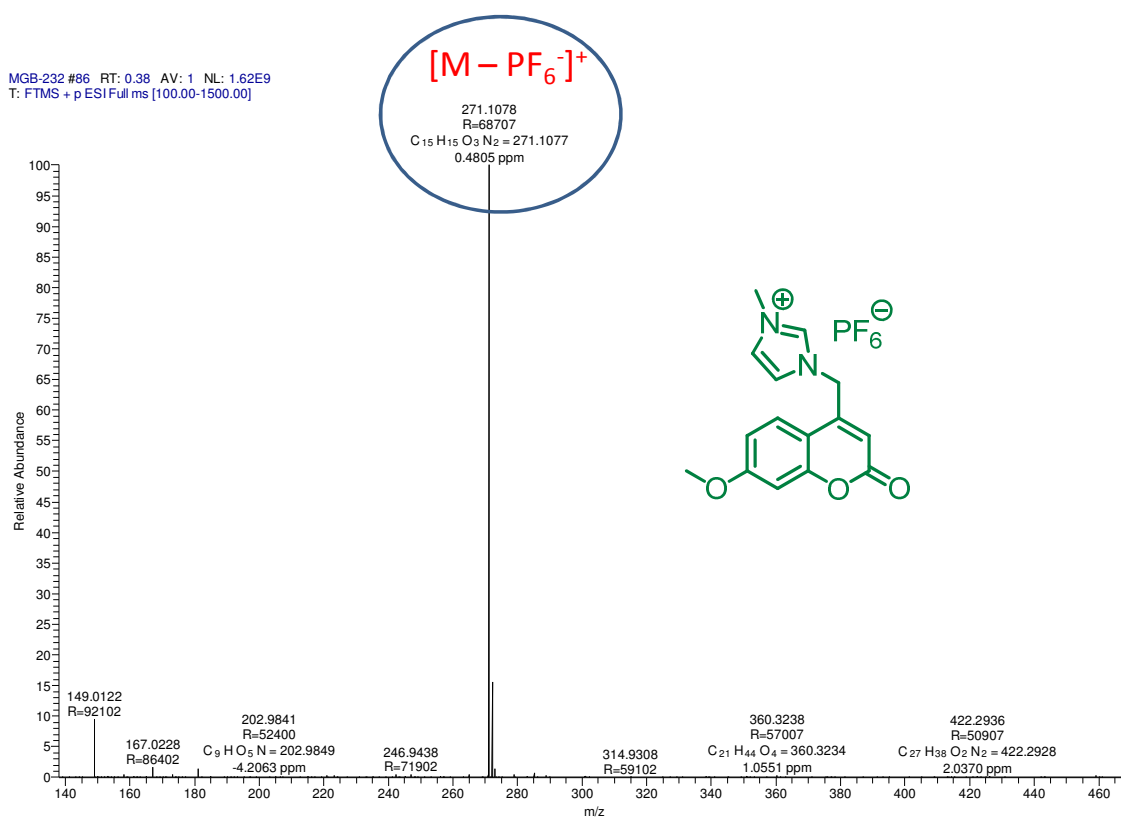


Figure 13. ^{13}C -NMR spectrum in CD_3CN at 298K



Appendix

Figure 14. HRMS spectrum in CH₃OH at 298K spectra

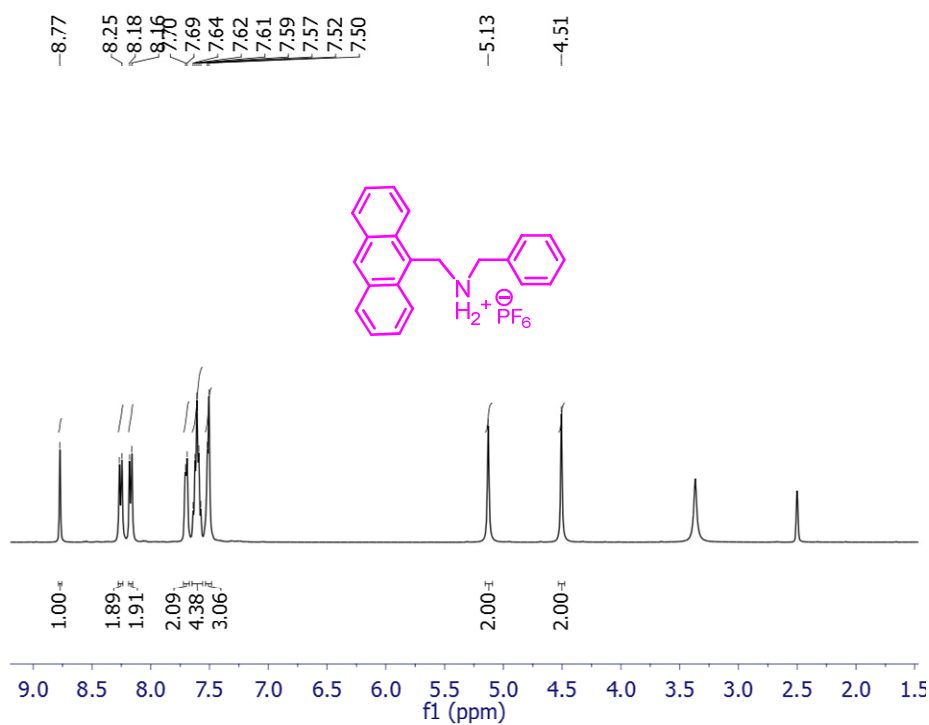


Figure 15. ¹H-NMR spectrum in DMSO-d₆ at 298K.

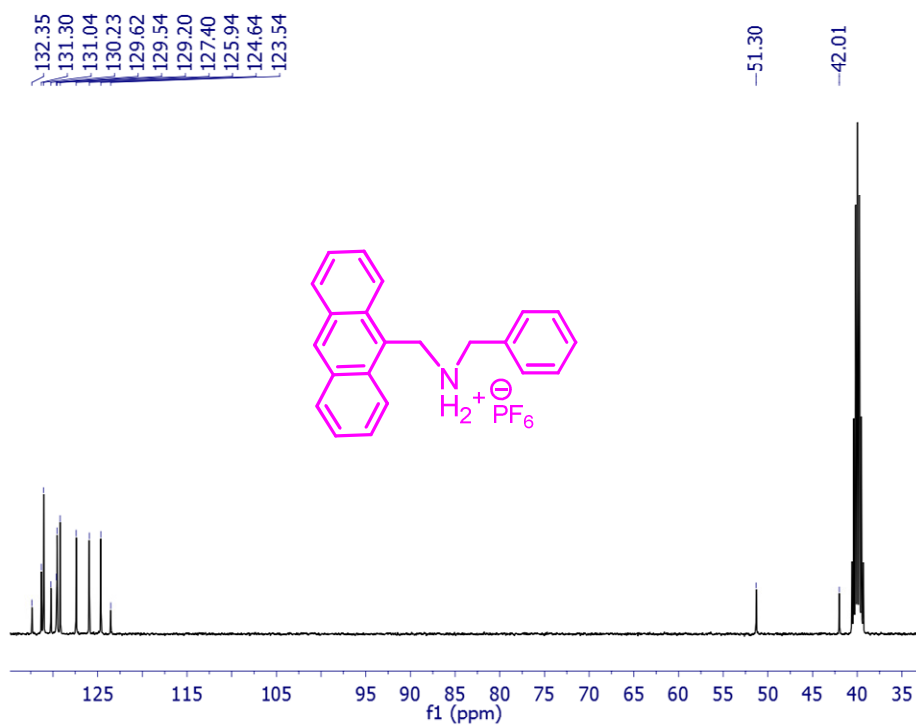


Figure 16. ¹³C-NMR spectrum in DMSO-d₆ at 298K spectra.

Appendix

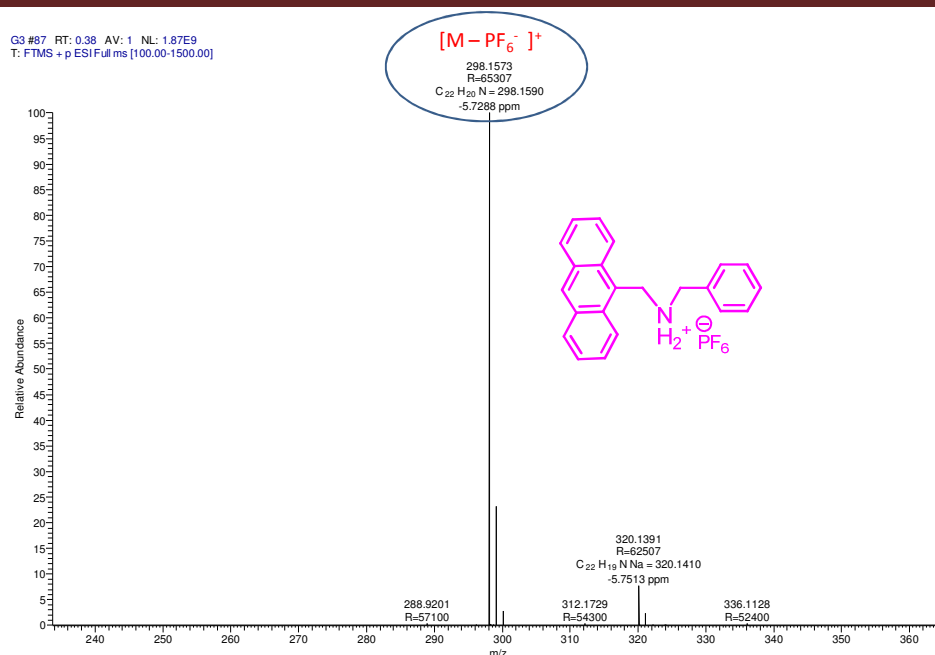


Figure 17. HRMS spectrum in CH₃OH at 298K spectra.

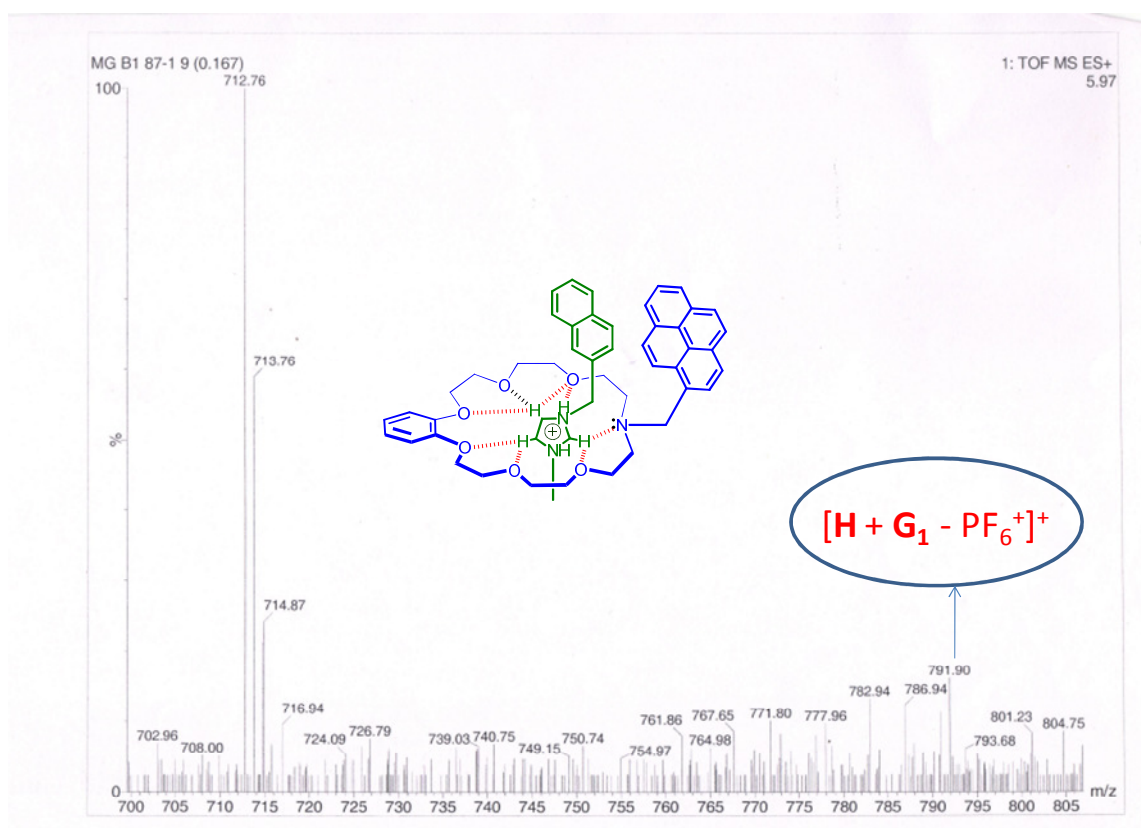


Figure 18. Mass spectrum for (1:1) mixture of H and G₁.

Appendix

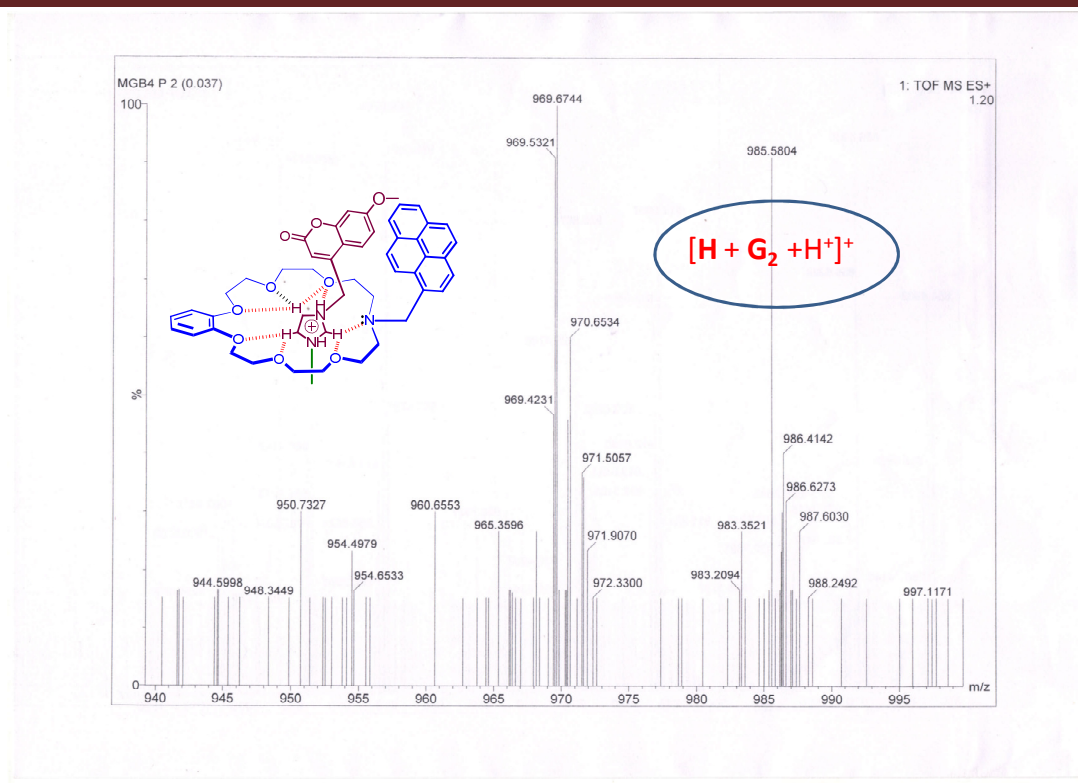


Figure 19. Mass spectrum for (1:1) mixture of **H** and **G₂**.

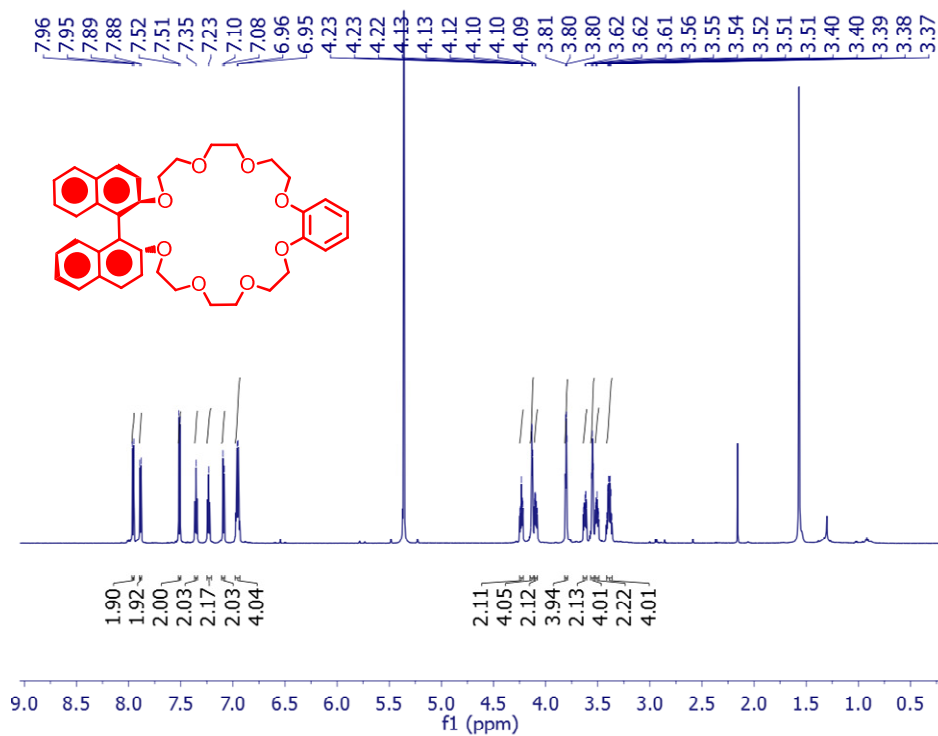


Figure 20. ¹H-NMR spectrum in CD₂Cl₂ at 298K.

Appendix

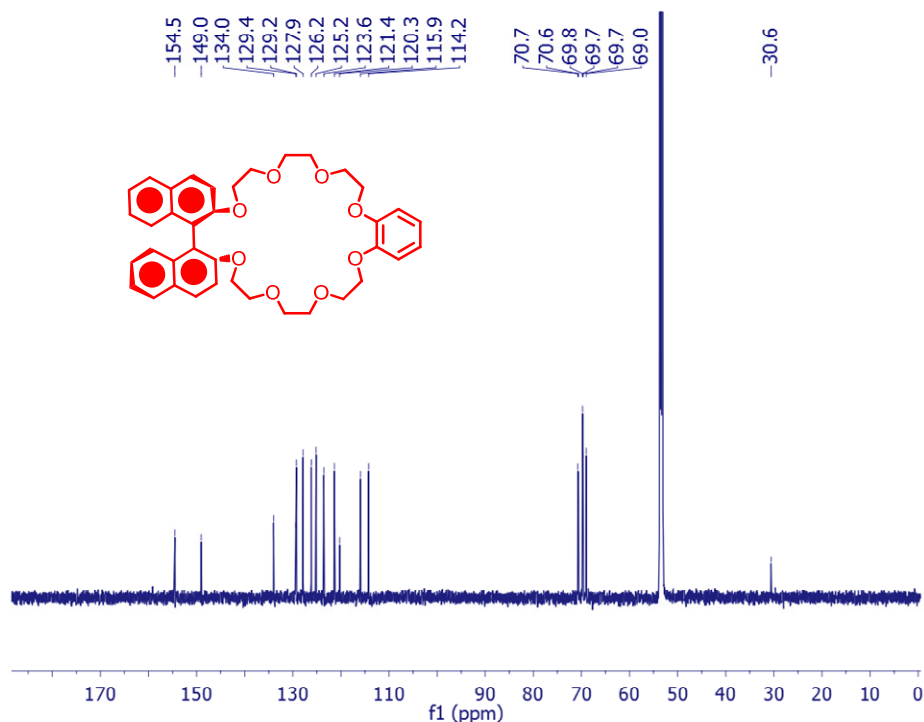


Figure 21. ^{13}C -NMR spectrum in CD_2Cl_2 at 298K.

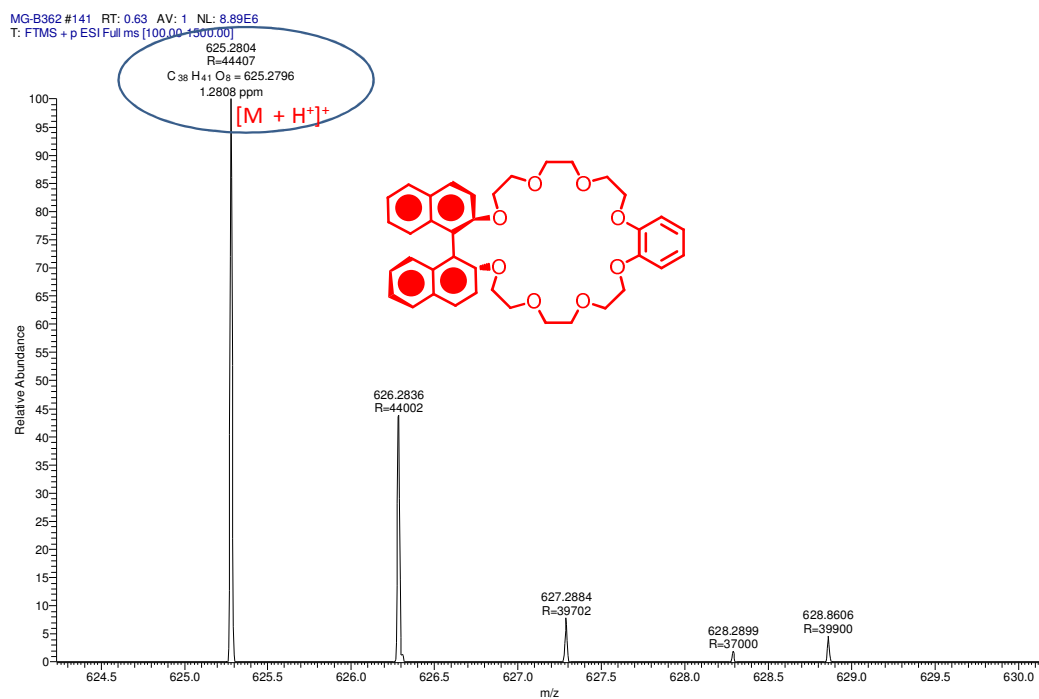


Figure 22. HRMS spectrum in CH_3OH at 298K spectra.

Appendix

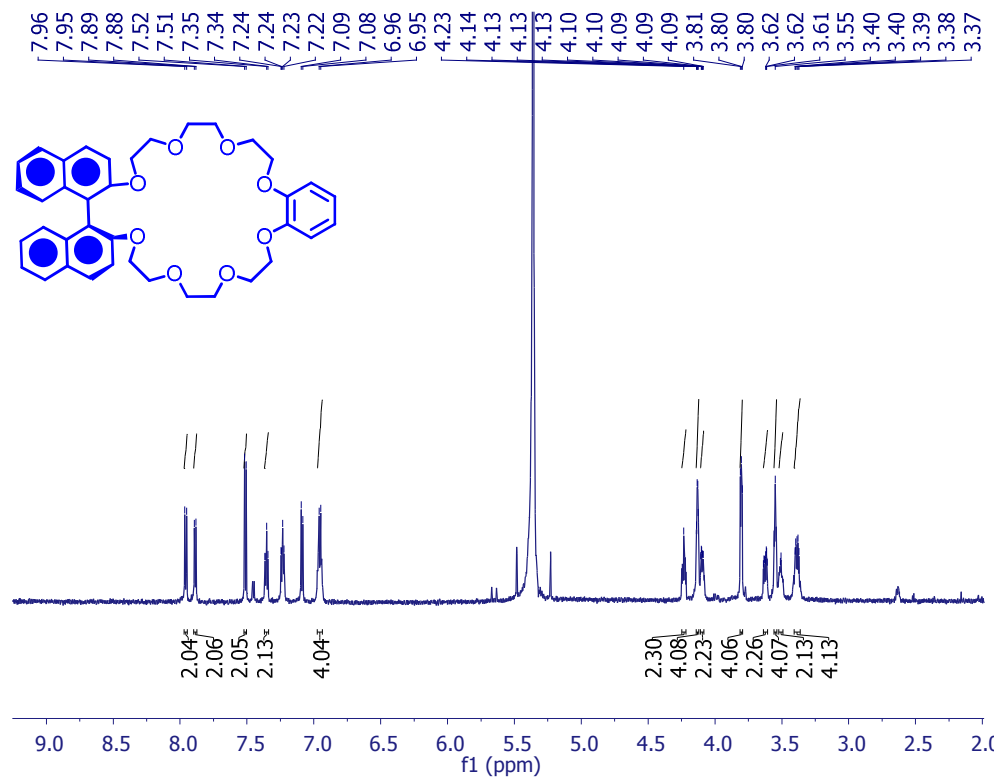


Figure 23. ¹H-NMR spectrum in CD₂Cl₂ at 298K spectra.

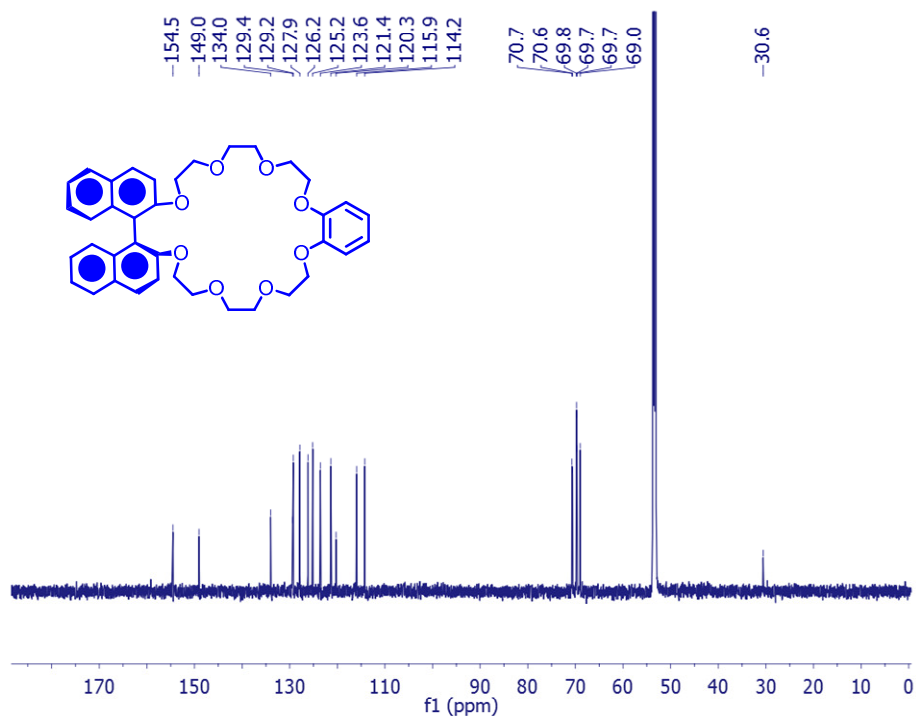


Figure 24. ¹³C-NMR spectrum in CD₂Cl₂ at 298K.

Appendix

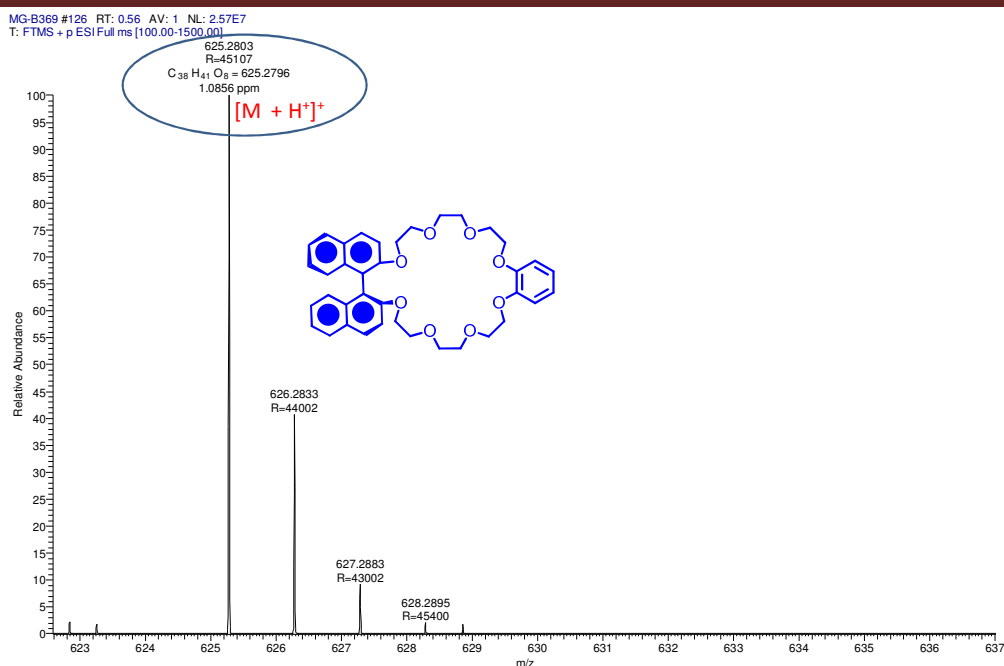


Figure 25. HRMS spectrum in CH₃OH at 298K.

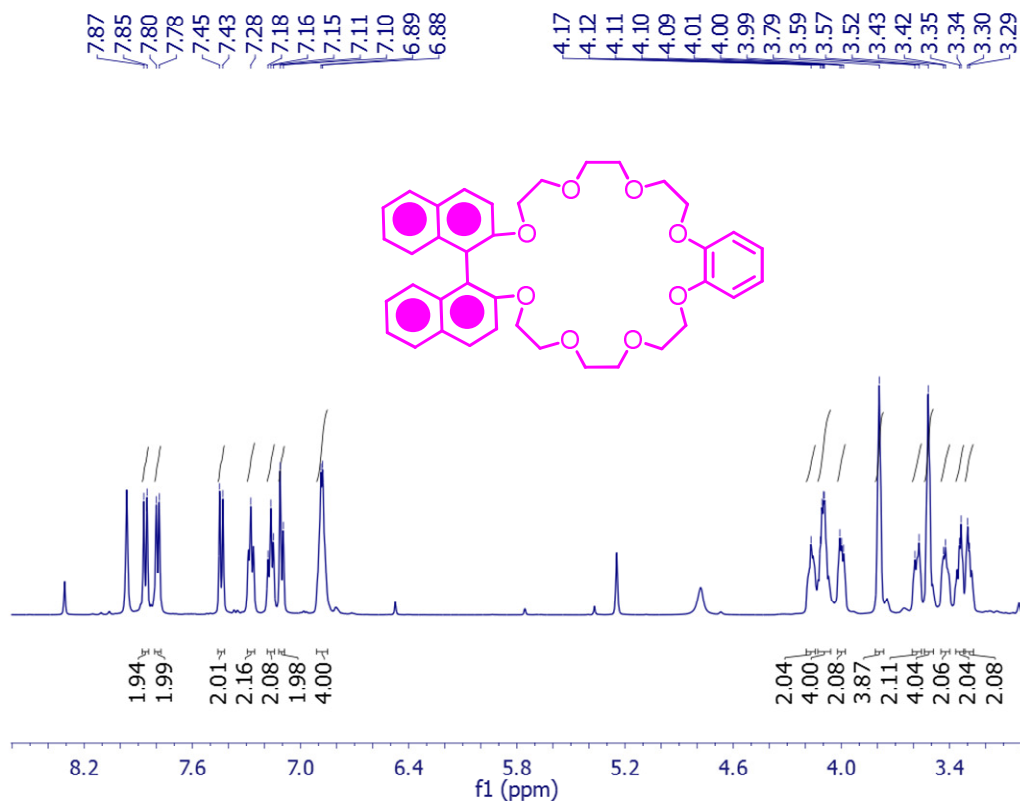


Figure 26. ¹H NMR spectra recorded in CD₂Cl₂.

Appendix

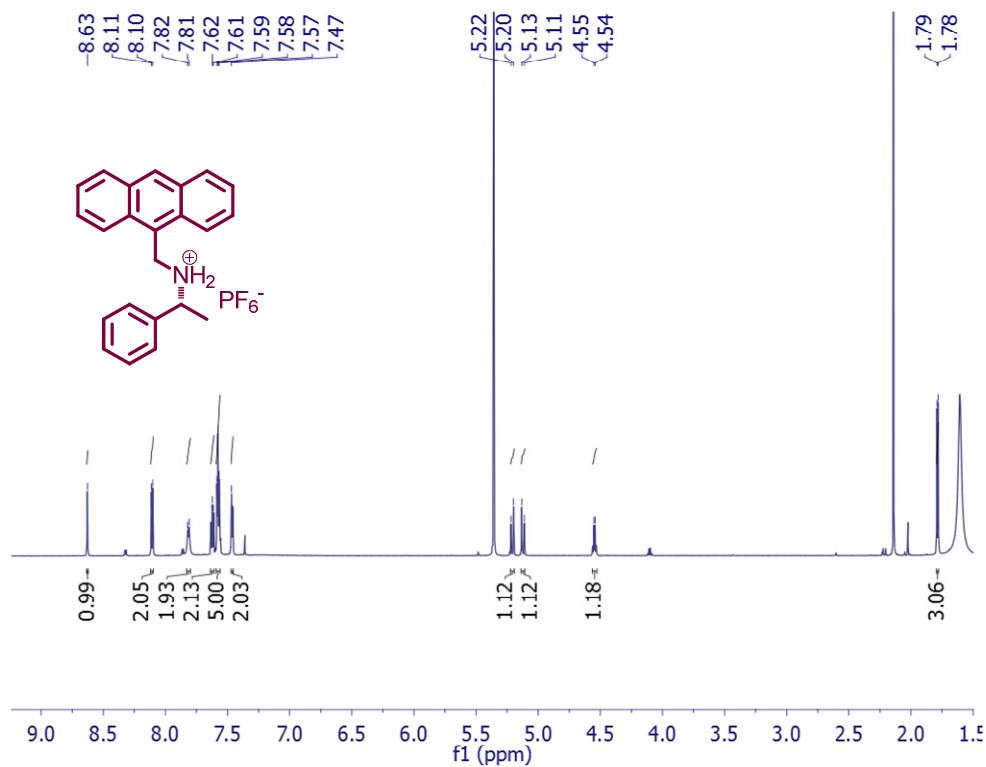


Figure 29. ¹H NMR spectra recorded in CD₂Cl₂.

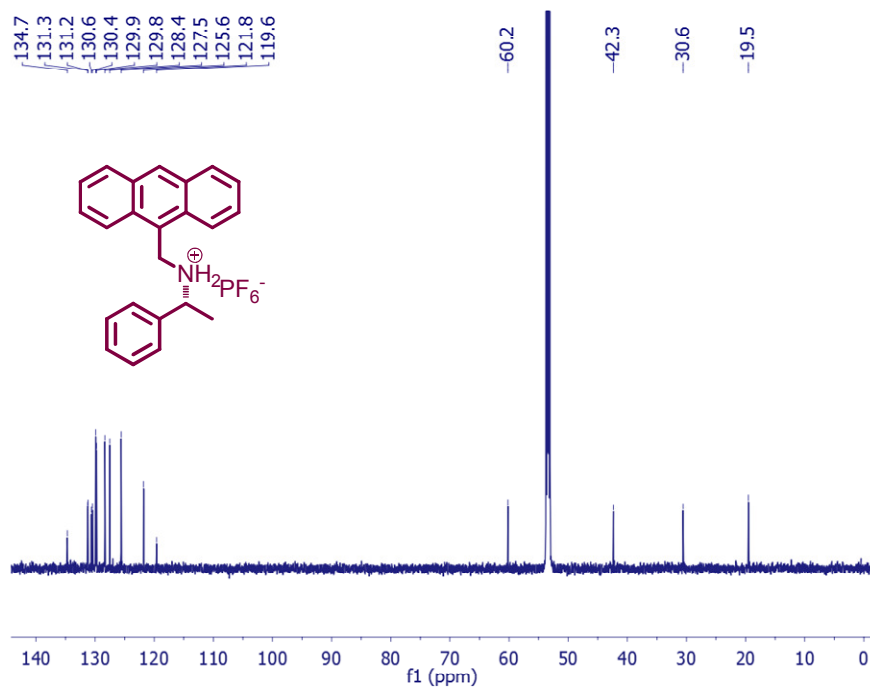


Figure 30. ¹³C NMR spectra recorded in CD₂Cl₂.

Appendix

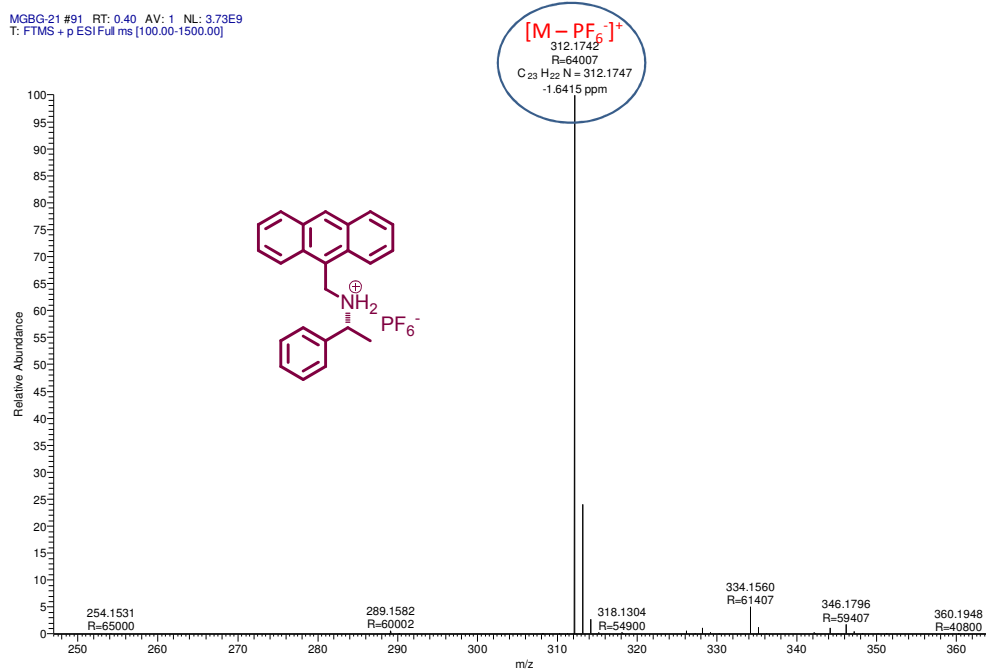


Figure 31. HRMS spectra recorded in CH_3OH .

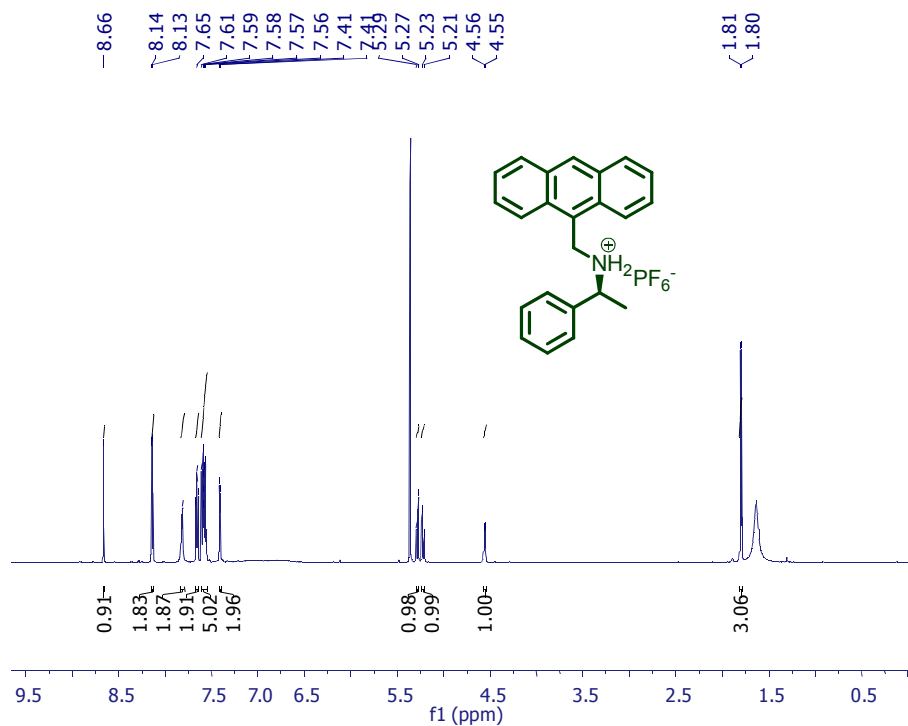


Figure 32. ^1H NMR spectra recorded in CD_2Cl_2 .

Appendix

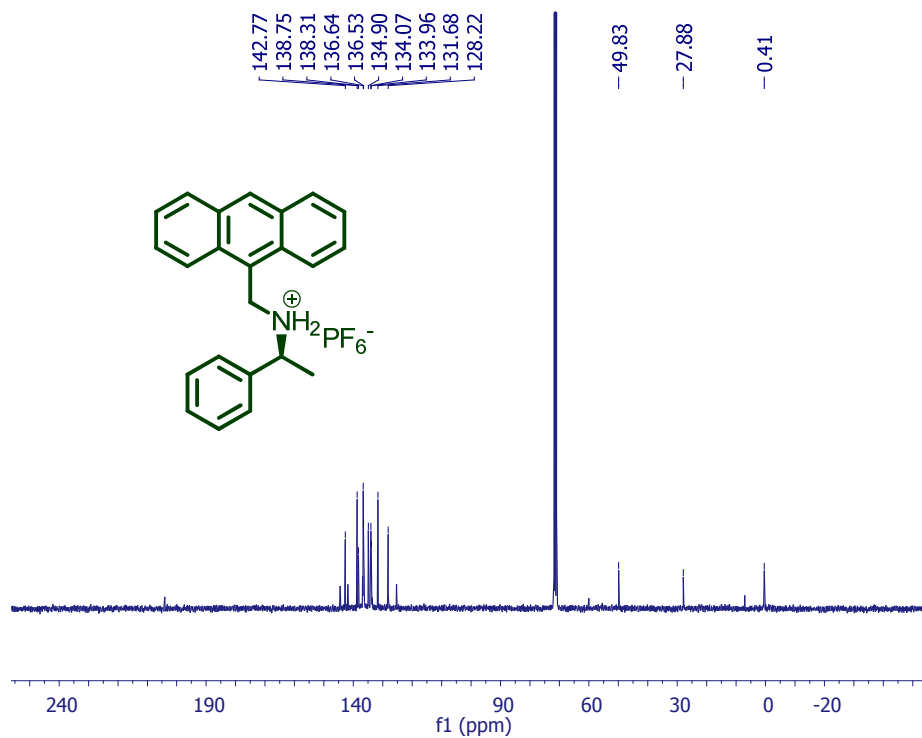


Figure 33. ^{13}C NMR spectra recorded in CD_2Cl_2 .

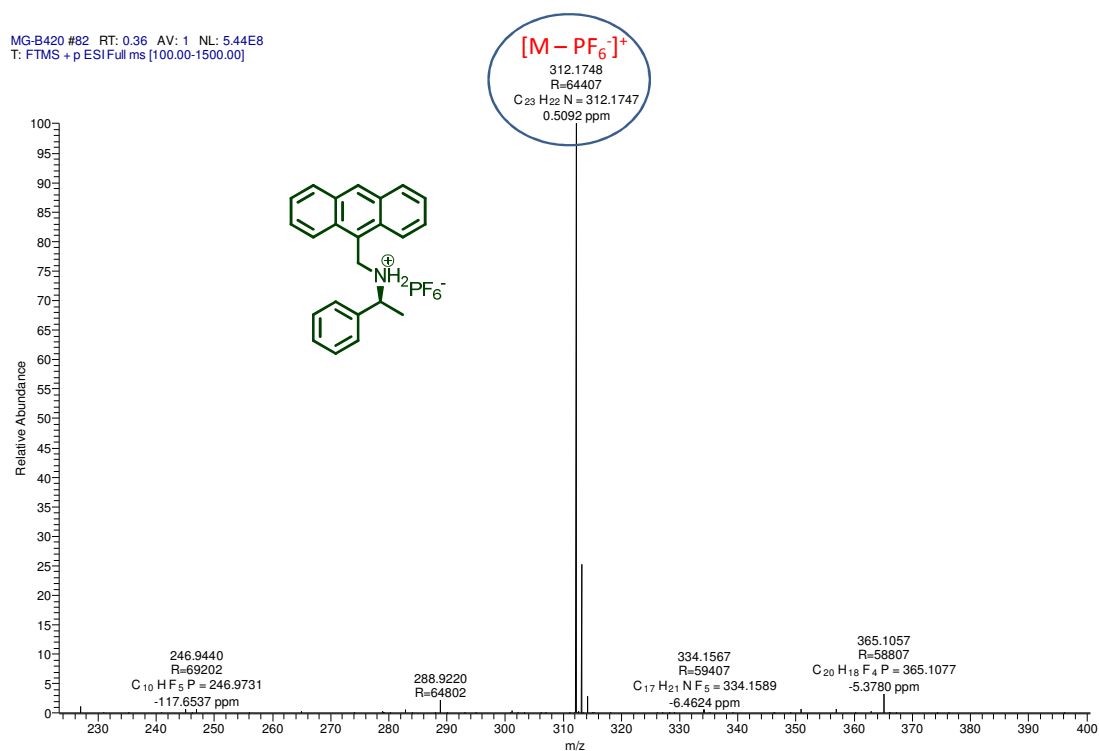


Figure 34. HRMS spectra recorded in methanol.

Appendix

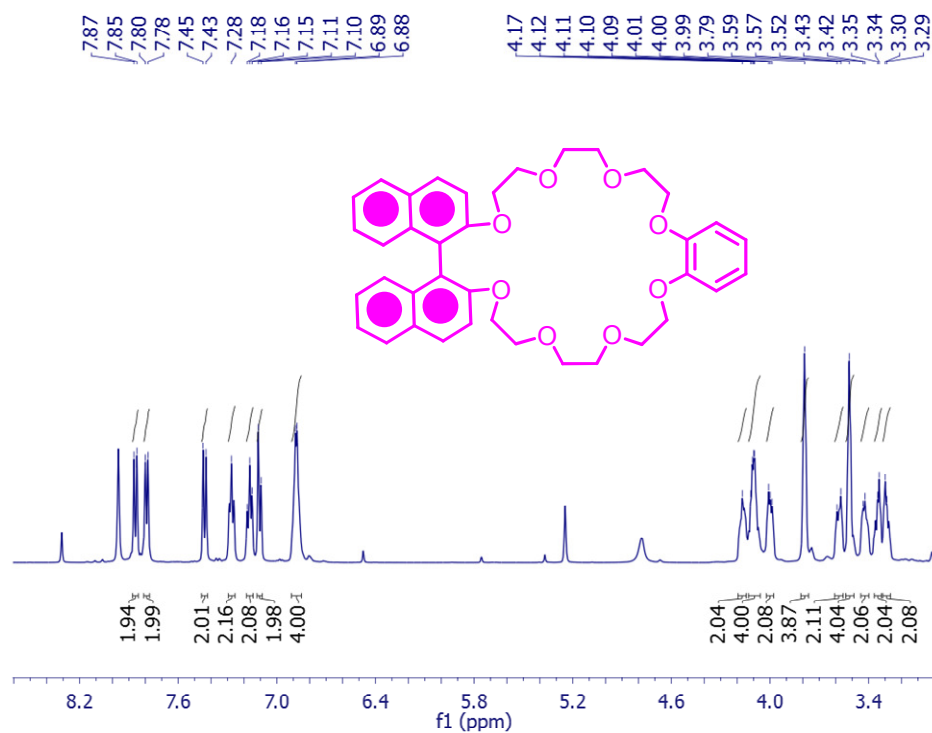


Figure 35. ¹H NMR spectra recorded in CD₂Cl₂.

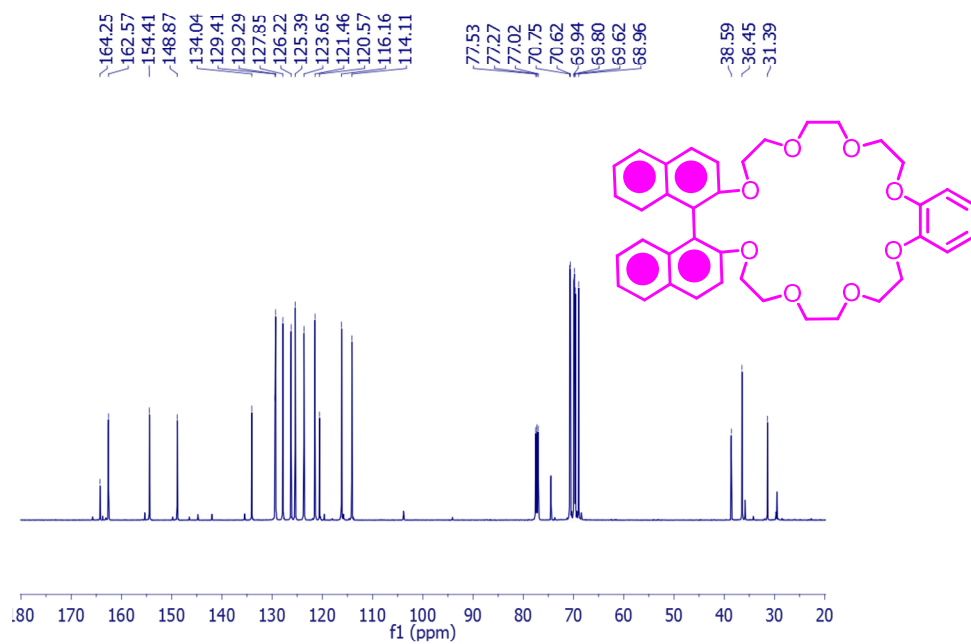


Figure 36. ¹³C NMR spectra recorded in CD₂Cl₂.

Appendix

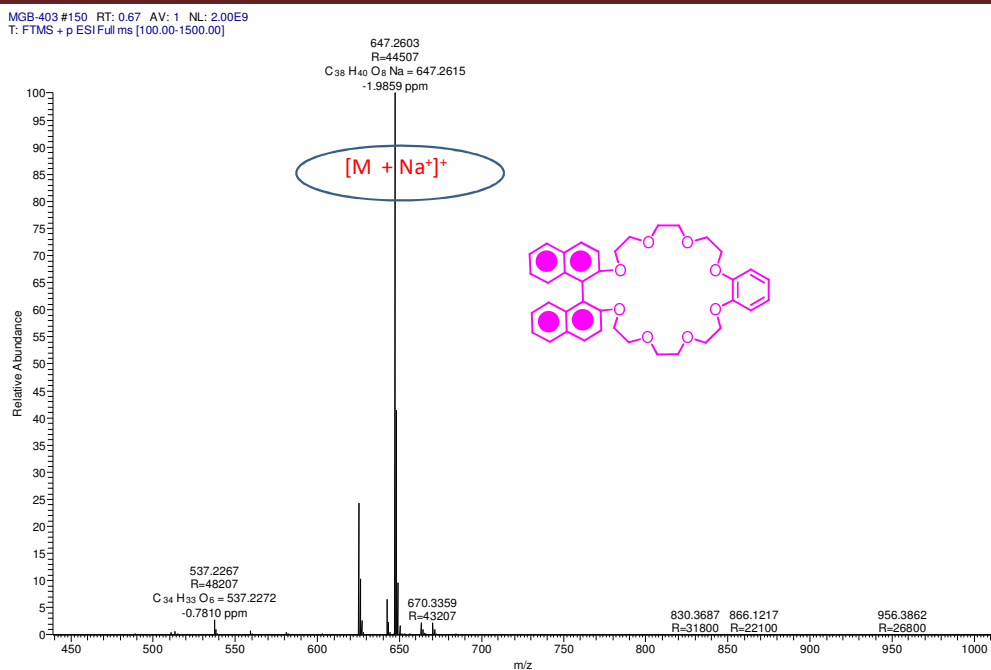


Figure 37. HRMS spectra recorded in methanol.

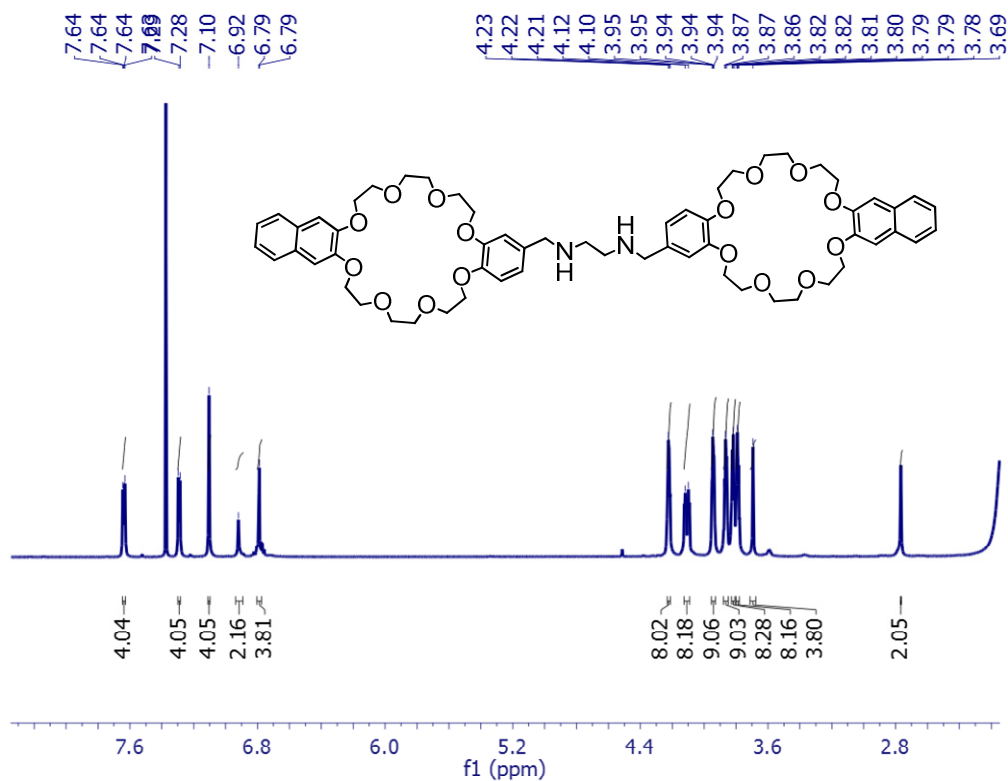


Figure 38. ¹H NMR spectra recorded in CD₂Cl₂.

Appendix

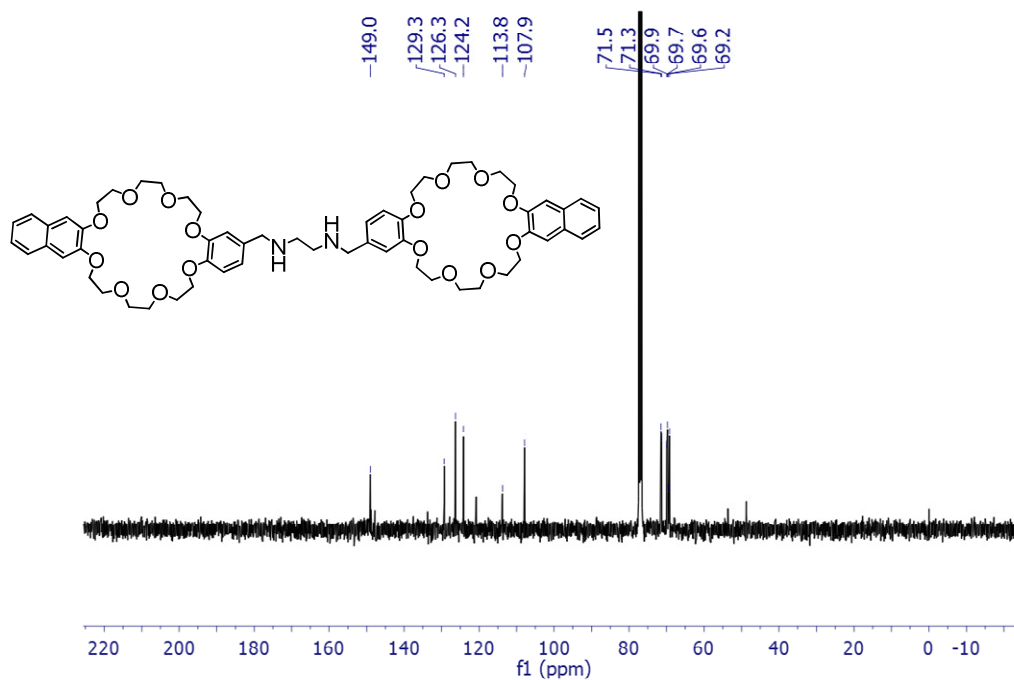


Figure 39. ^{13}C NMR spectra recorded in CDCl_3 .

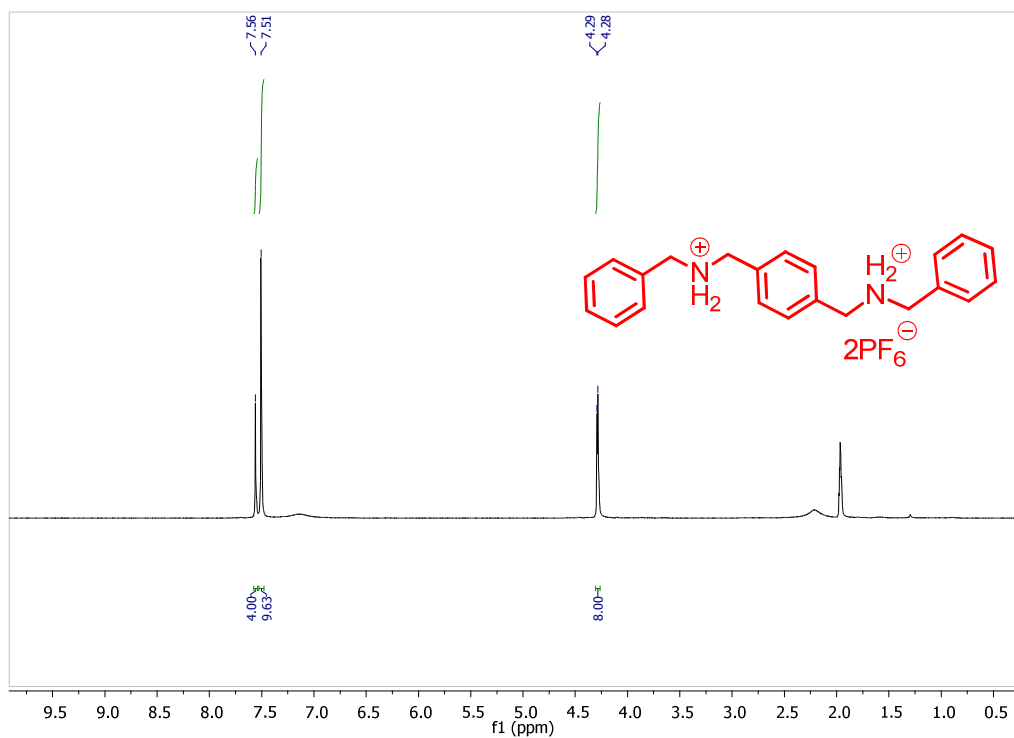


Figure 40. ^1H NMR spectra recorded in CD_3CN .

Appendix

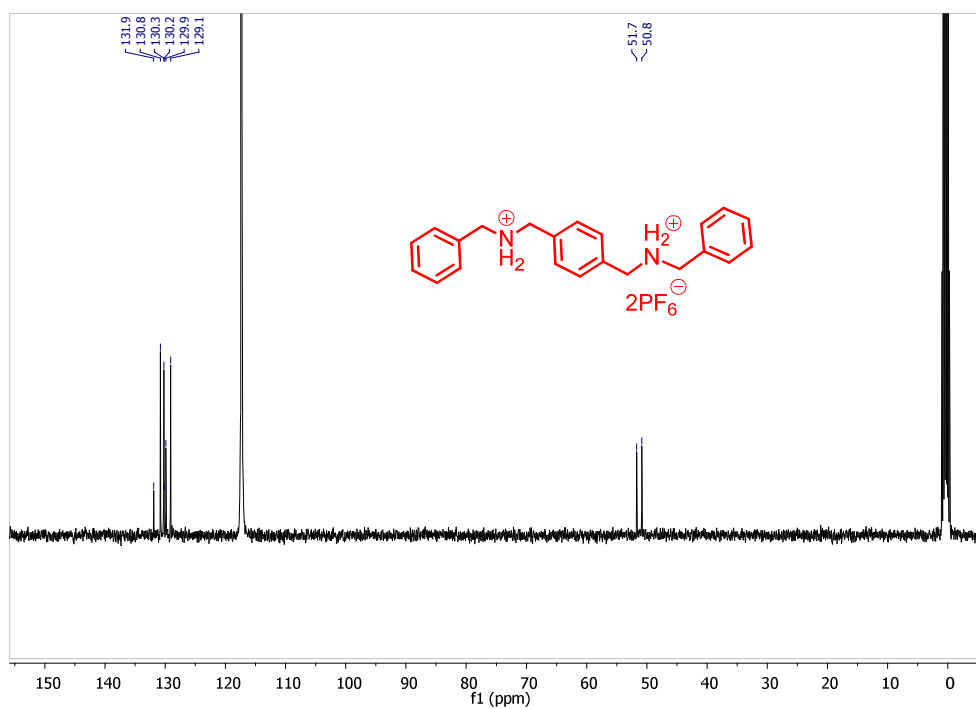


Figure 41. ^{13}C NMR spectra recorded in CD_3CN .

MGB-445 #100 RT: 0.44 AV: 1 NL: 2.52E7
T: FTMS + p ESI Full ms [100.00-1500.00]

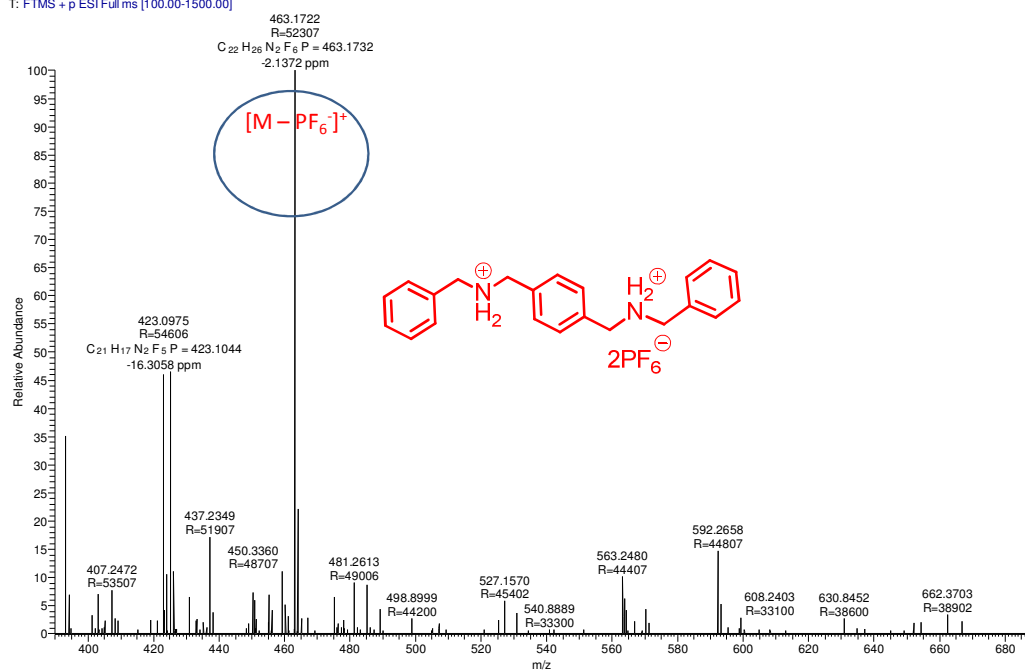


Figure 42. HRMS spectra recorded in ACN.

Appendix

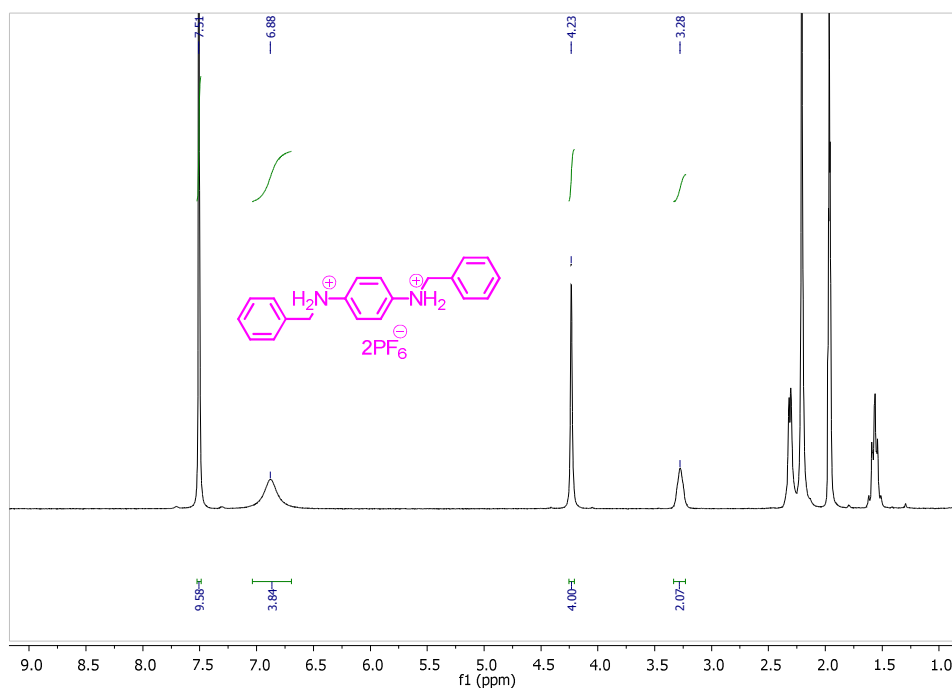


Figure 43. ¹H NMR spectra recorded in CD_3CN .

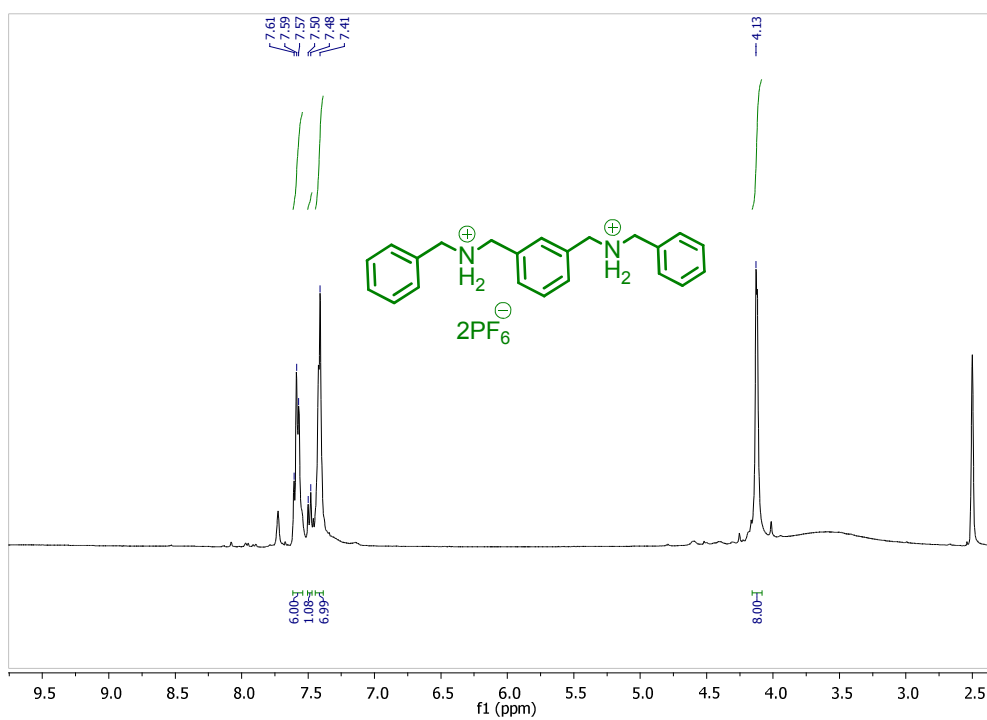


Figure 44. ¹H NMR spectra recorded in CD_3CN .

Appendix

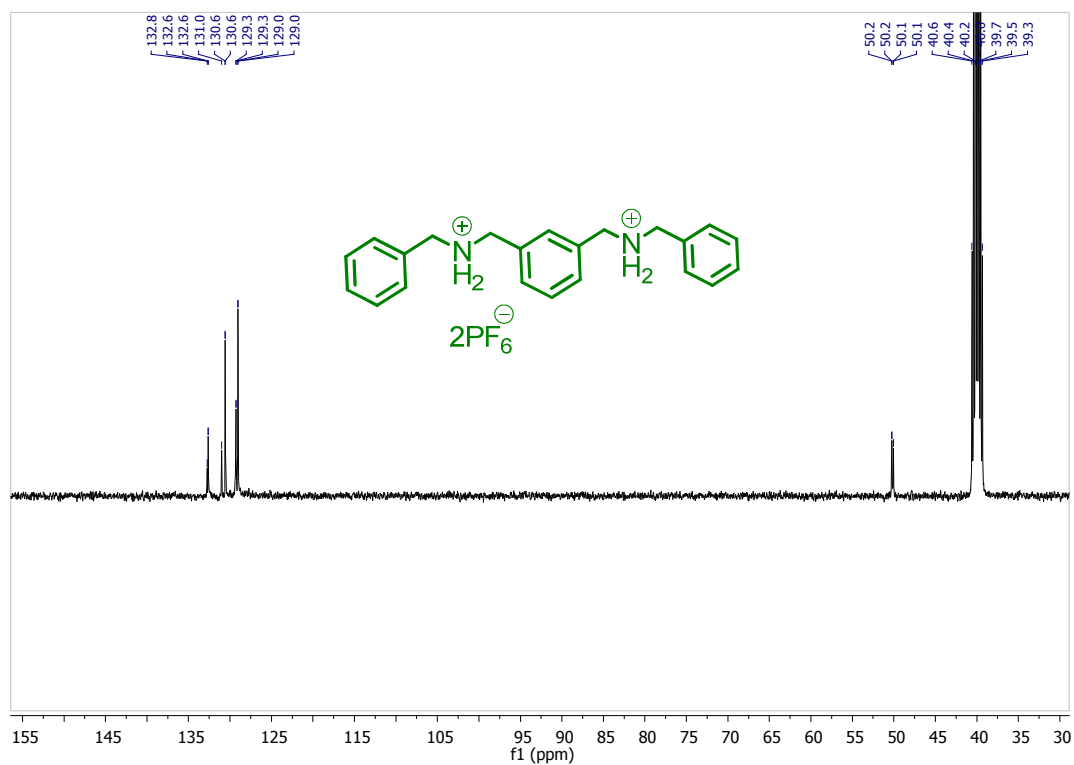


Figure 45. ^{13}C NMR spectra recorded in CD_3CN .

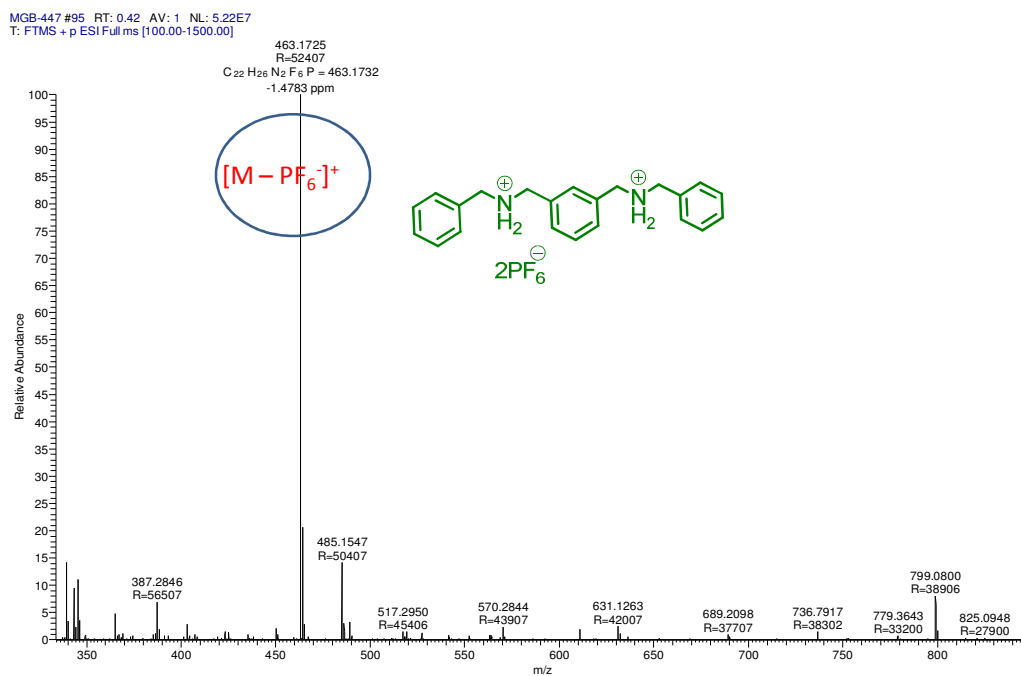


Figure 46. HRMS spectra recorded in ACN.

Appendix

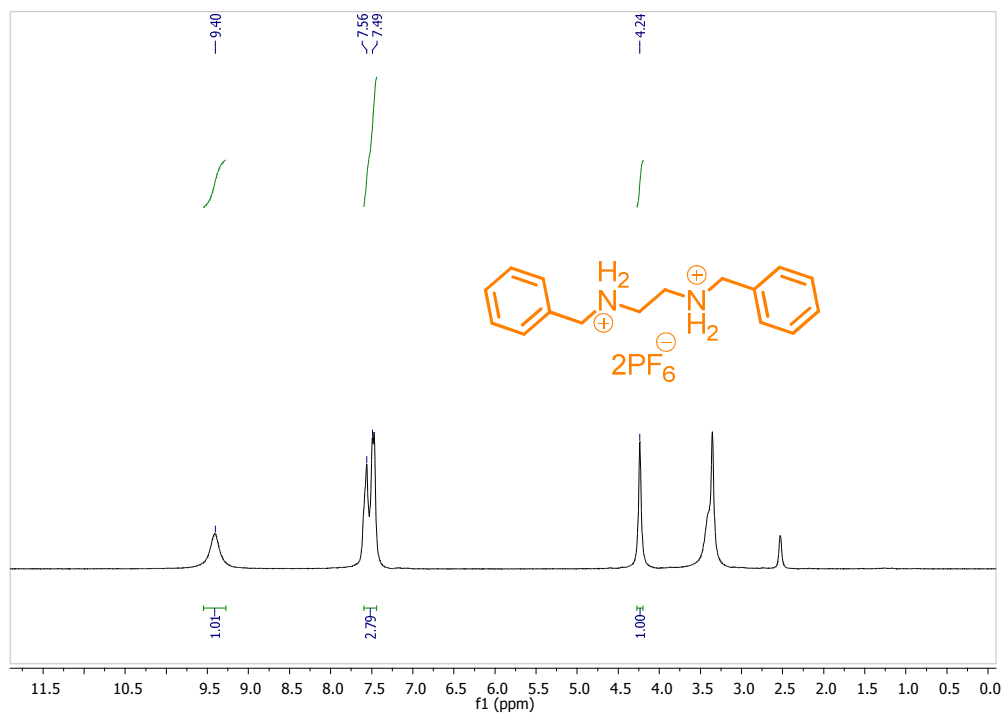


Figure 47. ^1H NMR spectra recorded in CD_3CN .

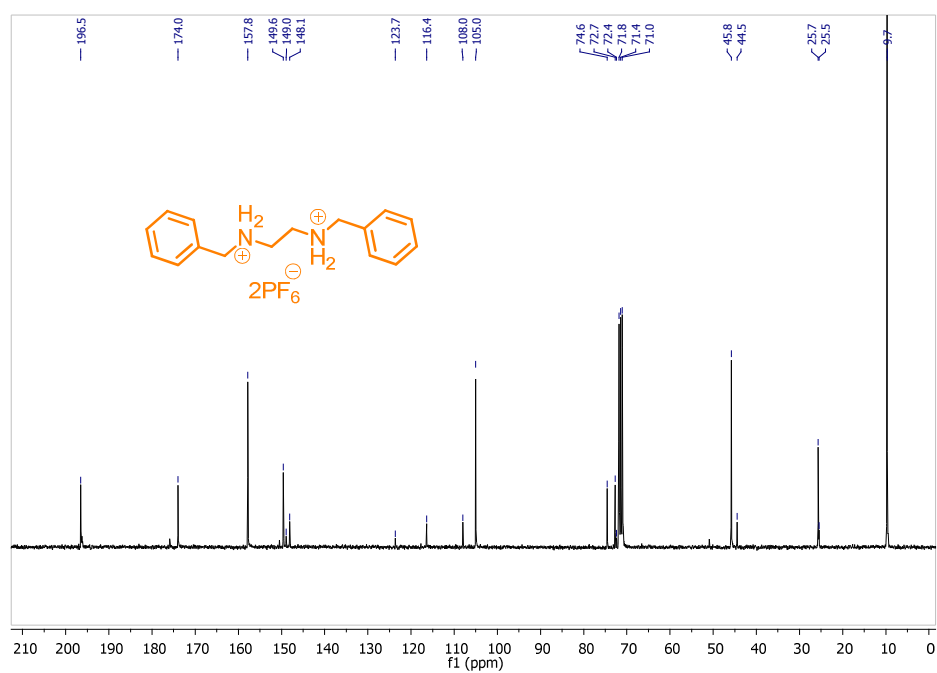


Figure 48. ^{13}C NMR spectra recorded in CD_3CN .

Appendix

MGB448 #87 RT: 0.39 AV: 1 NL: 1.90E7
T: FTMS - p ESI Full ms [100.00-1500.00]

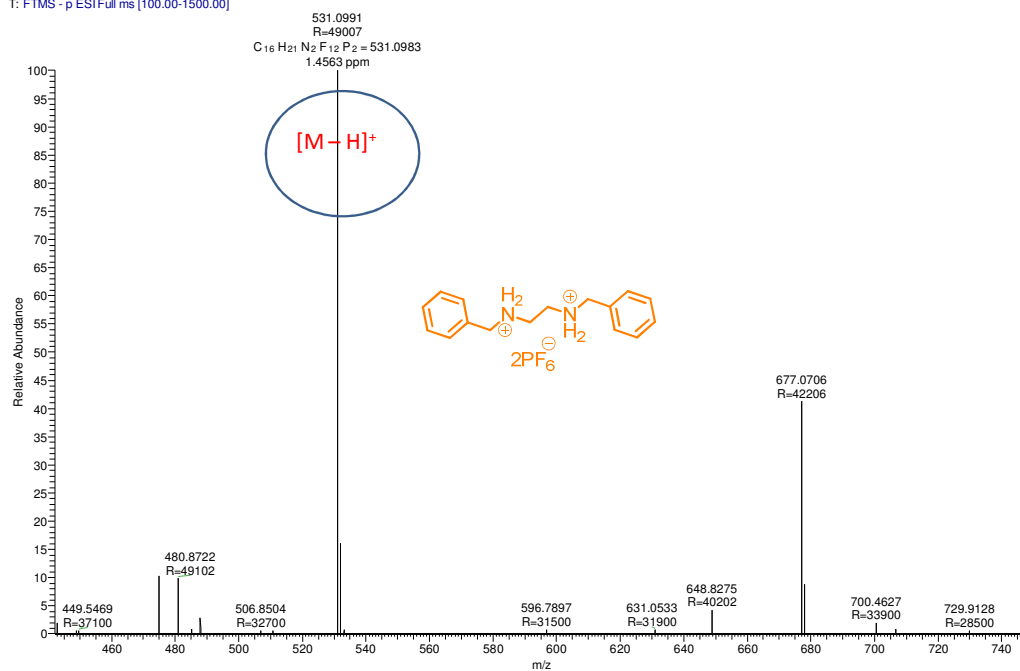


Figure 49. HRMS spectra recorded in ACN.

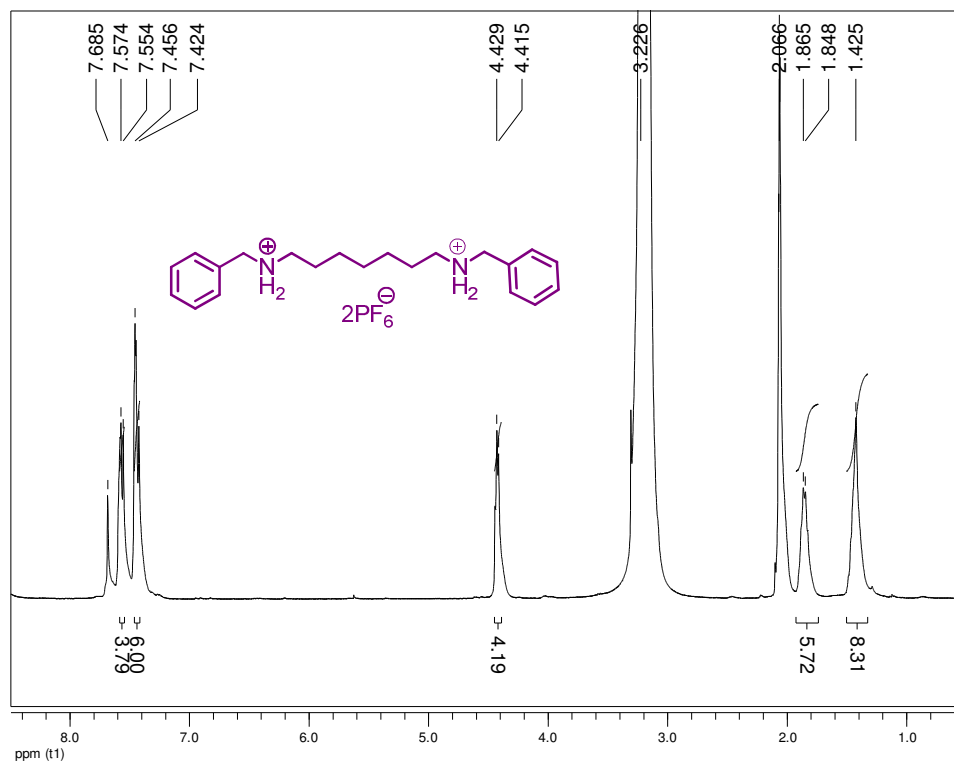


Figure 50. ¹H NMR spectra recorded in CD₃CN.

Appendix

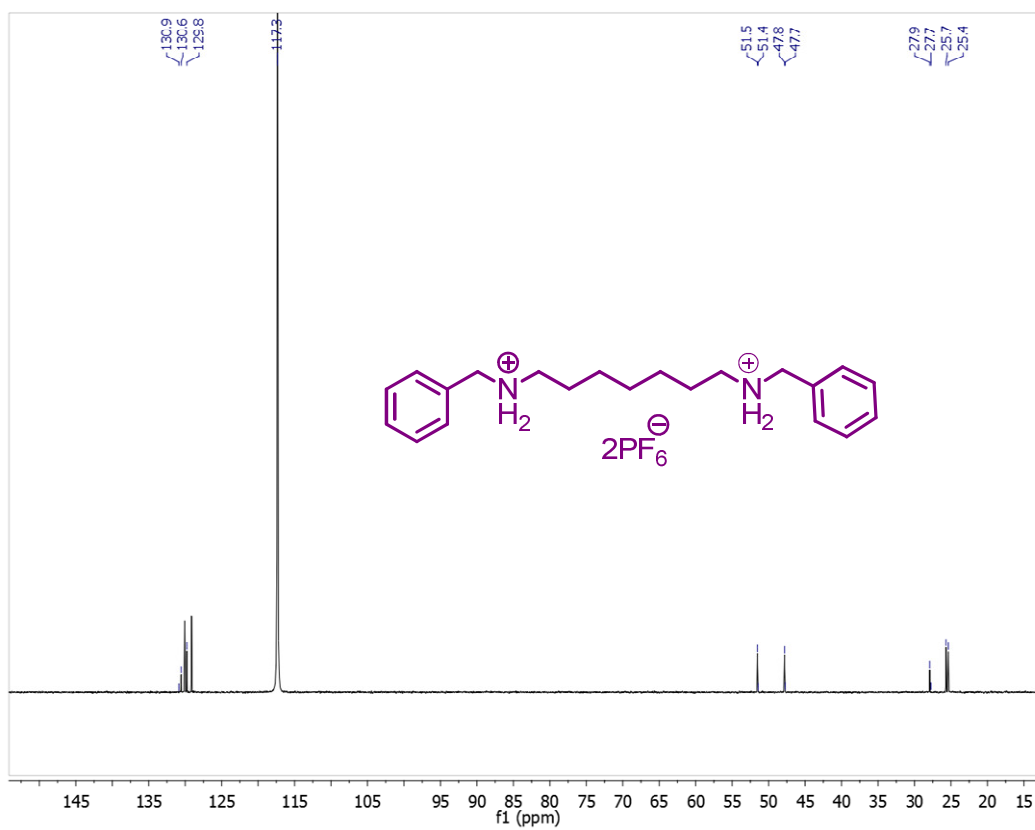


Figure 51. ^{13}C NMR spectra recorded in CD_3CN .

Publication

List of Publications Related To The Thesis

1. **Monalisa Gangopadhyay**, Amal K. Mandal, Arunava Maity, Sapna Ravindranathan, Pattuparambil R. Rajamohanan, and Amitava Das, *Tuning Emission Responses of a Triphenylamine Derivative in Host–Guest Complexes and an Unusual Dynamic Inclusion Phenomenon*, **J. Org. Chem.** 2016, 81, 512–521.
2. **Monalisa Gangopadhyay**, Arunava Maity, Ananta Dey, and Amitava Das, *[2]Pseudorotaxane Formation with FRET Based Luminescence Response: Demonstration of Boolean Operations through Self Sorting on Solid Surface* **J. Org. Chem.** 2016, 81, 8977–8987.
3. **Monalisa Gangopadhyay**, Arunava Maity, P. R. Rajamohanan, Sapna Ravindranathan and Amitava Das, Chiral Discrimination Through FRET Based Process in Supramolecular Assemblies. (To Be communicated)
4. **Monalisa Gangopadhyay**, and Amitava Das, Tuning of monomer/excimer emission of a bis crown ether by dicationic ammonium guests (To be communicated).

List of other Publications

1. Amal Kumar Mandal, Moorthy Suresh, Manoj K. Kesharwani, **Monalisa Gangopadhyay**, Manoj Agrawal, Vinod P. Boricha, Bishwajit Ganguly, and Amitava Das, **J. Org. Chem.** 2013, 78, 9004–9012.
2. Amal Kumar Mandal, **Monalisa Gangopadhyay** and Amitava Das, **Chem. Soc. Rev.**, 2015, 44, 663–676.
3. Hridesh Agarwalla, **Monalisa Gangopadhyay**, Dharmendar Kr. Sharma, Santanu Kr. Basu, Sameer Jadhav, Arindam Chowdhury, Amitava Das, **J. Mater. Chem. B**, 2015, 3, 9148–9156.
4. Arunava Maity, **Monalisa Gangopadhyay**, Arghya Basu, Sunil Aute, Sukumaran Santhosh Babu, and Amitava Das, **J. Am. Chem. Soc.**, 2016, 138, 11113–11116.

Conference

List of Conferences Attended

1. Poster presented in "**Trombay Symposium on Radiation & Photochemistry (TSRP-2016)**" which is held at BARC, Mumbai.
2. Participated in "**17th CRSI National Symposium in Chemistry**" this is held at National Chemical Laboratory, Pune 6-8 Feb 2015.
3. Poster presented in "**Trombay Symposium on Radiation & Photochemistry (TSRP-2014)**" which is held at BARC, Mumbai.
4. Participated in "**International Conference on Structural and Inorganic Chemistry**" which held at National Chemical Laboratory, Pune on 4th – 5th Dec 2014.
5. Poster Presented in "**National Science Day Celebration 2016**" at CSIR-National Chemical Laboratory, Pune on 25-26th of February 2015.
6. Poster Presented in "**National Science Day 2014 Celebration 2014**" at CSIR-National Chemical Laboratory, Pune on 25-26th of February 2014.



RightsLink®

[Home](#)[Create Account](#)[Help](#)

ACS Publications Title:
Most Trusted. Most Cited. Most Read.

Tuning Emission Responses of a Triphenylamine Derivative in Host–Guest Complexes and an Unusual Dynamic Inclusion Phenomenon

Author: Monalisa Gangopadhyay, Amal K. Mandal, Arunava Maity, et al

Publication: The Journal of Organic Chemistry

Publisher: American Chemical Society

Date: Jan 1, 2016

Copyright © 2016, American Chemical Society

[LOGIN](#)

If you're a [copyright.com user](#), you can login to RightsLink using your copyright.com credentials. Already a [RightsLink user](#) or want to [learn more?](#)

PERMISSION/LICENSE IS GRANTED FOR YOUR ORDER AT NO CHARGE

This type of permission/license, instead of the standard Terms & Conditions, is sent to you because no fee is being charged for your order. Please note the following:

- Permission is granted for your request in both print and electronic formats, and translations.
- If figures and/or tables were requested, they may be adapted or used in part.
- Please print this page for your records and send a copy of it to your publisher/graduate school.
- Appropriate credit for the requested material should be given as follows: "Reprinted (adapted) with permission from (COMPLETE REFERENCE CITATION). Copyright (YEAR) American Chemical Society." Insert appropriate information in place of the capitalized words.
- One-time permission is granted only for the use specified in your request. No additional uses are granted (such as derivative works or other editions). For any other uses, please submit a new request.

[BACK](#)[CLOSE WINDOW](#)

Copyright © 2017 [Copyright Clearance Center, Inc.](#) All Rights Reserved. [Privacy statement.](#) [Terms and Conditions.](#) Comments? We would like to hear from you. E-mail us at customercare@copyright.com



RightsLink®

[Home](#)[Create Account](#)[Help](#)

Title: [2]Pseudorotaxane Formation with FRET Based Luminescence Response: Demonstration of Boolean Operations through Self-Sorting on Solid Surface

Author: Monalisa Gangopadhyay, Arunava Maity, Ananta Dey, et al

Publication: The Journal of Organic Chemistry

Publisher: American Chemical Society

Date: Oct 1, 2016

Copyright © 2016, American Chemical Society

[LOGIN](#)

If you're a [copyright.com user](#), you can login to RightsLink using your copyright.com credentials. Already a [RightsLink user](#) or want to [learn more?](#)

PERMISSION/LICENSE IS GRANTED FOR YOUR ORDER AT NO CHARGE

This type of permission/license, instead of the standard Terms & Conditions, is sent to you because no fee is being charged for your order. Please note the following:

- Permission is granted for your request in both print and electronic formats, and translations.
- If figures and/or tables were requested, they may be adapted or used in part.
- Please print this page for your records and send a copy of it to your publisher/graduate school.
- Appropriate credit for the requested material should be given as follows: "Reprinted (adapted) with permission from (COMPLETE REFERENCE CITATION). Copyright (YEAR) American Chemical Society." Insert appropriate information in place of the capitalized words.
- One-time permission is granted only for the use specified in your request. No additional uses are granted (such as derivative works or other editions). For any other uses, please submit a new request.

[BACK](#)[CLOSE WINDOW](#)

Copyright © 2017 [Copyright Clearance Center, Inc.](#) All Rights Reserved. [Privacy statement.](#) [Terms and Conditions.](#) Comments? We would like to hear from you. E-mail us at customer care@copyright.com